The University of British Columbia

FACULTY OF GRADUATE STUDIES

PROGRAMME OF THE

FINAL ORAL EXAMINATION

FOR THE DEGREE OF

DOCTOR OF PHILOSOPHY

of

ROBERT CLOUDESLEY BRERETON

B. Eng., McGill University, 1959

WEDNESDAY, NOVEMBER 22, 1967, AT 10:30 a.m.

ROOM 208, MECHANICAL ENGINEERING ANNEX

COMMITTEE IN CHARGE

Chairman: I. McT. Cowan

J.P. Duncan	V.J. Modi
G.V. Parkinson	C.R. Hazell
A.C. Soudack	E.V. Bohn

External Examiner: J. Mar
Head, Space Mechanics Section
Defence Research Telecommunications
Establishment
Ottawa, Ontario

Research Supervisor: V.J. Modi

A STABILITY STUDY OF GRAVITY ORIENTED SATELLITES

ABSTRACT

The stability of gravitational gradient oriented satellites is examined by considering four simplified models. The investigation is carried out numberically and analytically. The techniques employed involve considerable computation and hence are particularly suited to solution by a digital computer.

The analysis of the planar motion of a rigid satellite leads to the concept of an invariant surface or integral manifold. Numerical integration of the equation of motion is employed to determine the manifolds. It is shown that for specified values of the parameters describing the satellite, the region in phase space that is consistent with stable motion corresponds to the largest invariant surface which can be found. It is also demonstrated that the manifolds are intimately connected with periodic solutions of the equation of motion and this knowledge permits determining limits on the parameters so as to ensure stable motion by a study of the solution of the variational equation. Several charts suitable for design purposes are presented.

The planar motion of a satellite containing a damping mechanism is studied using a simplified model. It is shown that for small dampers the motion eventuall becomes nearly identical with a periodic solution of the undamped case.

The third model represents a flexible satellite free to deform under the influence of solar heating. An analysis of the temperature distribution in the structure permits determination of the shape of the satellite solely in terms of its position. The resulting equation of motion is derived and it is shown that flexibility does not greatly affect the stability pro-

vided that the flexible member is not too long.

The case of an axi-symmetric satellite in a circular orbit is also considered. It is shown that in this case manifolds also exist although in some cases apparently ergodic motion can occur. Stability can be guaranteed if the Hamiltonian is less than a prescribed value. Values of the Hamiltonian larger than this may also permit stable motion and in this case an invariant surface is always described in phase space. The stability of the general motion is somewhat greater than that for the planar motion. Charts are presented giving the maximum permissible disturbances for stable motion.

GRADUATE STUDIES

Field of Study: Mechanical Engineering

Space Dynamics (I and II)	V.J. Modi
Mechanical Vibrations	C.A. Brockley
High Speed Gas Dynamics	G.V. Parkinson
Mechanics of Rarified Gases	G.V. Parkinson
Non-linear Systems	A.C. Soudack
Analogue Computers	E.V. Bohn

PUBLICATIONS

Modi, V.J., and Brereton, R.C., "Libration Analysis of a Dumbbell Satellite Using the WKBJ Method," Journal of Applied Mechanics, Vol. 33, No. 3, Sept. 1966, pp. 676-678.

Brereton, R.C., and Modi, V.J., "On the Stability of a Dumbbell Satellite in an Elliptic Orbit," Journal of the Royal Aeronautical Society, Vol. 70, Dec. 1966, pp. 1098-1102.

Brereton, R.C., and Modi, V.J., "Stability of the Planar Librational Motion of a Satellite in an Elliptic Orbit," Proceedings of the XVII International Astronautical Congress, Madrid, 1967.

Modi, V.J., and Brereton, R.C., "Stability Boundaries for Planar Librations of a Long Flexible Satellite, Paper No. 67-126, AIAA 5th Aerospace Sciences Meeting, New York, New York, Jan. 23-26, 1967.

Modi, V.J., and Brereton, R.C. "The Stability Analysis of Coupled Librational Motion of an Axi-Symmetric Satellite in a Circular Orbit," Proceedings of the XVIII International Astronautical Congress, Belgrad (in press).

A STABILITY STUDY OF GRAVITY ORIENTED SATELLITES

by

ROBERT CLOUDESLEY BRERETON
B. Eng., McGill University, 1959

A THESIS SUBMITTED IN PARTIAL FULFILMENT OF
THE REQUIREMENTS FOR THE DEGREE OF
DOCTOR OF PHILOSOPHY

in the Department
of
Mechanical Engineering

We accept this thesis as conforming to the
required standard

THE UNIVERSITY OF BRITISH COLUMBIA
September, 1967

In presenting this thesis in partial fulfilment of the requirements for an advanced degree at the University of British Columbia, I agree that the Library shall make it freely available for reference and study. I further agree that permission for extensive copying of this thesis for scholarly purposes may be granted by the Head of my Department or by his representatives. It is understood that copying or publication of this thesis for financial gain shall not be allowed without my written permission.

R.C. Brereton

Department of Mechanical Engineering

The University of British Columbia
Vancouver 8, Canada

Date 22 Nov 1967

ABSTRACT

The stability of gravitational gradient oriented satellites is examined by considering four simplified models. The investigation is carried out numerically and analytically. The techniques employed involve considerable computation and hence are particularly suited to solution by a digital computer.

The analysis of the planar motion of a rigid satellite leads to the concept of an invariant surface or integral manifold. Numerical integration of the equation of motion is employed to determine the manifolds. It is shown that for specified values of the parameters describing the satellite, the region in phase space that is consistent with stable motion corresponds to the largest invariant surface which can be found. It is also demonstrated that the manifolds are intimately connected with periodic solutions of the equation of motion and this knowledge permits determining limits on the parameters so as to ensure stable motion by a study of the solution of the variational equation. Several charts suitable for design purposes are presented.

The planar motion of a satellite containing a damping mechanism is studied using a simplified model. It is shown that for small dampers the motion eventually becomes nearly identical with a periodic solution of the undamped case.

The third model represents a flexible satellite free to deform under the influence of solar heating. An analysis of the temperature distribution in the structure permits determination of the shape of the satellite solely in terms of its position. The resulting equation of motion is derived and it is shown that flexibility does not greatly affect the stability provided that the flexible member is not too long.

The case of an axi-symmetric satellite in a circular orbit is also considered. It is shown that in this case manifolds also exist although at times apparently ergodic motion can occur. Stability can be guaranteed if the Hamiltonian is less than a prescribed value. Values of the Hamiltonian larger than this may also permit stable motion and in this case an invariant surface is always described in phase space. The stability of the general motion is somewhat greater than that for the planar motion. Charts are presented giving the maximum permissible disturbances for stable motion.

TABLE OF CONTENTS

LIST OF TABLES

LIST OF FIGURES

ACKNOWLEDGEMENT

The author wishes to express his thanks to Dr. V.J. Modi for the guidance given throughout the preparation of the thesis. His help and encouragement have been invaluable.

The numerical work in this thesis was carried out in the Computing Centre of the University of British Columbia. The use of these facilities is gratefully acknowledged.

LIST OF SYMBOLS

A	Coefficient in equation (2.100)
A_a	Aerodynamic reference area
A_e	Area from which radiation is emitted
A_i	Amplitude of the i^{th} normal mode of the satellite boom
A_{in}	Area on which radiation is incident
$A_{m,n}$	m^{th} Fourier coefficient in the solution of equation (2.14) of period $2\pi n$
A_r	Projected area of the satellite
A_δ	Arbitrary coefficient in the solution of the variational equation (2.64)
B	Coefficient in equation (2.100)
B_δ	Arbitrary coefficient in the solution of the variational equation (2.64)
C	Coefficient in equation (2.100)
$C_{b,n}$	Coefficient in equation (4.59)
C_c	Constant of integration in equation (2.16)
C_H	Constant value of the Hamiltonian, equation (5.26)
$C_{m_1,m_2,m_3,n}$	Coefficient in equation (2.23)
C_p	Aerodynamic pressure coefficient
$C_{s,n}$	n^{th} Fourier coefficient expressing the solar heat input to the satellite boom
$C_1, C_2, \bar{C}_1, \bar{C}_2$	Arbitrary constants
D	Coefficient in equation (2.100)
$\mathfrak{D}$	Parameter determining the nature of a conic section
$\mathcal{E}$	Modulus of elasticity

F	Function defined in equation (2.41)
$\mathcal{F}$	Dissipation function
F_i	Generalized force acting on the i^{th} normal mode of the satellite boom
F_L	Longitudinal force in the satellite boom
F_1, F_2	Functions defined in equation (5.29)
G	Function defined in equation (2.40)
H	Hamiltonian function
$\mathcal{H}$	Magnetic field strength
I	Large moment of inertia of an axi-symmetric satellite
I_b	Inertia of the cross-section of the satellite boom
I_i	Inertia of the i^{th} mode of vibration of the satellite boom, defined in equation (4.20)
I_r	Inertia of a satellite with a rigid boom
I_{xx}, I_{yy}, I_{zz}	Principal moments of inertia of the satellite
$\bar{I}$	Inertia variation parameter = $I_{zz_{max}}/I_r$
K	Elliptic integral of the first kind
K_d	Parameter describing the inertia of the satellite damper, equation (3.6)
K_i	Inertia parameter = $(I_{xx} - I_{zz})/I_{yy}$
K_x, K_z	Inertia variation parameters, defined in equation (4.82)
L	Length of the satellite boom
$\mathcal{L}$	Lagrangian function
L^*	Dimensionless length of the satellite boom = L/ℓ^*
$\mathcal{M}$	Residual magnetic moment of the satellite
$P_{m,n}$	Coefficient in equation (2.25)

Q	Quantity of heat
R_c	Radius of curvature of the satellite boom
T	Kinetic energy
T_b	Temperature of the satellite boom
$T_{b,n}$	The n^{th} Fourier coefficient describing the temperature distribution in the satellite boom
T_{ref}	Reference temperature
T_v	Vibrational kinetic energy
U	Potential energy
U_e	Elastic potential energy
U_g	Gravitational potential energy
W	Wronskian determinant
X_i	Shape function of the i^{th} normal mode of the satellite boom
Z	Dimensionless damper displacement
a	Value of the first solution of the variational equation when $\Theta = 2\pi n$
a_b	Diameter of the satellite boom
b	Value of the derivative of the first solution of the variational equation when $\Theta = 2\pi n$
b_b	Wall thickness of the satellite boom
c	Value of the second solution of the variational equation when $\Theta = 2\pi n$
c_b	Specific heat of the material in the satellite boom
c_d	Damping constant
c^*	Speed of light
d	Value of the derivative of the second solution of the variational equation when $\Theta = 2\pi n$

e	Orbit eccentricity
h	Step size employed in numerical integration
h_s	Angular momentum of the satellite boom as seen in rotating co-ordinates
h_θ	Angular momentum per unit mass of the satellite about the centre of force
i	Integer
k	Frequency eigenvalue of the satellite boom
k_b	Thermal conductivity of the material in the satellite boom
k_d	Spring constant of the damper
l_b	Length of an element of the satellite boom
l_{ref}	Reference length of an element of the satellite boom
l_x, l_y, l_z	Direction cosines of the local vertical in the principal co-ordinates
l^*	Thermal reference length of the satellite, defined in equation (4.76)
Δl_a	Distance between the line of action of the aerodynamic force and the centre of mass
Δl_r	Distance between the line of action of the force due to radiation pressure and the centre of mass
m	Integer
m_b	Mass of the satellite
m_d	Mass of the damper
m_s	Mass per unit length of the satellite boom
m_1, m_2, m_3	Integers
n	Integer
p_i	Generalized momentum conjugate to the co-ordinate q_i

P_r	Radiation pressure
P_λ	Momentum conjugate to the λ co-ordinate
P_ϕ	Momentum conjugate to the ϕ co-ordinate
P_ψ	Momentum conjugate to the ψ co-ordinate
q_{abs}	Rate at which heat is absorbed per unit area
q_{ext}	Rate of heat input from external sources per unit area
q_i	Generalized co-ordinate
q_{in}	Rate at which heat is incident on unit area
q_{int}	Rate of heat input from internal sources per unit area
q_{ref}	Rate at which heat is reflected per unit area
q_s	Rate of heat input from the sun per unit area
r	Radius
R	Distance between the centre of force and an element of mass
s	Distance along the satellite boom
t	Time
v	Velocity
x, y, z	Principal body co-ordinates
x_0, y_0, z_0 x_1, y_1, z_1 x_2, y_2, z_2	Intermediate body co-ordinates with origin at the centre of mass prior to the modified Eulerian rotations ψ , ϕ , λ respectively
$\bar{z}_0$	Damper off-set distance
$\bar{z}_1$	Damper displacement
Γ_a	Aerodynamic torque
Γ_b	Moment in the satellite boom
Γ_g	Moment due to gravitational gradient
Γ_m	Magnetic torque

Γ_r	Radiation torque
ϵ	Function describing the error in the numerically determined periodic solutions
Θ	Mean rotation angle of the perturbation solution
Ψ	Variable defined in equation (2.38)
$\bar{\Psi}_1, \bar{\Psi}_2$	Complementary solutions of equation (2.39)
$\bar{\Psi}^*$	Particular integral of equation (2.39)
Ω	Angle around satellite boom as measured from the sub-solar point
α	Solar aspect angle
α_s	Absorptivity of satellite boom material to solar energy
α_t	Coefficient of thermal expansion of boom material
α_θ	Specific value of α
β	$\psi + \Theta - \alpha$
γ	Characteristic root
γ_s	$\beta + \pi/2$
δ	Perturbation
δ_1, δ_2	Complementary solutions of variational equation
ϵ_b	Emissivity of boom material
ζ	Perturbation in ψ'
ζ_r	Distance between elements along satellite boom
η_b	Co-ordinate of deflected boom
θ	Position angle of satellite in its orbit as measured from pericentre
$\hat{\theta}$	Specified value of Θ
θ^*	$\Theta - \pi$

$\Delta\Theta$	Period of a periodic solution
λ	Co-ordinate defining the angle of spin of a satellite
$\lambda_n, \lambda_{r_1}, \lambda_{r_2}$	Angles used in the radiation analysis of the interior of the satellite boom (Figure 4-4)
μ	Gravitational field parameter
μ_r	Angle employed in the radiation analysis of the interior of the satellite boom (Figure 4-4)
γ	Function defined in equation (2.45)
ε	Perturbation in ψ
ε_b	Co-ordinate of deflected boom
ρ_a	Atmospheric density
ρ_b	Density of boom material
σ	Stefan-Boltzmann constant
σ_b	Stress in boom material
τ_d	Damper time constant
τ_n	Time constant of the n^{th} coefficient in the Fourier analysis of the temperature distribution of the satellite boom
τ_θ	Orbital period
τ^*	Dimensionless damper time constant, equation (3.14)
ϕ	Librational angle normal to the orbital plane
ϕ_b	Angle subtended by an element of the satellite boom of length ℓ_b
ϕ^*	Angle between the sun and the axis of an element of the satellite boom
ψ	Librational angle in the orbital plane
ψ_c	Value of ψ at $\Theta = 2\pi$
$\psi_{p,n}$	Periodic solution of equation (2.14) with period 2π n

ψ_*	$\psi - \pi/2$
$\hat{\psi}'$	ψ' Cos ϕ
ψ_1, ψ_2	Complementary solution of equation (2.37)
ψ^*	Particular integral of equation (2.37)
$\Delta\dot{\psi}$	Maximum allowable size of impulse for stability
ω	Solid angle
ω_d	Natural frequency of the damper
ω_i	Natural frequency of the i^{th} normal mode of the satellite boom
ω_L	Function defined in equation (2.45)
$\omega_x, \omega_y, \omega_z$	Angular velocities about the principal axes
ω_θ	Orbital frequency = $2\pi/\tau_\theta$
ω^*	Dimensionless damper natural frequency

Subscripts

f	Final value
i	Integer
max	Maximum
n	Value at $\Theta = 2\pi n$
steady	Steady state
o	Initial conditions

Dots and primes indicate differentiation with respect to t and Θ respectively

1. INTRODUCTION

1.1 Preliminary Remarks

The motion of a space vehicle involves two dynamical aspects of interest, namely, the analyses of its trajectory and of its orientation. The former, generally referred to as the orbital motion, is concerned with the determination of the motion of the mass centre and may be thought of as an extension of classical celestial mechanics. On the other hand, the motion of a satellite about its own centre of mass is called libration.

There are situations of practical importance where it is desirable to maintain a satellite in a fixed orientation relative to the earth. For example, proper functioning of communication satellites with directional antennae or of weather satellites scanning cloud cover requires attitude control. Unfortunately, the orientation of the satellite, even though positioned correctly in the beginning, deviates in time under the influence of external disturbances, e.g. micrometeorite impacts, solar radiation pressure, gravitational and magnetic field interactions. This leads to undesirable librational motion which must be controlled for the successful operation of the satellite.

Several methods of attitude control are available. They may be classified as active or passive techniques.

Active stabilization involves the expenditure of

energy which is a very expensive commodity aboard an instrument packed spacecraft. The main advantage of this technique is its ability to maintain the specified orientation with almost any desired degree of accuracy.

Passive stabilization techniques, which use no power, can provide the necessary attitude control if the orientation requirements are not too severe. Stabilization is obtained by employing the non-uniformities of the environment in conjunction with the physical properties of the satellite. The significant forces available for passive stabilization of a spacecraft arise from gravitational, solar, magnetic, and aerodynamic effects.[1,2]

The gravitational moment arises because of the local variation of the gravitational acceleration within the satellite. It tends to make the "long" axis (the axis of minimum moment of inertia) of the spacecraft point in the local vertical direction. There is no discrimination between "up" and "down." The maximum gravity-gradient torque is given by

$$\Gamma_g = \frac{3\mu}{2r^3}\left(I_{xx} - I_{zz}\right). \tag{1.1}$$

The electromagnetic radiation from the sun carries with it momentum and hence when absorbed or reflected exerts a pressure. A satellite with a large surface area placed asymmetrically with respect to the centre of mass will experience a moment which may be utilized to establish a

preferred orientation. The radiation pressure in the vicinity of the earth is given by

$$p_r = \frac{q_s}{c^*} = 9.7 \times 10^{-8} \ \text{lb/ft}^2 \tag{1.2}$$

so that the maximum radiation pressure torque is

$$\Gamma_r = p_r A_r \Delta \ell_r. \tag{1.3}$$

The earth's magnetic field extends for some distance into space. Within ten earth-radii it is relatively stable and varies approximately as the inverse third power of the distance. At larger distances it interacts with the solar wind and becomes quite unsteady.[3] The earth's magnetic field can interact with a spacecraft giving rise to a moment in three distinct ways.

Rotary motion of the conducting material in the spacecraft induces eddy currents which dissipate energy. The effect is to provide a moment which opposes the motion. Rotation with respect to the earth's magnetic field of ferromagnetic materials present in the satellite results in hysteresis losses and hence in a damping moment. The interaction between the residual magnetic moment of the spacecraft with the earth's field also produces a moment. In contrast to the previous two cases, this interaction is conservative. The maximum torque due to the magnetic moment is

$$\Gamma_m = 7.38 \times 10^{-8} \mathcal{M} \mathcal{H} \quad \text{lb ft.} \tag{1.4}$$

The problem is further complicated by the fact that the magnitude and direction of the earth's field change with the position of the satellite in its orbit.

Under certain conditions, aerodynamic forces may provide an effective means of stabilization with respect to the velocity vector. Unfortunately these forces cause the satellite to re-enter the earth's atmosphere thus limiting the application of the technique to a short interval. The maximum aerodynamic torque is given by

$$\Gamma_a = \rho_a v^2 A_a \Delta l_a \quad (C_p \approx 2). \tag{1.5}$$

King-Hele[4] has discussed the determination of ρ_a in considerable detail.

The variation of the moments given by equations (1), (3), (4) and (5) with altitude for the representative configuration[5] described in Table 1 is shown in Figure 1-1. A satellite, when stabilized by one of these moments, tends to attain the preferred direction associated with that moment. The remaining moments which act in different directions constitute disturbances. The chosen technique, therefore, must have a large maximum torque compared to the disturbing moments so that the perturbed motion is within the allowable limits.

Table I

Representative Gravity-Gradient Satellite Configuration[5]

Satellite		GEOS - A	
Moments of inertia,	I_{xx}	615.3	slug ft^2
	I_{zz}	20.8	slug ft^2
Projected area,	$A_r = A_a$	13.1	ft^2
Offset between centre of mass and centre of area,	$\Delta\ell_r = \Delta\ell_a$	5.75	ft
Residual magnetic moment,	$\mathcal{M}$	302	pole cm

1.2 Gravity-Gradient Stabilized Satellites

The dominance of the gravity-gradient torque over a large range of altitudes has led to considerable interest in this technique of stabilizing the attitude of artificial satellites. A survey of the literature reveals that the analysis of the problem has proceeded essentially along two paths. The major bulk of the literature is concerned either with the theoretical analysis of idealized models under restricted conditions or with the detailed simulation of specific configurations.

The purely theoretical analysis of the problem is limited by the fact that the governing non-linear coupled equations of motion do not possess a closed form solution. Moran[6] and Yu[7] found that some simplification of the problem is possible as the perturbations of the orbit due to

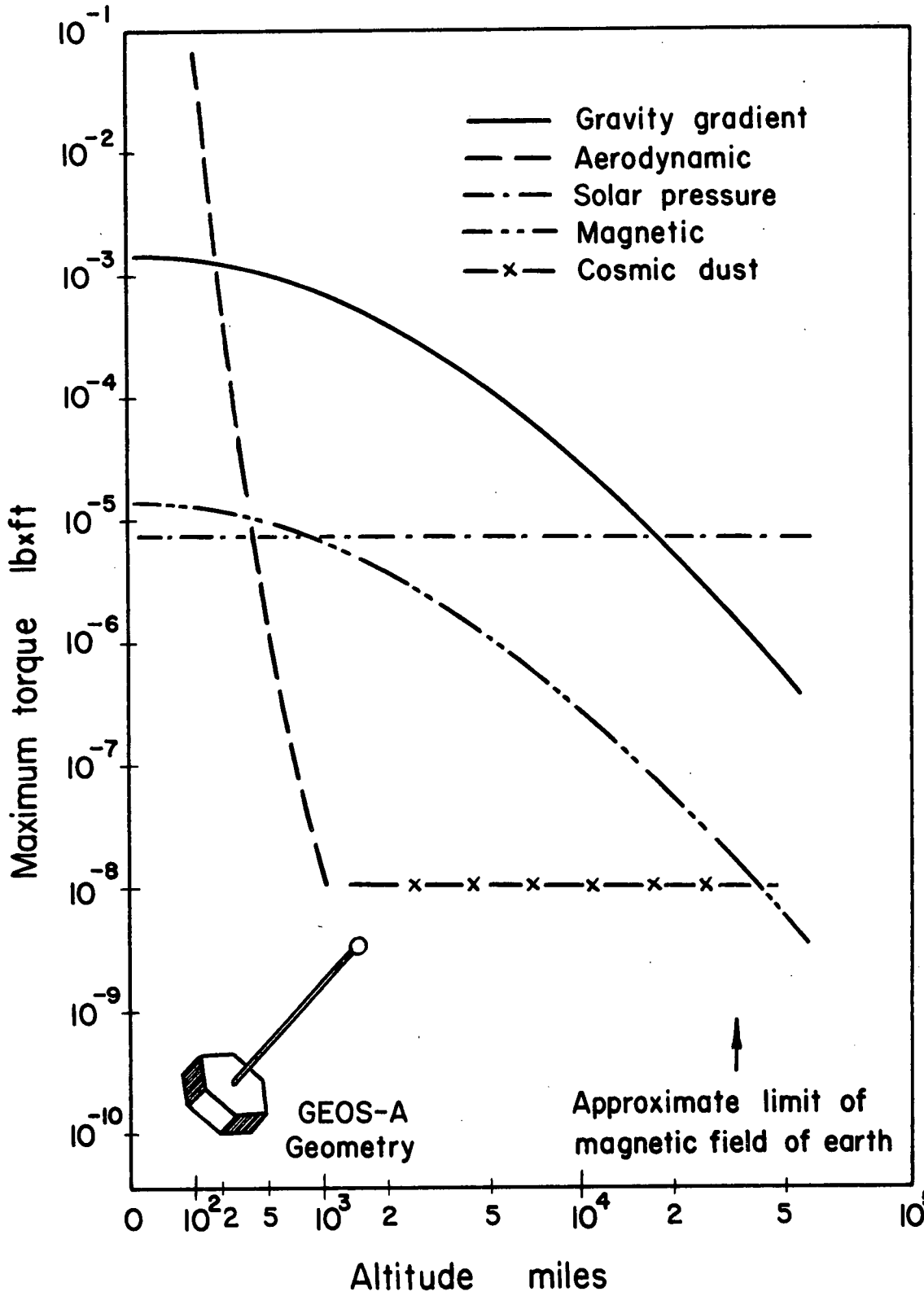

Figure 1-1 Magnitude of forces acting on a representative satellite

the librational motion of the satellite are negligibly small. This makes it possible to describe the orbital motion using the simple Keplerian equations.

Nelson and Loft[8] studied small amplitude librations of a rigid body in a circular orbit using linearized equations of motion. The approximation resulted in the decoupling of the motions in and normal to the orbital plane.

Klemperer[9] gave the exact solution for planar librations of a dumbbell satellite in a circular orbit. Schechter[10] attempted to extend this solution to the case of small orbital eccentricity by the method of perturbations. The method has limited applicability as the resulting perturbations grow without bound.

Baker[11] found periodic solutions with orbital frequency for a dumbbell satellite in an elliptic orbit. He showed that the amplitude of the motion is approximately proportional to the eccentricity of the orbit.

A recent paper by Zlatousov et al[12] is of considerable interest. These authors also obtained periodic solutions of the planar equations of motion. The solutions were functions of the orbit eccentricity and a parameter which described the geometry of the satellite. It was found that, in addition to the solutions predicted by Baker, there may be two other solutions for the same values of the parameters. Infinitesimal perturbations about these solutions were investigated for stability. It was shown that stable periodic motion was possible for all orbit eccentricities

by the proper choice of satellite geometry. Non-linear effects in the perturbation equations were not considered so that the magnitude of a finite disturbance which would yield stable motion was not determined.

These authors appear to have been the first to analyze the problem using the concept of a stroboscopic phase-plane. A plot in this plane may be regarded as the result of repeated application of a point transformation. Stable motion is represented by closed invariant curves and is associated with a periodic solution which appears as a set of fixed points.

The analysis involving the three degrees of freedom of a rigid satellite is very difficult. If the orbit is circular, the Hamiltonian is constant which specifies bounds on initial conditions to guarantee stability.[13]

DeBra[14] formulated the problem of the libration of a rigid arbitrarily shaped satellite in an elliptic orbit. He considered the general case with three degrees of freedom in the presence of a specific form of damping. The response of the satellite was determined for a limited set of initial conditions. Instability was attributed to the non-linear coupling existing between the degrees of freedom.

The detailed simulation technique has nearly always been concerned with satellites consisting of several bodies which are hinged together. The joints of such systems are conventionally equipped with springs and energy dissipating mechanisms. The introduction of articulated bodies increases

the complexity of the problem but, as pointed out by Hartbaum et al,[15] the configuration possesses considerable merit. The major advantages are very fast transient damping at all amplitudes of motion and considerable design flexibility.

Zajac[16] has analyzed the small amplitude planar motion of a two-body satellite (Figure 1-2-a) in a circular orbit. It was shown that in the presence of viscous damping the configuration reduces the time constant to 0.137 of the orbital period.

Multibody satellites have been investigated in detail by several authors. Etkin[17,18] has derived the equations of motion for a satellite consisting of rigid bodies (Figure 1-2-b). For an orbit of low eccentricity the equations of motion were linearized by assuming small amplitude librations of the constituent bodies. The roots of the resulting characteristic equation were evaluated for a wide range of configurations. This showed that the motion could be highly damped.

Fletcher, Rongved and Yu[19] formulated the equations of motion for a two-body communications satellite which was proposed originally by Paul, West and Yu[20] (Figure 1-2-c). A considerable amount of detailed simulation showed that the performance of such a device would be satisfactory.

Hartbaum et al[15] as well as Hughes[21] have attempted to optimize the configuration of articulated satellites (Figures 1-2-d and 1-2-b respectively) with respect to pointing accuracy.

Several configurations have been proposed which are simpler than the multi-body satellite discussed above. In 1963, Paul[22] investigated a satellite in which a mass was suspended from a "lossy" spring (Figure 1-2-e). The device damped oscillations only about axes perpendicular to that of the spring. This difficulty was eliminated in a study by Buxton, Campbell and Losch[23] where the spring was also permitted to execute torsional oscillations (Figure 1-2-f). Systems of this type are characterized by amplitude dependent damping.

Satellites designed for gravity-gradient stabilization are necessarily very long. Recently much attention has been focused on the effects of the resulting flexibility. Katucki and Moyer[24] have considered this to be a major factor affecting the librational dynamics as solar heating can produce large changes in the configuration. Ashley[25] investigated analytically the structural dynamics of several flexible bodies when excited by the gravitational gradient field. Dow et al[26] have presented the results of an extremely elaborate simulation of flexibility effects.

The simulation studies of this nature have been successful in predicting the performance of existing gravity-gradient satellites. The Geodetic Earth Orbiting Satellite, GEOS-A,[5] and the Gravity Gradient Test Satellite, GGTS,[27] are performing as expected.

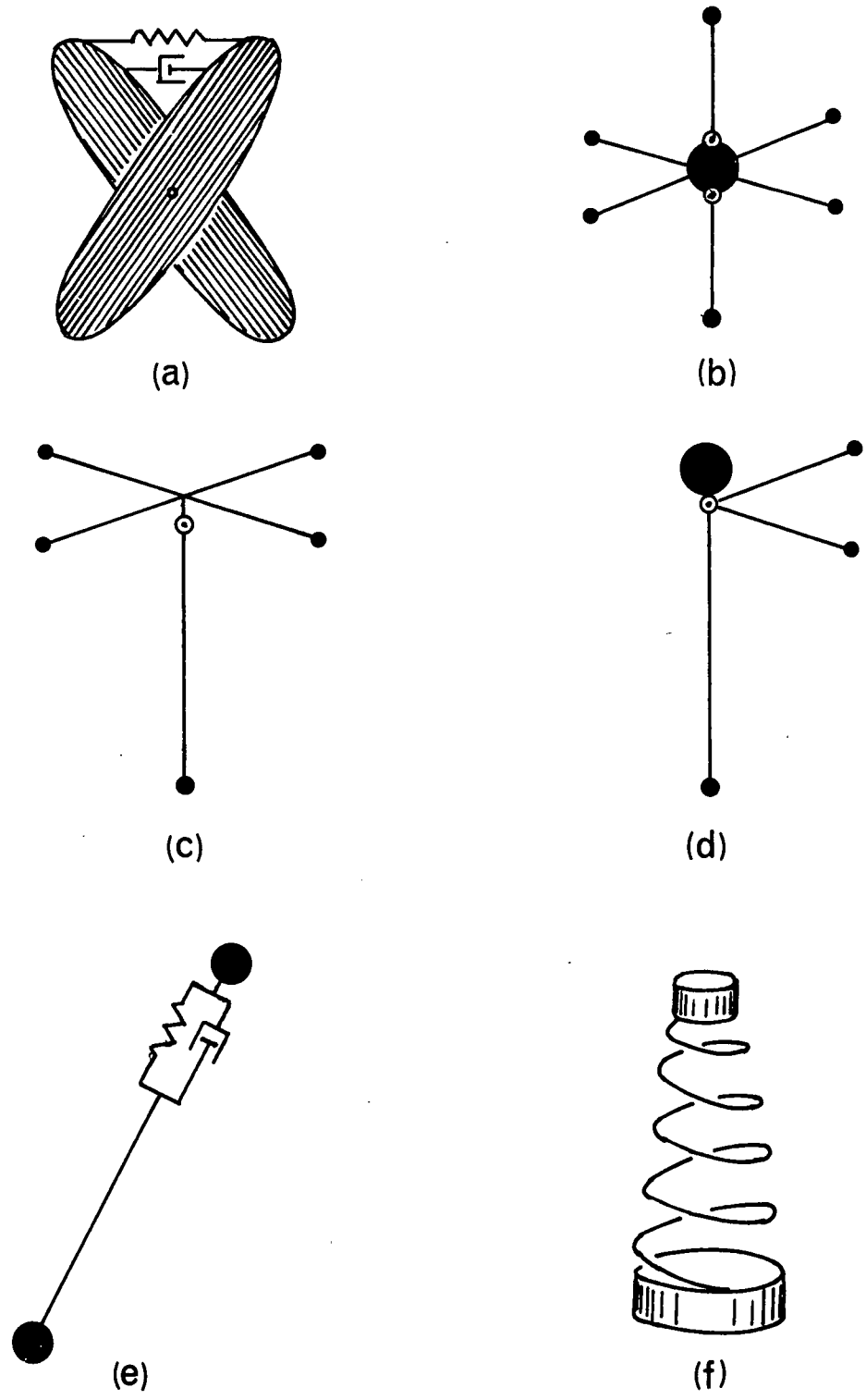

Figure 1-2 Models of multi-body satellites

1.3 Purpose and Scope of Investigation

The main purpose of this investigation is to obtain the limiting initial conditions for a gravity-gradient stabilized satellite as a function of design parameters. The secondary purpose is to investigate the nature of the motion and to establish procedures based on this knowledge which will speed and simplify the analysis. To these ends, several models are studied. In each case only those forces specifically mentioned are included in the analysis.

The first model is that of a rigid satellite executing librations in the plane of the orbit. The investigation assumes a non-dissipative configuration (Figure 2-1).

Model number two includes dissipation by the addition of a damper of the form proposed by Paul.[22] Planar motion is essential for the proper functioning of the model (Figure 3-1).

The third model assumes the satellite to be non-dissipative but subject to considerable distortion due to solar heating. The effects of varying the satellite's physical properties are considered (Figure 4-1).

The last model investigated is an axi-symmetric rigid satellite (Figure 5-1). The restriction to planar motion is removed although the orbit is assumed to be circular.

The first model is the simplest. It was specifically chosen to provide a basic understanding of the nature of the motion. In general the librational motion is two-dimensional

and model four serves as an appropriate extension. The influence of internal damping, which is always present, is idealized in model two. The importance of thermal distortion has been pointed out by several investigators.[24-26] The third model provides a convenient way of studying these effects.

2. PLANAR LIBRATIONAL MOTION OF A RIGID SATELLITE

2.1 Formulation of the Problem

The planar motion of a rigid satellite in a circular orbit has been solved by Klemperer[9] in terms of the elliptic sine function. In an elliptic orbit, the variations in the orbital angular velocity and the local gravitational gradient provide the satellite with a mechanism for exchanging energy between the librational and orbital degrees of freedom. In general, this leads to a reduction in the range of initial conditions that result in stable librational motion as compared to the corresponding range for a circular orbit. This chapter investigates the bounds that must be placed on the initial conditions as functions of orbit eccentricity and satellite geometry to guarantee stable motion.

Consider a rigid satellite of arbitrary shape with centre of mass at S executing planar librational motion while moving in an elliptic orbit about the centre of force O (Figure 2-1). The mass distribution of the central body is assumed spherical so that the orbit defines a plane. The position of the satellite is given by the orbit angle, θ, measured from the pericentre, P, in the direction of the orbital motion.

Let xyz be a set of orthogonal body co-ordinates with the y-axis normal to the plane of the orbit. The angle

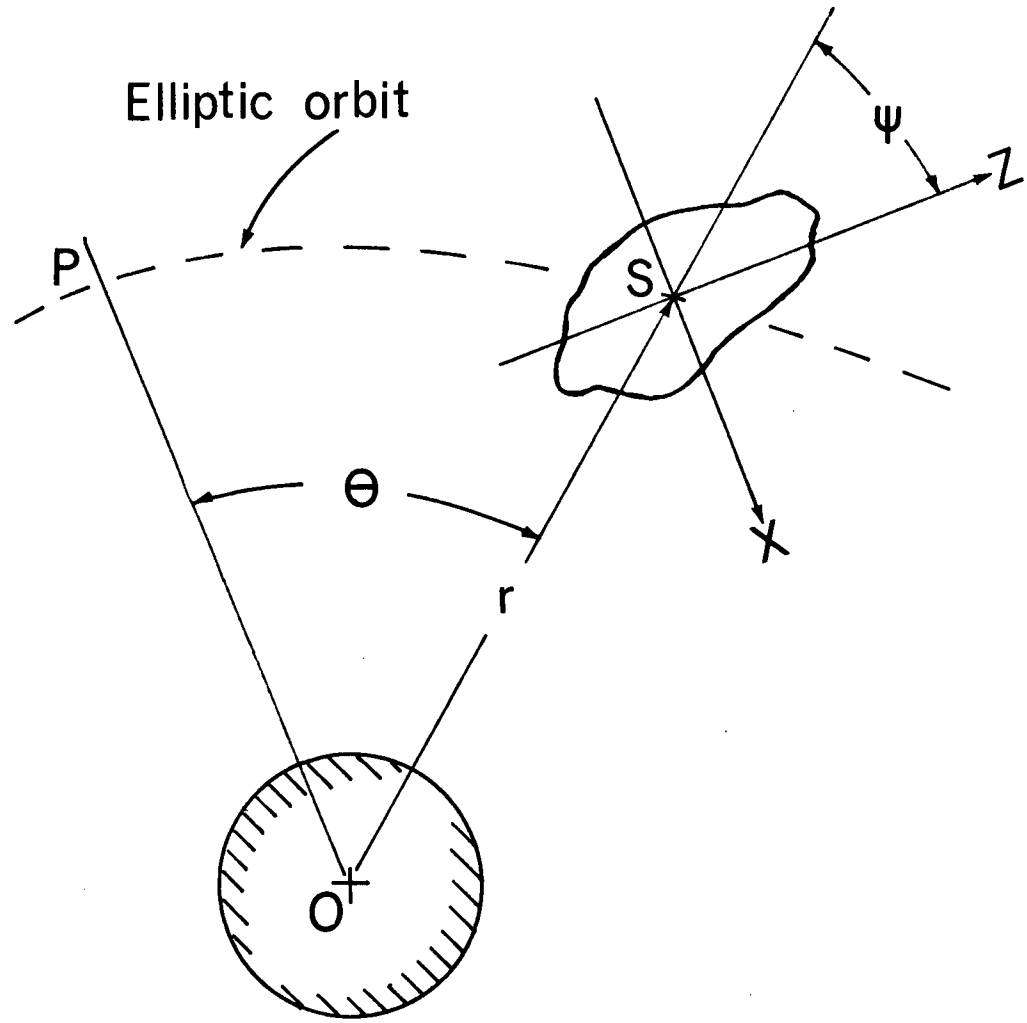

Figure 2-1 Geometry of planar motion of a rigid satellite

between the local vertical, OS, and the z-axis in the sense of the orbital motion defines the libration angle, ψ. For an element of mass, dm_b, of the satellite the expressions for the kinetic and potential energies can be written as

$$\begin{aligned} dT &= \frac{dm_b}{2}\left\{\left[r\dot{\theta}\cos\psi - \dot{r}\sin\psi + (\dot{\theta}+\dot{\psi})z\right]^2\right. \\ &\qquad \left. + \left[r\dot{\theta}\sin\psi + \dot{r}\cos\psi - (\dot{\theta}+\dot{\psi})x\right]^2\right\} \\ &= \frac{dm_b}{2}\left\{\dot{r}^2 + r^2\dot{\theta}^2 + (\dot{\theta}+\dot{\psi})^2(x^2+z^2)\right. \\ &\qquad + 2(\dot{\theta}+\dot{\psi})(zr\dot{\theta}\cos\psi - z\dot{r}\sin\psi \\ &\qquad \left. - xr\dot{\theta}\sin\psi - x\dot{r}\cos\psi)\right\} \end{aligned} \tag{2.1}$$

and

$$\begin{aligned} dU = -\frac{\mu dm_b}{r} &= \frac{-\mu\, dm_b}{\left[(r\sin\psi - x)^2 + (r\cos\psi + z)^2 + y^2\right]^{1/2}} \\ &= -\frac{\mu dm_b}{r}\left\{1 - \frac{1}{r}(z\cos\psi - x\sin\psi)\right. \\ &\qquad - \frac{x^2+y^2+z^2}{2r^2} + \frac{3}{2r^2}(z^2\cos^2\psi \\ &\qquad \left. - 2xz\sin\psi\cos\psi + x^2\sin^2\psi) + \cdots\right\}. \end{aligned} \tag{2.2}$$

If the origin of the xyz axes, S, is at the centre of mass,

$$\int dm_b = m_b \tag{2.3}$$

$$\int x\, dm_b = \int y\, dm_b = \int z\, dm_b = 0. \tag{2.4}$$

Moreover, if the axes are chosen to be the principal axes

$$\begin{aligned}
\int x^2\, dm_b &= \tfrac{1}{2}\left(I_{yy} + I_{zz} - I_{xx}\right) \\
\int y^2\, dm_b &= \tfrac{1}{2}\left(I_{zz} + I_{xx} - I_{yy}\right) \\
\int z^2\, dm_b &= \tfrac{1}{2}\left(I_{xx} + I_{yy} - I_{zz}\right) \\
\int xz\, dm_b &= 0.
\end{aligned} \tag{2.5}$$

With these relations the expressions for the kinetic and potential energies become

$$T = \frac{m_b}{2}\left(\dot{r}^2 + r^2\dot{\theta}^2\right) + \frac{I_{YY}}{2}\left(\dot{\theta} + \dot{\psi}\right)^2 \tag{2.6}$$

$$U = -\frac{\mu m_b}{r} + \frac{\mu}{2r^3}\left\{\left(2I_{xx} - I_{yy} - I_{zz}\right) - 3\left(I_{xx} - I_{zz}\right)\cos^2\psi\right\}. \tag{2.7}$$

Using the Lagrangian formulation the equations of motion corresponding to the three degrees of freedom can be written as

$$\ddot{r} - r\dot{\theta}^2 + \frac{\mu}{r^2} = \frac{3\mu}{2m_b r^4}\left\{2I_{xx} - I_{yy} - I_{zz} - 3\left(I_{xx} - I_{zz}\right)\cos^2\psi\right\} \tag{2.8}$$

$$r^2\dot{\theta} + \frac{I_{YY}}{m_b}\left(\dot{\theta} + \dot{\psi}\right) = \text{constant} = h_\theta \tag{2.9}$$

$$\ddot{\psi} + \ddot{\theta} + \frac{3\mu}{r^3}\left[\frac{I_{xx} - I_{zz}}{I_{yy}}\right]\sin\psi\cos\psi = 0. \tag{2.10}$$

These equations are essentially those of Yu.[7] The terms involving moments of inertia in equations (2.8) and (2.9) represent perturbations of the usual two-body equations of motion. Their presence can be attributed to the finite dimensions of the satellite. Moran[6] and Yu[7] found approximate solutions to (2.10) and showed that for typical satellites the contribution of the perturbation terms is extremely small. Neglecting the perturbations in the orbit due to the librational motion of the satellite, the solution of equations (2.8) and (2.9) leads to the classical Keplerian relations

$$r^2\dot{\theta} = h_\theta$$
$$r = \frac{h_\theta^2}{\mu(1 + e\,\mathrm{Cos}\,\theta)} . \tag{2.11}$$

Noting that

$$\frac{d}{dt} = \frac{h_\theta}{r^2}\frac{d}{d\theta} \tag{2.12}$$

and

$$\frac{d^2}{dt^2} = \dot{\theta}^2\frac{d^2}{d\theta^2} + \ddot{\theta}\frac{d}{d\theta}$$
$$= \frac{h_\theta^2}{r^4}\frac{d^2}{d\theta^2} - \frac{2h_\theta^2}{r^5}\frac{dr}{d\theta}\frac{d}{d\theta} \tag{2.13}$$

equation (2.10) can be rewritten as

$$(1 + e\cos\theta)\psi'' - 2e\sin\theta(\psi'+1) + 3K_i\sin\psi\cos\psi = 0. \qquad (2.14)$$

This form of the equation of motion was presented independently by Zlatousov et al.[12]

In general, the governing non-linear, non-autonomous differential equation with periodic coefficients does not admit of any closed form solution. The non-linearity is similar to that of a "soft" spring thus raising the possibility of amplitude dependent instability.

2.2 Simple Exact Solutions

2.2.1 Circular Orbit (e = 0)

When the orbit of the satellite is circular, equation (2.14) assumes the autonomous form

$$\psi'' + 3K_i\sin\psi\cos\psi = 0 \qquad (2.15)$$

which has the first integral

$$\psi'^2 + 3K_i\sin^2\psi = \text{constant} = C_c. \qquad (2.16)$$

Equation (2.16) defines regions of stability in the ψ-ψ' phase-plane. For values of the constant less than $3K_i$ the trajectories are closed and the resulting motion is periodic. Figure 2-2 illustrates the effect of varying the constant of integration.

Different values of K_i result in different trajec-

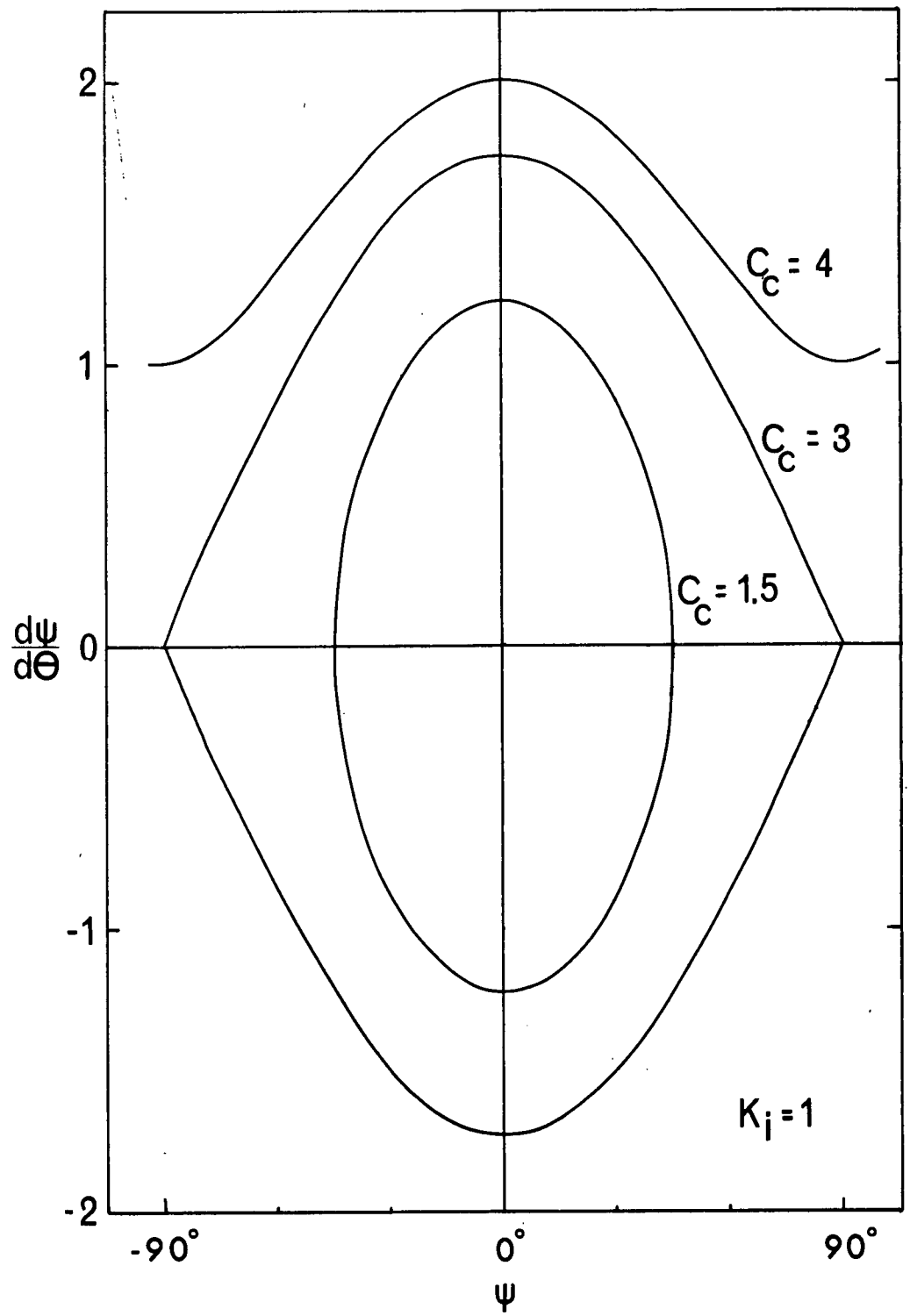

Figure 2-2 Phase plane trajectories describing the solution when e = 0

tories which for $C_c = 3K_i$ are shown in Figure 2-3. It is noteworthy that these curves are invariant with respect to Θ, hence the regions of stability may be considered to be cylinders with the cross-sections depicted here.

For periodic motion ($C_c < 3K_i$) equation (2.15) yields a solution in terms of the elliptic sine function,

$$\psi = \sin^{-1}\left[\sin\psi_{max}\ sn\left(\sqrt{3K_i}(\theta-\theta_o)\middle|\sin\psi_{max}\right)\right] \tag{2.17}$$

where $\psi = 0$ and $\psi' = \sqrt{C_c} = \sqrt{3K_i}\ \sin\psi_{max}$ at $\theta = \theta_o$.

The change in the orbital angle during one complete cycle of the librational motion is given by

$$\Delta\theta = \frac{4}{\sqrt{3K_i}} K(\sin\psi_{max}). \tag{2.18}$$

Of particular interest are solutions where $\Delta\theta = 2\pi\ n/m$ indicating m oscillations in n orbits.

The initial conditions required to generate these solutions may be taken to be

$$\begin{aligned} \psi_{P,1}(0) &= 0 \\ \psi'_{P,1}(0) &= \sqrt{3K_i}\ \sin\psi_{max}. \end{aligned} \qquad (m=n=1) \tag{2.19}$$

The variation of $\psi'_{P,1}(0)$ required to produce periodic solutions with specified values of m and n is plotted in Figure 2-4 as a function of K_i.

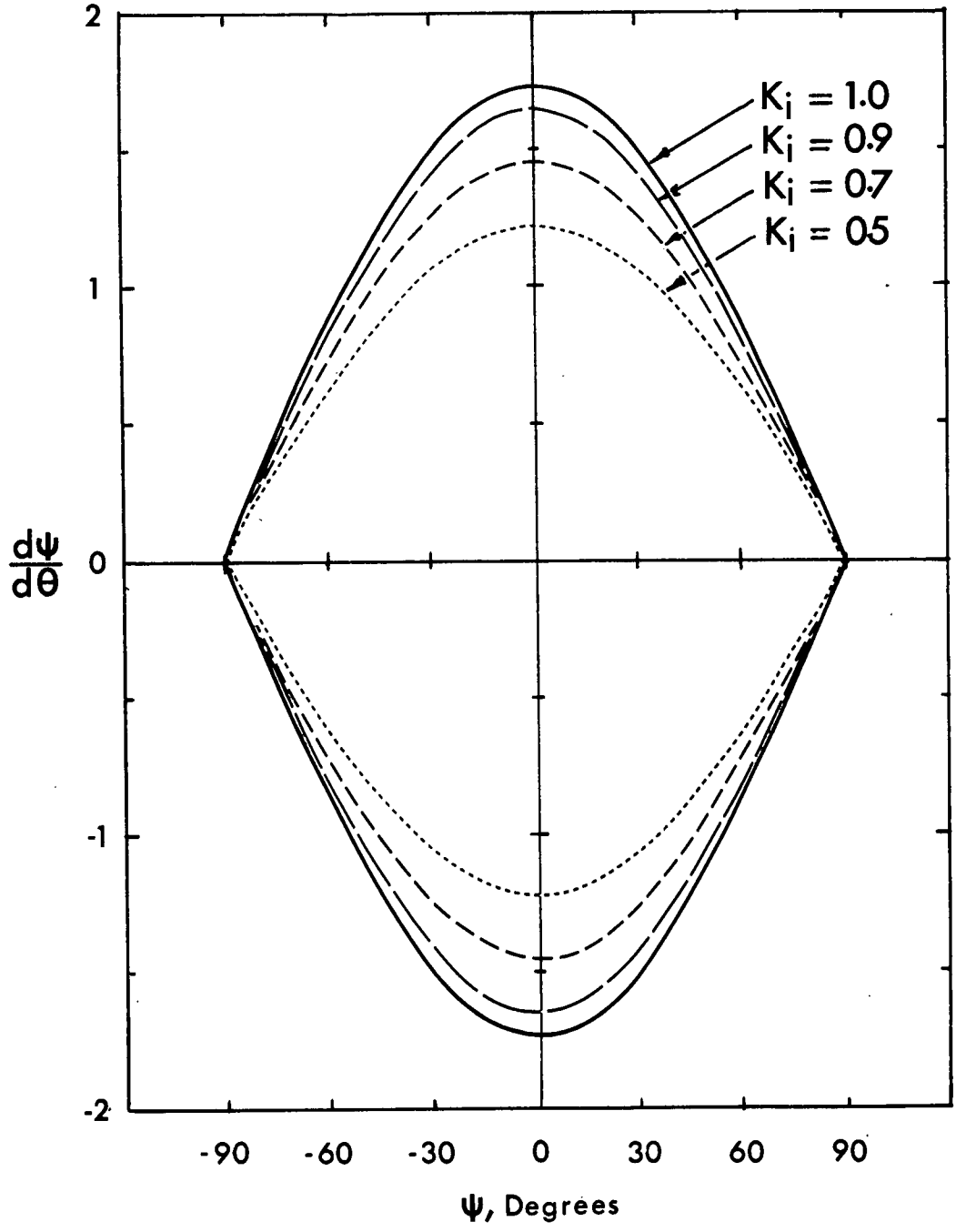

Figure 2-3 Limiting phase plane trajectories for e = 0

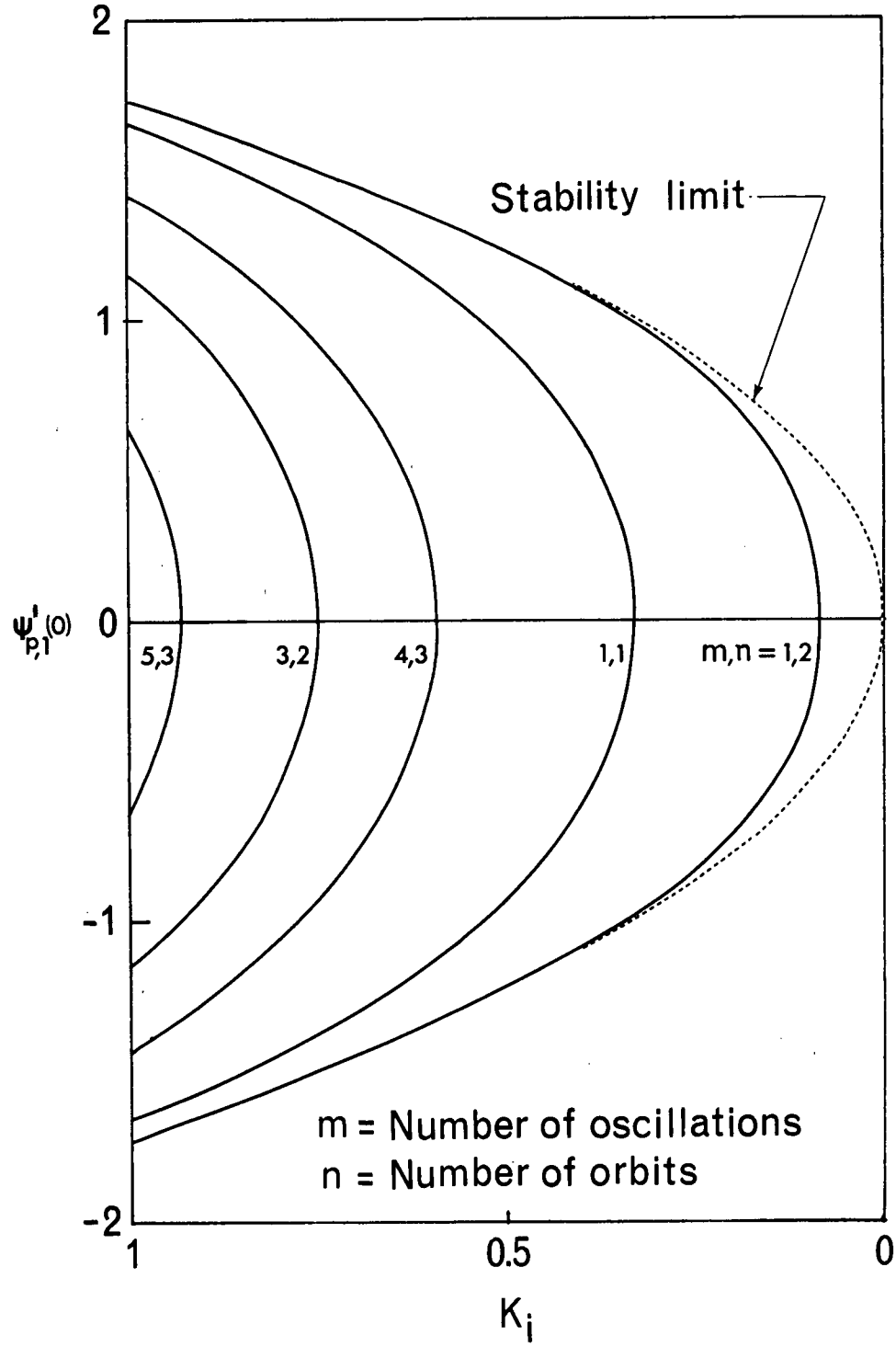

Figure 2-4 Initial angular velocities required to produce specified periodic solutions (e = 0)

2.2.2 Periodic Solutions Using the Method of Harmonic Balance

The non-linear term in the governing equation of motion (2.14) may be represented by the Taylor's series

$$\begin{aligned} \sin\psi\cos\psi &= \frac{1}{2}\sin 2\psi \\ &= \psi - \frac{2}{3}\psi^3 + \frac{2}{15}\psi^5 - \cdots . \end{aligned} \tag{2.20}$$

Consider now a solution of equation (2.14) of the form

$$\psi_{P,n} = \sum_{m=1}^{\infty} A_{m,n} \sin\frac{m\theta}{n} \; ; \quad (n = 1,2,3\cdots) \tag{2.21}$$

which has a period of $2\pi n$. The first two derivatives may be written as

$$\begin{aligned} \psi'_{P,n} &= \sum_{m=1}^{\infty} \frac{m}{n} A_{m,n} \cos\frac{m\theta}{n} \\ \psi''_{P,n} &= -\sum \left(\frac{m}{n}\right)^2 A_{m,n} \sin\frac{m\theta}{n} \end{aligned} \tag{2.22}$$

and the expansion for ψ^3 leads to an expression of the form

$$\psi^3_{P,n} = \sum_{m_1=1}^{\infty}\sum_{m_2=1}^{\infty}\sum_{m_3=1}^{\infty} C_{m_1,m_2,m_3;n} \sin\frac{m_1\theta}{n}\sin\frac{m_2\theta}{n}\sin\frac{m_3\theta}{n}$$

$$\psi^{3}_{P,n} = \sum_{m_1=1}^{\infty}\sum_{m_2=1}^{\infty}\sum_{m_3=1}^{\infty} \frac{1}{4} C_{m_1,m_2,m_3;n}$$

$$\times\left\{ \sin\frac{(m_1+m_2-m_3)\theta}{n} + \sin\frac{(m_2+m_3-m_1)\theta}{n} \right. \tag{2.23}$$

$$\left. + \sin\frac{(m_3+m_1-m_2)\theta}{n} + \sin\frac{(m_1+m_2+m_3)\theta}{n} \right\}.$$

Similar expressions can be obtained for ψ^5, ψ^7, ... so that the Taylor's series expansion for $\sin 2\psi$ in (2.20) introduces only sine terms. Recognizing that

$$\frac{d\psi}{d\theta}\sin\theta = \sum_{m=1}^{\infty} \frac{m}{n} A_{m,n} \sin\frac{n\theta}{n}\cos\frac{m\theta}{n}$$

$$= \frac{1}{2}\sum_{m=1}^{\infty} \frac{m}{n} A_{m,n}\left\{\sin\frac{(n+m)\theta}{n} + \sin\frac{(n-m)\theta}{n}\right\}$$

(2.24)

$$\frac{d^2\psi}{d\theta^2}\cos\theta = -\sum_{m=1}^{\infty}\left(\frac{m}{n}\right)^2 A_{m,n}\cos\frac{n\theta}{n}\sin\frac{m\theta}{n}$$

$$= \frac{-1}{2}\sum_{m=1}^{\infty}\left(\frac{m}{n}\right)^2 A_{m,n}\left\{\sin\frac{(m+n)\theta}{n} + \sin\frac{(m-n)\theta}{n}\right\}$$

equation (2.14) becomes

$$\sum_{m=1}^{\infty} P_{m,n}(A_{m,n}; e, K_i) \sin \frac{m\theta}{n} = 0. \tag{2.25}$$

The principle of harmonic balance requires the coefficient of each trigonometric term to be individually zero thus providing a sufficient number of equations to solve for the $A_{n,i}(i = 1,2,....)$. The equations are non-linear and, for a significant number of terms in the assumed solution, are difficult to solve. However, the important conclusion can be drawn, that the assumed form of the solution is correct.

Periodic solutions of (2.14) are odd functions of θ. The non-linearity of the equations also indicates that there may be more than one solution for specific values of the parameters.

There are other families of periodic solutions which are closely related to those already investigated. Let

$$\theta^* = \theta - \pi \tag{2.26}$$

then

$$\begin{aligned} \sin \theta &= -\sin \theta^* \\ \cos \theta &= -\cos \theta^* \end{aligned} \tag{2.27}$$

$$\frac{d}{d\theta} = \frac{d}{d\theta^*}$$

$$\frac{d^2}{d\theta^2} = \frac{d^2}{d\theta^{*2}} \qquad (2.27)\ \text{cont'd}$$

and equation (2.14) becomes

$$(1 - e\cos\theta^*)\frac{d^2\psi}{d\theta^{*2}} + 2e\sin\theta^*\left(\frac{d\psi}{d\theta^*} + 1\right) + 3K_i \sin\psi\cos\psi = 0. \qquad (2.28)$$

Equation (2.28) has essentially the same form as (2.14) except for the sign of e, hence the same form of solution is valid and periodic solutions of the form

$$\psi_{p,n} = \sum_{m=1}^{\infty} A_{m,n} \sin\frac{m(\theta-\pi)}{n} \qquad (2.29)$$

exist. These solutions appear as odd functions about the point $\theta = \pi$. In some cases, the solutions thus determined are identical to those which are odd about the point $\theta = 0$, e.g., n = 1.

The fact that the eccentricity is negative implies that the apocentre corresponds to $\theta = 0$. If the solution is such that at pericentre $\psi \neq 0$, the solution is different from that obtained earlier.

There also exists a third family of periodic solutions. Let

$$\psi_* = \psi - \frac{\pi}{2} \tag{2.30}$$

then

$$\frac{d\psi}{d\theta} = \frac{d\psi_*}{d\theta}$$

$$\frac{d^2\psi}{d\theta^2} = \frac{d^2\psi_*}{d\theta^2} \tag{2.31}$$

$$\sin\psi\cos\psi = -\sin\psi_*\cos\psi_*$$

so that (2.14) becomes

$$(1 + e\cos\theta)\psi_*'' - 2e\sin\theta(\psi_*' + 1) - 3K_i\sin\psi_*\cos\psi_* = 0. \tag{2.32}$$

This is identical to equation (2.14) with K_i replaced by $-K_i$. The equation may be solved using the techniques discussed above and yields the similar solution

$$\psi_{p,n} = \frac{\pi}{2} + \sum_{m=1}^{\infty} A_{m,n}\sin\frac{m\theta}{n} \tag{2.33}$$

In physical terms, the motion represents an oscillation about the local horizontal. It is interesting to note that Zlatousov et al[12] obtained periodic solutions of this type numerically for n = 1 without establishing the general form of the solution presented here.

Periodic solutions determined with negative values of e and K_i thus correspond to realizable situations when the parameters are restricted to the interval between zero and one. Larger values of these parameters have no physical meaning as for $e \geq 1$ the orbital motion is not periodic and $K_i > 1$ is physically impossible.

2.2.3 Numerical Determination of Periodic Solutions

The preceding section has indicated a method of determining the periodic solutions of (2.14). The actual solution of the resulting equations is quite involved as the number of terms required for an accurate solution is astronomical. Fortunately, the knowledge of the form helps considerably in the numerical evaluation of the periodic solutions.

The numerical determination of the periodic solutions was accomplished as follows. A digital computer was programmed to solve equation (2.14) using a numerical algorithm. Initial conditions were chosen consistent with the known form

$$\begin{aligned} \psi(0) &= 0 \\ \psi'(0) &= \psi'_0 \end{aligned} \tag{2.34}$$

and equation (2.14) was integrated until $\Theta = 2\pi n$. The final values of ψ_f and ψ'_f which were, in general, different from (2.34) were noted. A correction was then made to the

value of ψ_o' so as to cause the final condition to become identical with the initial condition. When a periodic solution exists, the process converges to give the required value of ψ_o' and the solution of the interval.

Typical periodic solutions with orbital frequency (i.e. n = 1) are presented in Figures 2-5 and 2-6. The initial derivatives, $\psi'_{P,1}(0)$, required to produce solutions of this type are plotted in Figure 2-7. A similar diagram was presented independently in reference 12. The diagram indicates that for K_i less than 1/3 there is only one periodic solution while for larger values of K_i there may be as many as three. This result is in accord with the curves presented in Figure 2-4.

The numerical technique can produce periodic solutions of any desired accuracy. A reliable estimate of the error may be made by computing the function

$$\mathcal{E}(\theta) = \frac{1}{2}\left[\psi_{P,n}(n\pi+\theta) + \psi_{P,n}(n\pi-\theta)\right] \qquad (2.35)$$

over the interval $0 \leq \theta \leq n\pi$. The exact solution is odd with respect to the point $\theta = n\pi$ so that $\mathcal{E}$ should be identically zero. Several typical situations are shown in Figure 2-8. The maximum observed value of $\mathcal{E}$, which occurred at high eccentricity, was .003 radians and may be attributed to the nearly discontinuous behaviour of the solution.

It is also possible to search for solutions of longer

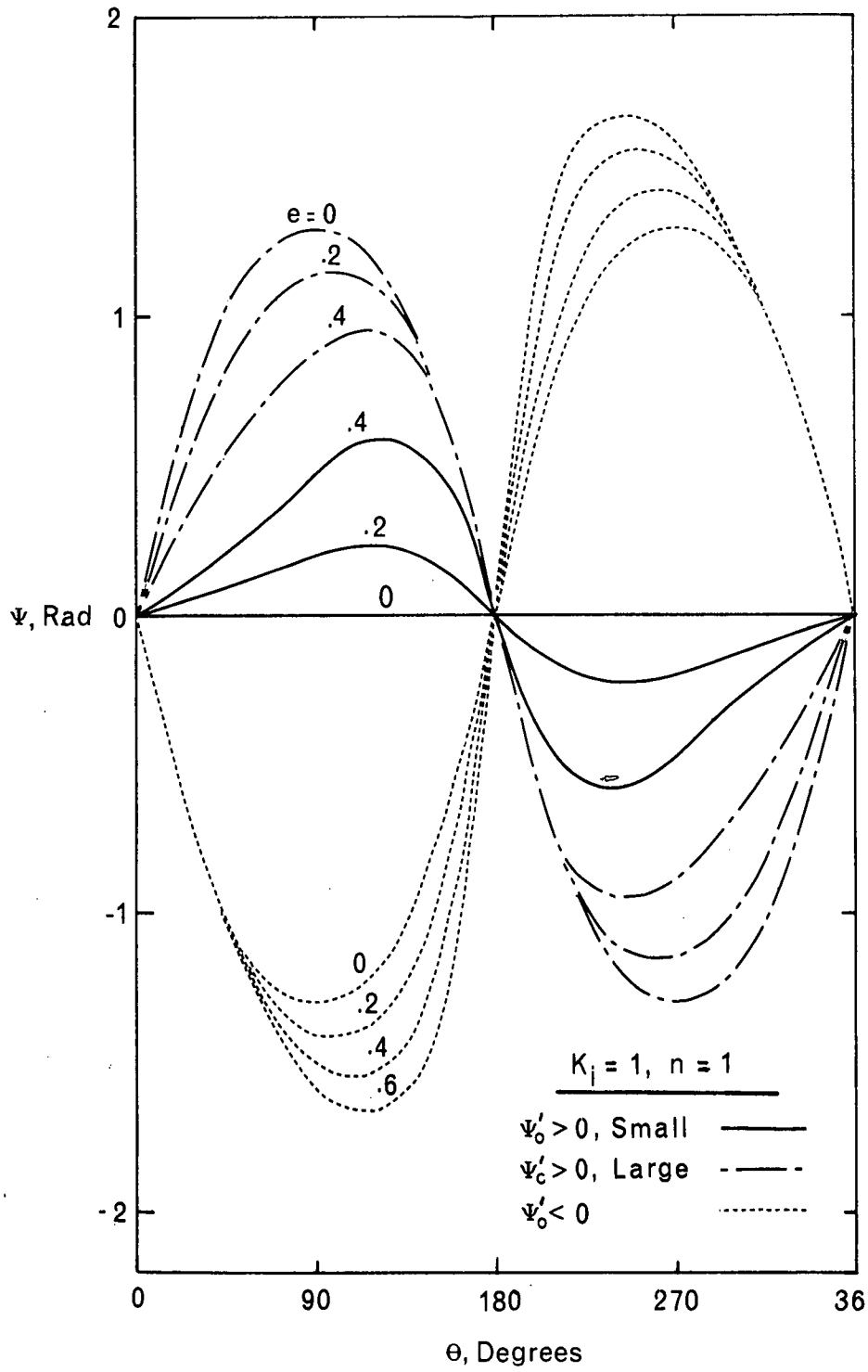

Figure 2-5 Periodic solutions as functions of eccentricity (K_i = 1, n = 1)

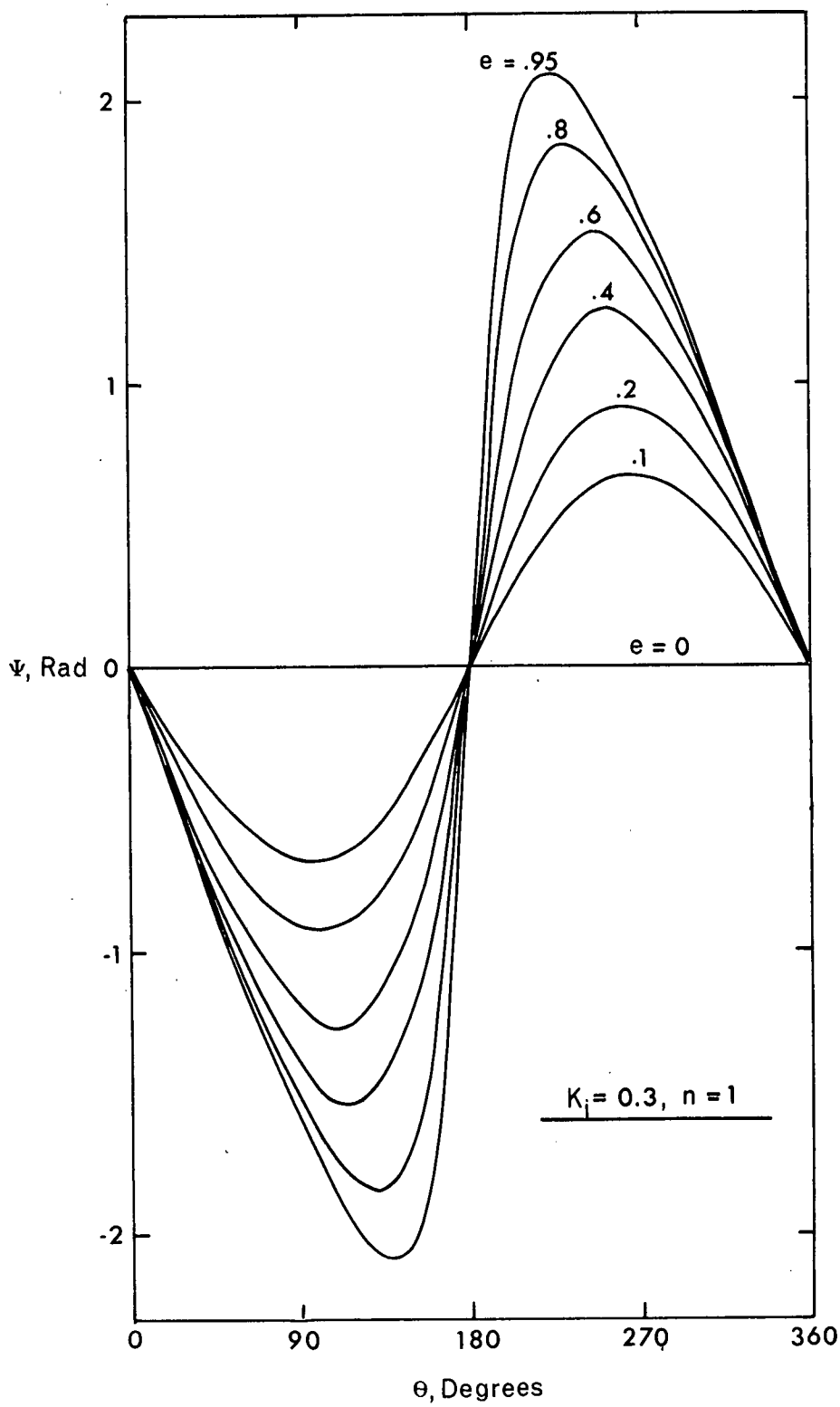

Figure 2-6 Periodic solutions as functions of eccentricity (K_i = 0.3, n = 1)

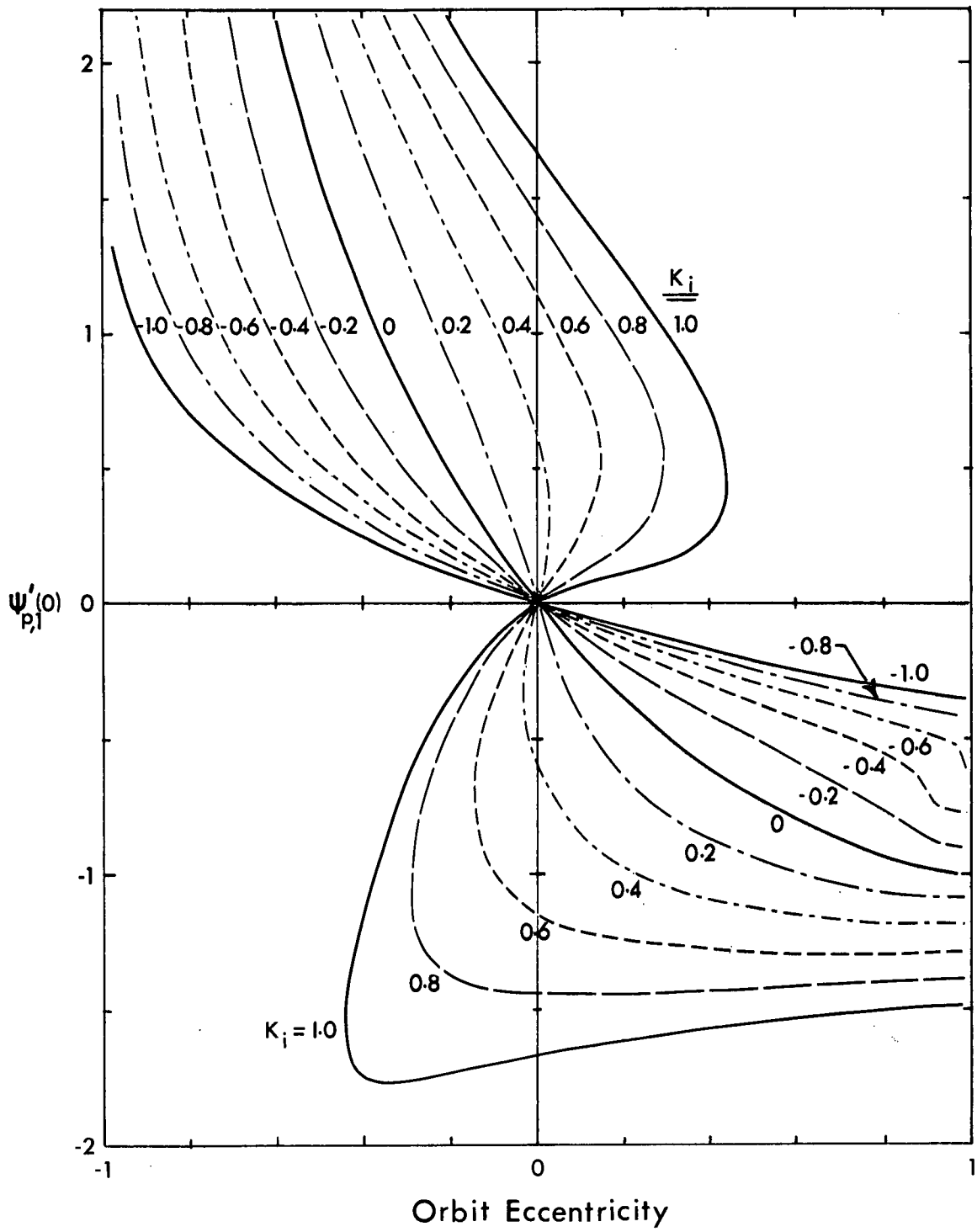

Figure 2-7 Initial derivative required to produce solutions with period of 2π

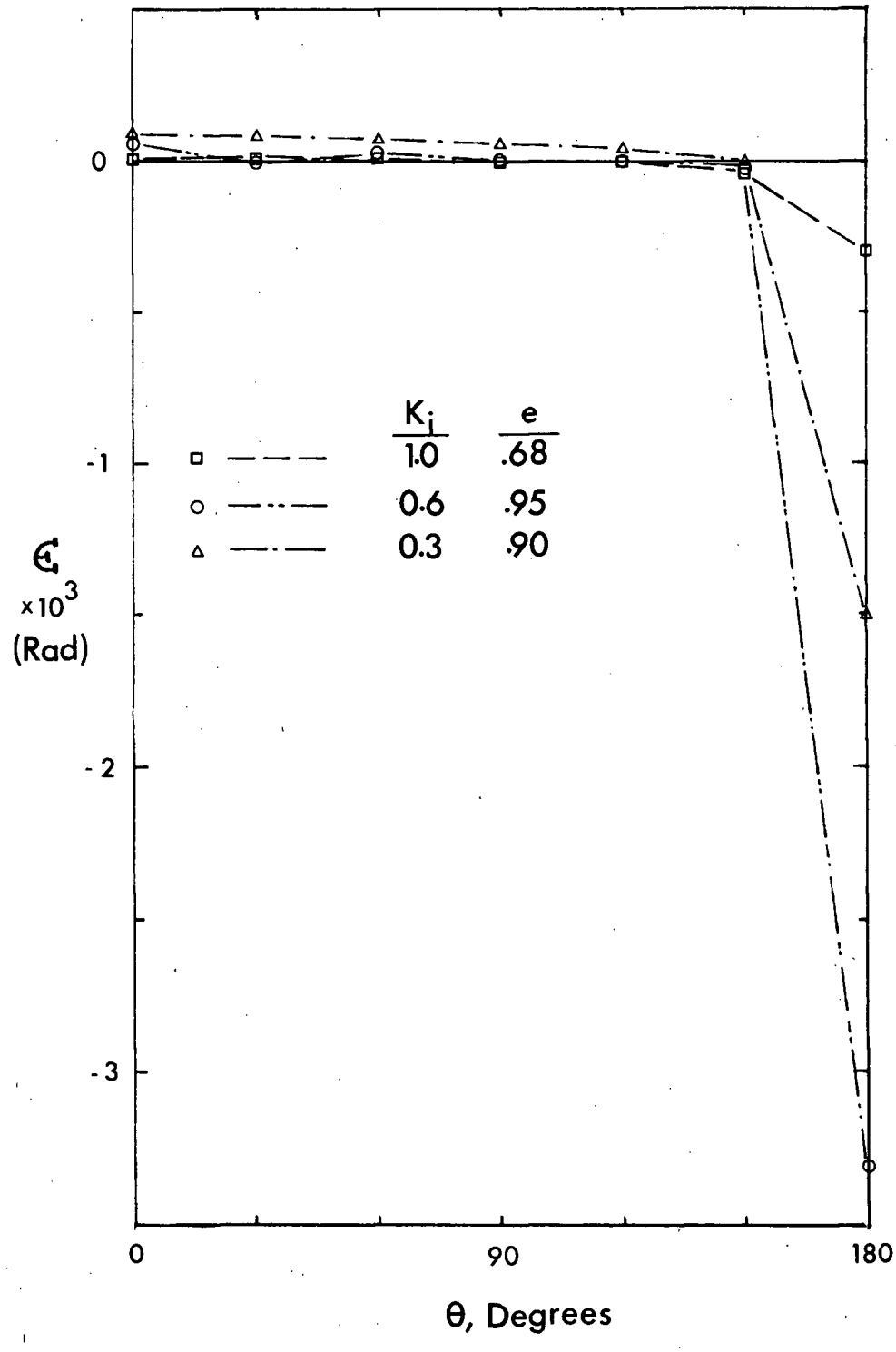

Figure 2-8 Typical variations of the error found in the numerical determination of periodic solutions

period ($n > 1$). The numerical technique is quite versatile in this respect. Figure 2-9 illustrates periodic solutions with a period of 4π. Note the degeneration of a solution which oscillates three times at $e = 0$ into one which oscillates only twice at $e \approx 0.35$. Initial values of the derivatives, $\psi'_{p,2}(0)$, for the solutions are presented in Figure 2-10. Vertical tangents to these curves correspond to the points where the solutions become identical to those periodic over 2π.

2.3 Approximate Solutions

2.3.1 WKBJ Method[28]

For small amplitude motion, equation (2.14) may be linearized by introducing the approximations

$$\begin{aligned} \sin\psi &\approx \psi \\ \cos\psi &\approx 1. \end{aligned} \tag{2.36}$$

The equation of motion reduces to

$$(1 + e\cos\theta)\psi'' - 2e\sin\theta\,\psi' + 3K_i\psi = 2e\sin\theta \tag{2.37}$$

which may be transformed by means of the transformation

$$\Psi = (1 + e\cos\theta)\psi \tag{2.38}$$

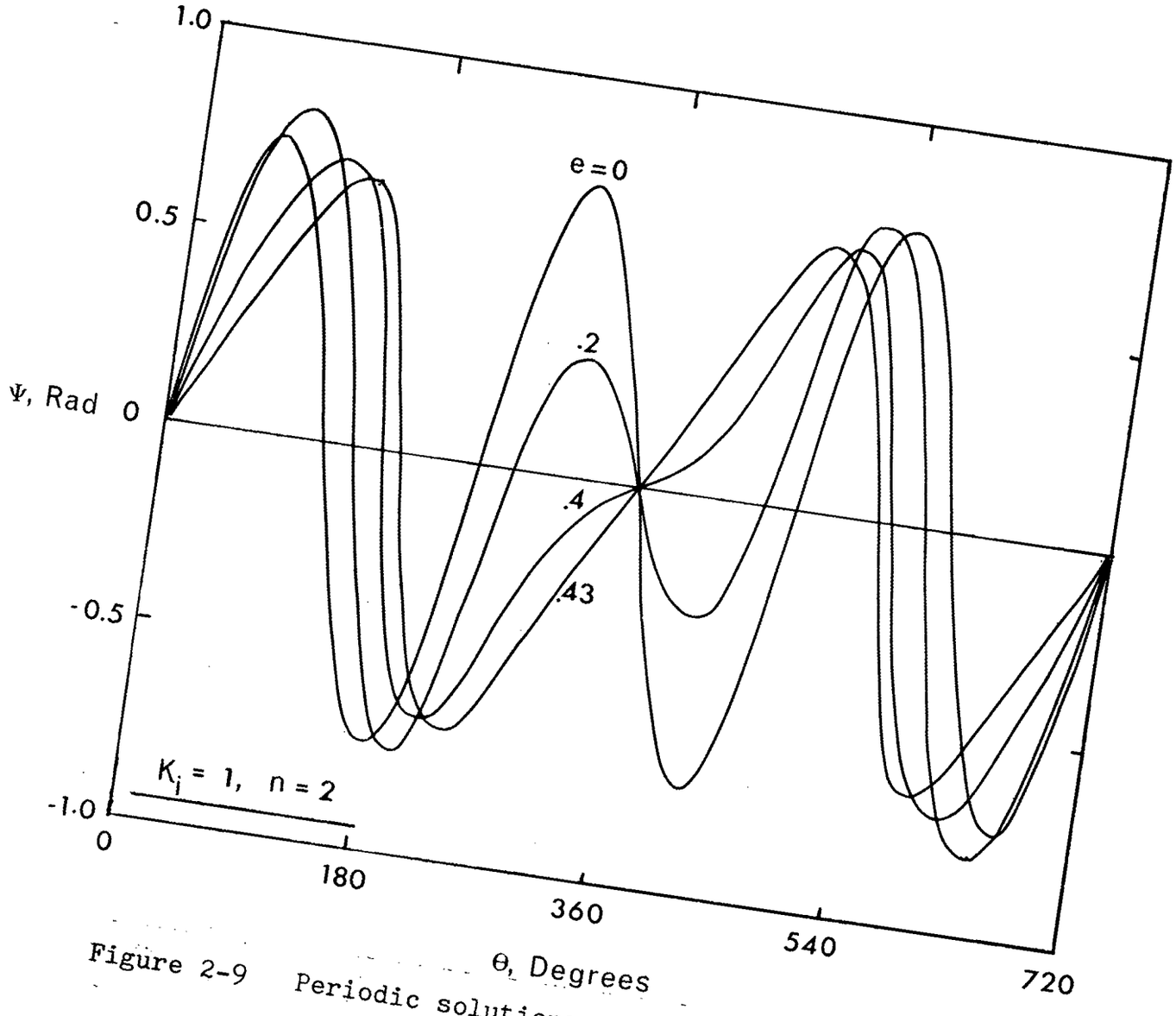

Figure 2-9 Periodic solutions with period of 4π ($K_i = 1$)

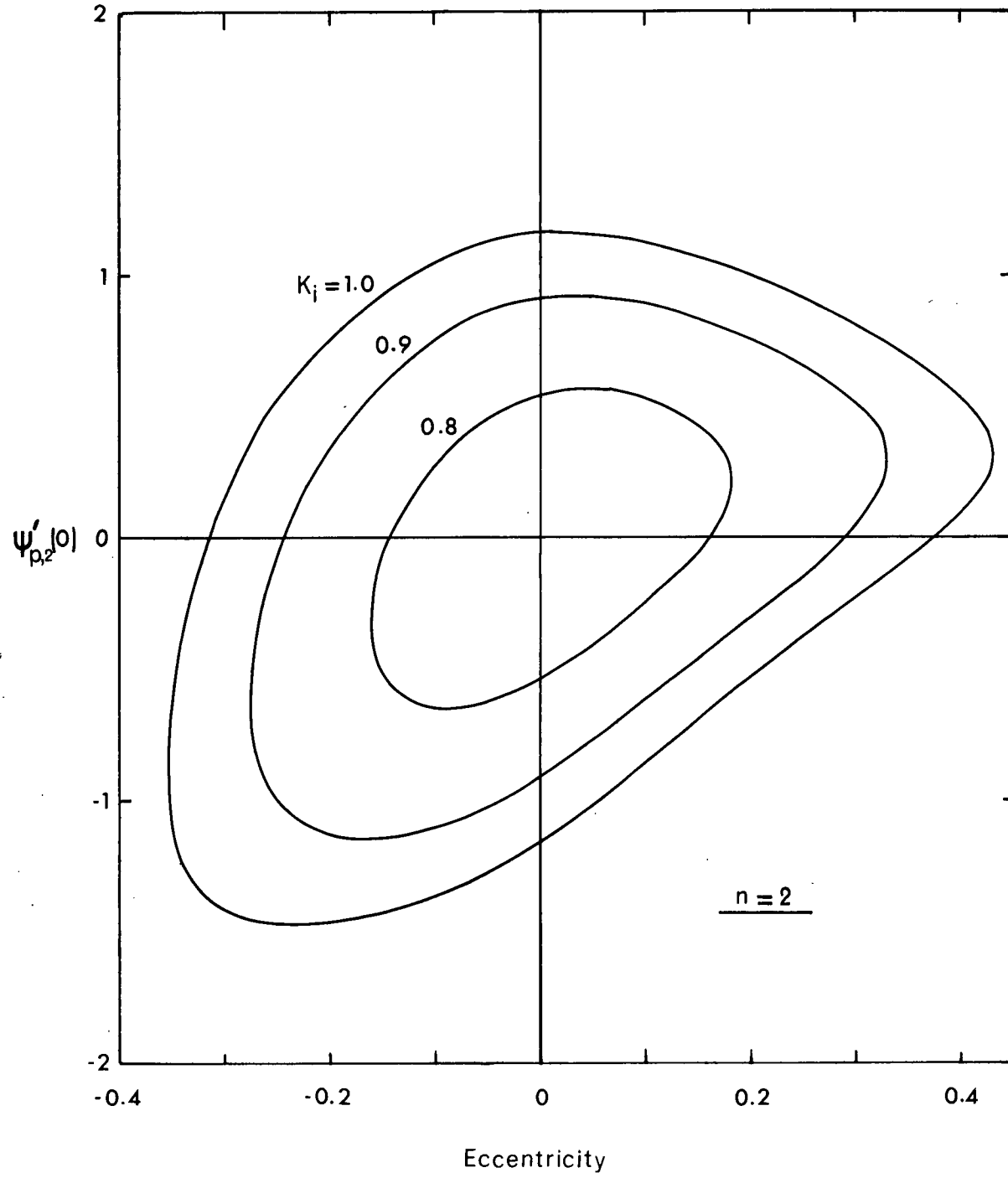

Figure 2-10 Initial derivative required to produce periodic solutions with period of 4π

to

$$\Psi'' + G^2\Psi = 2e \sin\theta \tag{2.39}$$

where

$$G^2 = \frac{3K_i + e\cos\theta}{1 + e\cos\theta}. \tag{2.40}$$

The complementary solution to (2.39) can be obtained approximately using the WKBJ method provided the function $G^2(\theta)$ satisfies the inequality

$$F = \frac{1}{G^2}\left|\frac{G''}{2G} - \frac{3}{4}\left(\frac{G'}{G}\right)^2\right| << 1. \tag{2.41}$$

Figure 2-11 shows the variation of F with θ for several values of e and $K_i = 1$. It is evident that, even for large values of the eccentricity, the inequality in (2.41) is reasonably well satisfied.

The approximate solution to (2.39) is then given by

$$\Psi = C_1\Psi_1 + C_2\Psi_2 + \Psi^* \tag{2.42}$$

where

$$\Psi_1 = \frac{1}{\sqrt{G}}\cos\left(\int_0^\theta G\, d\theta\right)$$
$$\Psi_2 = \frac{1}{\sqrt{G}}\sin\left(\int_0^\theta G\, d\theta\right) \tag{2.43}$$

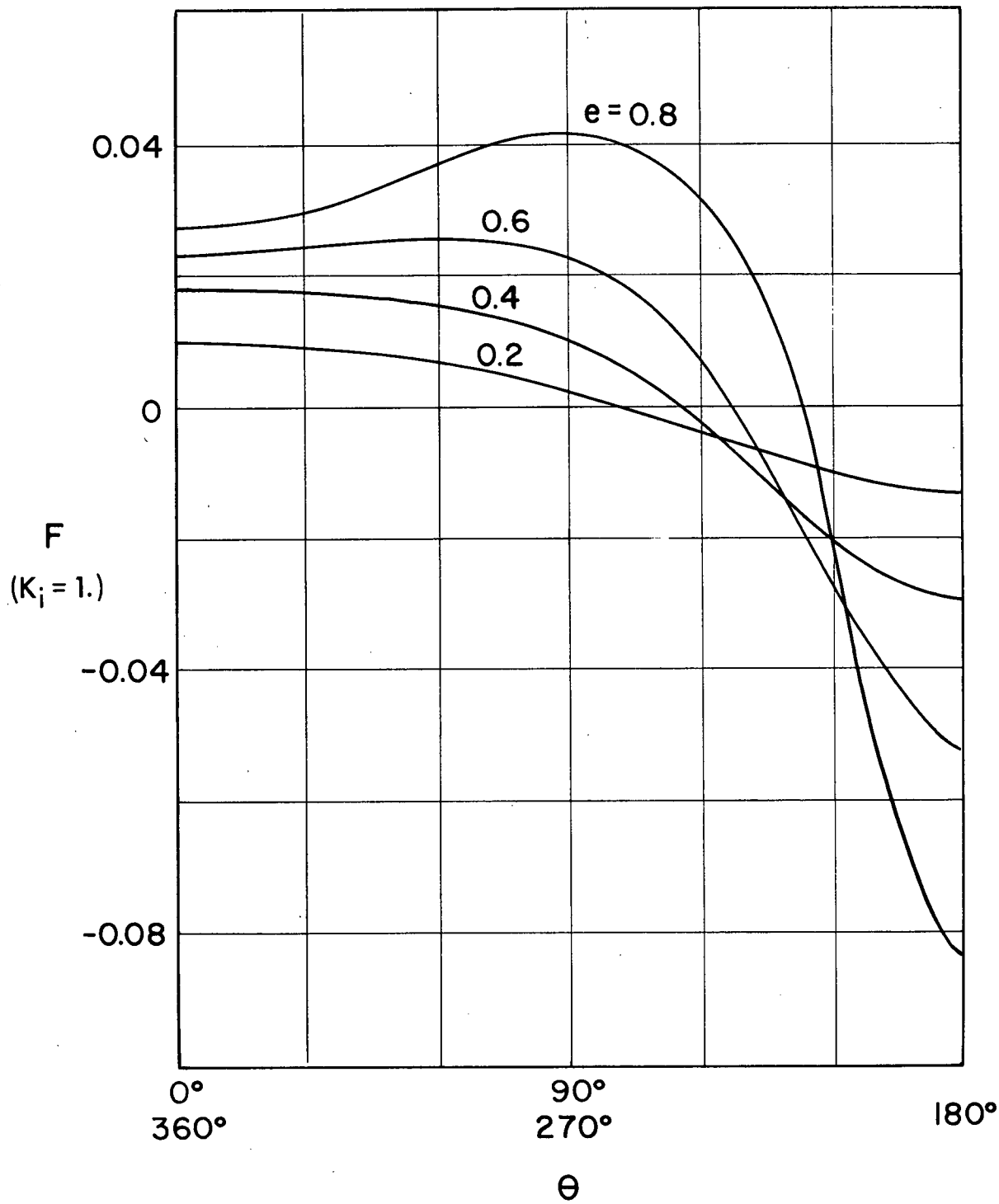

Figure 2-11 The variation of F with orbit angle and orbit eccentricity (K_i = 1)

and Ψ^* represents the particular integral obtained using the method of variation of parameters

$$\Psi^* = \Psi_2 \int_0^\theta \frac{2e \sin\theta \ \Psi_1}{\Psi_1 \Psi_2' - \Psi_1' \Psi_2} d\theta - \Psi_1 \int_0^\theta \frac{2e \sin\theta \ \Psi_2}{\Psi_1 \Psi_2' - \Psi_1' \Psi_2} d\theta . \tag{2.44}$$

In general, the evaluation of the WKBJ solution can be achieved only numerically and involves a large amount of computation. Considerable simplification is possible without substantially affecting the accuracy of the WKBJ approximation by adopting the following procedure.

Neglecting second and higher degree terms in e and putting

$$\omega_L^2 = 3K_i$$
$$\nu = \frac{3K_i - 1}{6K_i} \tag{2.45}$$

the required functions can be approximated as

$$G \approx \omega_L (1 - \nu e \cos\theta)$$
$$\frac{1}{\sqrt{G}} \approx \frac{1}{\sqrt{\omega_L}} \left(1 + \frac{\nu e}{2} \cos\theta\right) \tag{2.46}$$
$$\sin\left(\int_0^\theta G \, d\theta\right) \approx \sin\left(\omega_L\theta - e\nu\omega_L \sin\theta\right)$$
$$\approx \sin\omega_L\theta - e\nu\omega_L \sin\theta \cos\omega_L\theta$$

$$\cos\left(\int_0^\theta G\, d\theta\right) \approx \cos\left(\omega_L\theta - e\nu\omega_L \sin\theta\right)$$

$$\approx \cos\omega_L\theta + e\nu\omega_L \sin\theta \sin\omega_L\theta . \qquad (2.46)\ \text{cont'd}$$

Thus, within a multiplicative constant, the solutions (2.43) become

$$\Psi_1 \approx \cos\omega_L\theta + e\nu\left(\frac{1}{4} - \frac{\omega_L}{2}\right)\cos(\omega_L+1)\theta + e\nu\left(\frac{1}{4} + \frac{\omega_L}{2}\right)\cos(\omega_L-1)\theta \qquad (2.47)$$

$$\Psi_2 \approx \sin\omega_L\theta + e\nu\left(\frac{1}{4} - \frac{\omega_L}{2}\right)\sin(\omega_L+1)\theta + e\nu\left(\frac{1}{4} + \frac{\omega_L}{2}\right)\sin(\omega_L-1)\theta . \qquad (2.48)$$

The first derivative is missing from equation (2.39) so that the denominators in (2.44) are equal to a constant which is

$$\Psi_1\Psi_2' - \Psi_1'\Psi_2 = \omega_L + O(e^2). \qquad (2.49)$$

The particular integral already involves the first power of

the eccentricity so that

$$\Psi^* = \frac{2e}{\omega_L}\left\{\sin\omega_L\theta\int_0^\theta \sin\theta\cos\omega_L\theta\,d\theta - \cos\omega_L\theta\int_0^\theta \sin\theta\sin\omega_L\theta\,d\theta\right\} + O(e^2)$$

$$= \frac{2e}{\omega_L(\omega_L^2-1)}\left(\omega_L\sin\theta - \sin\omega_L\theta\right) + O(e^2);\quad (\omega_L \neq 1). \tag{2.50}$$

Using the transformation (2.38) the solution for ψ is

$$\psi = \bar{c}_1\psi_1 + \bar{c}_2\psi_2 + \psi^* \tag{2.51}$$

where

$$\psi_1 = \cos\omega_L\theta + e\left(\frac{\nu}{4} - \frac{\omega_L\nu}{2} - \frac{1}{2}\right)\cos(\omega_L+1)\theta + e\left(\frac{\nu}{4} + \frac{\omega_L\nu}{2} - \frac{1}{2}\right)\cos(\omega_L-1)\theta + O(e^2)$$

$$\psi_2 = \sin\omega_L\theta + e\left(\frac{\nu}{4} - \frac{\omega_L\nu}{2} - \frac{1}{2}\right)\sin(\omega_L+1)\theta + e\left(\frac{\nu}{4} + \frac{\omega_L\nu}{2} - \frac{1}{2}\right)\sin(\omega_L-1)\theta + O(e^2) \tag{2.52}$$

$$\psi^* = \frac{2e}{\omega_L(\omega_L^2-1)}\left(\omega_L\sin\theta - \sin\omega_L\theta\right) + O(e^2).$$

Figures 2-12 and 2-13 compare the WKBJ solution

(2.42 - 2.44) and its approximation (2.51, 2.52) with the exact numerical solution of equation (2.14). It is apparent that the simplification to the WKBJ method does not increase the error already present.

The approximation to the WKBJ solution follows the exact solution in a general fashion for a long period of time. This is illustrated in Figure 2-14, where the librational motion is shown over eight revolutions, and discussed on page 47. The WKBJ solution is not plotted because it is nearly coincident with the approximate result.

The analysis does provide useful information about the maximum value of the amplitude of libration. From (2.51),

$$|\psi|_{max} = \frac{2e}{\omega_L^2 - 1} + \sqrt{\bar{C}_1^2 + \left(\bar{C}_2 - \frac{2e}{\omega_L(\omega_L^2 - 1)}\right)^2} + e\left(1 - \frac{\nu}{2}\right)\sqrt{\bar{C}_1^2 + \bar{C}_2^2} \tag{2.53}$$

which has a minimum when

$$\bar{C}_1 = 0$$
$$\bar{C}_2 = \frac{2e}{\omega_L(\omega_L^2 - 1)} \tag{2.54}$$

provided $\omega_L^2 > (e/(4-3e))$. Hence the amplitude of libration is always greater than $2e/(\omega_L^2 - 1) + O(e^2)$. The method predicts the "period" of libration with considerable accuracy.

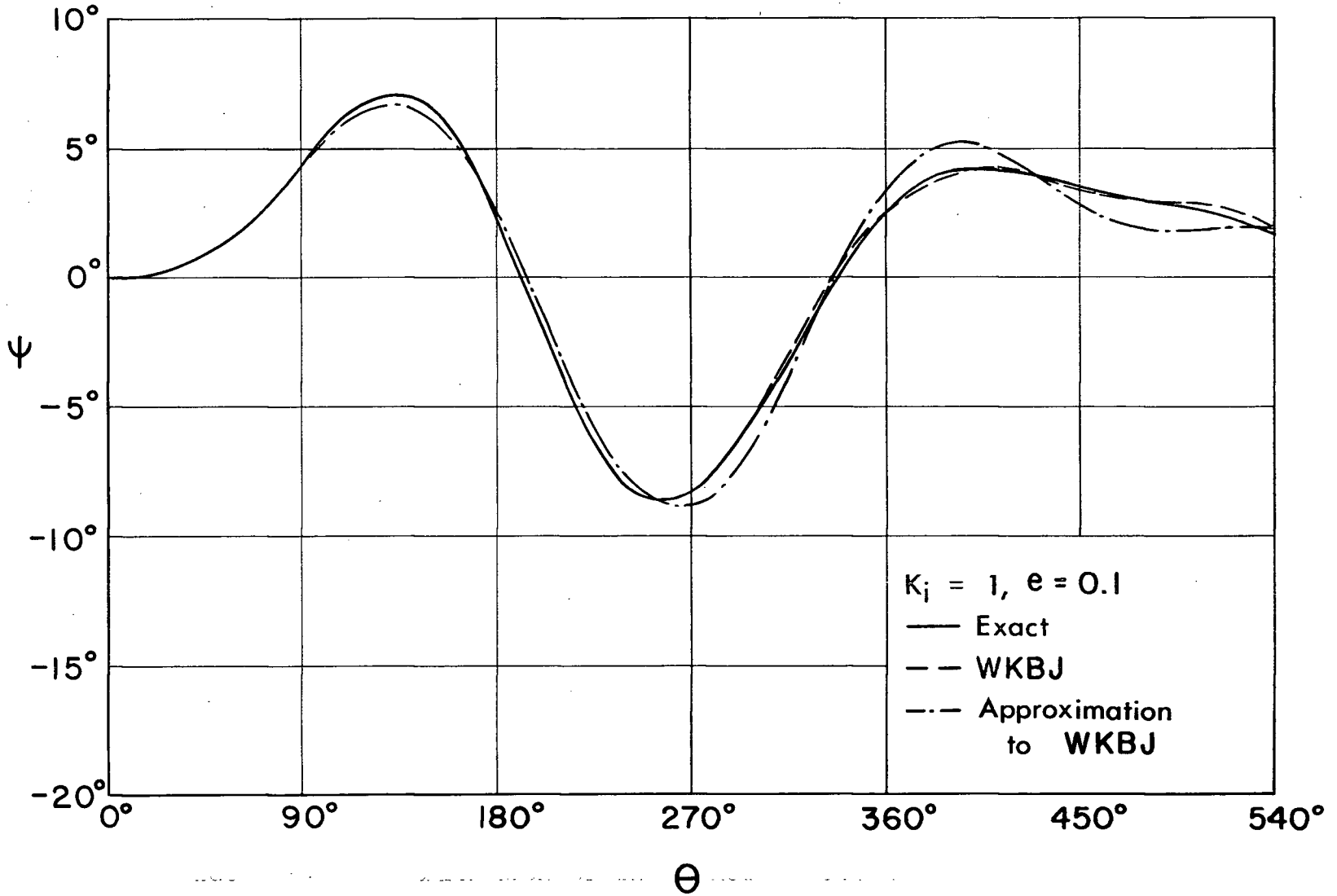

Figure 2-12 Comparison of the exact solution of the equation of motion with that determined by the WKBJ method and the approximate WKBJ method (K_i = 1, e = 0.1)

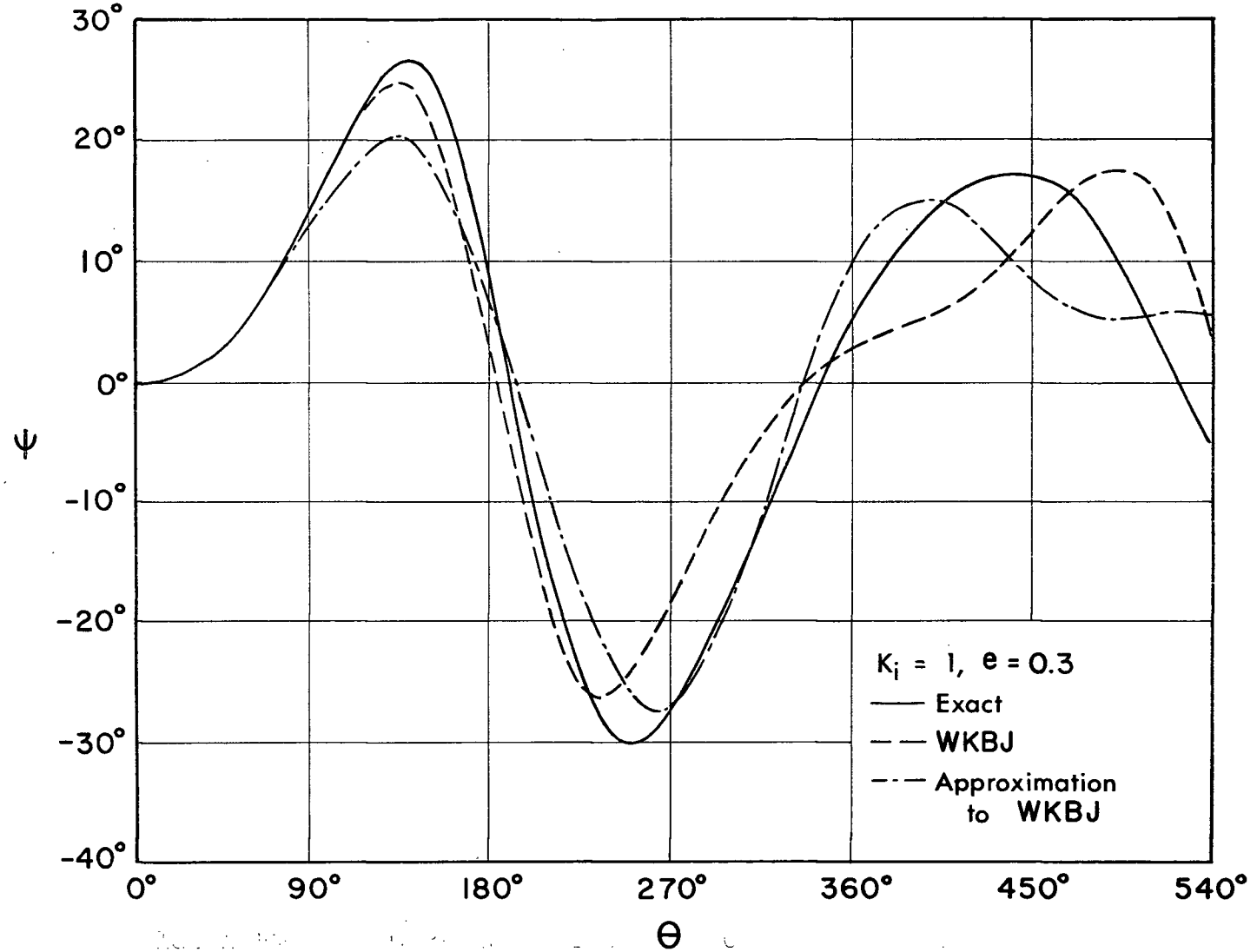

Figure 2-13 Comparison of the exact solution of the equation of motion with that determined by the WKBJ method and the approximate WKBJ method (K_i = 1, e = 0.3)

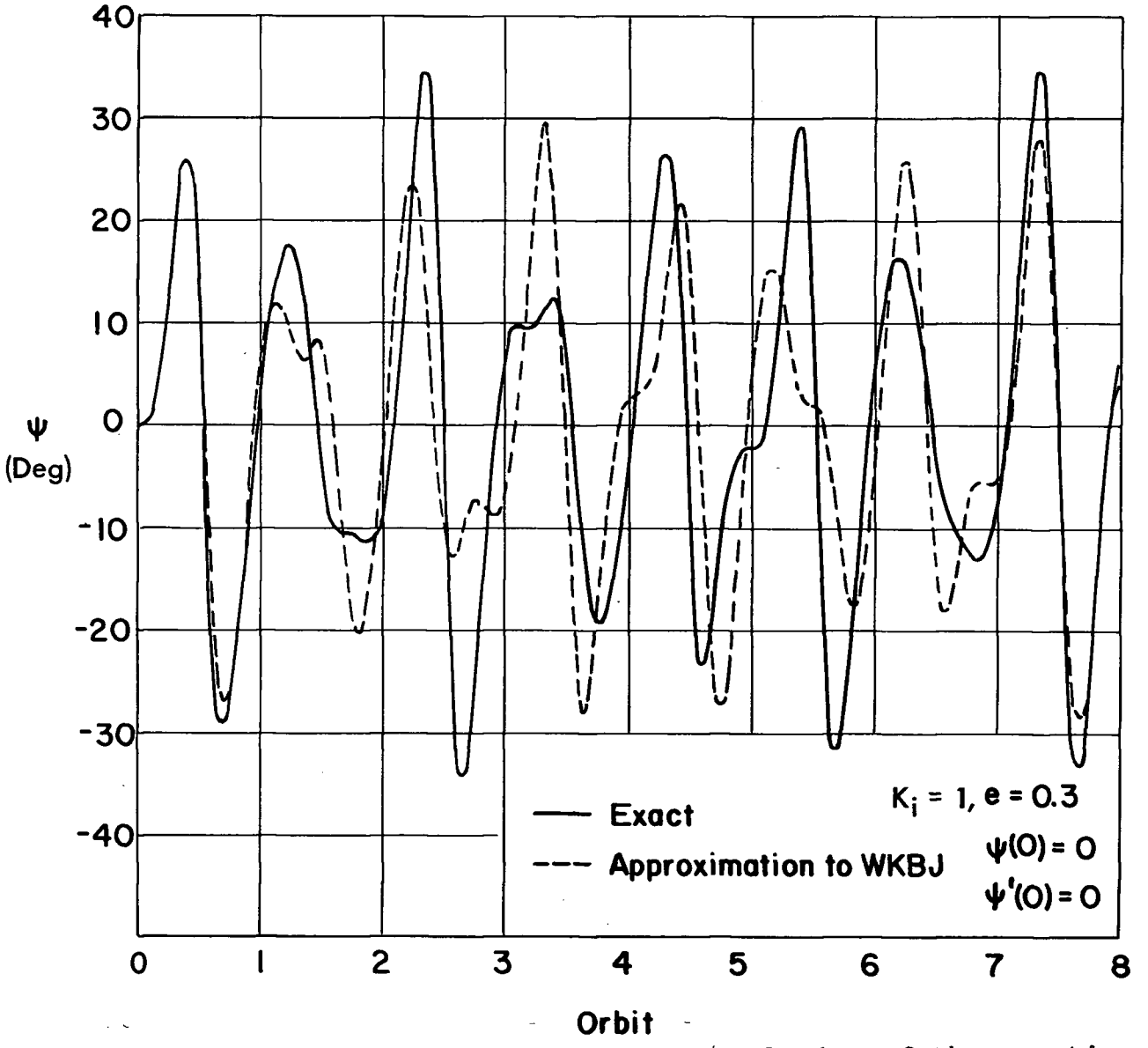

Figure 2-14 Comparison of the exact solution of the equation of motion with that determined by the approximate WKBJ method over eight orbits (K_i = 1, e = 0.3)

For the particular case of e = 0 and K_i = 1, it provides the well known result that, for small amplitudes, the librational frequency is $\sqrt{3}$ times the orbital frequency. Further, the presence of a particular solution indicates that a body in an elliptic orbit always executes librational motion.

It may be pointed out that the frequency spectrum associated with the librational motion consists of the orbital frequency, the frequency of libration in a circular orbit, and the modulation products of the two foregoing frequencies. The resulting motion acquires an apparently random character due to the superposition of the various frequencies. This also explains the unusual irregularities which may be noted in Figure 2-14. The frequency of libration is also dependent on the amplitude of the motion. This introduces a phase shift between the exact and approximate solutions.

The major source of error is the non-linearity of equation (2.14). The amplitudes of ψ definitely indicate that the system is operating in the non-linear region. However, it appears that the approximation to the WKBJ method presented here may prove adequate for preliminary design purposes.

2.3.2 Principle of Harmonic Balance

The method outlined in section 2.2.2 may be considered exact. Unfortunately the amount of computational work involved is prohibitive.

Consider for example the three term series solution

$$\psi_{P,1} = A_{1,1} \sin\theta + A_{2,1} \sin 2\theta + A_{3,1} \sin 3\theta \,. \tag{2.55}$$

The $\sin\psi \cos\psi$ term may be represented by the first two terms of the Taylor's series (2.20) so that it retains its inherent non-linear character. Substituting equation (2.55) into (2.14), collecting terms and applying the principle of harmonic balance results in the three equations

$$\begin{aligned}
A_{1,1}\left[6K_i - 2 - 3K_i\left(A_{1,1}^2 + 2A_{2,1}^2 + 2A_{3,1}^2\right)\right] &= 4e + 3K_i A_{3,1}\left(A_{2,1}^2 - A_{1,1}^2\right) \\
A_{2,1}\left[6K_i - 8 - 3K_i\left(A_{2,1}^2 + 2A_{1,1}^2 + 2A_{3,1}^2 + 2A_{1,1}A_{3,1}\right)\right] &= 3e\left(A_{1,1} + A_{3,1}\right) \\
A_{3,1}\left[6K_i - 18 - 3K_i\left(A_{3,1}^2 + 2A_{2,1}^2 + 2A_{1,1}^2\right)\right] &= 8e\,A_{2,1} + K_i A_{1,1}\left(3A_{2,1}^2 - A_{1,1}^2\right).
\end{aligned} \tag{2.56}$$

This set of equations does not possess any simple solution, hence an iterative procedure was adopted. For example, when $e = 0.3$ and $K_i = 1$ three solutions were obtained. The coefficients were found to be :

$$A_{1,1} = 0.333;\ 0.975;\ -1.286$$
$$A_{2,1} = -0.116;\ -0.114;\ 0.097 \qquad (2.57)$$
$$A_{3,1} = 0.021;\ 0.065;\ -0.010.$$

Even with this three term approximation, the amount of computational effort is comparable to that for the exact numerical solution (section 2.2.3). The procedure can be simplified further by putting $A_{3,1} = 0$, i.e. by considering a two term series solution. The equations relating the coefficients then reduce to

$$A_{1,1}\left[6K_i - 2 - 3K_i\left(A_{1,1}^2 + 2A_{2,1}^2\right)\right] = 4e$$
$$A_{2,1}\left[6K_i - 8 - 3K_i\left(A_{2,1}^2 + 2A_{1,1}^2\right)\right] = 3e\,A_{1,1} \qquad (2.58)$$

which can be rewritten in a more convenient form as

$$A_{1,1} = \frac{-e}{4K_i A_{2,1}} \pm \sqrt{\left(\frac{e}{4K_i A_{2,1}}\right)^2 - \frac{4}{3K_i} - \frac{A_{2,1}^2}{2} + 1} \qquad (2.59)$$

$$A_{2,1} = \pm\sqrt{1 - \frac{1}{3K_i} - \frac{A_{1,1}^2}{2} - \frac{2e}{3K_i A_{1,1}}} \qquad (2.60)$$

For specified values of e and K_i equations (2.59) and (2.60) define curves in an $A_{1,1}$, $A_{2,1}$-plane (Figures 2-15-i to 2-15-vi) where the points of intersection give the required values of $A_{1,1}$ and $A_{2,1}$. Since

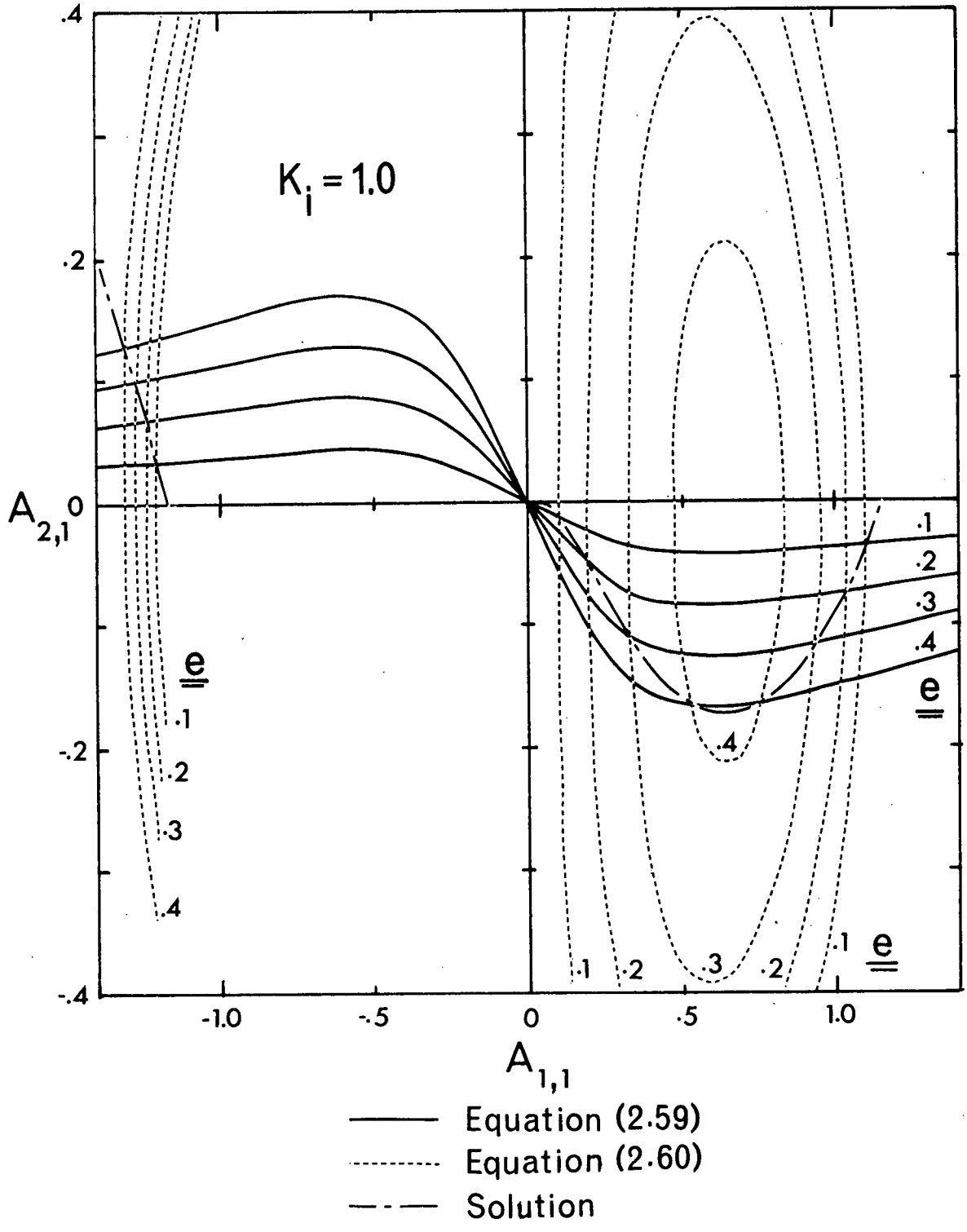

Figure 2-15-i Determination of the first two terms of the sine series solution (K_i = 1.0)

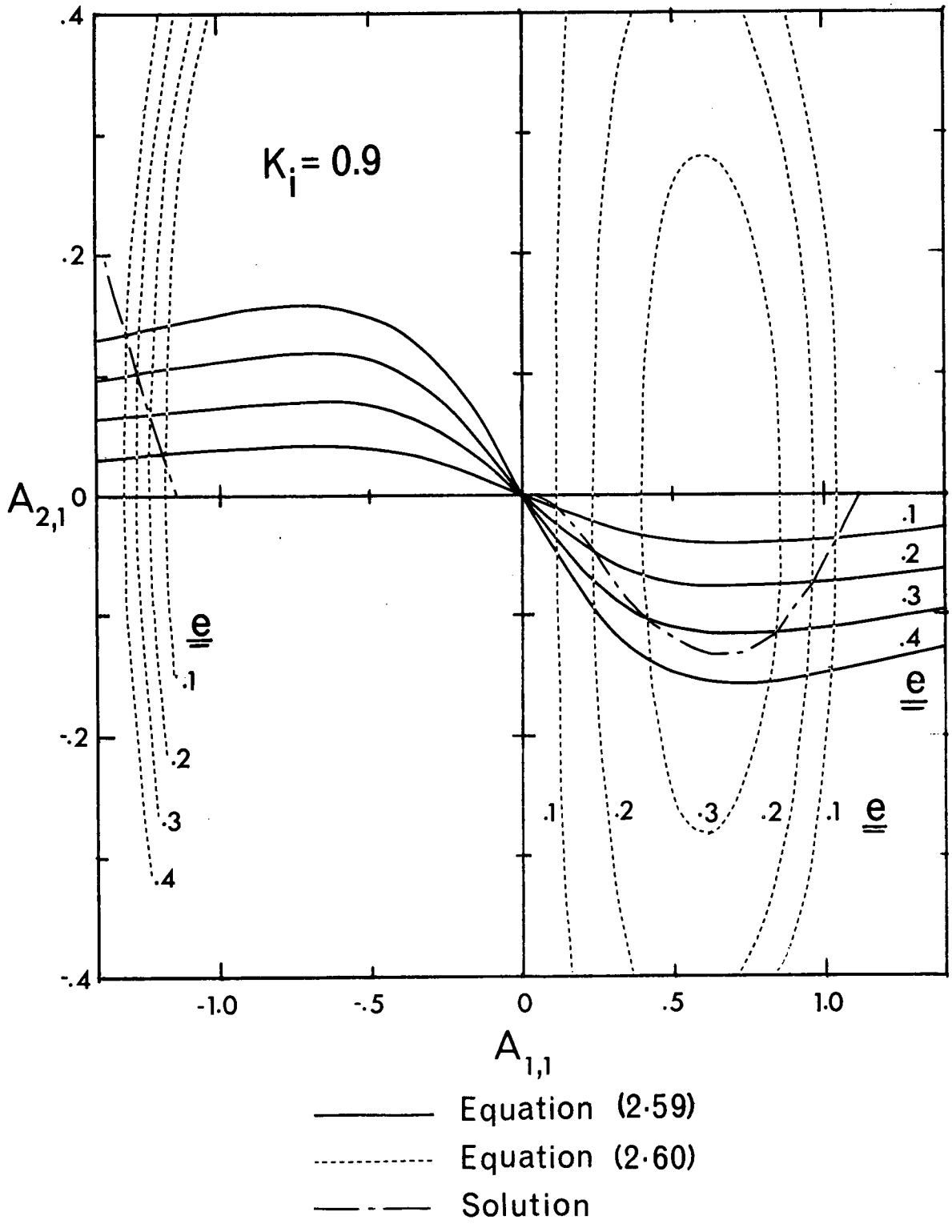

Figure 2-15-ii Determination of the first two terms of the sine series solution ($K_i = 0.9$)

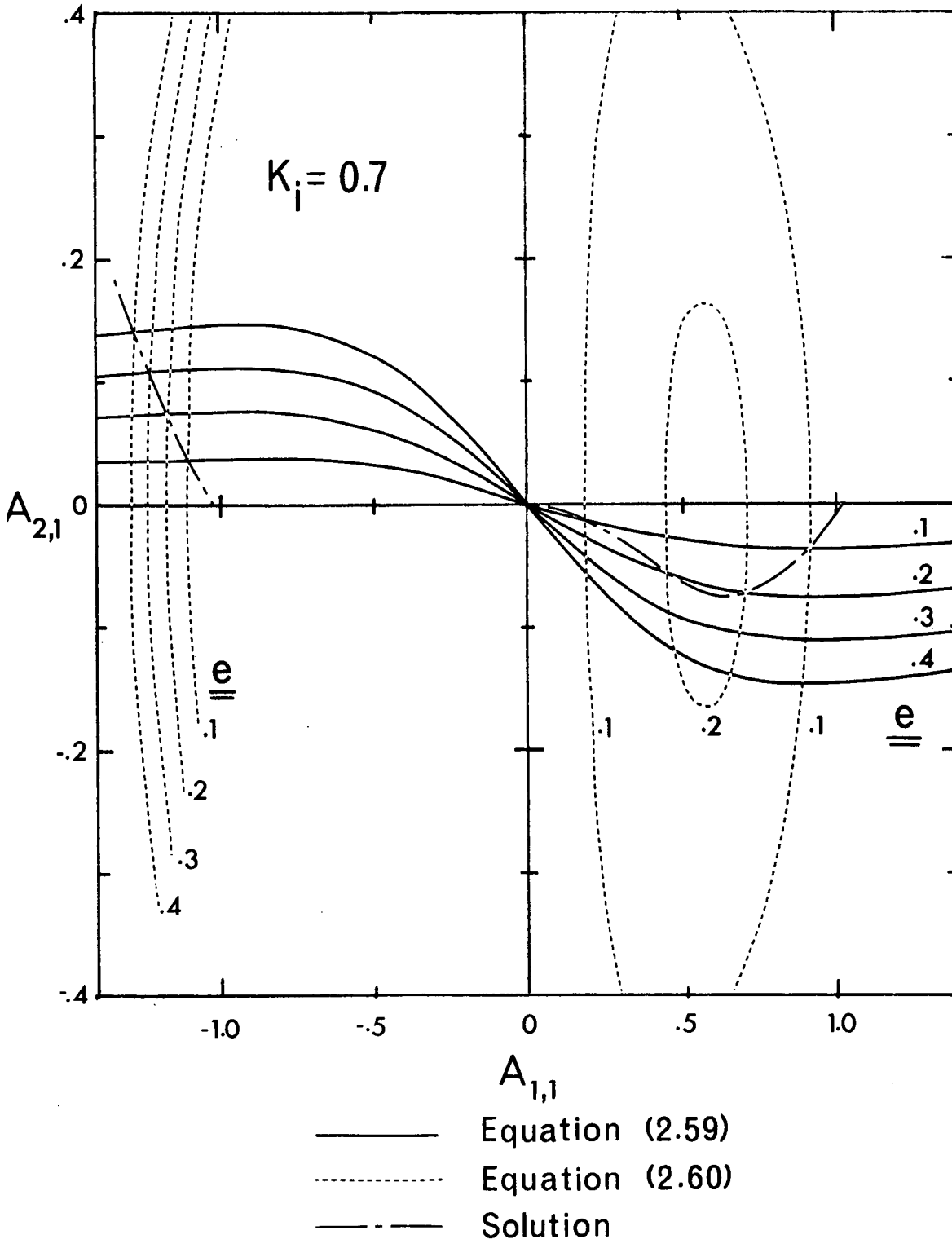

Figure 2-15-iii Determination of the first two terms of the sine series solution ($K_i = 0.7$)

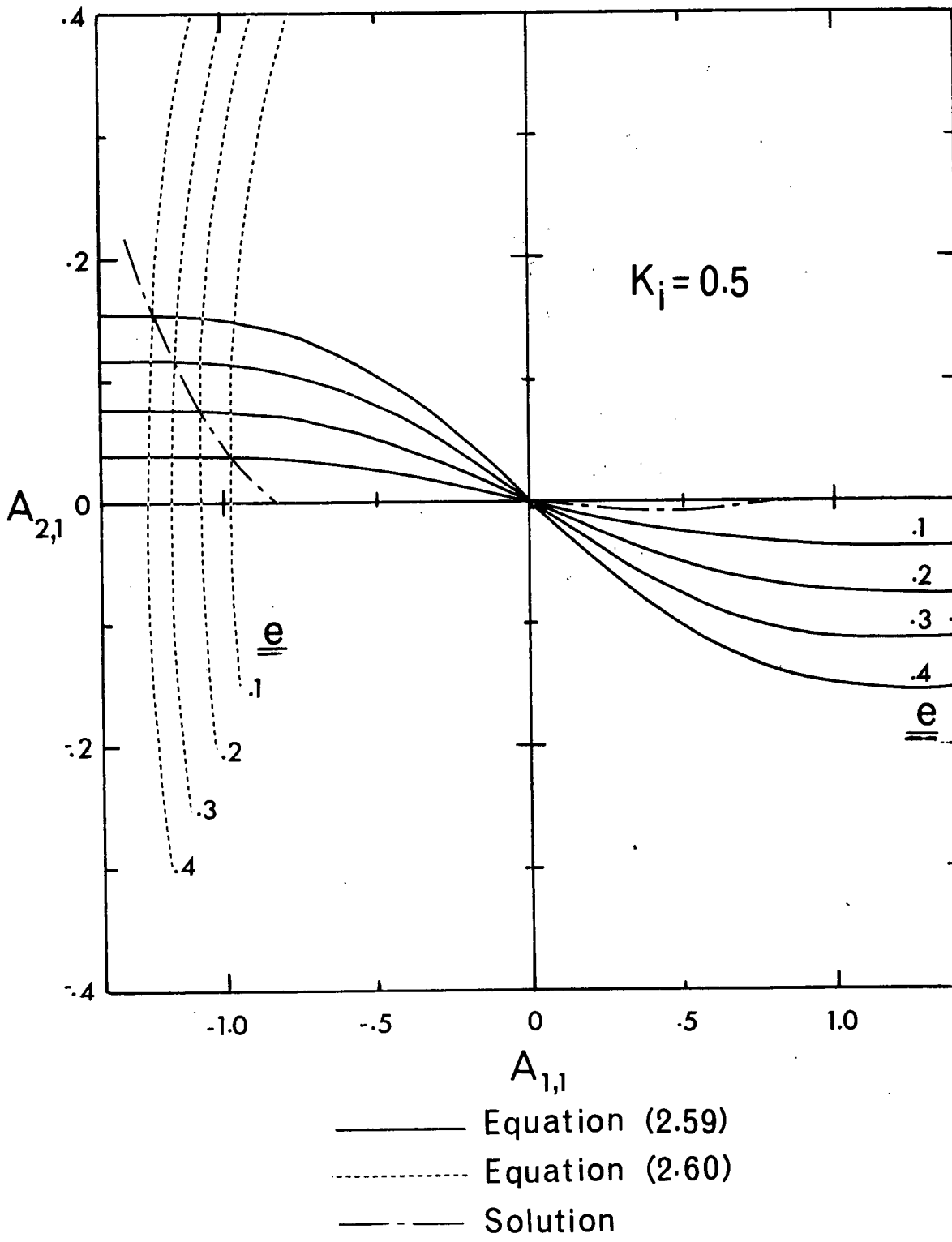

Figure 2-15-iv Determination of the first two terms of the sine series solution ($K_i = 0.5$)

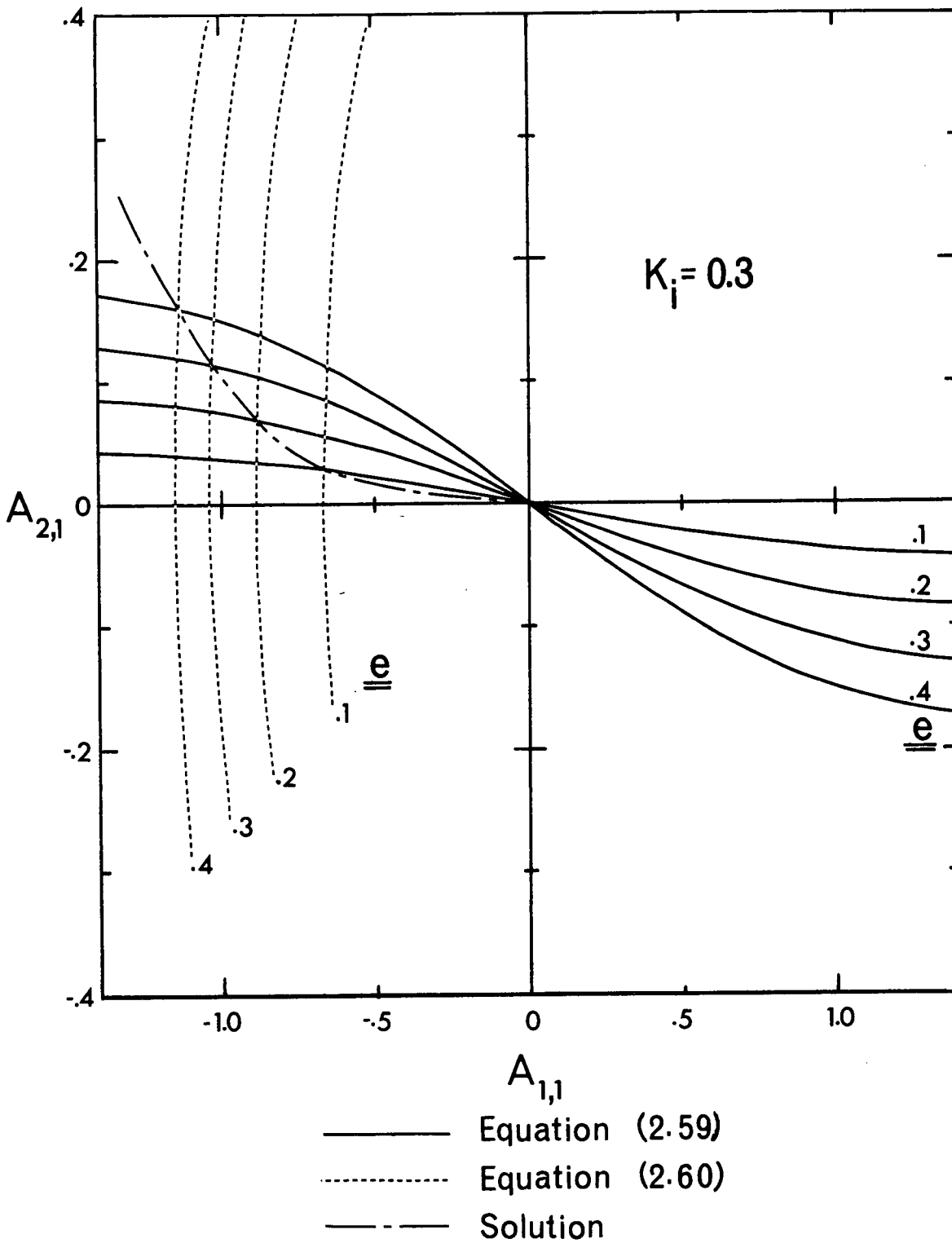

Figure 2-15-v Determination of the first two terms of the sine series solution (K_i = 0.3)

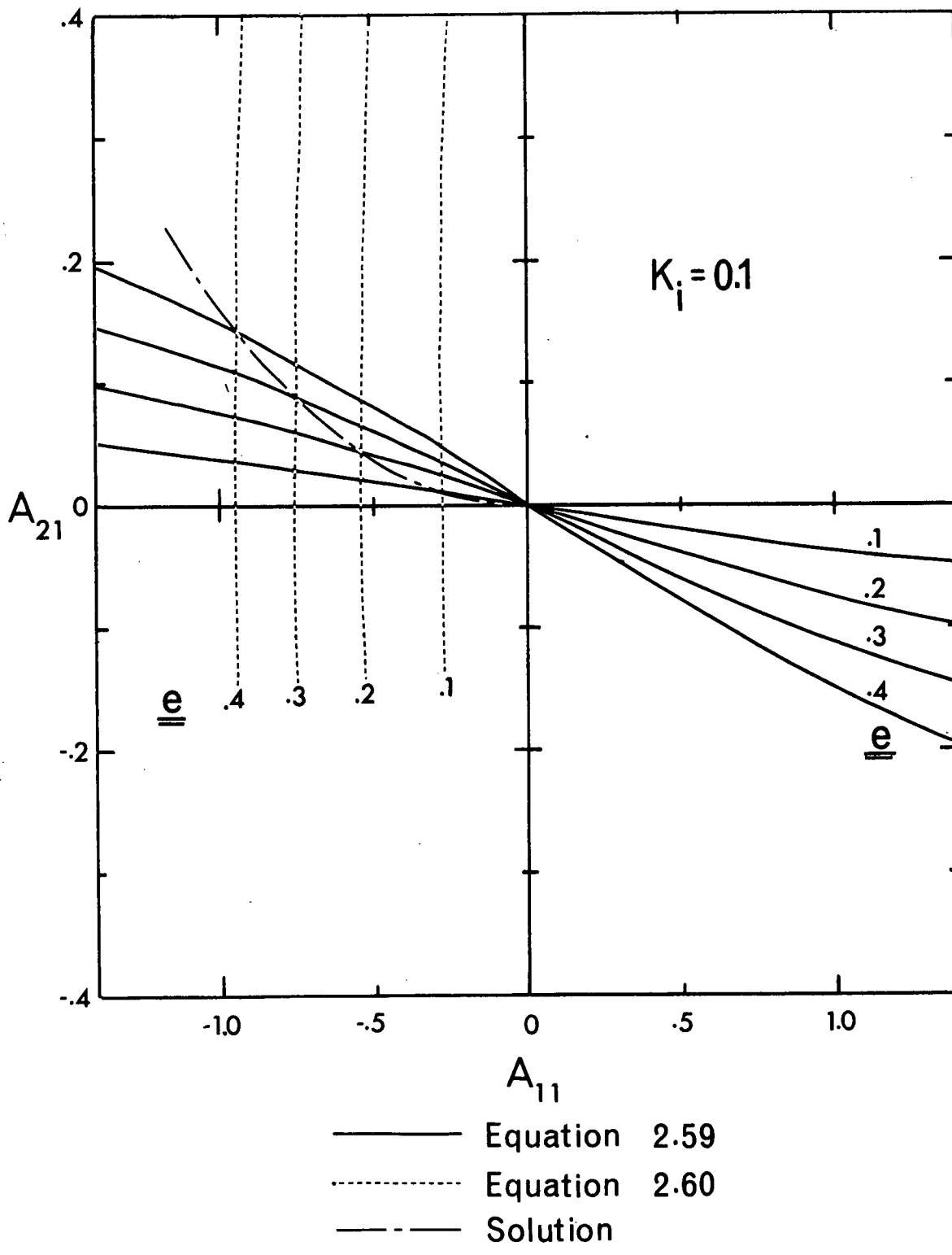

Figure 2-15-vi Determination of the first two terms of the sine series solution ($K_i = 0.1$)

$$\psi'_{p,1}(0) = A_{1,1} + 2A_{2,1} \tag{2.61}$$

the initial derivative of the periodic solutions can also be estimated. Figure 2-16 shows the value of $\psi'_{p,1}(0)$ obtained in this manner. A comparison with Figure 2-7 indicates that the general characteristics of the diagram are quite accurate. In particular, the approximate scheme predicts the maximum value of the eccentricity and the minimum value of K_i for which three periodic solutions exist with considerable precision.

Figure 2-17 compares the results of the simple two and three term analysis with the exact numerical solution of the equation of motion for the three cases listed in equation (2.57). The accuracy of the two term solution is rather poor (maximum error $\approx$ 20%). The addition of the third term improves the accuracy only of the solution of smallest amplitude. To achieve greater accuracy requires that more terms in the Taylor's expansion of the non-linear term be retained.

2.3.3 Perturbation of Periodic Solutions

Consider the periodic solution $\psi_{p,n}$ developed in 2.2.2 or 2.2.3. Let δ represent a perturbation so that the actual librational angle is given by

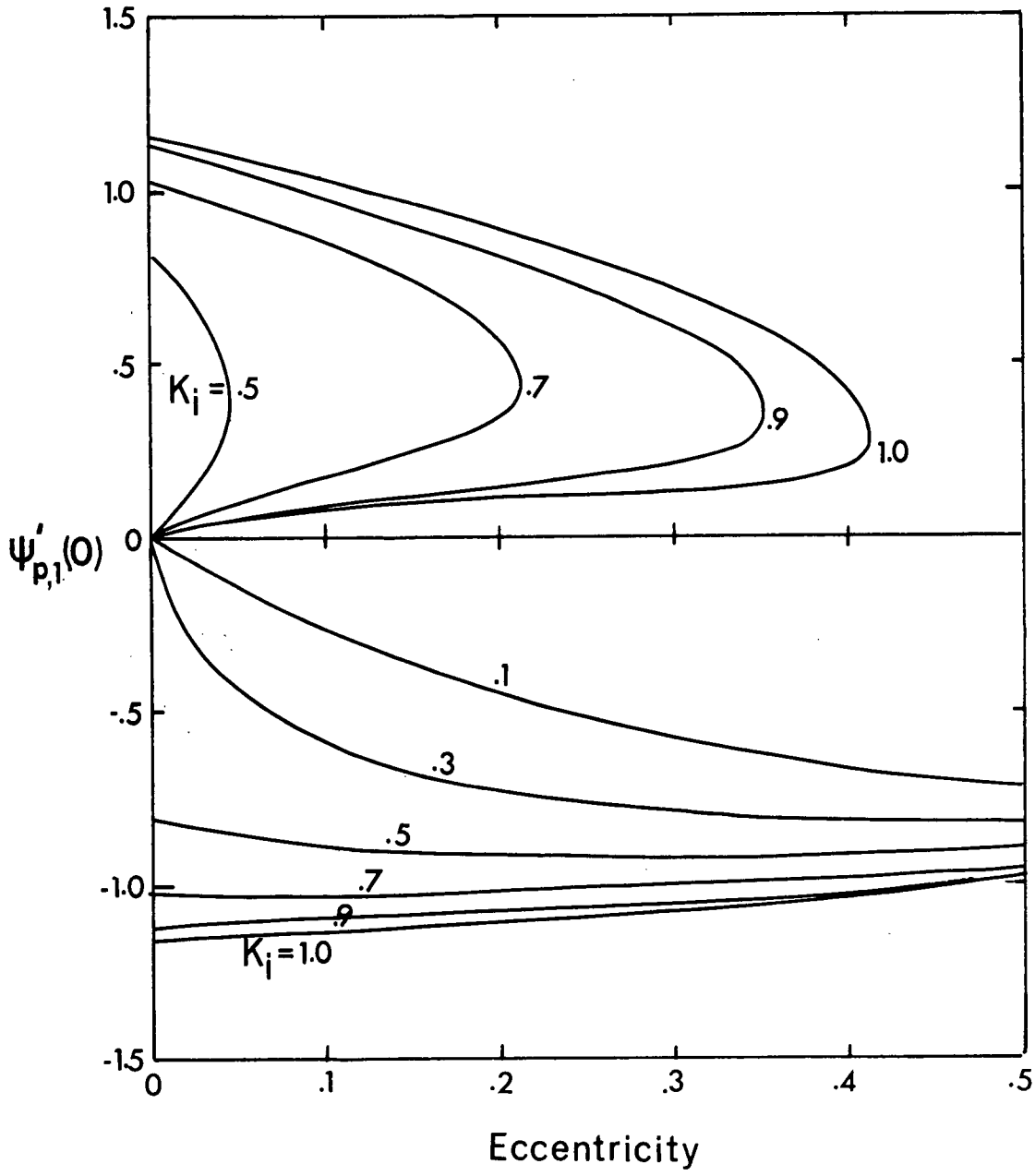

Figure 2-16 Values of the initial derivative required to produce solutions with period of 2π as determined by the first two terms of the sine series solution

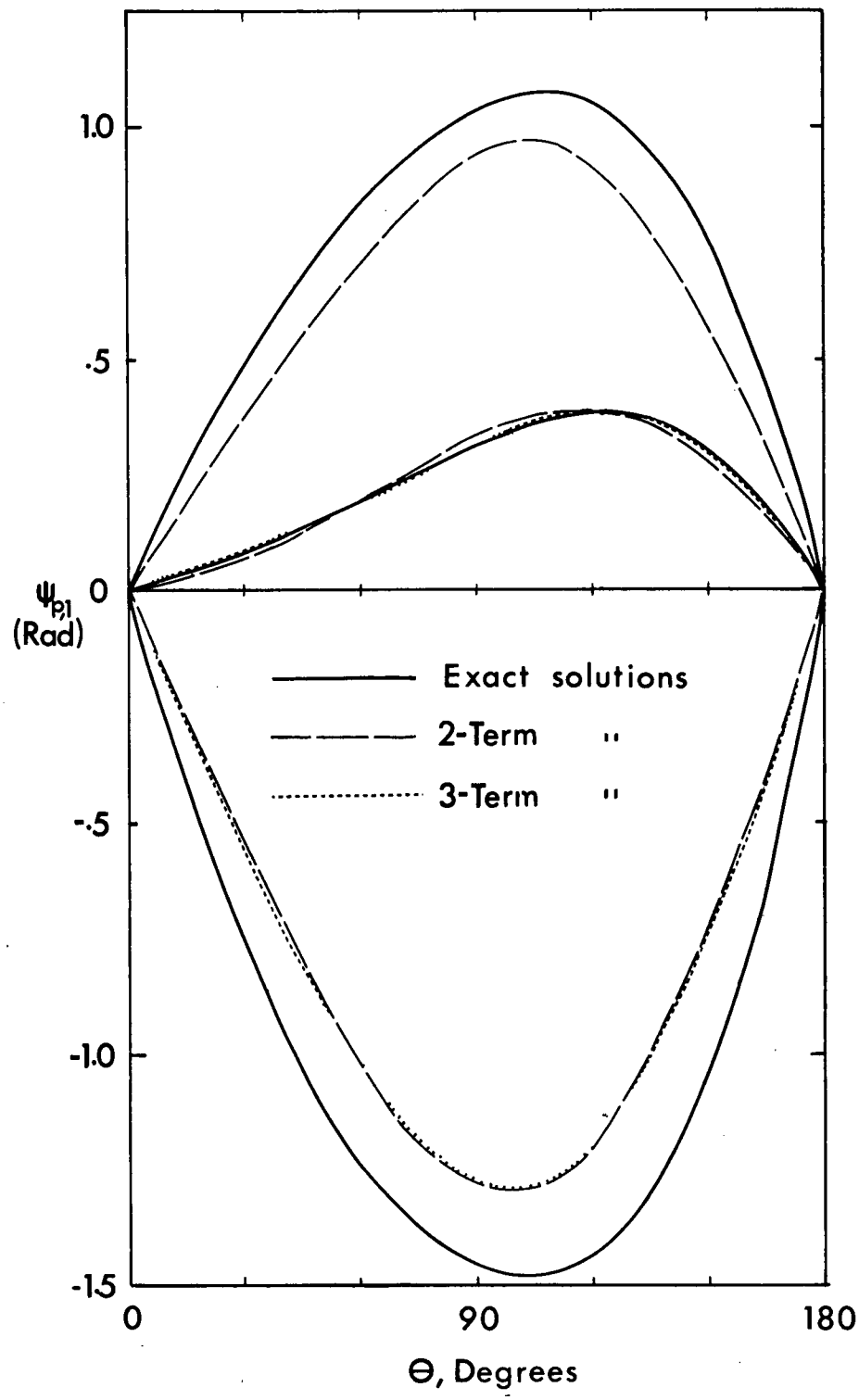

Figure 2-17 Comparison of exact periodic solutions with two and three term sine series solutions

$$\psi = \psi_{P,n} + \delta \tag{2.62}$$

Substituting (2.62) into (2.14) results in

$$\begin{aligned}&(1 + e\cos\theta)\psi''_{P,n} - 2e\sin\theta(\psi'_{P,n} + 1)\\ &+ (1 + e\cos\theta)\delta'' - 2e\sin\theta\,\delta'\\ &+ 3K_i \sin\psi_{P,n}\cos\psi_{P,n}\cos 2\delta + 3K_i\cos 2\psi_{P,n}\sin\delta\cos\delta = 0\end{aligned} \tag{2.63}$$

which for small δ reduces to the variational equation

$$(1 + e\cos\theta)\delta'' - 2e\sin\theta\,\delta' + 3K_i\cos 2\psi_{P,n}\,\delta = 0. \tag{2.64}$$

This is a linear differential equation with periodic coefficients which possesses two linearly independent solutions, $\delta_1(\theta)$ and $\delta_2(\theta)$, defined by the initial conditions

$$\begin{aligned}\delta_1(0) &= 1\\ \delta_1'(0) &= 0\\ \delta_2(0) &= 0\\ \delta_2'(0) &= 1.\end{aligned} \tag{2.65}$$

The solution to (2.64) subject to the initial conditions

$$\begin{aligned} \delta(0) &= \xi_0 \\ \delta'(0) &= \gamma_0 \end{aligned} \tag{2.66}$$

is given by

$$\delta(\theta) = \xi_0 \delta_1(\theta) + \gamma_0 \delta_2(\theta) . \tag{2.67}$$

Now, for $\theta = 2\pi$, equation (2.67) gives

$$\begin{aligned} \delta(2\pi) &= \xi_0 \delta_1(2\pi) + \gamma_0 \delta_2(2\pi) \\ \delta'(2\pi) &= \xi_0 \delta_1'(2\pi) + \gamma_0 \delta_2'(2\pi) \end{aligned} \tag{2.68}$$

and since equation (2.64) is invariant when θ is replaced by $\theta + 2\pi$, the solution in (2.67) can be extended over the interval $2\pi \leq \theta \leq 4\pi$ by considering (2.68) to be new initial conditions and writing the analogous relation

$$\begin{aligned} \delta(\theta) = &\left\{\xi_0 \delta_1(2\pi) + \gamma_0 \delta_2(2\pi)\right\} \delta_1(\theta) \\ &+ \left\{\xi_0 \delta_1'(2\pi) + \gamma_0 \delta_2'(2\pi)\right\} \delta_2(\theta) . \end{aligned} \tag{2.69}$$

This process may be continued indefinitely. Thus the complete solution for δ may be written in terms of the solution over the interval $0 \leq \theta \leq 2\pi$.

Because equation (2.64) remains invariant when δ is replaced by $-\delta$ and θ by $-\theta$, the δ_2 solution must be an odd function of θ. i.e.,

$$\begin{aligned} \delta_2(-\theta) &= -\delta_2(\theta) \\ \delta_2'(-\theta) &= \delta_2'(\theta). \end{aligned} \tag{2.70}$$

The initial conditions

$$\begin{aligned} \delta(0) &= -\delta_2(2\pi) \\ \delta'(0) &= \delta_2'(2\pi) \end{aligned} \tag{2.71}$$

define a solution

$$\delta(\theta) = -\delta_2(2\pi)\delta_1(\theta) + \delta_2'(2\pi)\delta_2(\theta) \tag{2.72}$$

in the interval $0 \leq \theta \leq 2\pi$ which matches the δ_2 solution in the interval $-2\pi \leq \theta \leq 0$. The final conditions at $\theta = 2\pi$ must then be

$$\begin{aligned} \delta(2\pi) &= \delta_2(0) = 0 \\ \delta'(2\pi) &= \delta_2'(0) = 1 . \end{aligned} \tag{2.73}$$

Hence, from (2.72)

$$\delta(2\pi) = -\delta_2(2\pi)\delta_1(2\pi) + \delta_2'(2\pi)\delta_2(2\pi) = 0 \tag{2.74}$$

and

$$\delta'(2\pi) = -\delta_2(2\pi)\delta_1'(2\pi) + \delta_2'(2\pi)\delta_2'(2\pi) = 1 \tag{2.75}$$

i.e.

$$\delta_1(2\pi) = \delta_2'(2\pi) \tag{2.76}$$

and

$$\delta_1(2\pi)\delta_2'(2\pi) - \delta_1'(2\pi)\delta_2(2\pi) = 1 = W(2\pi). \tag{2.77}$$

The left hand side of (2.77) is the Wronskian of the differential equation and can be determined from the coefficients.[29] For equation (2.64) the relation is

$$\frac{dW}{W} = \frac{2e\,\sin\theta}{1+e\,\cos\theta}\,d\theta \tag{2.78}$$

or

$$W(\theta) = W(0)\left(\frac{1+e}{1+e\,\cos\theta}\right)^2 \tag{2.79}$$

and therefore

$$W(0) = W(2\pi) = 1. \tag{2.80}$$

Consider the solution (2.67) when $\theta = 2n\pi$ and let

$$\begin{aligned} \delta(2\pi n) &= \Sigma_n \\ \delta'(2\pi n) &= J_n \end{aligned} \tag{2.81}$$

then, by (2.68)

$$\delta(2\pi n + 2\pi) = \xi_{n+1} = a\xi_n + b\eta_n$$
$$\delta'(2\pi n + 2\pi) = \eta_{n+1} = c\xi_n + d\eta_n \tag{2.82}$$

where

$$a = \delta_1(2\pi)$$
$$b = \delta_2(2\pi) \tag{2.83}$$
$$c = \delta_1'(2\pi)$$
$$d = \delta_2'(2\pi)$$

and (2.82) represents a pair of linear difference equations. Taking a solution of the form

$$\xi_n = A_s \gamma^n \tag{2.84}$$
$$\eta_n = B_s \gamma^n$$

and substituting in (2.82) results in

$$A_s \gamma^{n+1} = A_s a \gamma^n + B_s b \gamma^n \tag{2.85}$$
$$B_s \gamma^{n+1} = A_s c \gamma^n + B_s d \gamma^n$$

or

$$A_s(\gamma - a) - B_s b = 0 \tag{2.86}$$

$$-A_\delta c + B_\delta(\gamma - d) = 0. \qquad (2.86)\ \text{cont'd}$$

For a non-trivial solution, it is required that

$$\gamma^2 - (a+d)\gamma + (ad - bc) = 0. \qquad (2.87)$$

It may be pointed out that the analysis due to Floquet[30] yields an equation for the characteristic roots that is identical to equation (2.87) which simplifies, using (2.76) and (2.77), to

$$\gamma^2 - 2a\gamma + 1 = 0 \qquad (2.88)$$

giving

$$\gamma_i = a \pm \sqrt{a^2 - 1} \quad ; (i = 1,2) \qquad (2.89)$$

and equation (2.89) when substituted into (2.86) gives

$$B_{\delta_i} = \frac{(\gamma_i - a)A_{\delta i}}{b} = \pm \frac{\sqrt{a^2-1}}{b} A_{\delta i}\ ;\ (i=1,2). \qquad (2.90)$$

The solution (2.84) may be written as the sum of the two solutions

$$\varepsilon_n = A_{\delta_1}\gamma_1^n + A_{\delta_2}\gamma_2^n \qquad (2.91)$$

$$\begin{aligned}\delta_n &= B_{\delta_1}\gamma_1^n + B_{\delta_2}\gamma_2^n \\ &= \frac{\sqrt{a^2-1}}{b} A_{\delta_1}\gamma_1^n - \frac{\sqrt{a^2-1}}{b} A_{\delta_2}\gamma_2^n\end{aligned} \qquad (2.92)$$

hence

$$\frac{b\zeta_n}{\sqrt{a^2-1}} = A_{\delta_1}\gamma_1^n - A_{\delta_2}\gamma_2^n . \tag{2.93}$$

Taking the sum and difference of (2.91) and (2.93) gives

$$\begin{aligned} \xi_n + \frac{b\zeta_n}{\sqrt{a^2-1}} &= 2A_{\delta_1}\gamma_1^n \\ \xi_n - \frac{b\zeta_n}{\sqrt{a^2-1}} &= 2A_{\delta_2}\gamma_2^n \end{aligned} \tag{2.94}$$

whose product yields the relation

$$\xi_n^2 - \frac{b^2}{a^2-1}\zeta_n^2 = 4A_{\delta_1}A_{\delta_2}(\gamma_1\gamma_2)^n = 4A_{\delta_1}A_{\delta_2} . \tag{2.95}$$

This result shows that, if the solution of equation (2.64) is inspected each time the independent variable equals $2\pi n$, the values of the function and its derivative, when plotted in the ξ,ζ -plane, lie on a certain curve. For $|a| > 1$ the curve is a hyperbola so that δ eventually becomes very large. On the other hand if $|a| < 1$ the curve is an ellipse and δ is bounded. It may be concluded that in the latter case, small perturbations about the periodic solutions are stable and for $\theta = 2\pi n$ may be found on a single curve in the ψ, ψ' -plane which surrounds the point $(\psi_p(0), \psi_p'(0))$.

For values of θ other than zero, a point on the curve

transforms into

$$\begin{aligned} \delta(\theta) &= \xi\,\delta_1(\theta) + \int \delta_2(\theta) \\ \delta'(\theta) &= \xi\,\delta_1'(\theta) + \int \delta_2'(\theta) \end{aligned} \tag{2.96}$$

where ξ and $\int$ lie on the curve defined by (2.95). Hence

$$\xi = \frac{\delta(\theta)\,\delta_2'(\theta) - \delta'(\theta)\,\delta_2(\theta)}{W(\theta)} \tag{2.97}$$

$$\int = \frac{\delta'(\theta)\,\delta_1(\theta) - \delta(\theta)\,\delta_1'(\theta)}{W(\theta)} \tag{2.98}$$

which when substituted into (2.95) determine the shape of the curve at the specified value of θ

$$\begin{aligned} &\delta^2(\theta)\left\{\delta_2'^2(\theta) - \frac{b^2}{a^2-1}\,\delta_1'^2(\theta)\right\} \\ &-2\,\delta(\theta)\,\delta'(\theta)\left\{\delta_2(\theta)\,\delta_2'(\theta) - \frac{b^2}{a^2-1}\,\delta_1(\theta)\,\delta_1'(\theta)\right\} \\ &+\delta'^2(\theta)\left\{\delta_2^2(\theta) - \frac{b^2}{a^2-1}\,\delta_1^2(\theta)\right\} = 4A_{\delta_1}A_{\delta_2}W^2(\theta) \end{aligned} \tag{2.99}$$

that is,

$$A(\theta)\,\delta^2(\theta) + B(\theta)\,\delta'^2(\theta) + C(\theta)\,\delta(\theta)\,\delta'(\theta) + D(\theta) = 0. \tag{2.100}$$

The nature of the curve at the specified value of θ

is determined by the sign of the parameter

$$\mathcal{D}(\theta) = 4A(\theta)B(\theta) - C^2(\theta) \tag{2.101}$$

such that for $\mathcal{D} > 0$ the curve is an ellipse and for $\mathcal{D} < 0$, a hyperbola. From equations (2.99) and (2.100) there is obtained

$$\mathcal{D}(\theta) = -\frac{4b^2}{a^2-1} W^2(\theta) \tag{2.102}$$

therefore, $\mathcal{D} < 0$ if $|a| > 1$ and $\mathcal{D} > 0$ if $|a| < 1$.

Thus, depending upon the value of $|a|$ the curve defined by successive passages of the solution at fixed θ is either an ellipse or a hyperbola. In the first case a tubular surface is defined.

Linear perturbation analysis predicts that initial conditions which do not lead to exactly periodic motion may still permit the motion to remain in the neighbourhood of the periodic solution. There is also the possibility that the motion may drift away from the generating solution. The criterion determining the kind of motion is the magnitude of the δ_2 -type of solution of the variational equation at $\theta = 2\pi$. For $|\delta_2(2\pi)| > 1$, the variation increases with time, but if $|\delta_2(2\pi)| < 1$ the difference between the actual and the periodic solutions remains bounded. In fact, in the latter case, the solutions lie on a surface in ψ, ψ', θ -space which always surrounds the periodic solution and has

an elliptic cross section.

Figure 2-18 presents the regions in an e, K_i parameter space for which the perturbations about the various periodic solutions of orbital frequency are stable. This diagram was determined numerically and represents an extension in the region near $e = 1$ of the work by Zlatousov et al.[12] In general there are three periodic solutions to consider. One, with large positive initial derivative, always leads to unstable perturbations. The other two solutions, having either a small positive or large negative initial derivative may yield stable perturbations.

Figure 2-19 presents similar data for periodic solutions which complete three oscillations in two orbits. It may be emphasized that there is only one class of solution in this case ($n = 2$) because solutions with the positive slope at $\theta = 0$ required in Figure 2.10 have at $\theta = 2\pi$ the negative slope also found in this Figure (see also Figure 2-9).

When the parameter a in equation (2.88) lies between +1 and -1, the perturbations are confined to a surface with elliptical cross-section. In general, as time increases the point of intersection of the trajectory with the $\theta = 0$ plane moves around the ellipse. In fact, since

$$\gamma = a \pm i\sqrt{1-a^2} = e^{\pm i\Theta} \qquad (2.103)$$

where

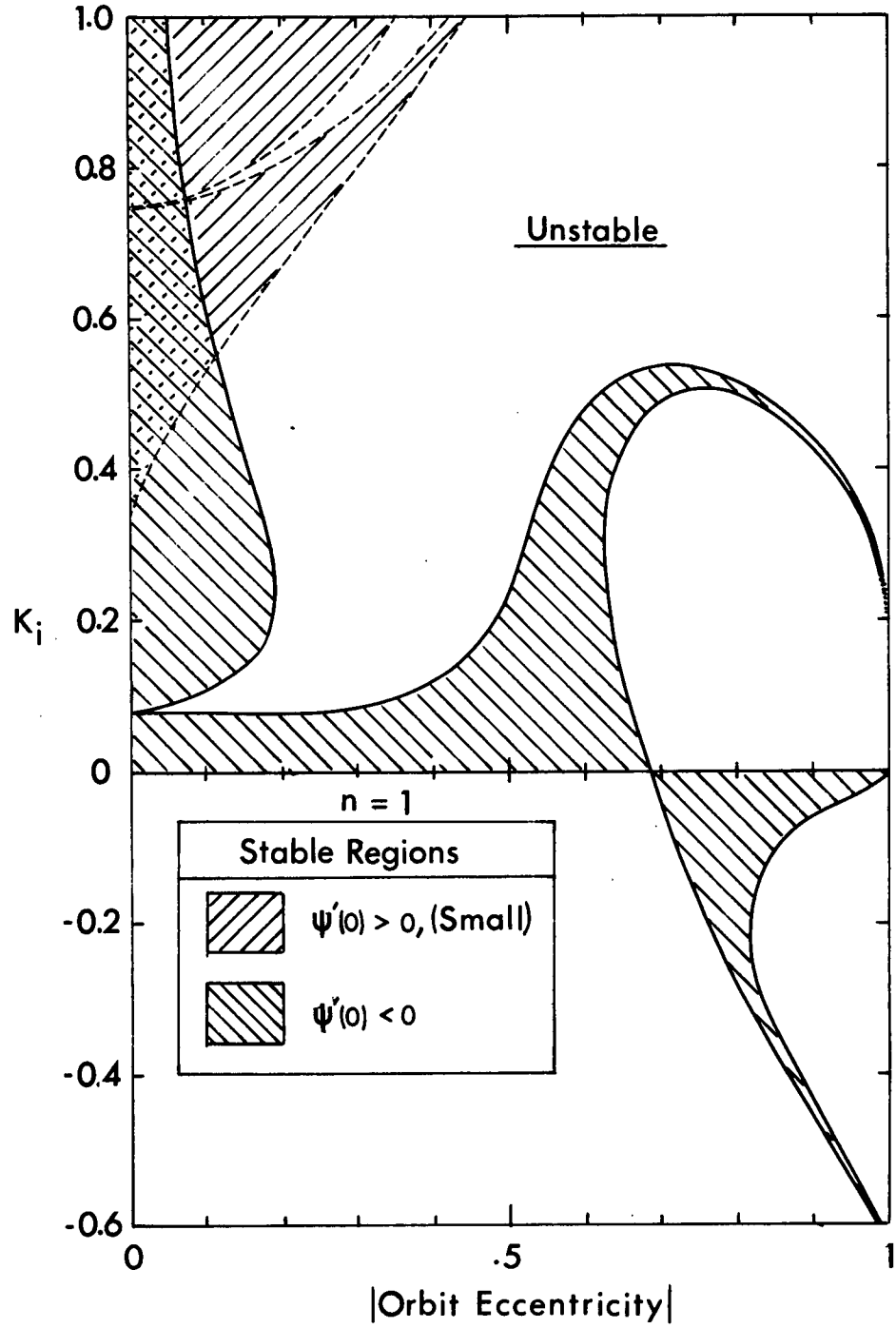

Figure 2-18 Values of K_i and e which lead to variationally stable periodic solutions of period 2π

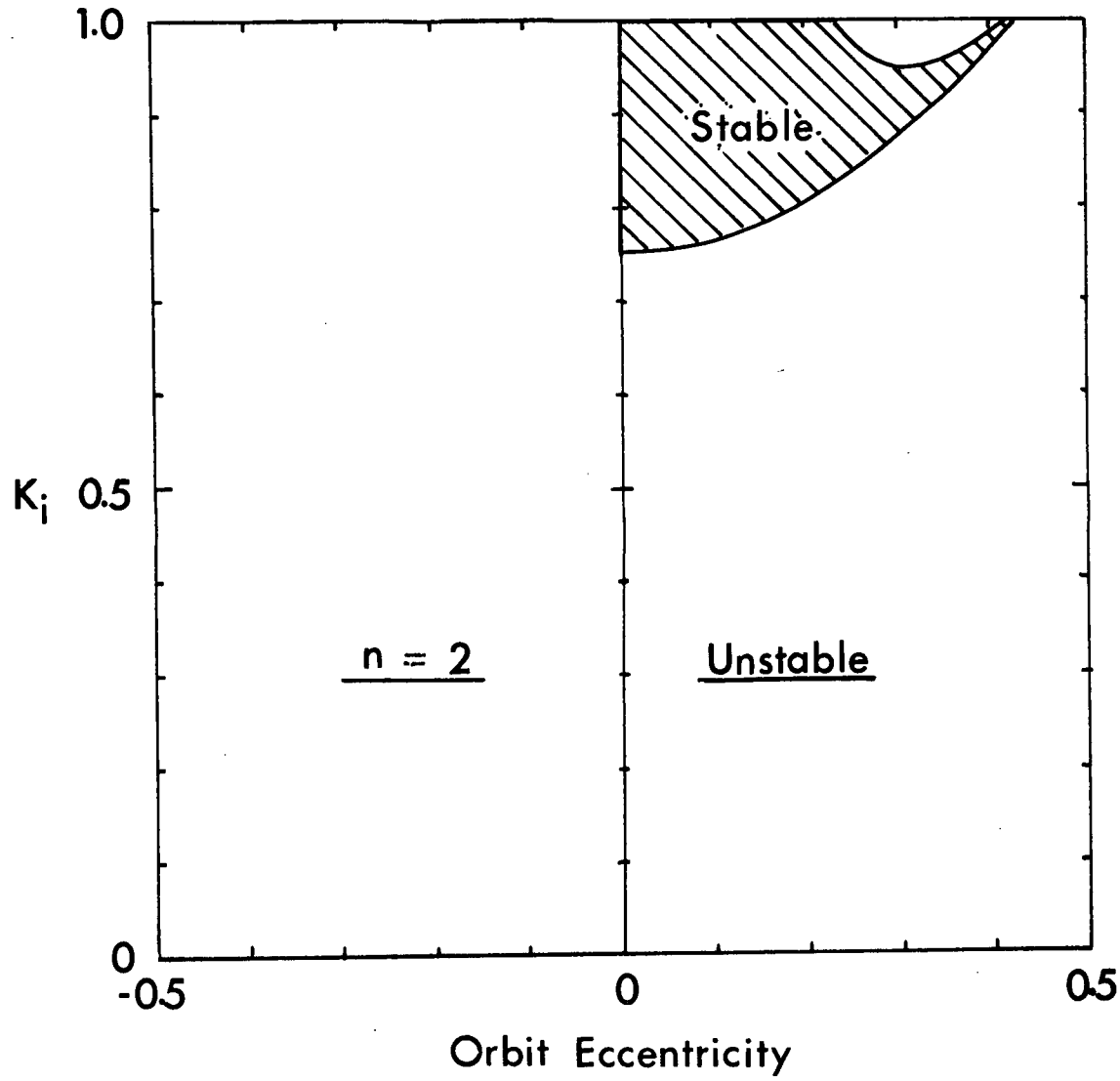

Figure 2-19 Values of K_i and e which lead to variationally stable periodic solutions of period 4π

$$\Theta = \cos^{-1} a, \tag{2.104}$$

it is evident from equations (2.82) that the point representing the perturbation solution in the ψ, ψ' -plane rotates around the ellipse at the average rate of Θ radians per orbit. In particular, if Θ is a rational sub-multiple of 2π the points defined by (2.82) appear stationary. Thus the perturbation solution has itself become periodic. This occurrence is the manifestation of the coalescence with the original periodic solution of another solution characterized by a period equal to that of the perturbation.

For example, referring to Figures 2-7, 2-9, and 2-10 it is seen that one type of solution of period 4π becomes identical with that of period 2π at $e \approx 0.43$. Figures 2-20 and 2-21 indicate that for both periodic solutions $|a| = 1$ at this point, hence $\Theta = 0, 180^{\circ}$.

2.4 Phase Space and Invariant Surfaces

The equation of motion (2.14) may be written as a pair of first order differential equations

$$\begin{aligned} \frac{d\psi}{d\theta} &= \psi' \\ \frac{d\psi'}{d\theta} &= \frac{2e\sin\theta(\psi'+1) - 3K_i\sin\psi\cos\psi}{1+e\cos\theta} \end{aligned} \tag{2.105}$$

This parallels the usual Hamiltonian formulation where the

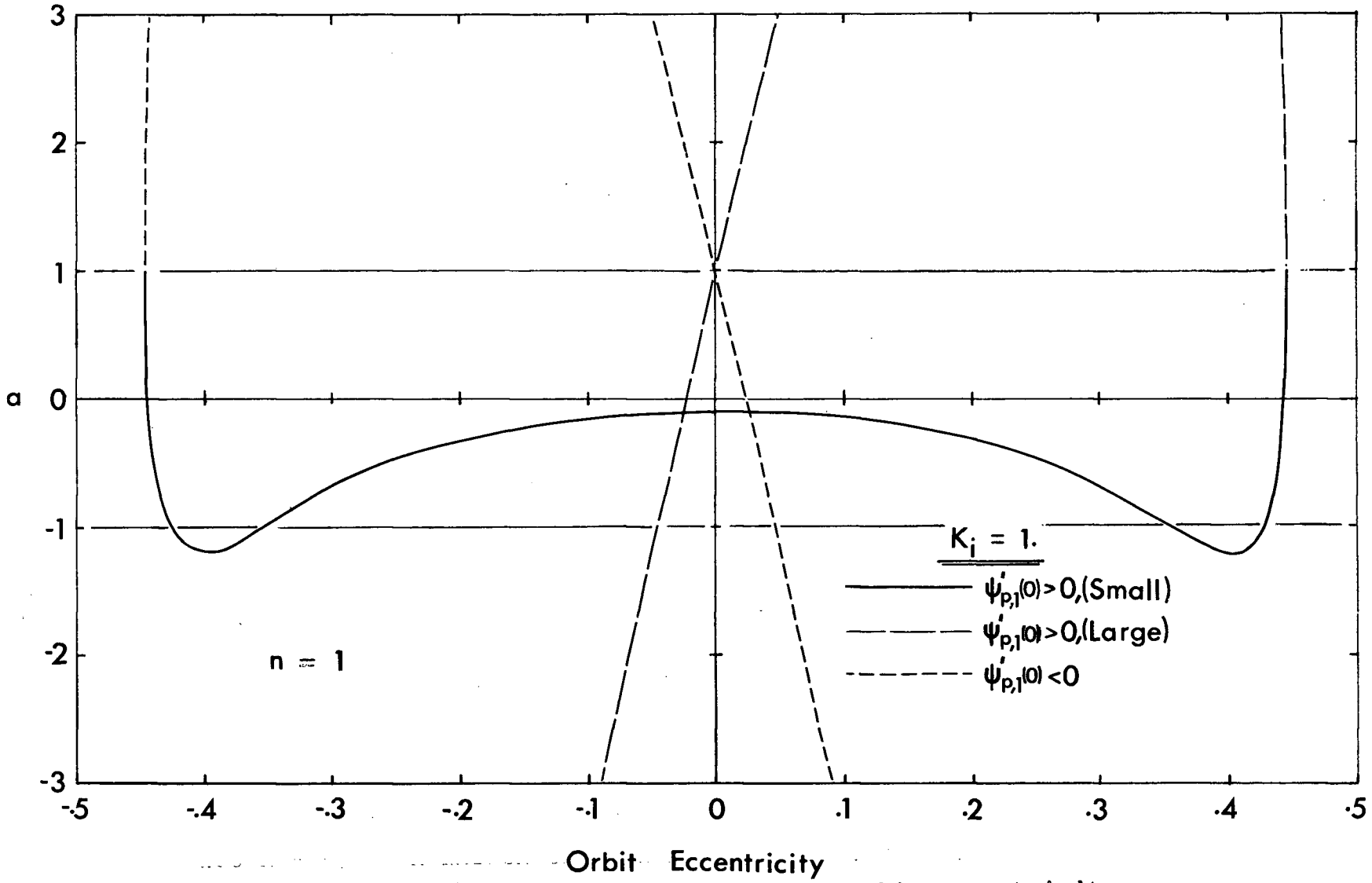

Figure 2-20 Variation of parameter a with orbit eccentricity (K_i = 1) for solutions of period 2π

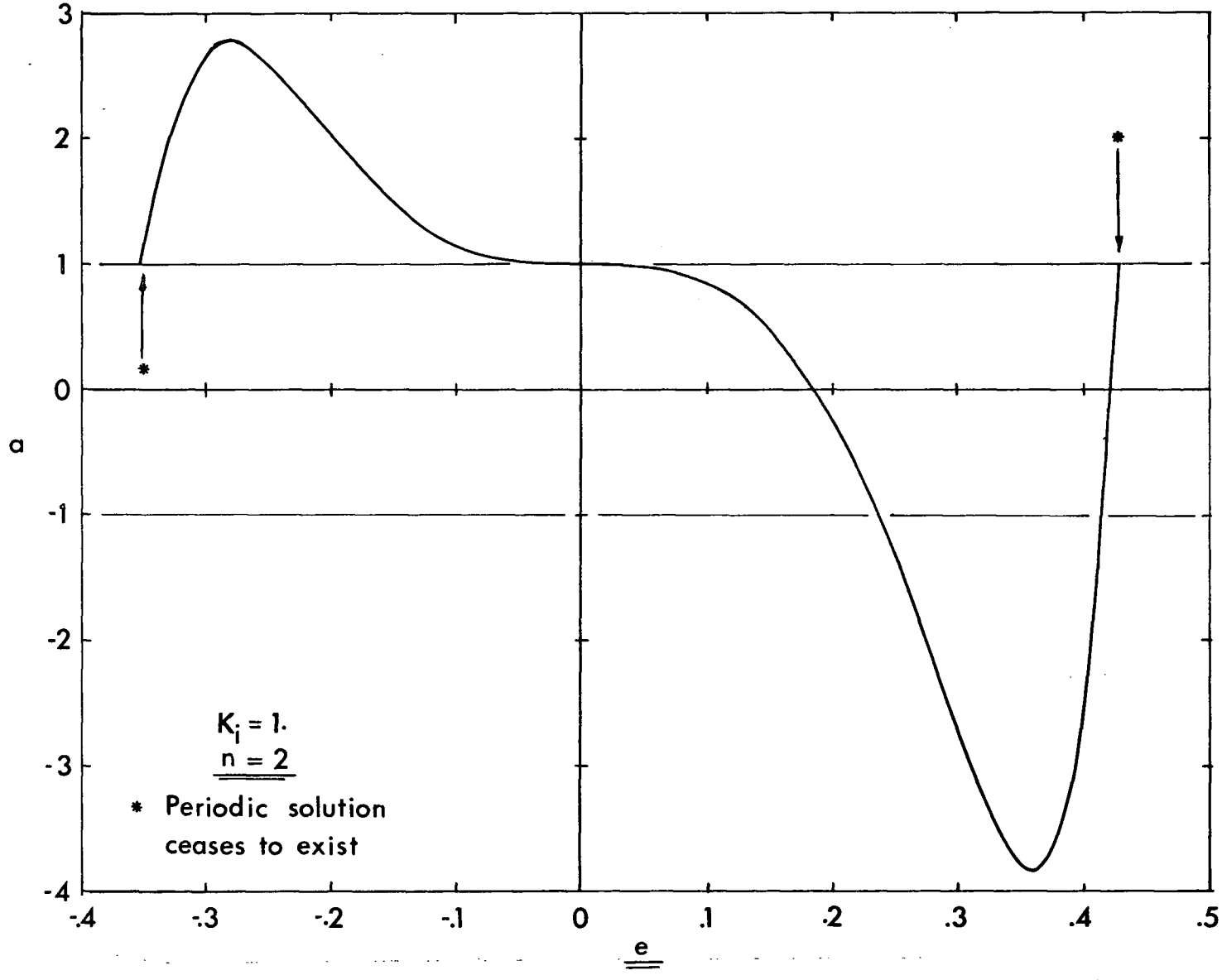

Figure 2-21 Variation of parameter a with orbit eccentricity for solutions of period 4π ($K_i = 1$)

distinction between co-ordinates and momenta nearly disappears. The solution of (2.105) depends on the starting values of both ψ and ψ', as well as the value of the independent variable, at the initial point ($\theta = \theta_0$). This suggests that the state of the system can be represented by a point in a phase space formed by the three orthogonal co-ordinates ψ, ψ', and θ.

As shown in section 2.2.1 for e = 0, the existence of a first integral (2.16) indicates that the stable state of the system is represented by a point which lies on the closed curve,

$$\psi'^2 + 3K_i \sin^2\psi = C_c \leq 3K_i . \qquad (2.106)$$

The curve can be thought of as defining a cylindrical surface with oval cross-section (Figure 2-3).

The governing non-linear, non-autonomous differential equation does not admit of a simple solution for $e \neq 0$. However, it seems logical to expect that closed curves analogous to those of Figure 2-3 should continue to exist for non-zero eccentricity. These curves would then be functions of θ and thus define a surface in the three dimensional ψ, ψ', θ -space. It is apparent that equation (2.14) is periodic in θ with period 2π, hence the surface need only be determined over that interval.

The surface may be generated by what Hénon and Heiles[31] refer to as a "numerical experiment." An initial point, $\psi = \psi_0$, $\psi' = \psi'_0$, $\theta = 0$ is chosen and equations (2.105) are integrated until θ equals 2π. This produces a "consequent"

point $\psi = \psi_c$, $\psi' = \psi'_c$, $\theta = 2\pi$ which may be considered as a new initial point with $\theta = 0$. The process may be thought of as a transformation, defined by equations (2.105), of the initial point.

The new starting point may itself be transformed repeatedly thus leading to a series of points in the ψ, ψ' -plane at $\theta = 0$. If any of the transformed points lies outside the region $|\psi| \leq \pi/2$, then all the points determined by the process lead to tumbling motion and may be plotted in the unstable region. Alternatively, the points may lie inside the region indicating stable operation and, when plotted, appear to define a curve. This is an invariant curve of the transformation. That is, the transformation of the curve lying in the $\theta = 0$ plane results in the same curve being generated at $\theta = 2\pi$. The two curves are connected by an infinity of trajectories thereby defining a surface which may be called an "invariant surface" or "integral manifold." The existence of such surfaces for librational motion in a circular orbit is evident from earlier discussion, and, as pointed out by Moser,[32] their existence can be proven for $e \neq 0$ as follows.

The concept of a transformation which converts a point (ψ_o, ψ'_o) in the $\theta = 0$ plane into another (ψ_c, ψ'_c) in the $\theta = 2\pi$ plane is very helpful in this regard. Periodic solutions appear as sets of fixed points in the two planes and hence are characterized by an identity transformation.

The period of the solutions may be taken as long as desired by making $n \to \infty$. Hence there will be a countably infinite number of points which satisfy an identity transformation. Since the density of these points may be made as high as desired, the mapping defined in this manner must be area preserving.

Now, the period of oscillation of the system for $e = 0$ is given by (2.18) as a monotonically increasing function of ψ_{max}. The period is bounded by

$$\frac{2\pi}{\sqrt{3K_i}} \leq \Delta\theta < \infty; \left(0 \leq \psi_{max} < \frac{\pi}{2}\right). \qquad (2.107)$$

Moser's theorem then asserts that there exist curves in the neighbourhood of the curves (2.106) which remain invariant under the mapping for small e. Figure 2-22 represents such an invariant surface schematically.

The surfaces generated by equation (2.14) have certain symmetry properties. This differential equation remains unchanged if both θ and ψ change sign. Thus, the solution and its derivative defined by the conditions $\psi(0) = 0$, $\psi'(0) = \psi'_0$, are odd and even functions respectively. Consequently, the points defined in the $\theta = 2\pi m$ $(m = 1,2,\ldots)$ planes are reflections about the ψ'-axis of the points defined in the $\theta = 2\pi m$ $(m = -1, -2, \ldots)$ planes. Hence the cross-sections of the surface at $\theta = 0$ and 2π are symmetrical about the ψ'-axis. This is illustrated in Figure 2-23.

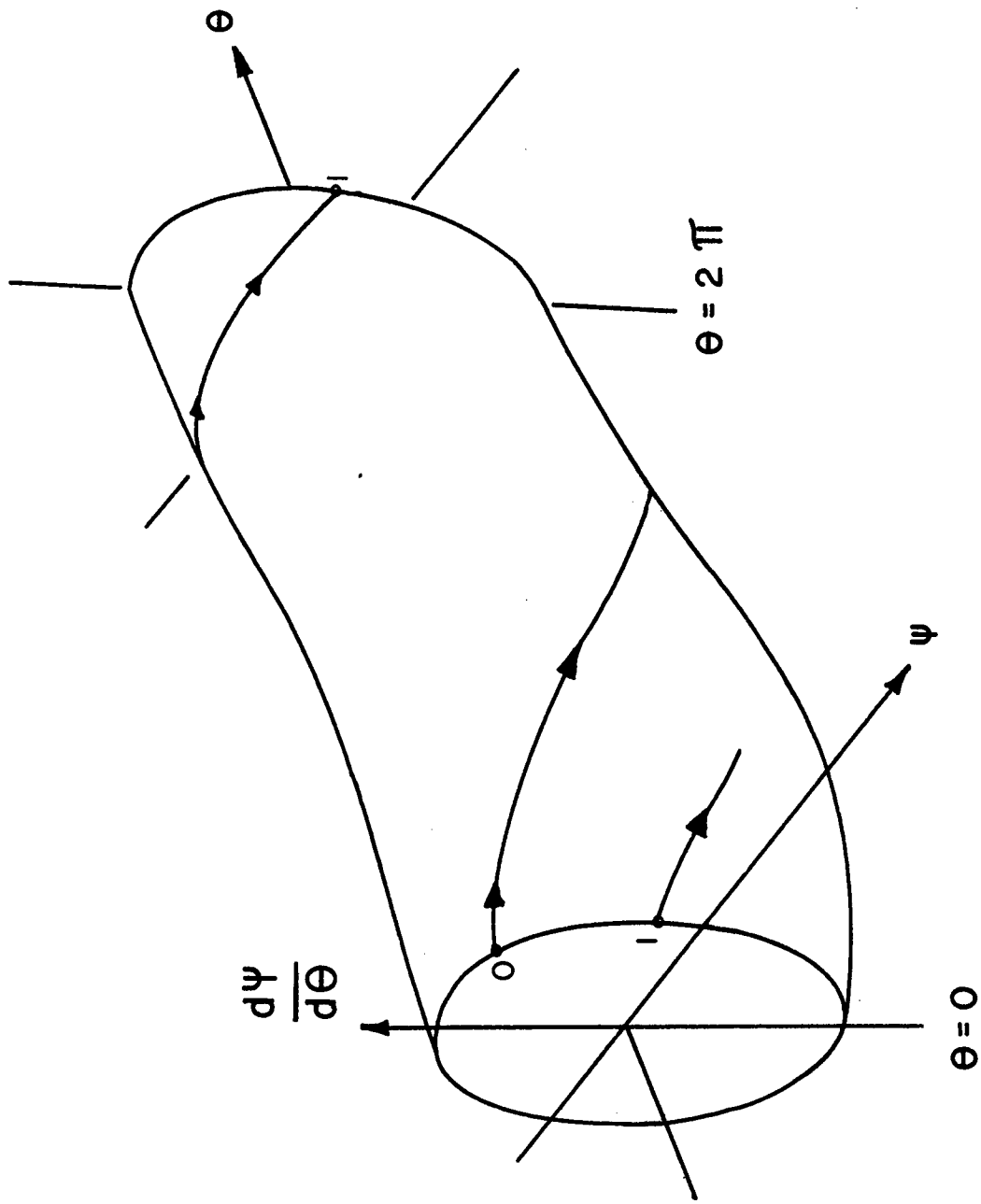

Figure 2-22 Schematic view of an invariant surface

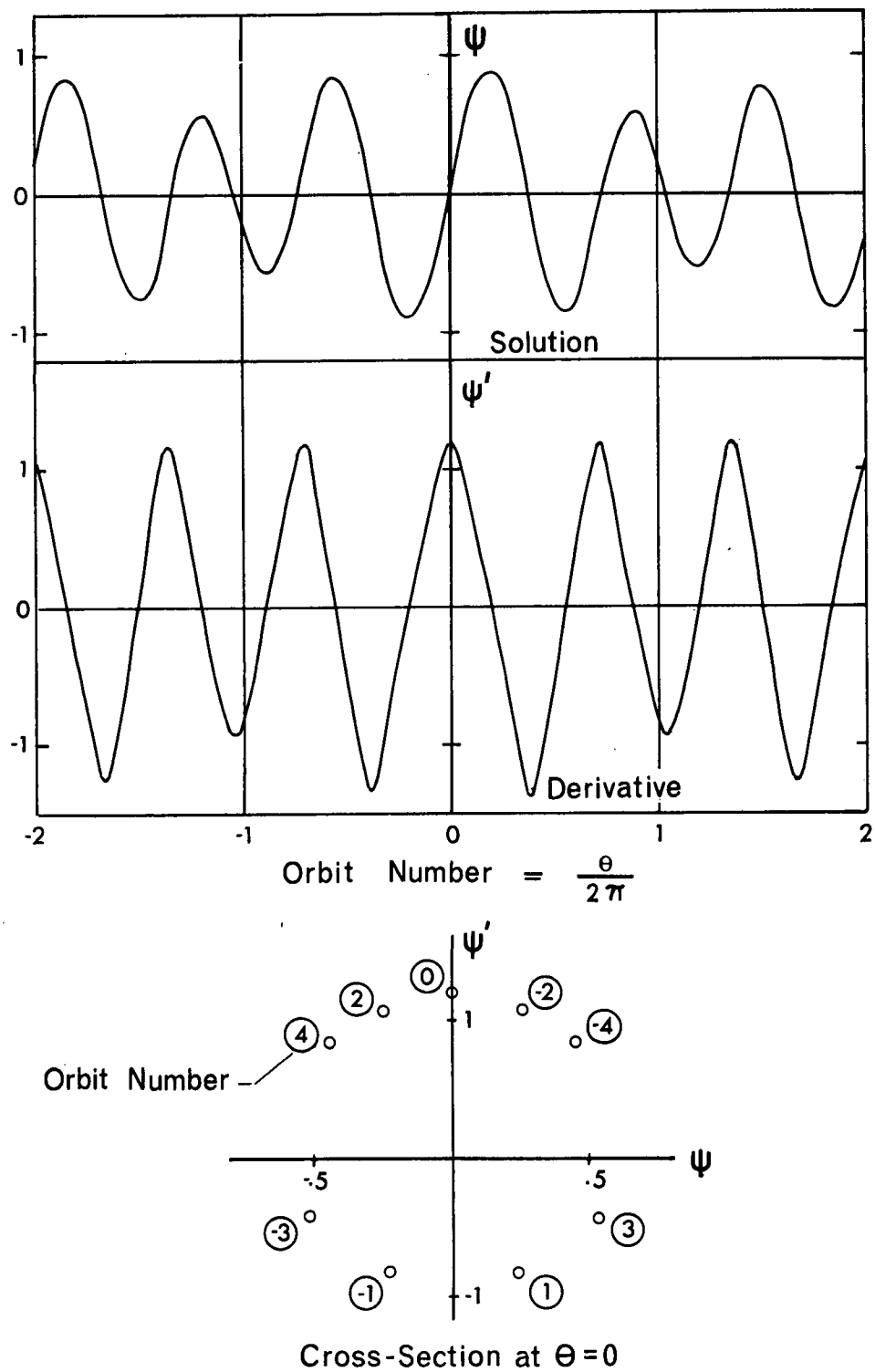

Figure 2-23 A specific solution which illustrates the symmetry properties of the invariant surface

Further, the points defined in the $\theta = \hat{\theta}$ plane will be the mirror image about the ψ'-axis of the points defined in the $\theta = -\hat{\theta}$ plane, or equivalently in the $\theta = 2\pi - \hat{\theta}$ plane. Thus the cross-section of the invariant surface at $\theta = \hat{\theta}$ is a mirror image about the ψ'-axis of the cross-section at $\theta = 2\pi - \hat{\theta}$. Hence, the cross-section at $\theta = \pi$ is also symmetric about the ψ'-axis. Several cross-sections of an invariant surface taken at various orbit angles are presented in Figure 2-24 for specific values of e and K_i.

An initial point taken within a given manifold generates a different trajectory and hence a new surface. The property of uniqueness guarantees that the new trajectory does not intersect the old one. The new invariant surface must therefore lie completely within the original.

On the other hand, an external initial condition generates an external surface provided that the motion continues to be stable. The desired region of stability may be represented as the largest closed invariant surface that can be constructed. Typical invariant surfaces are shown in Figures 2-25-i and 2-25-ii. The symmetry properties are readily observed.

This concept of a limiting surface in the phase space is very important. For given values of the parameters it provides all possible combinations of initial angles and velocities to which a satellite may be subjected at any point in its orbit without causing it to become unstable.

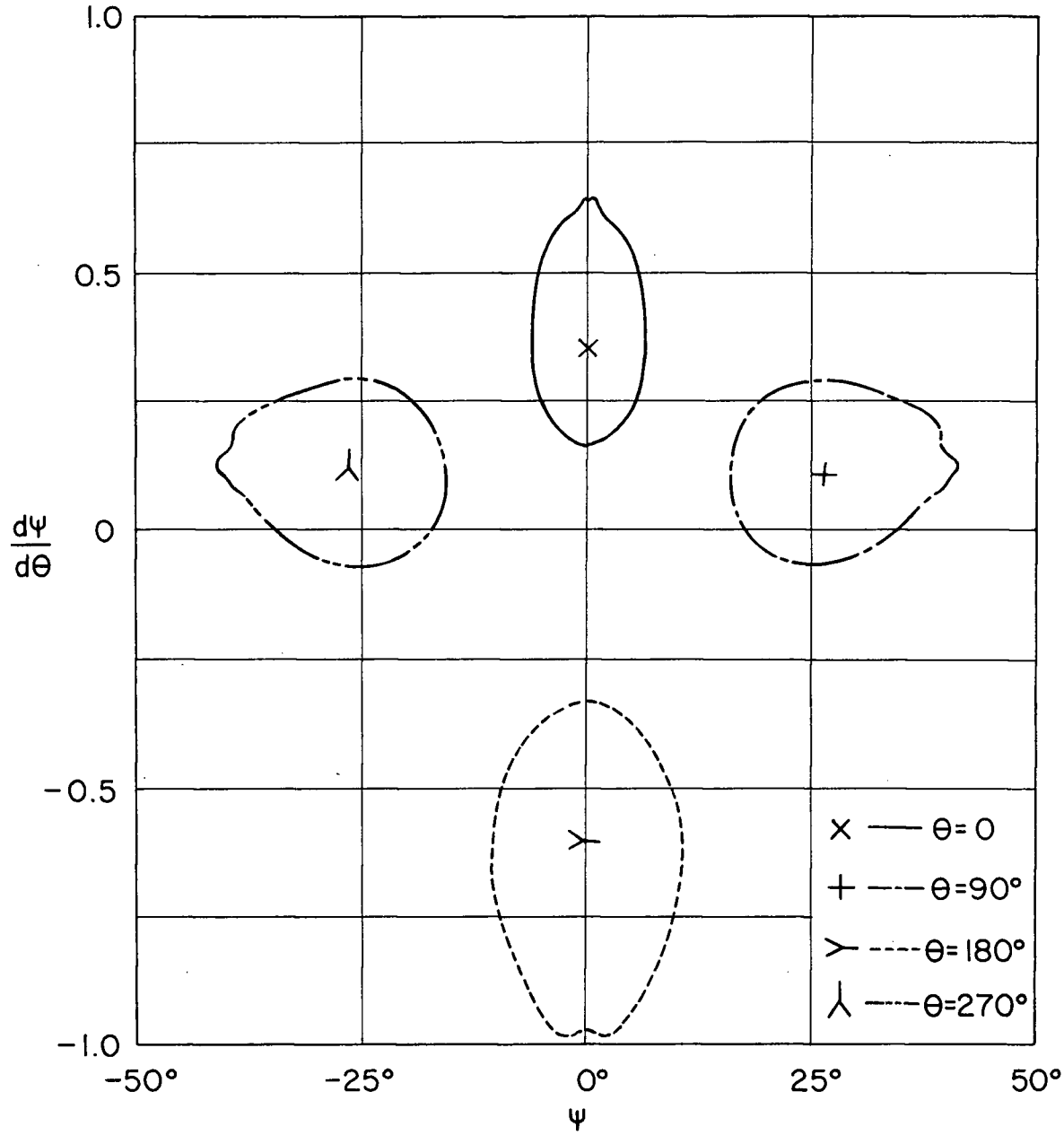

Figure 2-24 Cross-sections of an invariant surface at various orbit angles (K_i = 0.7, e = 0.2)

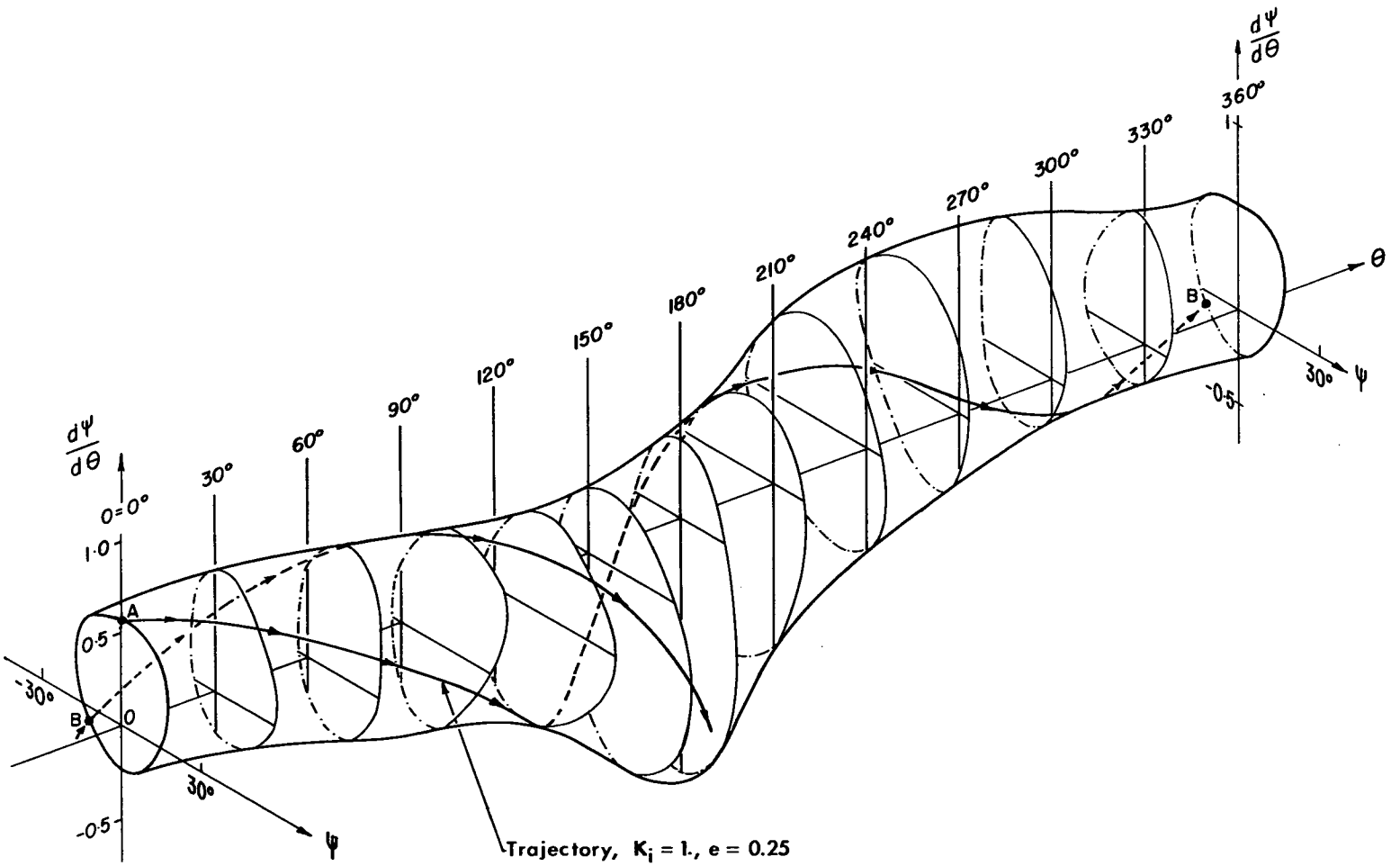

Figure 2-25-i Typical invariant surface (K_i = 1, e = 0.25)

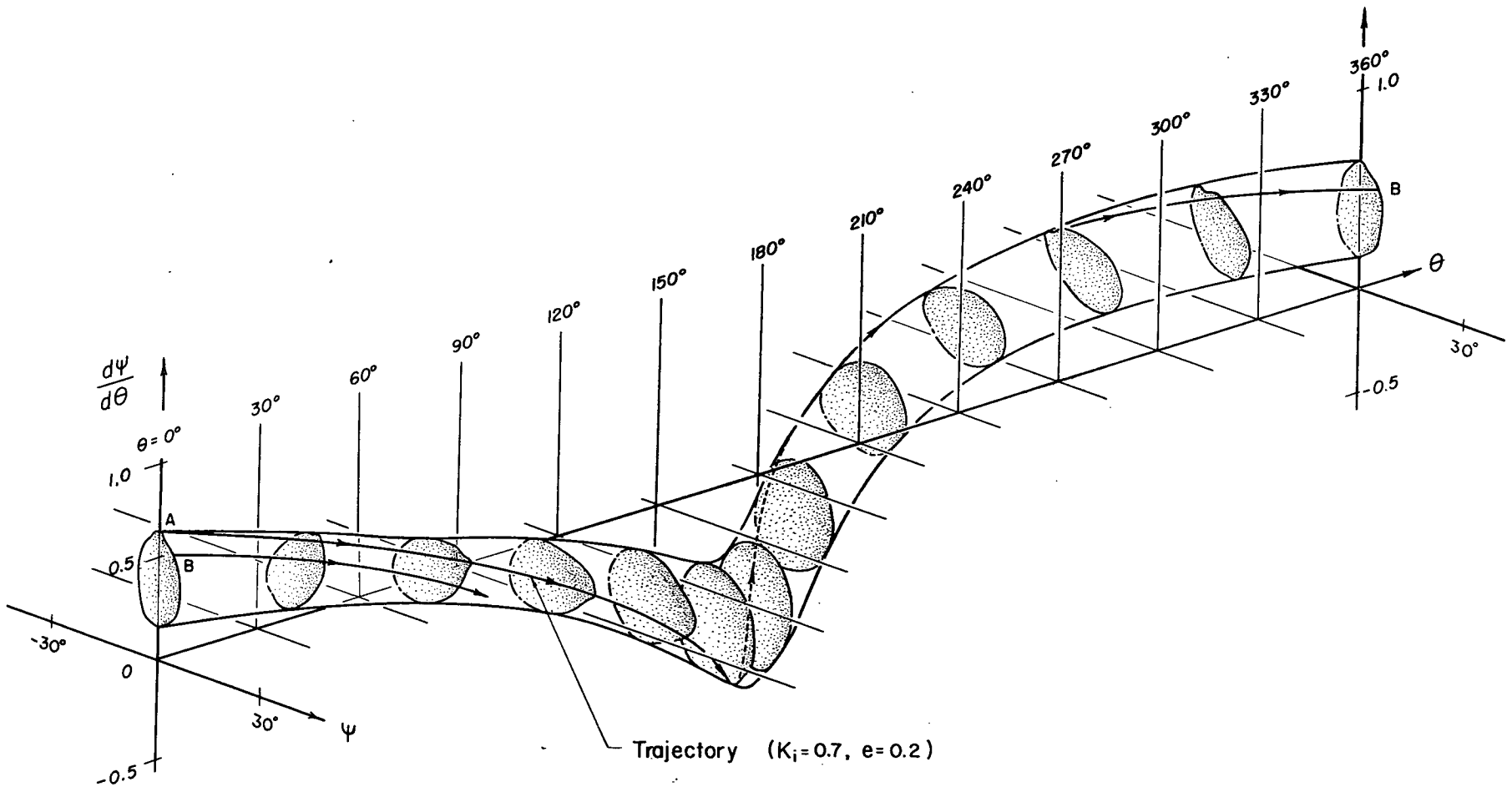

Figure 2-25-ii Typical invariant surface (K_i = 0.7, e = 0.2)

In this respect it is an improvement of the work of Zlatousov et al.[12]

The existence of an integral manifold raises doubts as to the applicability of Lyapunov's direct method in the determination of stability. In this method a Lyapunov V-function, which may be taken to be positive definite, is sought. According as its time derivative is negative definite, zero, or positive definite the motion is either asymptotically stable, neutrally stable, or unstable.

When an integral manifold exists, the point representing the state of motion always lies on the same surface. Therefore the motion must be neutrally stable. Hence the derivative of the V-function is identically zero and the V-function must be a constant of the motion. That is, the integral manifold is a surface on which the V-function is constant.

Near such a surface an approximate V-function will possess a time derivative of variable sign so that no information regarding stability can be obtained by an approximate analysis. On the other hand, the determination of the V-function with $dV/dt = 0$ is exactly equivalent to the determination of the integral manifold so that no saving in effort is to be expected.

Using an approximate V-function and requiring that the state vector be larger than some specified value, it is possible to estimate bounds on the conditions which lead to

instability. These bounds are only approximate and only the more exact numerically determined bounds are considered.

It is possible that a particular set of parameters (e, K_i) may be associated with more than one region of stability. This is illustrated in Figure 2-26. There is a single central "mainland" accompanied by one or more "islands." The smaller invariant surfaces wrap themselves around the main surface in a helical manner. The region between the surfaces represents unstable initial conditions.

The symmetry properties of the invariant surface provide a means of condensing considerable information into a single diagram. The line in phase space defined by the intersection of the planes $\psi = 0$ and $\theta = 0$ forms an axis of symmetry of the surface. The intercepts made by the limiting manifold on this line represent bounds that must be placed on the derivative for the given configuration ($\psi = \theta = 0$) to ensure stable motion. For a specified value of K_i the points of intersection can be plotted as a function of eccentricity (Figures 2-27-i to 2-27-vi). Qualitatively such a diagram measures the size of the region of stability.

The spikes in the diagrams indicate the presence of the secondary islands of stability discussed earlier. The irregular edges of the stable regions are caused by the presence of many additional small spikes. The Figures also indicate that the region of stability shrinks rapidly with increasing eccentricity. At some upper limit, e_{max}, the stability region shrinks to a point; or in the phase space

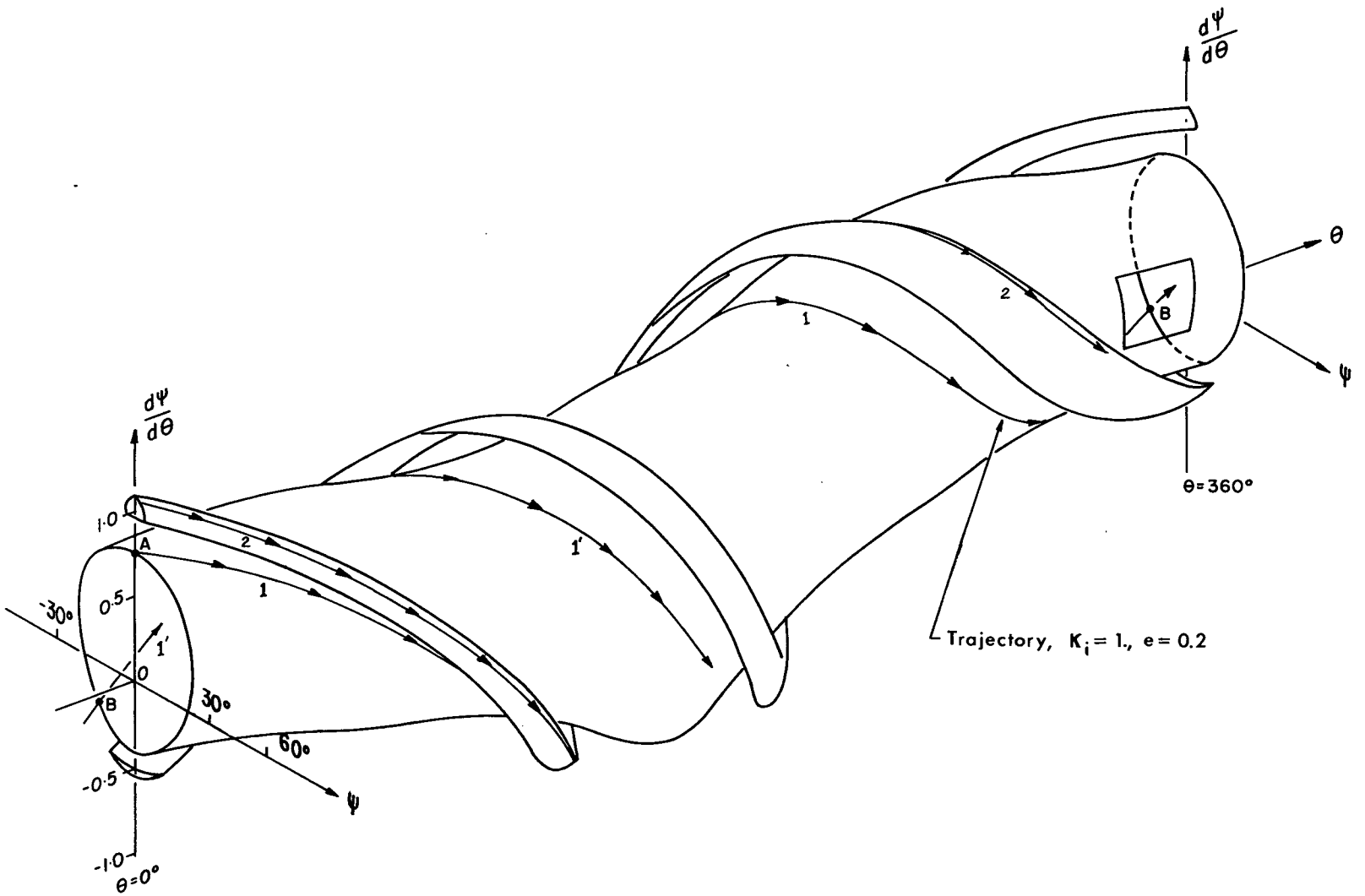

Figure 2-26 Typical invariant surface with "islands"

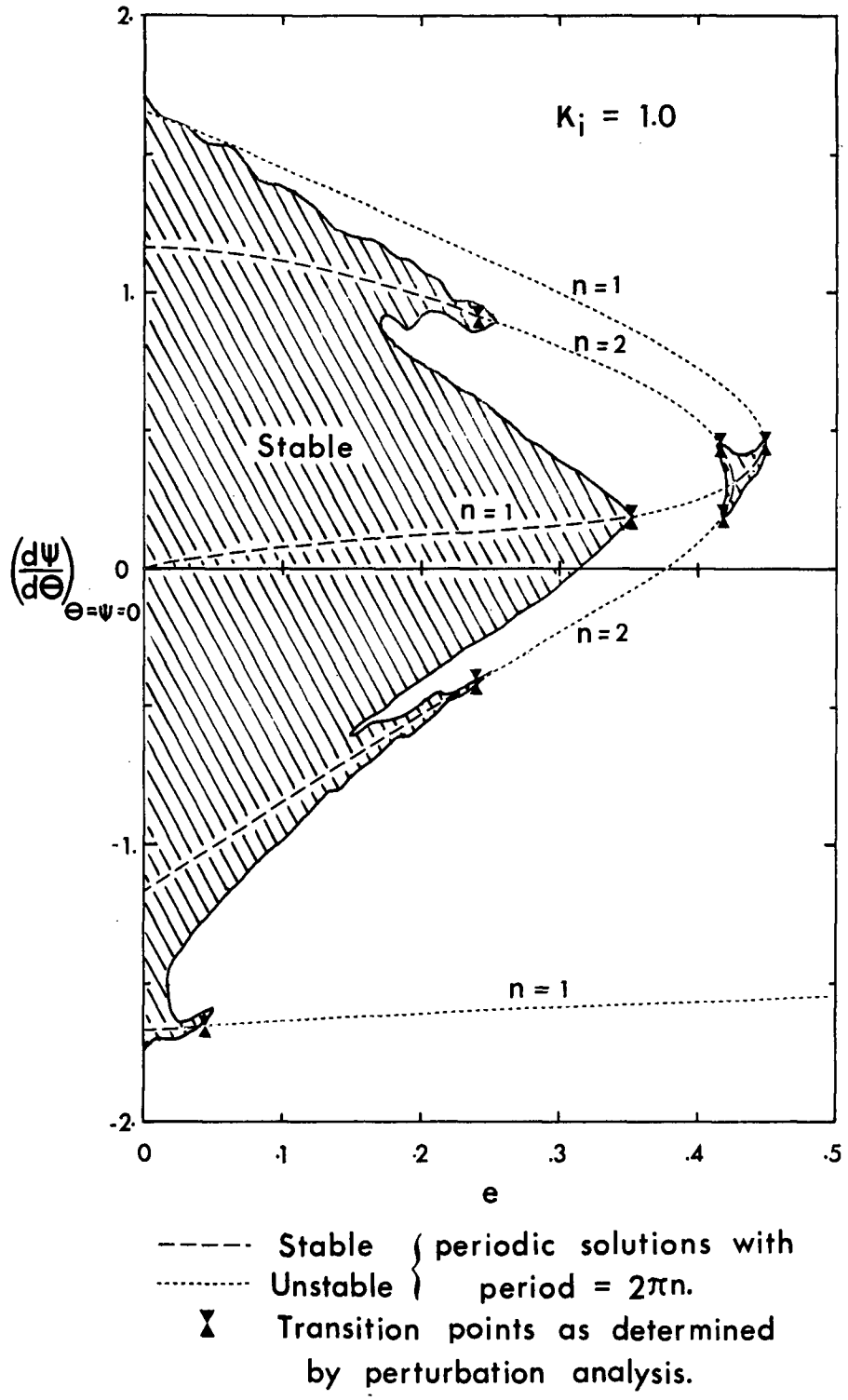

Figure 2-27-i Range of values of the derivative when $\psi = \theta = 0$ for stable motion ($K_i = 1.0$)

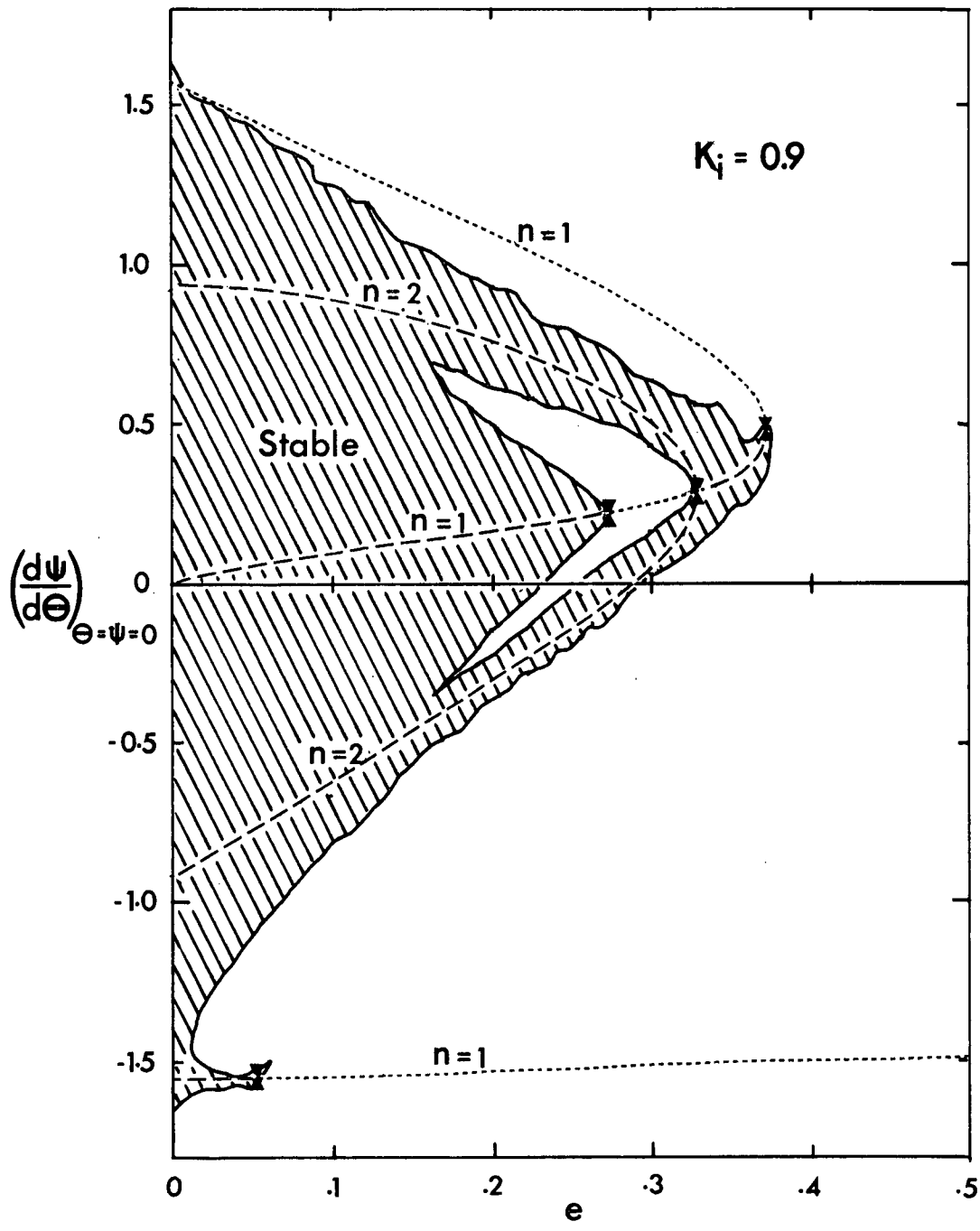

Figure 2-27-ii Range of values of the derivative when $\psi = \theta = 0$ for stable motion ($K_i = 0.9$)

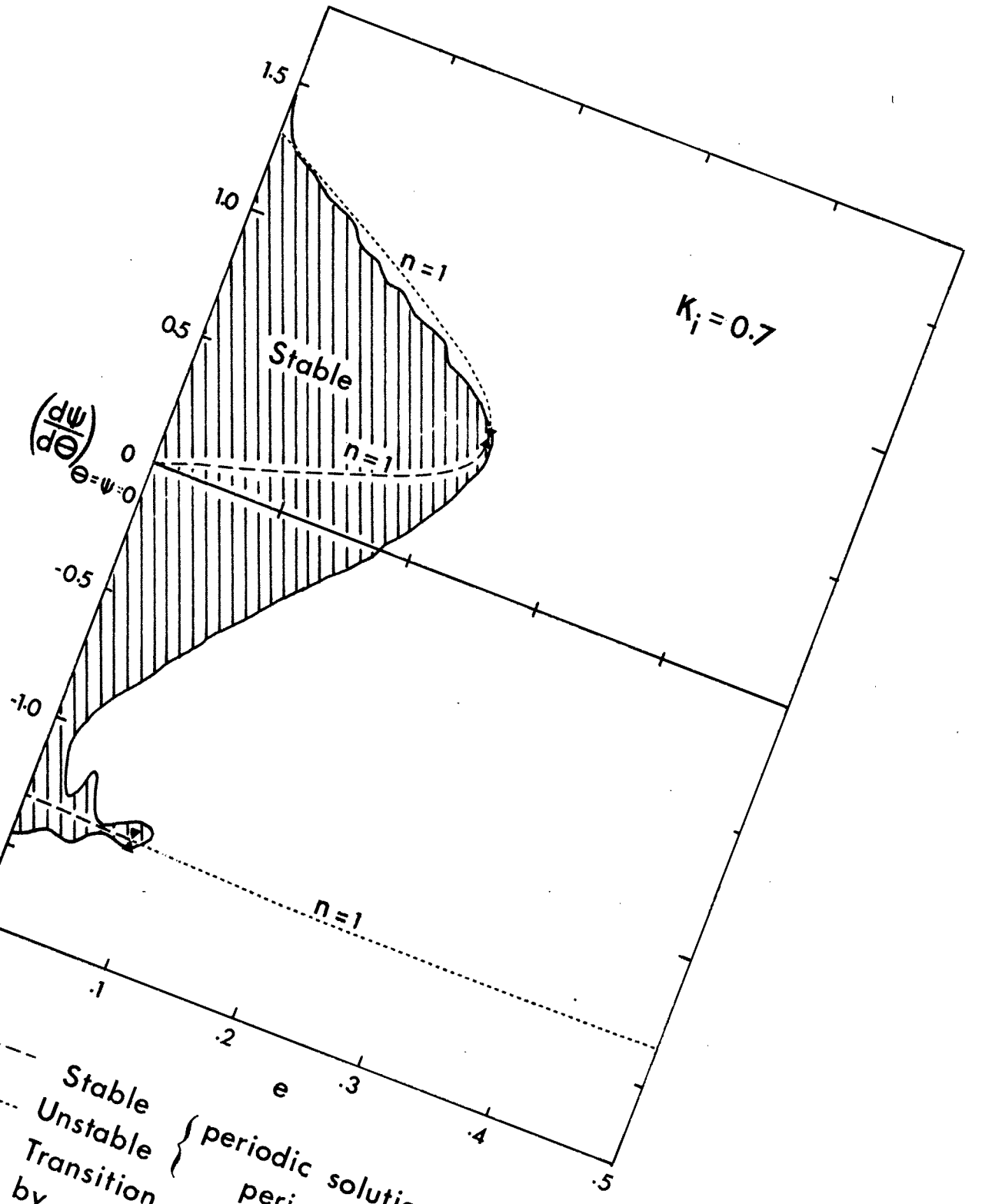

Figure 2-27-iii Range of values of the derivative when $\psi = \theta = 0$ for stable motion ($K_i = 0.7$)

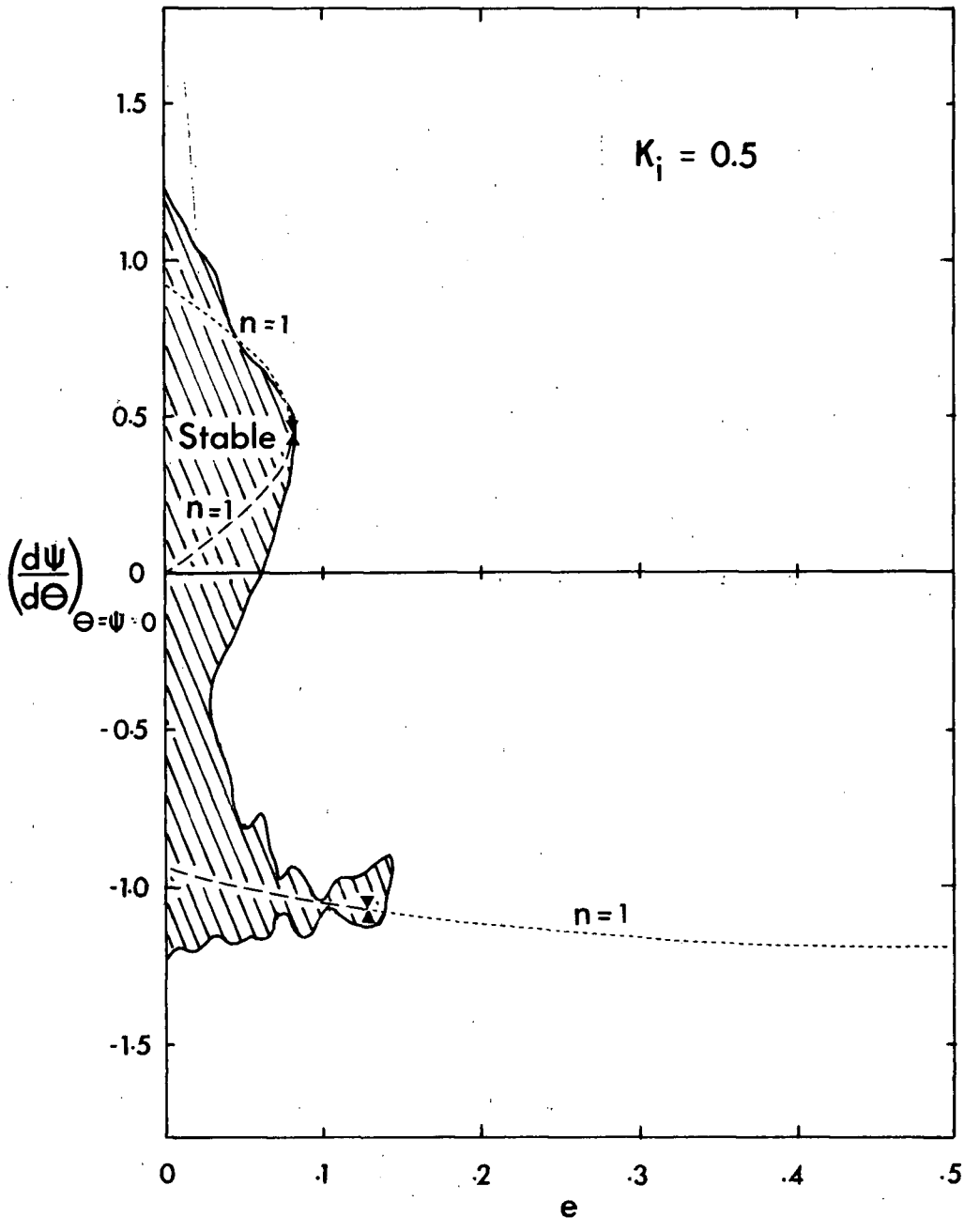

----- Stable } periodic solutions with
..... Unstable } period = $2\pi n$.

X Transition points as determined by perturbation analysis.

Figure 2-27-iv Range of values of the derivative when $\psi = \Theta = 0$ for stable motion ($K_i = 0.5$)

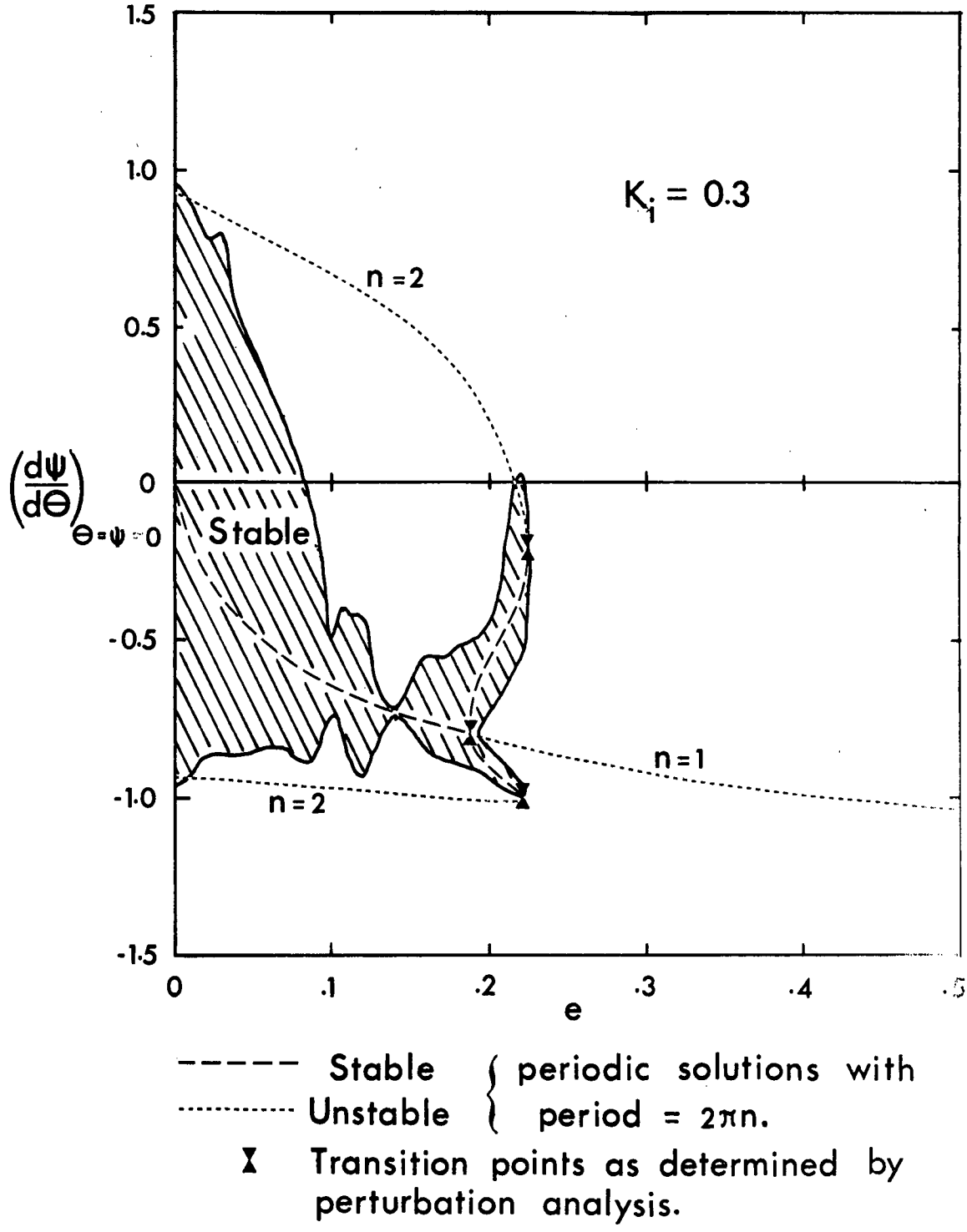

Figure 2-27-v Range of values of the derivative when $\psi = \theta = 0$ for stable motion ($K_i = 0.3$)

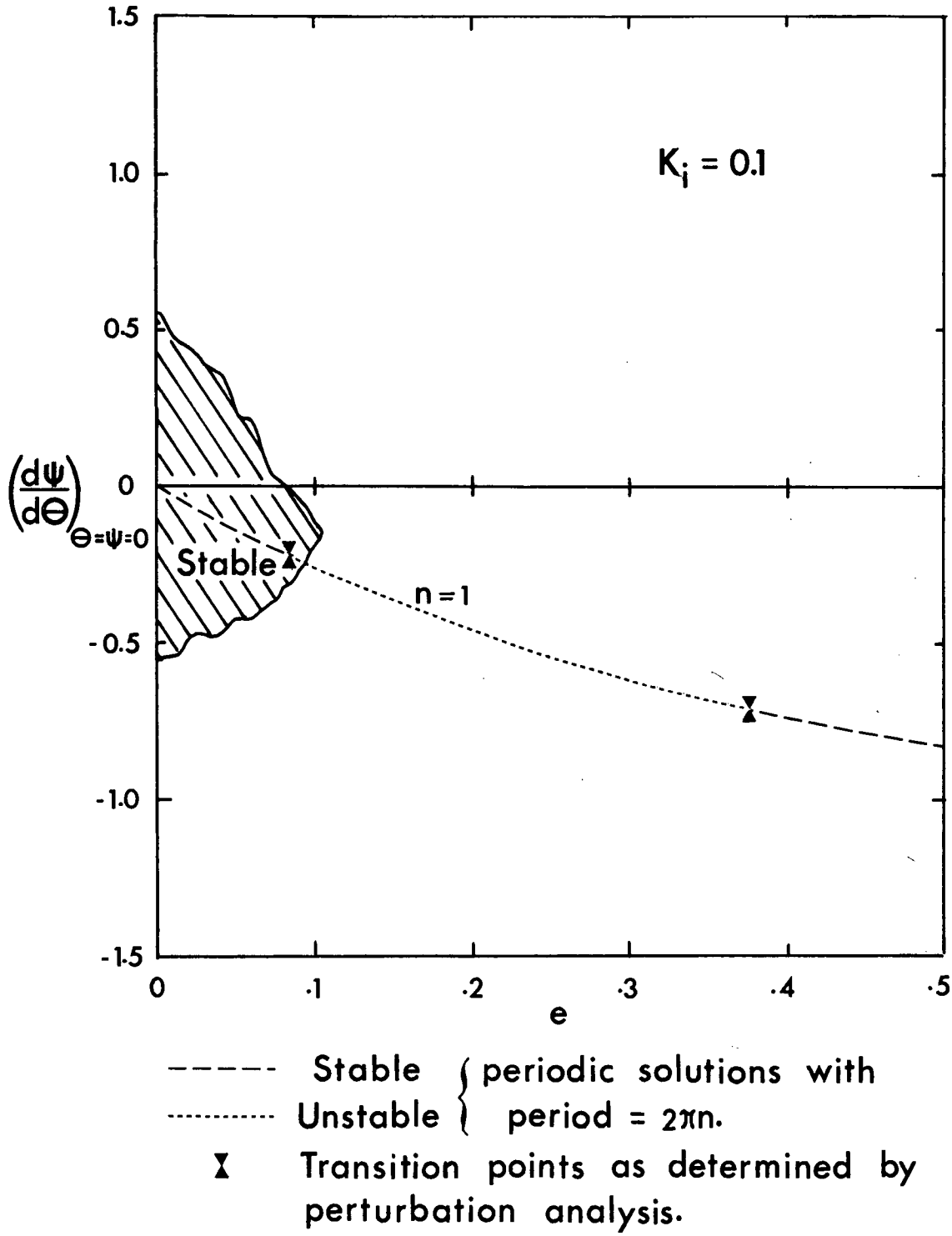

Figure 2-27-vi Range of values of the derivative when $\psi = \theta = 0$ for stable motion ($K_i = 0.1$)

representation the invariant surface degenerates to a single trajectory. Thus, beyond a certain critical value of eccentricity, stable motion is not possible. At still higher eccentricities, stability may return but the size of the region is so small as to be of no practical importance.

2.5 Accuracy of the Method

There are several sources of error in the method outlined in section 2.4. They are all due to the finite nature of the numerical process.

A large discrepancy may arise in the solution due to the truncation error of the numerical integration process and "roundoff" generated in the computer.

The truncation error varies as h^4 for the Adams-Bashforth and Runge-Kutta techniques employed.[33] The roundoff error, on the other hand, tends to increase as $1/h$. Thus there is an optimum step size which minimizes the total error. At times a situation may arise where the critical step size is too small for rapid computation and the resulting precision may not be essential for the analysis.

To illustrate this point, several step sizes were chosen for the integration of equation (2.14) over 30 orbits. The resulting values of the final conditions (Table II) indicate that the errors can be reduced to .0001 radians by employing a step size of 3°.

Figure 2-28-i presents the invariant curve in the $\theta = 0$ plane as given by the most accurate solution ($h = 1.5^{\circ}$).

TABLE II

The Effect of Varying Integration Step Size

Inertia parameter, K_i = 1.0

Orbit eccentricity, e = 0.1

Initial displacement, ψ_o = 0

Initial velocity, ψ_o' = 1.18

h Degrees	$\psi(60\pi)$ Radians	$\psi'(60\pi)$ -
30	Unstable after 4.5 orbits	
15	Unstable after 18.3 orbits	
7.5	-0.18556	1.12282
3	-0.18910	1.11949
1.5	-0.18911	1.11948

Also plotted in the Figure are selected points determined from the numerical solution obtained with h = 7.5°. It is interesting to note that the difference between the two cross-sections is much smaller than that between the two solutions indicated in Table II. Mitropolskiy[34] indicates that this is frequently observed in systems which possess integral manifolds. There does not appear to be a theoretical explanation for this behaviour, but it does permit the use of large step sizes. Although the resulting solutions have large errors the invariant surfaces are usually of sufficient accuracy. The errors appear to cause displacements around the manifold rather than normal to it.

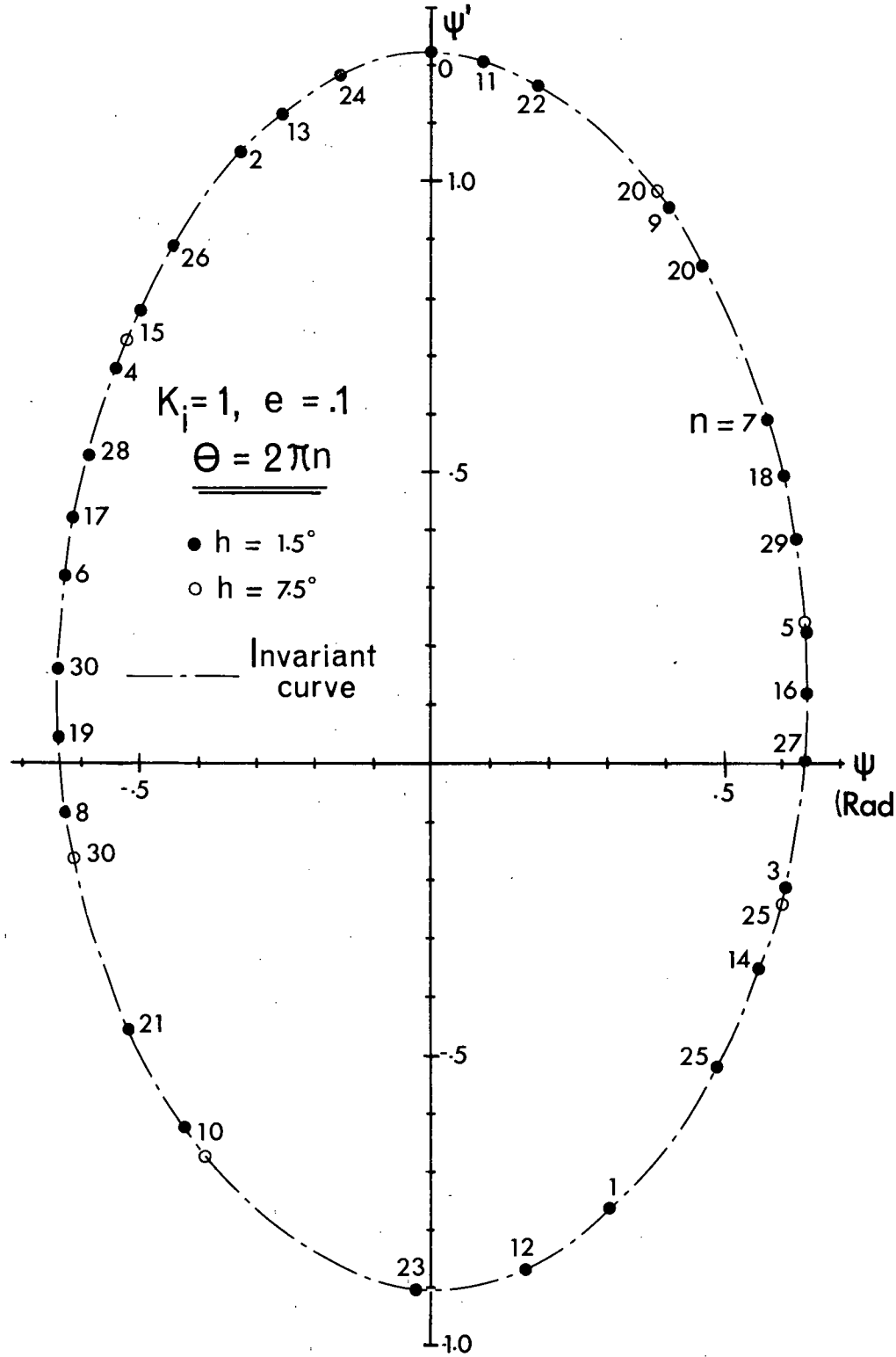

Figure 2-28-i Comparison of the invariant surfaces generated using different integration step sizes (Non-limiting surface)

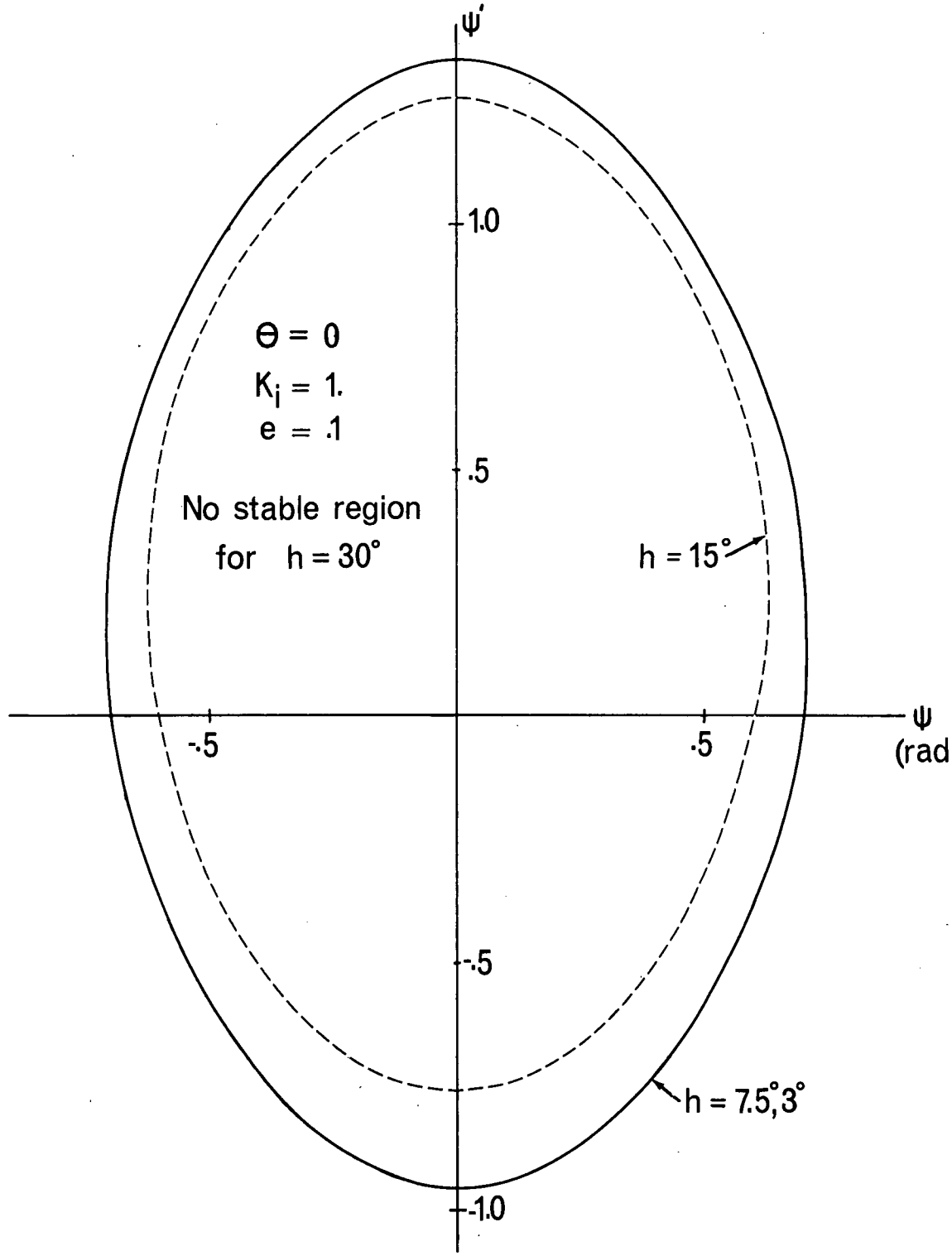

Figure 2-28-ii Comparison of the invariant surfaces generated using different integration step sizes. (Limiting surfaces)

The determination of the limiting invariant surface involves additional difficulties. Here, even a small discrepancy can lead to erroneous results regarding stability. As indicated by Table II the errors bring about early instability and hence cause the size of the limiting invariant surface to be underestimated (Figure 2-28-ii).

The results suggest that any error which displaces the representative point into the unstable region leads to further growth of this error. Any subsequent error which acts towards the stable region will have to be somewhat larger than the original error to regain stability. On the other hand, the effect of an error which takes the representative point into the stable region may be immediately cancelled by an error of the same size but in the opposite sense. Thus, assuming that both kinds of error are equally probable, there will be a drift towards instability from a thin "skin" which lies inside the limiting invariant surface. In the majority of cases studied this tendency towards instability was noted.

A second error in the determination of the limiting manifold is due to the termination of the numerical integration after a finite time. This may result in an unstable solution appearing stable. Careful plotting of the results can usually detect any tendency of this type. This error acts to increase the size of the limiting invariant surface.

Thirdly, the process of numerical experimentation is

necessarily discrete. That is, bounds can be placed on initial conditions which separate stable and unstable solutions. These bounds may be made as fine as desired providing sufficient computing time is used. There is, therefore, a practical limit to the precision with which the limiting manifold can be determined. This results in the numerically evaluated limiting manifold lying inside the true one.

The majority of the numerical integrations were performed using a step size of 7.5°. The resulting limiting surfaces were compared with more exact results in several cases using the data at $\theta = \psi = 0$ as a standard. The results with $h = 7.5^{\circ}$ lay within -.07 and +.05 units in of the more precise results. In the majority of cases the error was less than .03 units.

2.6 The Significance of Periodic Solutions

2.6.1 The Relationship Between Manifolds and Periodic Solutions

In section 2.4 it was shown that an initial condition chosen inside a specific manifold results in the generation of a new manifold which lies completely within the first. A succession of initial conditions may thus be chosen which determine progressively smaller manifolds, finally resulting in a surface which has zero cross-section. Because of the periodicity exhibited by the invariant surface, this manifold must then represent a periodic solution. Hence periodic solutions act as spines upon which the invariant surfaces are

built. The general motion can then be thought of as a bounded perturbation about the appropriate periodic solution.

The numerical results presented in section 2.4 indicate that with increasing eccentricity the size of the limiting invariant surface shrinks. Ultimately, the cross-section becomes a set of points so that the manifold degenerates into a periodic solution. The importance of the periodic solutions is now evident; as at the largest orbit eccentricity for stable motion the only available solution is a periodic one. Because at this critical value of eccentricity the invariant surface is infinitesimal in size, the linear perturbation analysis should correctly predict a change from stable to unstable perturbations. The maximum eccentricity for stable motion can thus be determined with great precision by the variational analysis of the appropriate periodic solution.

The details of the analysis were presented in section 2.3.3 and the limiting values of eccentricity were plotted in Figures 2-18 and 2-19. They are also indicated in Figures 2-27-i to 2-27-vi to compare the accuracy of the strictly numerical search for the limiting manifold with the more theoretical determination of the characteristic exponents. The agreement is quite good, but tends to become poorer as K_i decreases. This is due to a multiplicity of periodic solutions appearing and disturbing the numerical search near the maximum eccentricity. Because the numerical integrations involved are performed only over finite intervals and are not

"open ended" as in the case of the numerical search, the accuracy may be improved to any desired degree. These results also explain the apparently anomolous behaviour of the region of stability between $K_i = 0.5$ and 0.3. Figures 2-7 and 2-18 indicate that the upper spike disappears with decreasing K_i (it can be shown that the spike vanishes for $K_i = 1/3$) while the lower one continues to grow until $K_i \approx 0.25$.

Occasionally unstable periodic solutions appear inside the manifold cross-sections. Figure 2-29 presents several cross-sections of invariant surfaces evaluated for $K_i = 1$, $e = .2$. The closed curves surround stable periodic solutions and the pointed invariant plots are associated with unstable solutions. This is in agreement with the analysis (section 2.3.3) where it was shown that the perturbations lie along ellipses or hyperbolae in the vicinity of the periodic solutions. In the stroboscopic phase plane stable periodic solutions appear like centres while the unstable periodic solutions have the appearance of saddle points. Thus the inspection of the periodic solutions provides qualitative information concerning the nature of the stroboscopic phase plane and hence of the motion.

2.6.2 Determination of a Complete Set of Periodic Solutions

Section 2.2.2 indicated the existence of periodic solutions that could be represented as a sine series. An extensive numerical search for these solutions resulted in the

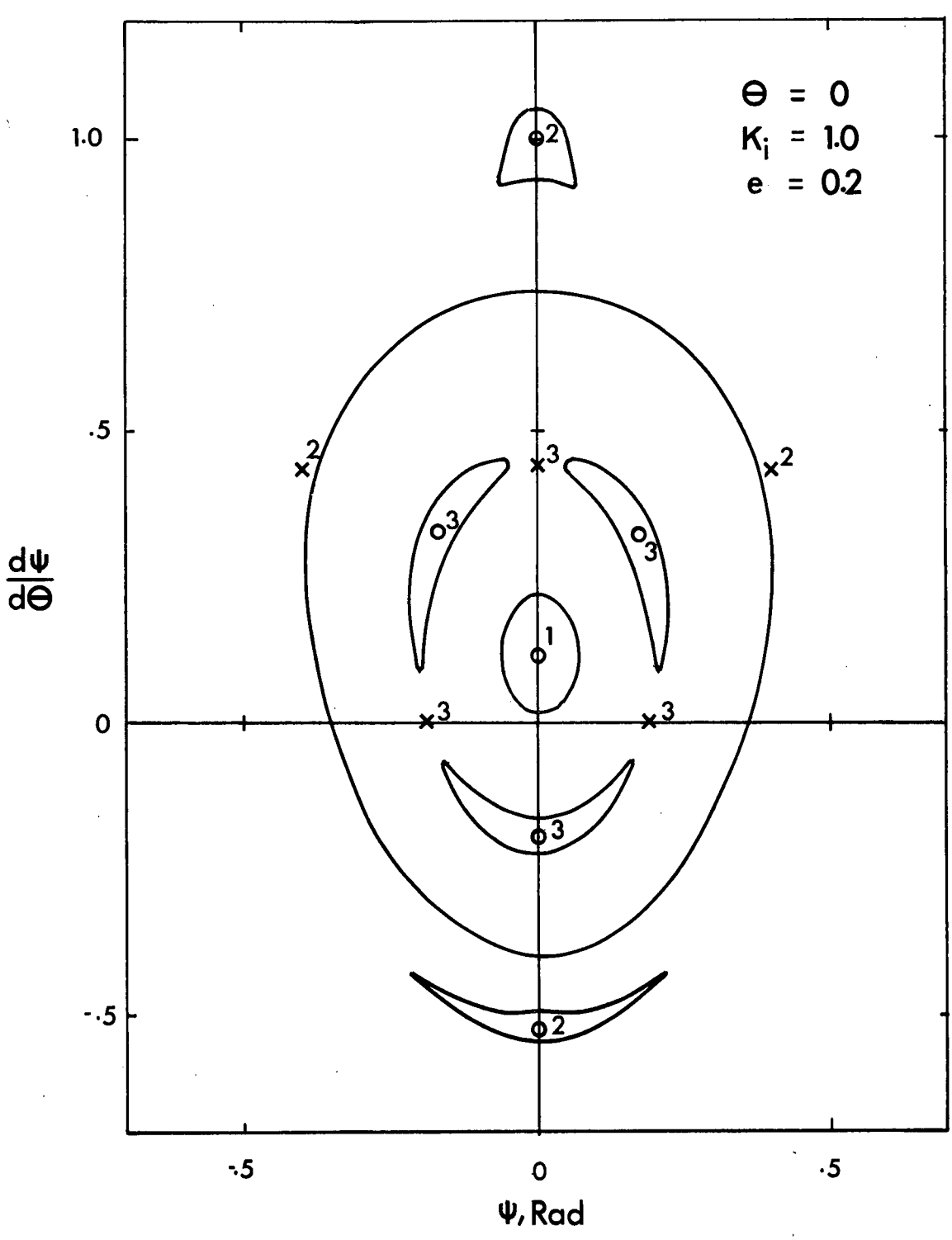

Figure 2-29 Invariant surface illustrating the appearance of stable and unstable periodic solutions in the stroboscopic phase plane

data presented in section 2.2.3. No attempt was made, however, to determine if the solutions obtained constituted a complete set. The importance of periodic solutions in determining the limiting values of eccentricity and the general shape of the invariant surfaces makes the knowledge of a complete set desirable.

Earlier the process of integration of equation (2.14) from $\theta = 0$ to $\theta = 2\pi n$ was described as a transformation between the two planes. In terms of such a transformation, a periodic solution appears as a fixed point. Thus enumeration of a complete set of periodic solutions requires the determination of all the fixed points of the transformation. Although this is a simple concept it involves an enormous amount of work because of the large number of trajectories which must be computed.

Figure 2-30 presents for $K_i = 1$, $e = 0$, contours in the $\theta = 2\pi$ plane which correspond to lines of constant ψ in the $\theta = 0$ plane. A curve may be drawn which passes through those points such that ψ is invariant under the transformation. The corresponding plots for constant ψ' are shown in Figure 2-31.

The points of intersection of the ψ -invariant and the ψ'-invariant curves constitute a complete set of fixed points for the given values of the parameters (Figure 2-32). Note that because the eccentricity is zero, there are an infinite number of invariant points which define a closed

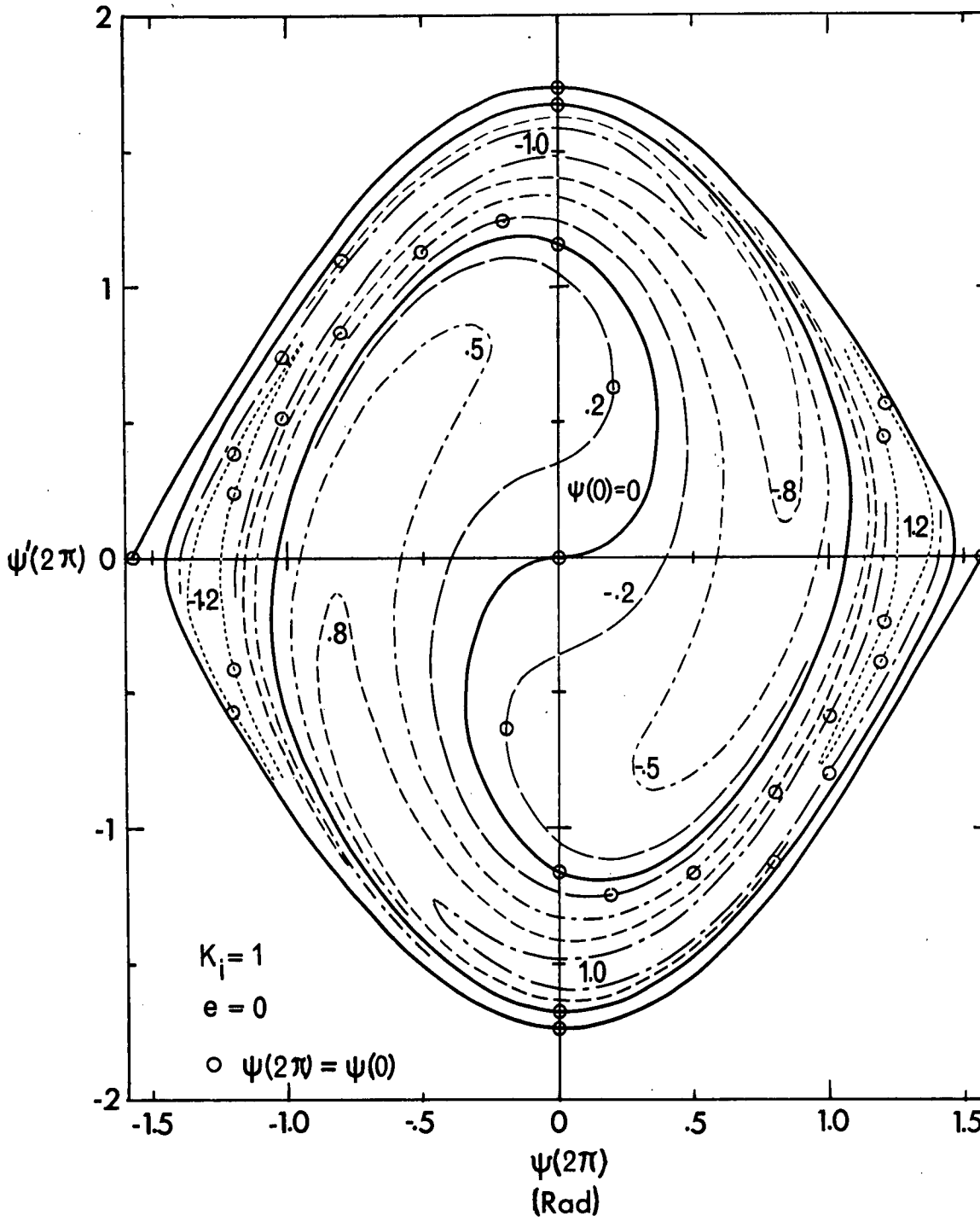

Figure 2-30 The transformation of lines of constant ψ when the equation of motion is integrated over 2π ($K_i = 1$, $e = 0$)

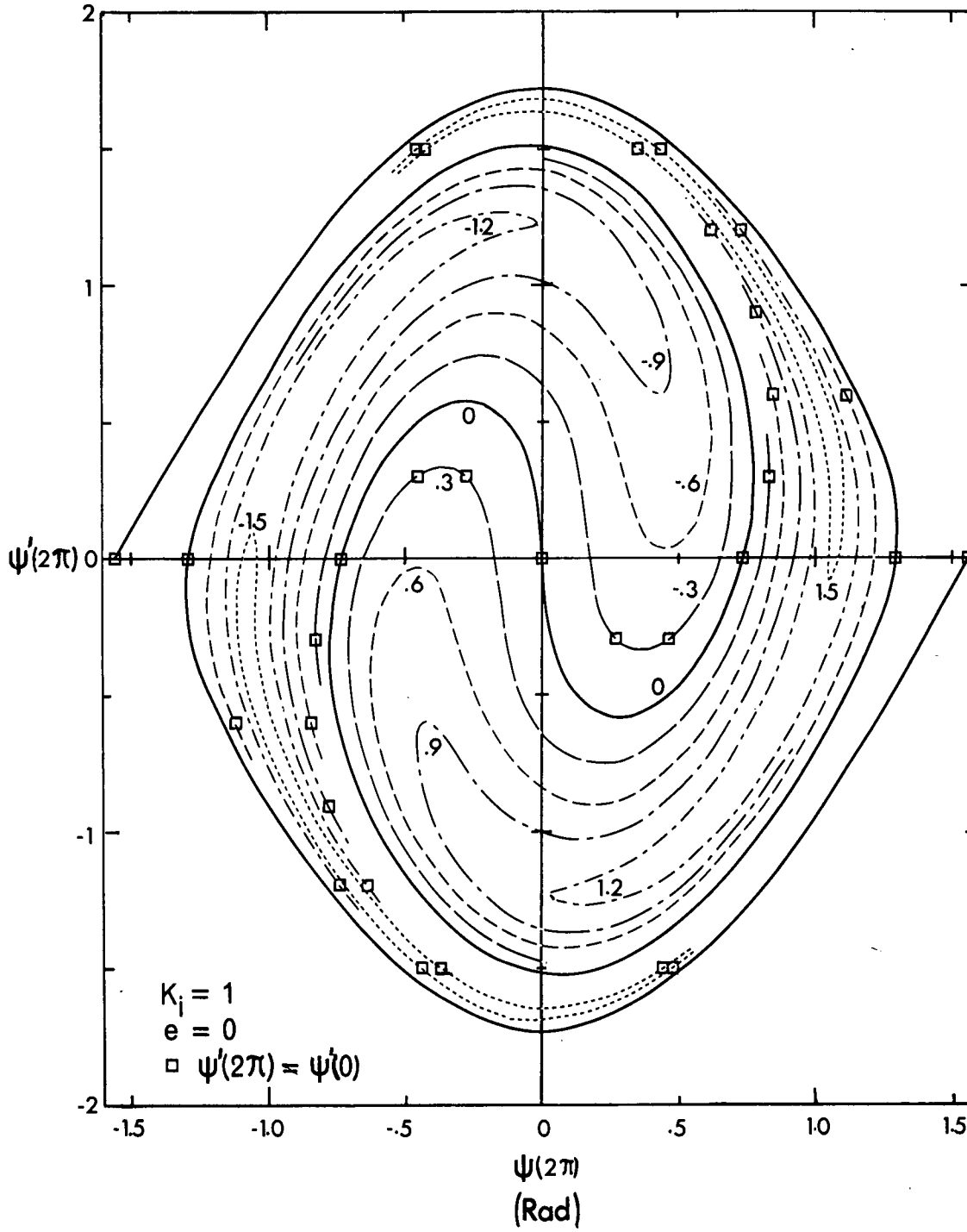

Figure 2-31 The transformation of lines of constant ψ' when the equation of motion is integrated over 2π ($K_i = 1$, $e = 0$)

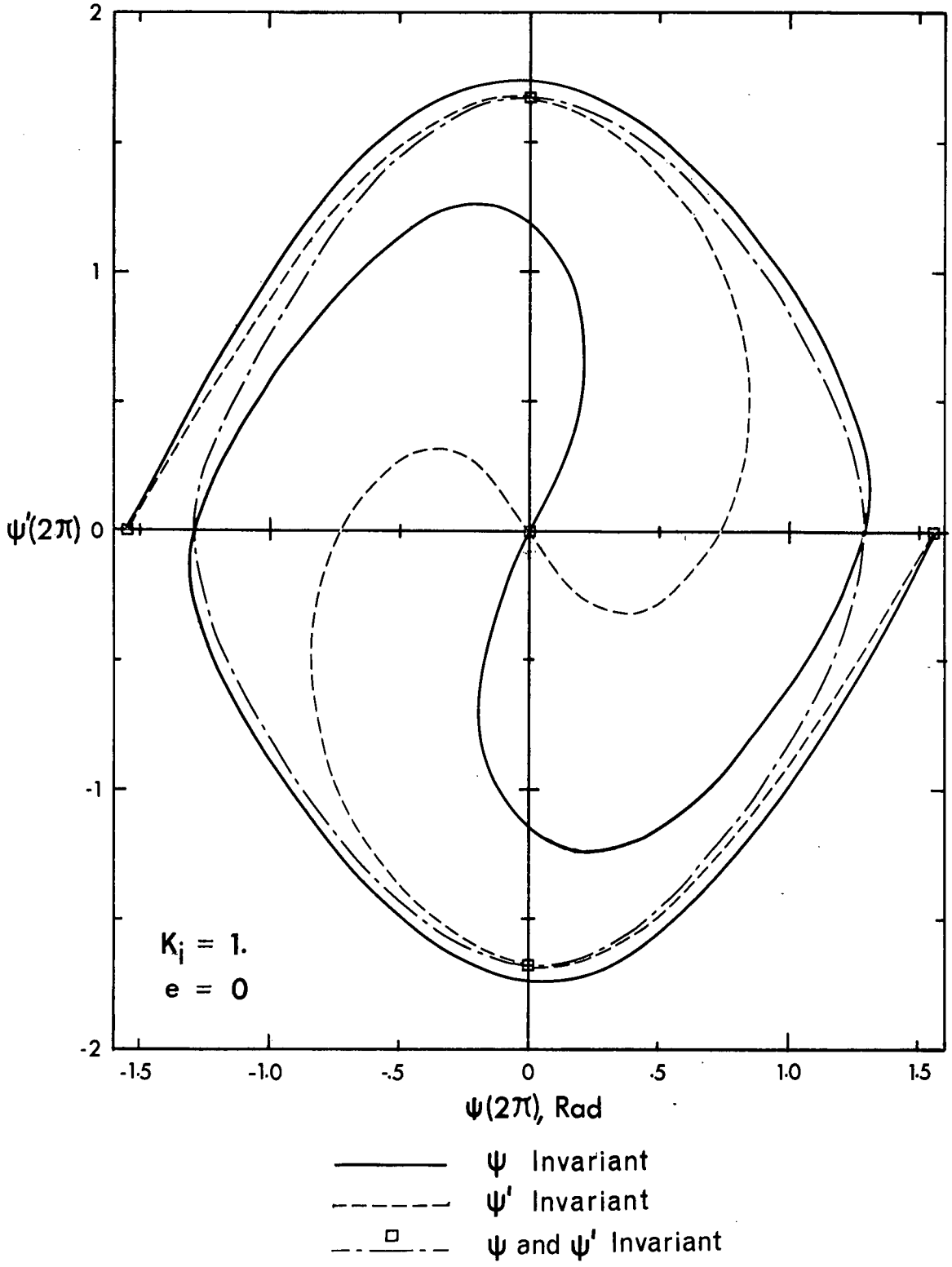

Figure 2-32 Determination of a complete set of fixed points of the transformation ($K_i = 1$, $e = 0$)

curve. This is consistent with the exact solution arrived at in section 2.2.1.

Figures 2-33, 2-34, and 2-35 present the corresponding set of curves for $K_i = 1$, $e = 0.1$. In this case the three solutions on the ψ'-axis are immediately evident. Because the transformation studied is for $n = 1$, these three solutions also lie on the ψ'-axis at $\theta = \pi$ and hence are also members of the second family of periodic solutions. There are also solutions of the third family at $\psi = \pm\pi/2$ as indicated by Zlatousov et al.[12]

No other periodic solutions exist so that those determined in section 2.2.2 form a complete set for $n = 1$.

2.6.3 The Degree of Stability

As already mentioned, any state of motion within the region of stability will give rise to a surface which lies within the limiting surface at all times. Since the major disturbances are essentially stochastic in nature, the distance between the surface corresponding to the actual motion of the satellite and the limiting surface would be a measure of the long term stability. Further, since the phase space representation shows that the various surfaces are nested, this distance becomes a maximum when the surface becomes as small as possible, i.e. a single trajectory. This state corresponds to a periodic motion of the satellite with period 2π.

The necessary momentum change at $\theta = 0$ can be obtained

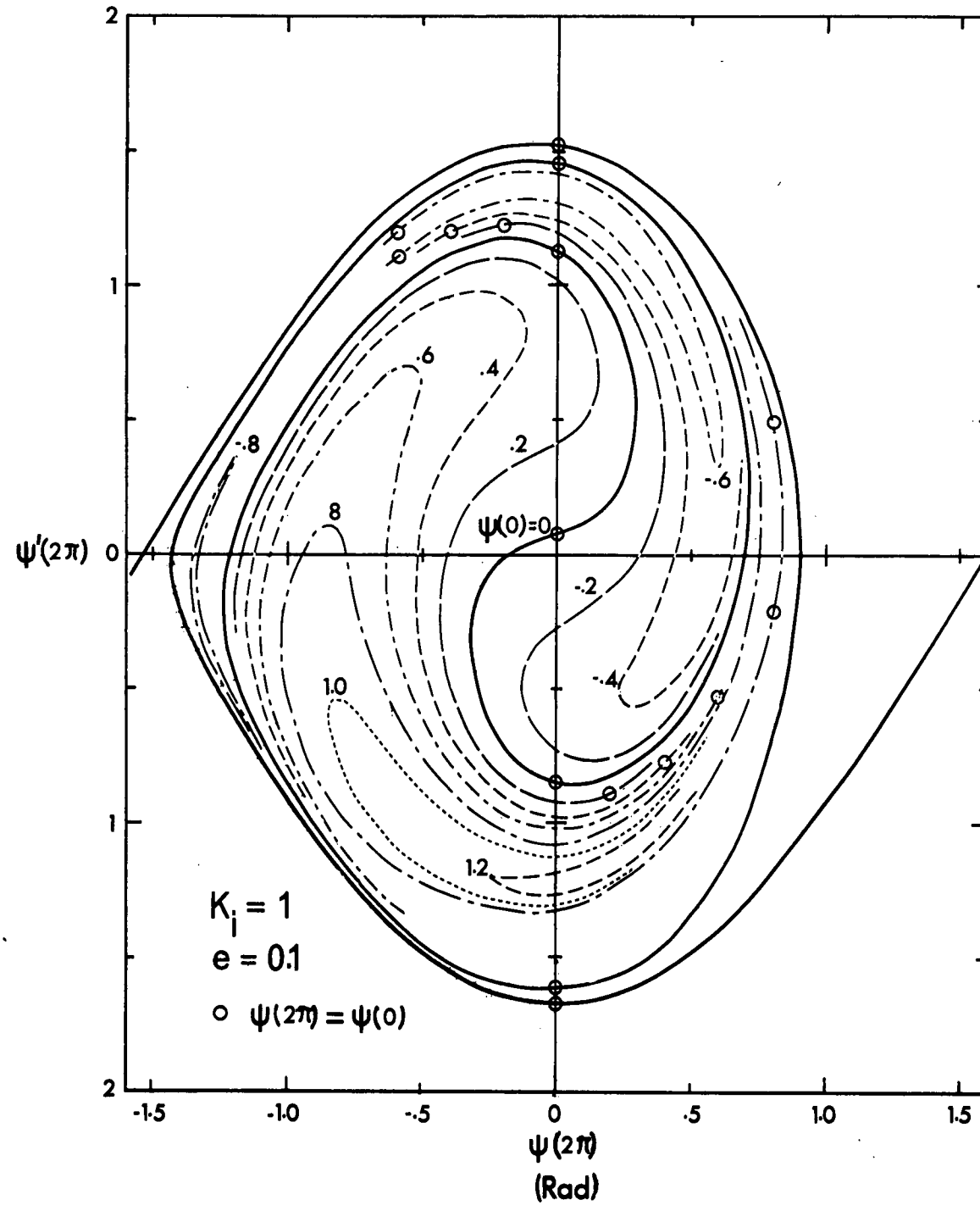

Figure 2-33 The transformation of lines of constant ψ when the equation of motion is integrated over 2π ($K_i = 1$, $e = 0.1$)

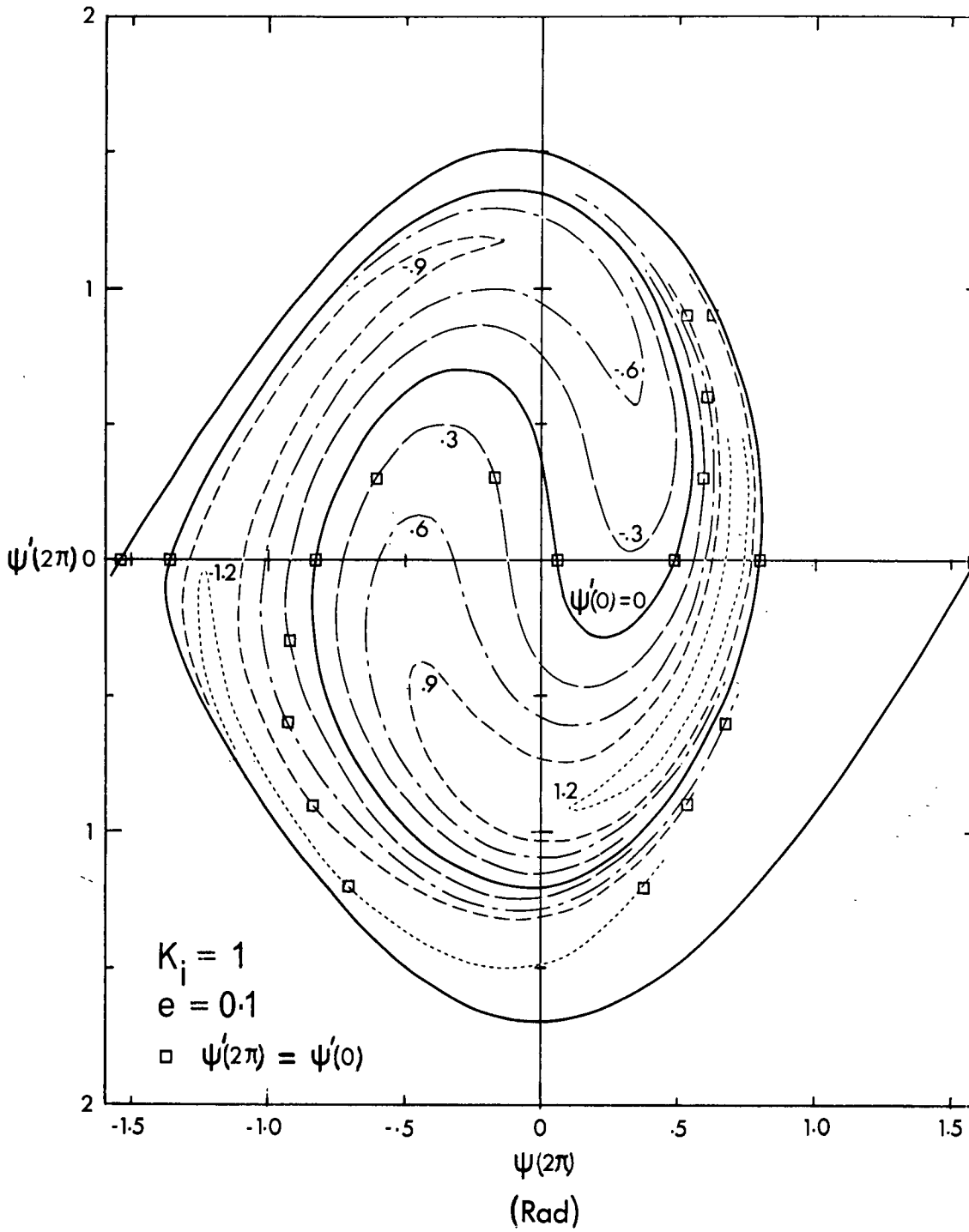

Figure 2-34 The transformation of lines of constant ψ' when the equation of motion is integrated over 2π ($K_i = 1$, $e = 0.1$)

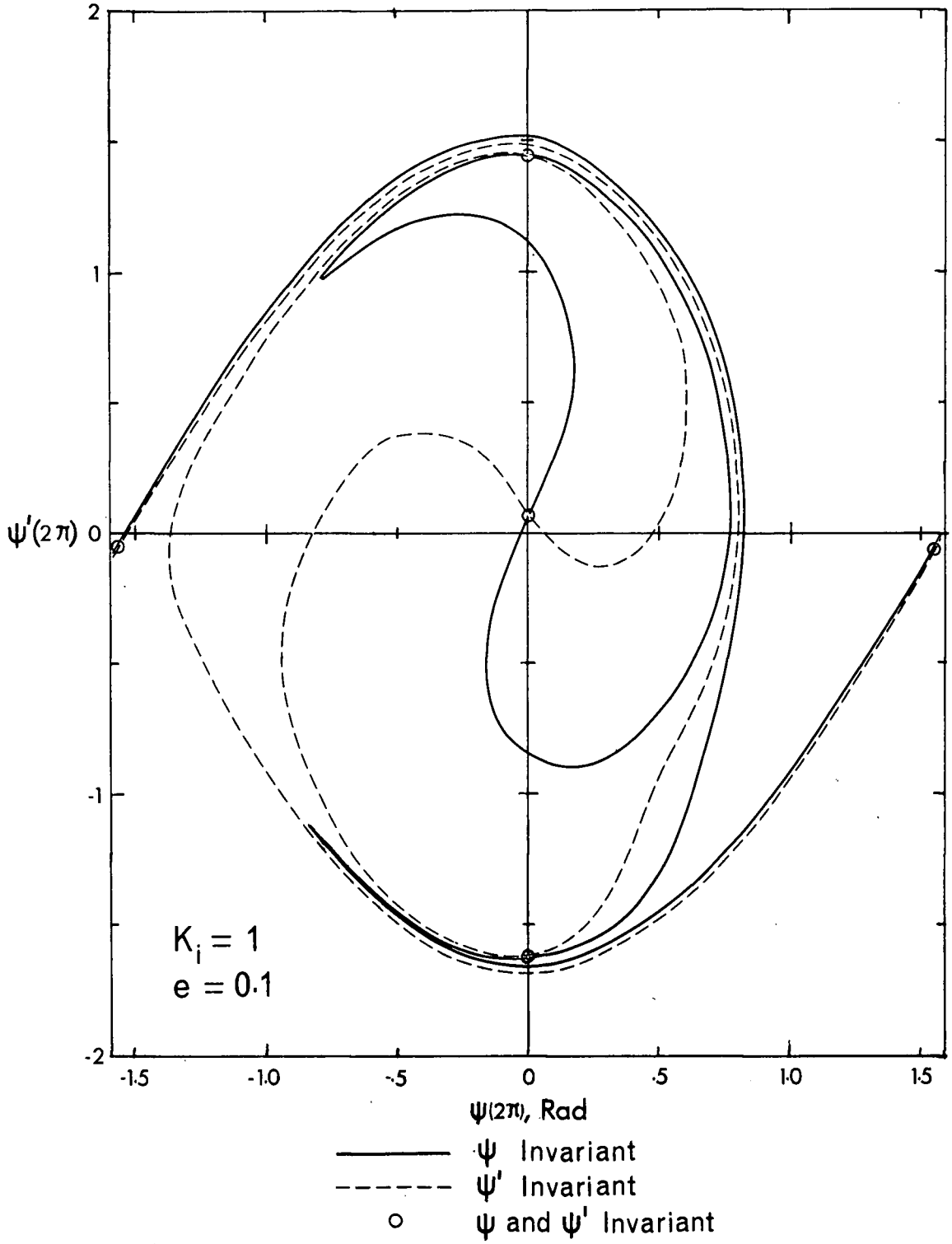

Figure 2-35 Determination of a complete set of fixed points of the transformation (K_i = 1, e = 0.1)

from Figures 2-27-i to 2-27-vi. The plots in Figures 2-36-i through 2-36-vi present the size of the destabilizing impulse as a function of orbit angle for several values of eccentricity and inertia parameter. Only the largest invariant surfaces have been used to prepare these diagrams. Moreover, the presence of spikes has been ignored so that the margin of stability shown in the Figures represents a conservative estimate. It is apparent that orbit angle does not affect the degree of stability greatly. Eccentricity of the orbit, on the other hand, is a powerful destabilizing factor. Values of e greater than 0.15 lead to a substantial loss of stability.

2.7 Concluding Remarks

The essential features of the analysis presented in this chapter and the conclusions based on them may be summarized as follows:

(i) The analysis demonstrated the existence of various periodic solutions which may be determined by analytical or numerical means.

(ii) The concept of a three dimensional phase space has been introduced. This has the valuable property that the trajectories described in the phase space by the representative points are unique and non-intersecting.

(iii) The periodic solutions appear as helical trajectories in the phase space. The general character of the motion is displayed by the integral manifolds which have been determined numerically. The manifolds are also non-

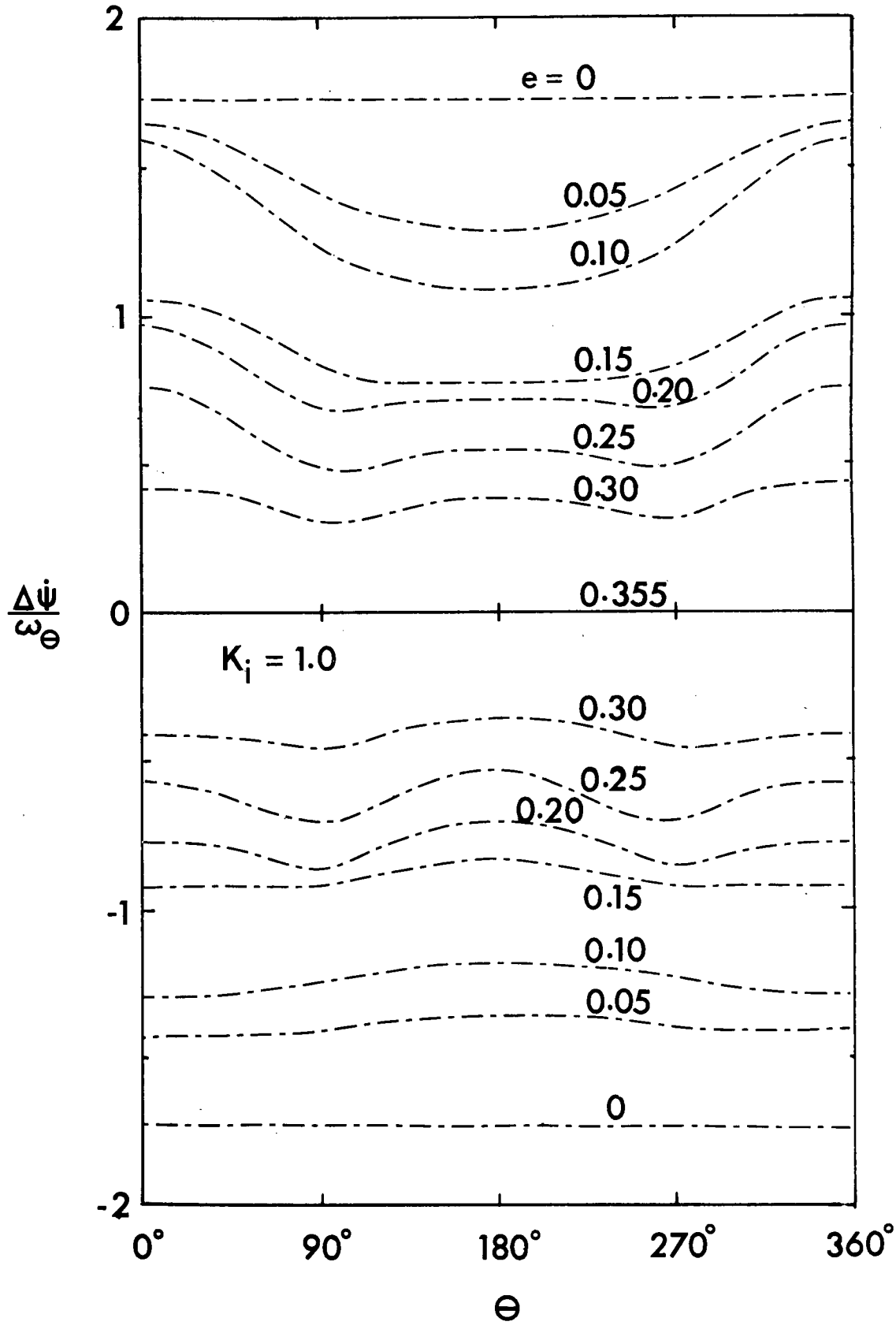

Figure 2-36-i Maximum momentum change required to destabilize a satellite (K_i = 1.0)

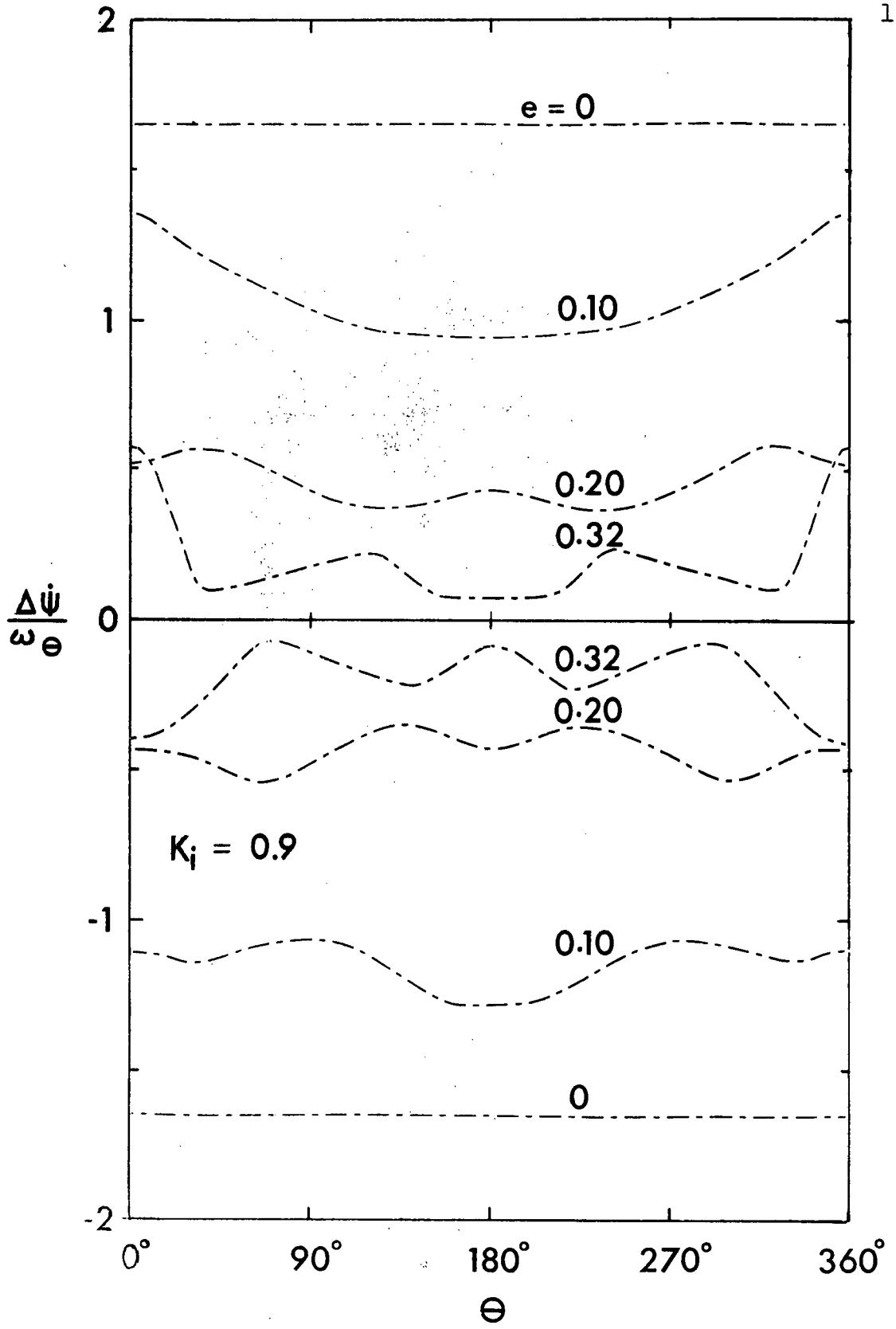

Figure 2-36-ii Maximum momentum change required to destabilize a satellite (K_i = 0.9)

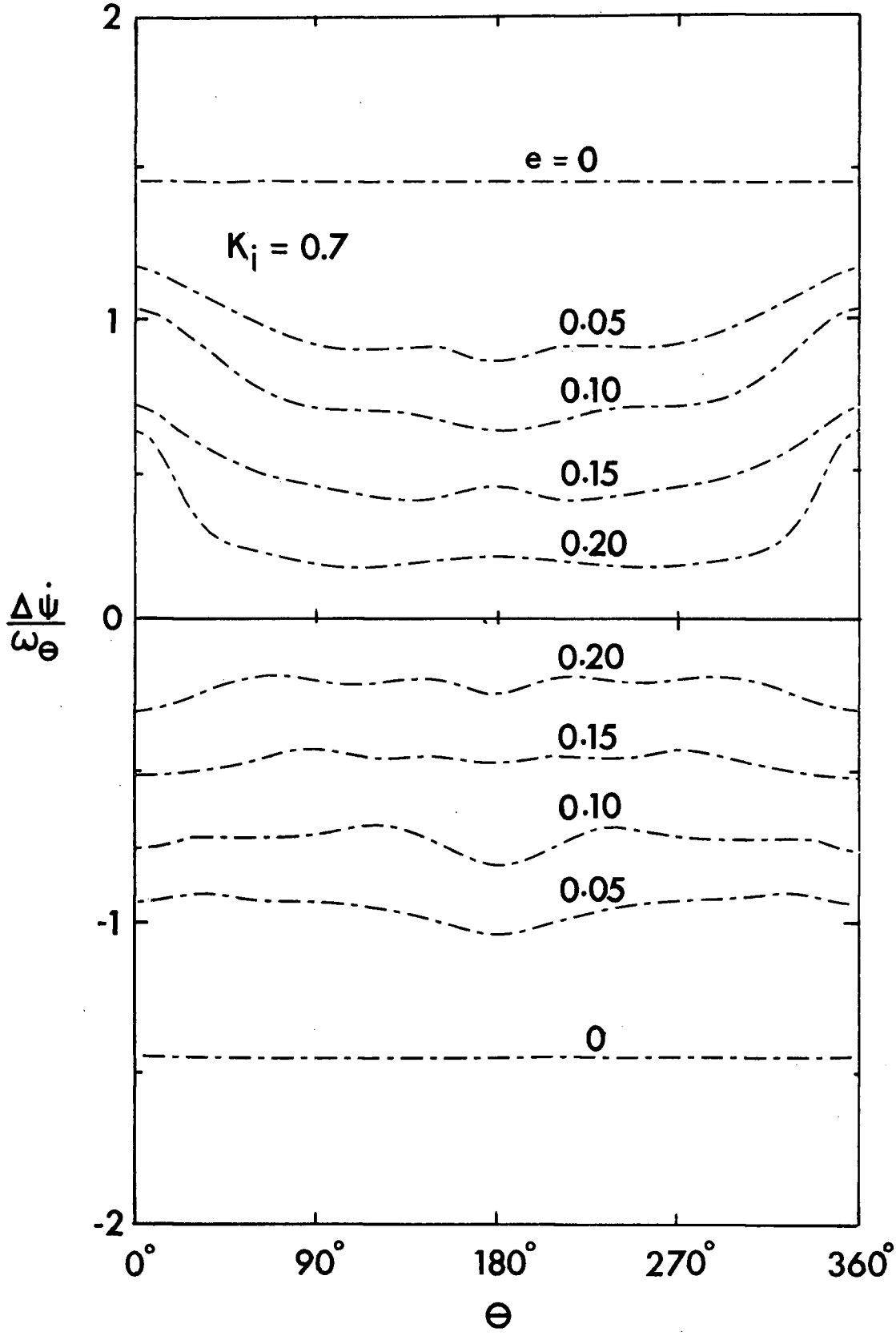

Figure 2-36-iii Maximum momentum change required to destabilize a satellite (K_i = 0.7)

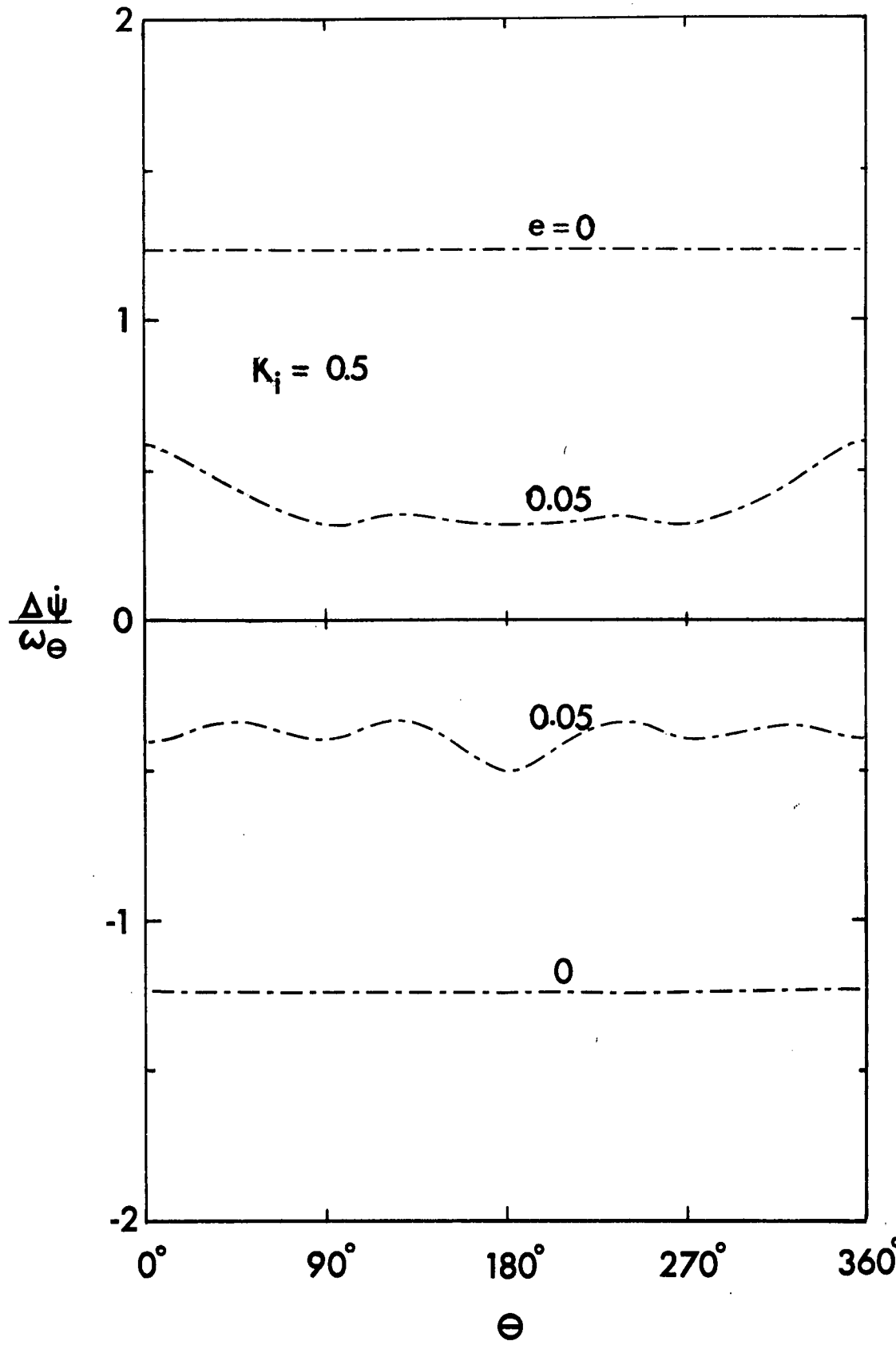

Figure 2-36-iv Maximum momentum change required to destabilize a satellite (K_i = 0.5)

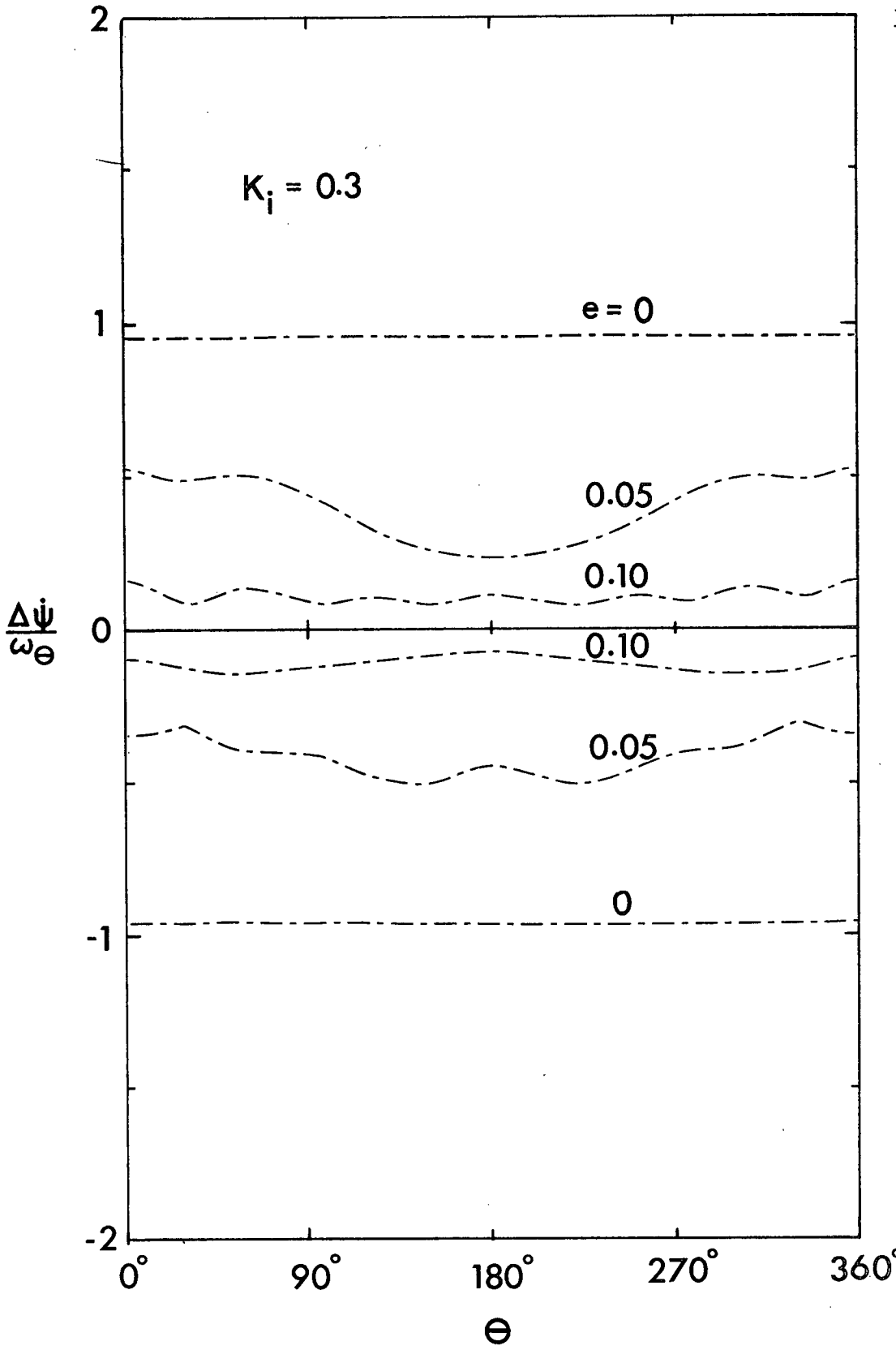

Figure 2-36-v Maximum momentum change required to destabilize a satellite ($K_i = 0.3$)

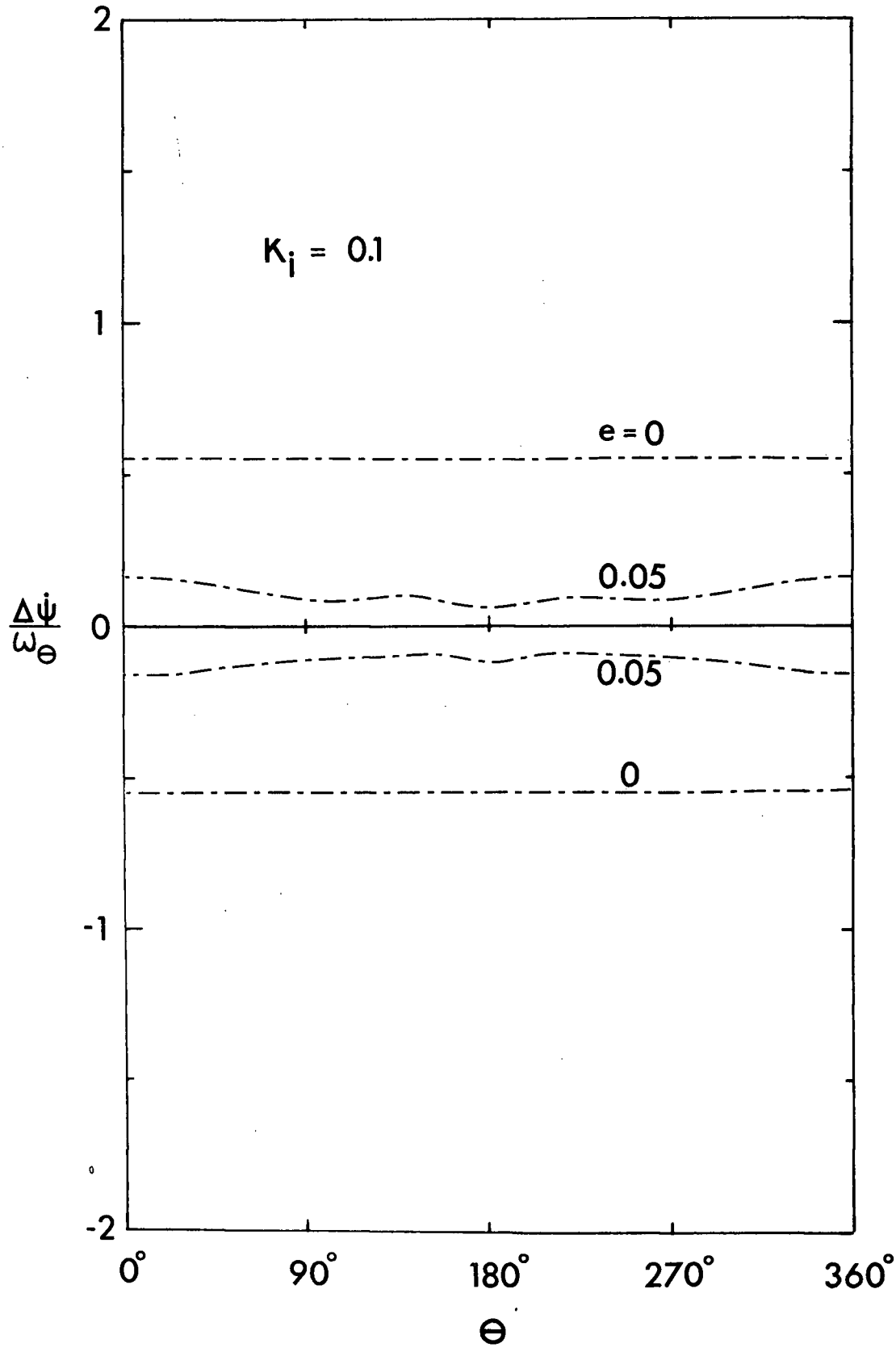

Figure 2-36-vi Maximum momentum change required to destabilize a satellite (K_i = 0.1)

intersecting and exhibit a close relationship with the periodic solutions.

(iv) The region of stability is represented by the largest integral manifold which can be constructed. The importance of such a surface cannot be over emphasized as for given values of the parameters it provides all possible combinations of disturbances to which a satellite may be subjected at any given point in its orbit without causing it to tumble.

(v) For a circular orbit the invariant surfaces in the phase space are cylinders with simple cross-sections. For finite eccentricity the surfaces are helical and exhibit substantial variation in cross-section with orbital angle.

(vi) As eccentricity increases, the size of the limiting surface decreases and for $e = e_{max}$ it collapses to a line, i.e. to a periodic solution. There is a limit to the value of orbit eccentricity for stable librational motion. This critical value depends on the geometry of the satellite. The numerically obtained value was checked by linear perturbation analysis of the periodic solutions.

(vii) The analysis suggests that a small value of eccentricity and a large value of inertia parameter would help to ensure stability. For e larger than about 0.38 practical gravitational gradient stabilization of a satellite is not possible. If the size of the limiting invariant surface is interpreted as a measure of the disturbances which

a satellite will tolerate and still continue to execute librational motion, it has been shown that even quite moderate values of eccentricity would seriously reduce the ability of the satellite to withstand external disturbances.

3. PLANAR LIBRATIONS OF A DAMPED SATELLITE

3.1 Formulation of the Problem

The analysis of the planar librations of a rigid satellite was presented in the preceding chapter. By constructing the satellite so that relative motion can occur between various members and inserting energy dissipating mechanisms which oppose this relative motion it is possible to hasten the capture of the satellite by the gravity-gradient field and to reduce the effects of external disturbances on its orientation.

Several designs have been proposed in the literature (section 1.2). Some of these are quite complex as they attempt to stabilize the satellite about all three body axes. If only planar librations are considered, the damper proposed by Paul[22] is adequate. This device consists of two point masses constrained to move along the axis of the satellite and connected by a linear spring-dashpot arrangement.

The configuration studied by Paul is unduly restrictive and a more general configuration has been selected for study (Figure 3-1). Note that the mean position of the damper mass is offset from the centre of mass of the main body.

The kinetic and potential energies of the system may be written as

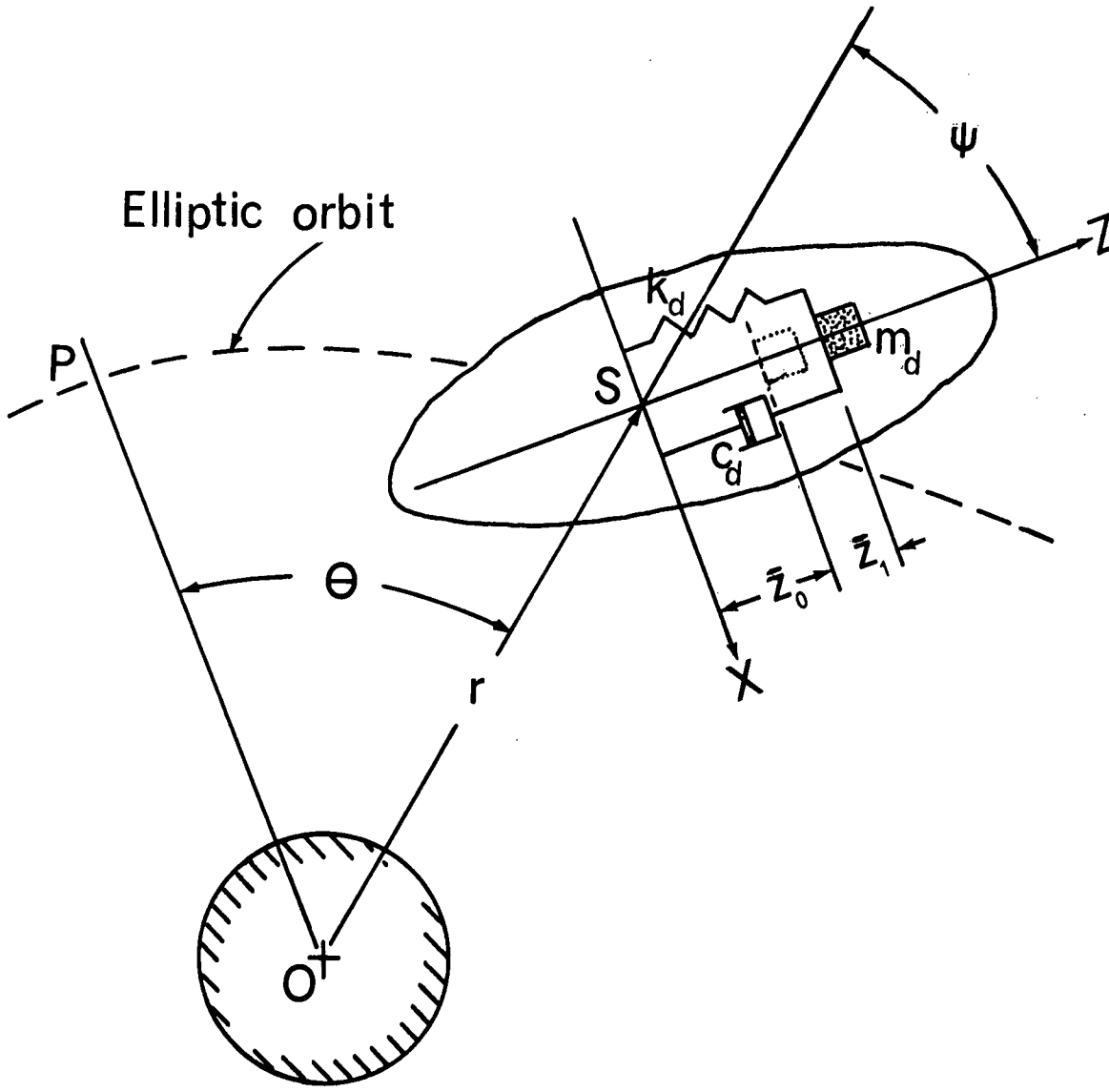

Figure 3-1 Geometry of motion of a damped satellite

$$T = \frac{1}{2}(m_b + m_d)(\dot{r}^2 + r^2\dot{\theta}^2) + \frac{1}{2}m_d\dot{\bar{z}}_1^2 + \frac{1}{2}(I_{yy} + m_d(\bar{z}_0 + \bar{z}_1)^2)(\dot{\theta} + \dot{\psi})^2 \tag{3.1}$$

$$U = -\frac{\mu}{r}(m_b + m_d) + \frac{\mu}{2r^3}\{2I_{xx} - I_{yy} - I_{zz} + m_d(\bar{z}_0 + \bar{z}_1)^2 - 3(I_{xx} - I_{zz} + m_d(\bar{z}_0 + \bar{z}_1)^2)\cos^2\psi\} + \frac{1}{2}k_d\bar{z}_1^2 . \tag{3.2}$$

Writing the dissipation function as

$$\mathcal{F} = \frac{1}{2}c_d\dot{\bar{z}}_1^2 \tag{3.3}$$

and using Lagrange's formulation gives the equations of motion in the ψ and z_1 degrees of freedom

$$(I_{yy} + m_d(\bar{z}_0 + \bar{z}_1)^2)(\ddot{\theta} + \ddot{\psi}) + 2m_d(\bar{z}_0 + \bar{z}_1)\dot{\bar{z}}_1(\dot{\theta} + \dot{\psi}) + \frac{3\mu}{r^3}(I_{xx} - I_{zz} + m_d(\bar{z}_0 + \bar{z}_1)^2)\sin\psi\cos\psi = 0 \tag{3.4}$$

$$m_d\ddot{\bar{z}}_1 + c_d\dot{\bar{z}}_1 + \frac{\mu m_d}{r^3}(\bar{z}_0 + \bar{z}_1)(1 - 3\cos^2\psi) - m_d(\bar{z}_0 + \bar{z}_1)(\dot{\theta} + \dot{\psi})^2 + k_d\bar{z}_1 = 0 . \tag{3.5}$$

Putting

$$K_i = \frac{I_{xx} - I_{zz}}{I_{yy}}$$

$$K_d = \frac{m_d \bar{z}_o^2}{I_{yy}}$$

$$Z = \bar{z}_1 / \bar{z}_o \tag{3.6}$$

$$\omega_d^2 = k_d / m_d$$

$$\tau_d = m_d / c_d$$

the governing equations may be rewritten as

$$(1 + K_d(1+Z)^2)(\ddot{\theta} + \ddot{\psi}) + 2K_d(1+Z)\dot{Z}(\dot{\theta} + \dot{\psi}) + \frac{3\mu}{r^3}\left(K_i + K_d(1+Z)^2\right)\sin\psi\cos\psi = 0 \tag{3.7}$$

$$\ddot{Z} + \frac{\dot{Z}}{\tau_d} + \left\{\omega_d^2 + \frac{\mu}{r^3}(1 - 3\cos^2\psi) - (\dot{\theta}+\dot{\psi})^2\right\} Z = \left\{(\dot{\theta}+\dot{\psi})^2 - \frac{\mu}{r^3}(1 - 3\cos^2\psi)\right\}. \tag{3.8}$$

The use of the awkward relations governing r, θ, and $\dot{\theta}$ as functions of time can be avoided by changing the independent variable to θ using the relations (2.11)-(2.13) and noting that

$$\frac{\mu}{r^3} = \frac{\dot{\theta}^2}{1 + e\cos\theta}\,. \tag{3.9}$$

For an elliptical orbit it is possible to write a relationship for $\dot{\theta}$ in terms of the orbital period

$$\dot{\theta} = \frac{h_\theta}{r} = \frac{2\pi}{\tau_\theta}\frac{(1+e\cos\theta)^2}{(1-e^2)^{3/2}} = \omega_\theta \frac{(1+e\cos\theta)^2}{(1-e^2)^{3/2}} \tag{3.10}$$

so that the parameters describing the damper may be written

$$\frac{1}{\tau_d} = \frac{\dot{\theta}}{\tau_d \dot{\theta}} = \dot{\theta}\frac{(1-e^2)^{3/2}}{\tau_d \omega_\theta (1+e\cos\theta)^2}$$

$$\omega_d^2 = \dot{\theta}^2\left(\frac{\omega_d}{\dot{\theta}}\right)^2 = \dot{\theta}^2\left(\frac{\omega_d}{\omega_\theta}\right)^2\frac{(1-e^2)^3}{(1+e\cos\theta)^4}. \tag{3.11}$$

Using these relations, the system equations (3.8) and (3.9) may be written as

$$\left(1+K_d(1+z^2)\right)\left(\psi'' - \frac{2e\sin\theta}{1+e\cos\theta}(\psi'+1)\right)$$

$$+ 2K_d(1+z)z'(\psi'+1) \tag{3.12}$$

$$+ \frac{3(K_i + K_d(1+z)^2)}{1+e\cos\theta}\sin\psi\cos\psi = 0$$

and

$$z'' + \left[\frac{(1-e^2)^{3/2}}{\tau^*(1+e\cos\theta)^2} - \frac{2e\sin\theta}{1+e\cos\theta}\right]z'$$

$$+\left[\frac{\omega^{*2}(1-e^2)^3}{(1+e\cos\theta)^4}+\frac{1-3\cos^2\psi}{1+e\cos\theta}-(\psi'+1)^2\right]z \tag{3.13}$$

$$=\left[(\psi'+1)^2-\frac{1-3\cos^2\psi}{1+e\cos\theta}\right]$$

where

$$\tau^* = \omega_\theta \tau_d \tag{3.14}$$

$$\omega^* = \omega_d/\omega_\theta$$

The system involves a large number of variables which complicates the analysis. To better understand the basic character of the system it is convenient to consider a particular situation where the mass, m_d, is critically damped, i.e.

$$\frac{1}{\tau^*} = 2\omega^* \tag{3.15}$$

Furthermore, the parameter K_1 will be taken to be unity thus representing a slender, dumbbell type satellite.

3.2. Numerical Results

The damping present in the model causes the phase space trajectories to gradually approach a limit cycle. The dissipation of energy in the damping mechanism precludes employ-

ing the process which made possible the generation of an invariant surface. For a damped system there is no closed invariant surface, however, the representation of the behaviour of the system in the stroboscopic phase plane is still very helpful.

For a given value of θ, a point in the stroboscopic ψ, ψ'-plane determines the state of the satellite while a corresponding point in a Z, Z' -plane specifies the state of the damper. For simplicity only the phase plane representing the state of the satellite is studied here.

A typical short history of the satellite motion is presented in Figure 3-2. The corresponding stroboscopic phase plane is shown in Figure 3-3. The diagrams indicate that the damper is causing the amplitude of the motion to decay. Similar results for several cases are presented in Figures 3-4 and 3-5. Note that the apparent curves in these diagrams do not indicate the actual motion of the satellite, but serve only to indicate the inward trend of successive points. The number of apparent curves is of no special significance.

It may be pointed out that after a considerable period of time successive points in the stroboscopic phase plane fall progressively closer together. The system thus approaches a periodic solution or limit cycle.

Figures 3-6 to 3-8 compare the limit cycles given by different dampers with the periodic solutions obtained in section 2.2.3 for the same values of e and K_1. Of the three

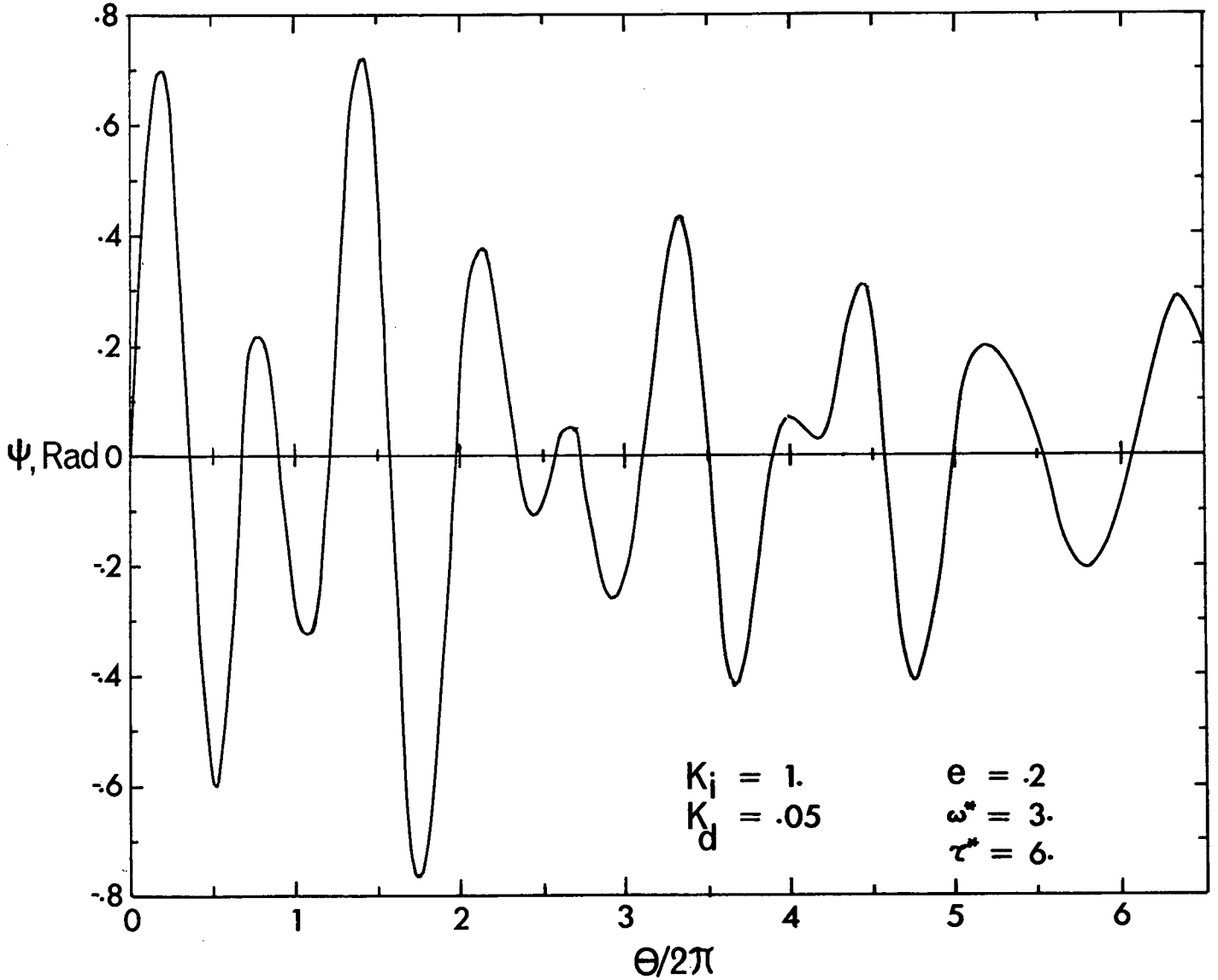

Figure 3-2 Solution of equation of motion illustrating the effect of the damper

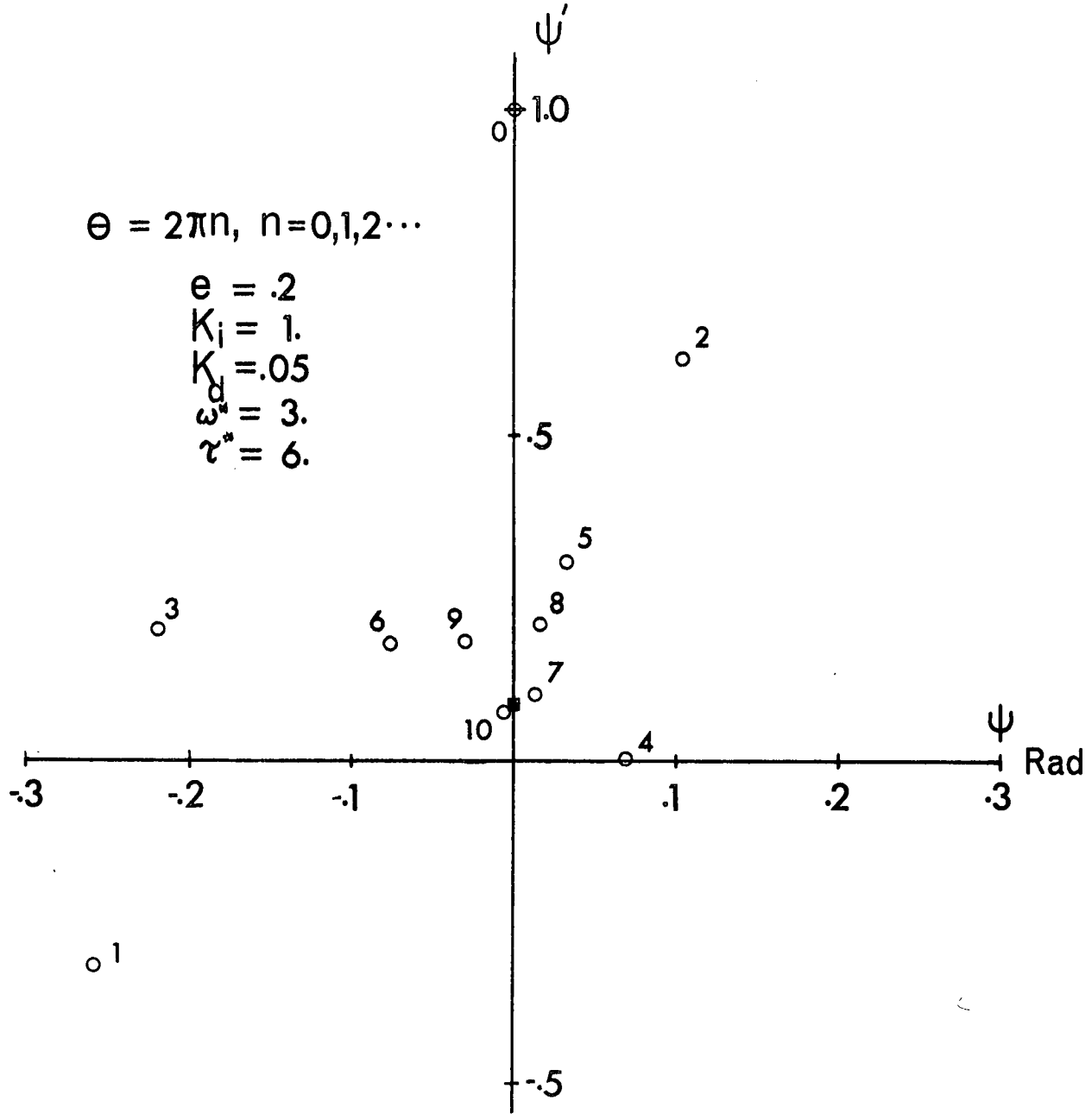

$\circ^n$ Point representing the state of the system at $\Theta = 2\pi n$.

■ Limit cycle.

Figure 3-3 Stroboscopic phase plane of the solution illustrated in Figure 3-2

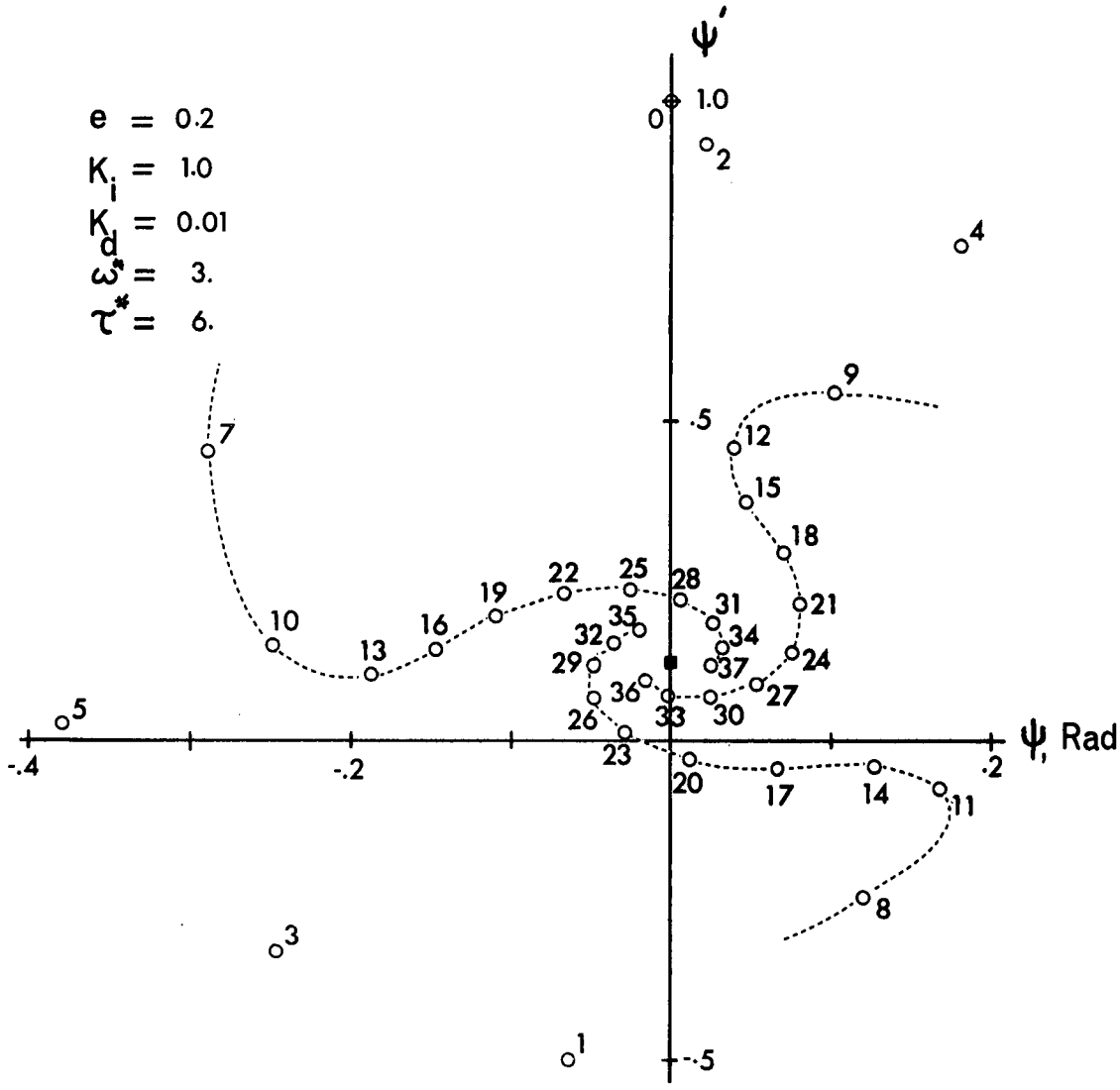

o^n Point representing the state of the system at $\Theta=2\pi n$.

■ Limit cycle.

····· Apparent curves defined by groups of points.

Figure 3-4 Typical stroboscopic phase plane of a damped satellite

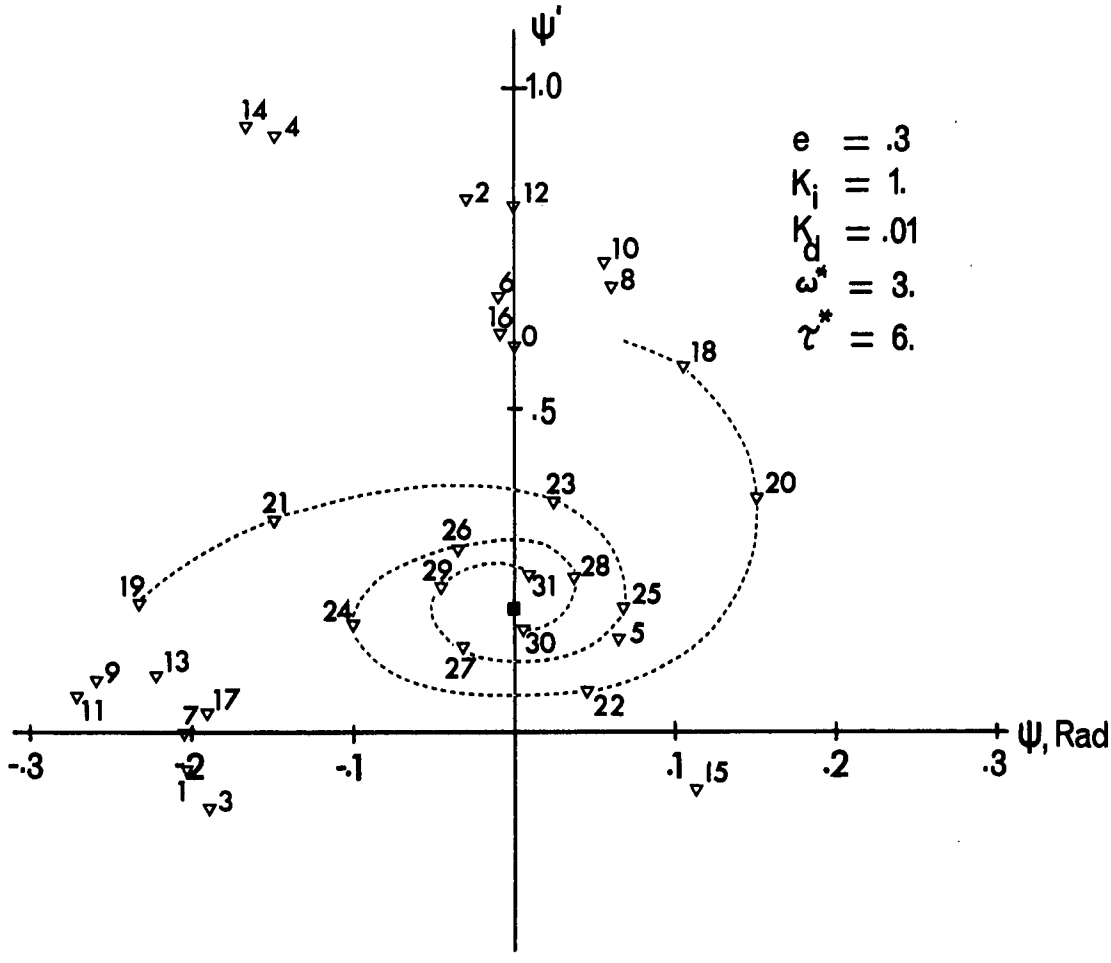

∇^n Point representing the state of the system at $\Theta = 2\pi n$.

■ Limit cycle

..... Apparent curves defined by groups of points.

Figure 3-5 Typical stroboscopic phase plane of a damped satellite

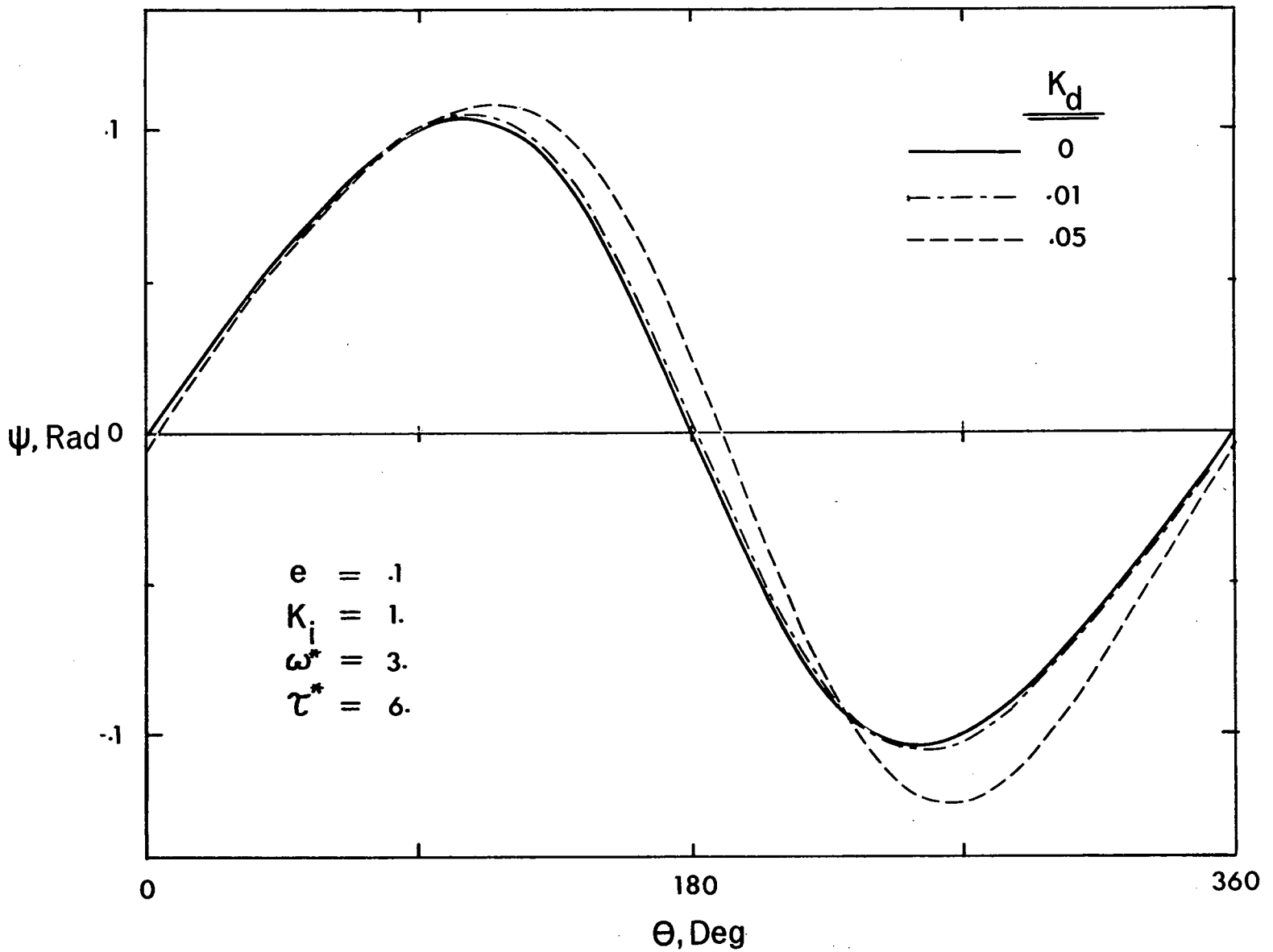

Figure 3-6 Limit cycles (K_i = 1.0, e = 0.1)

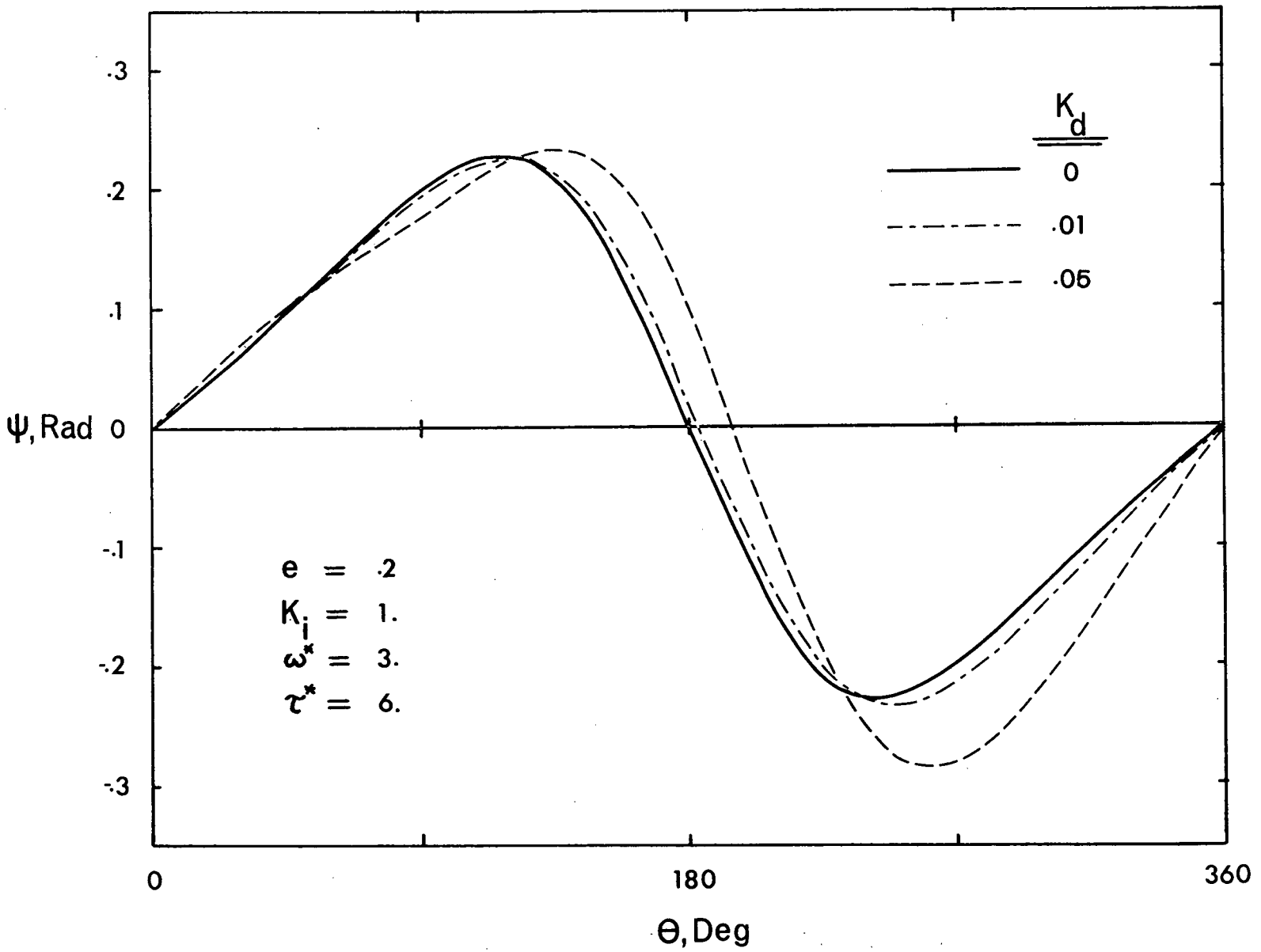

Figure 3-7 Limit cycles (K_i = 1.0, e = 0.2)

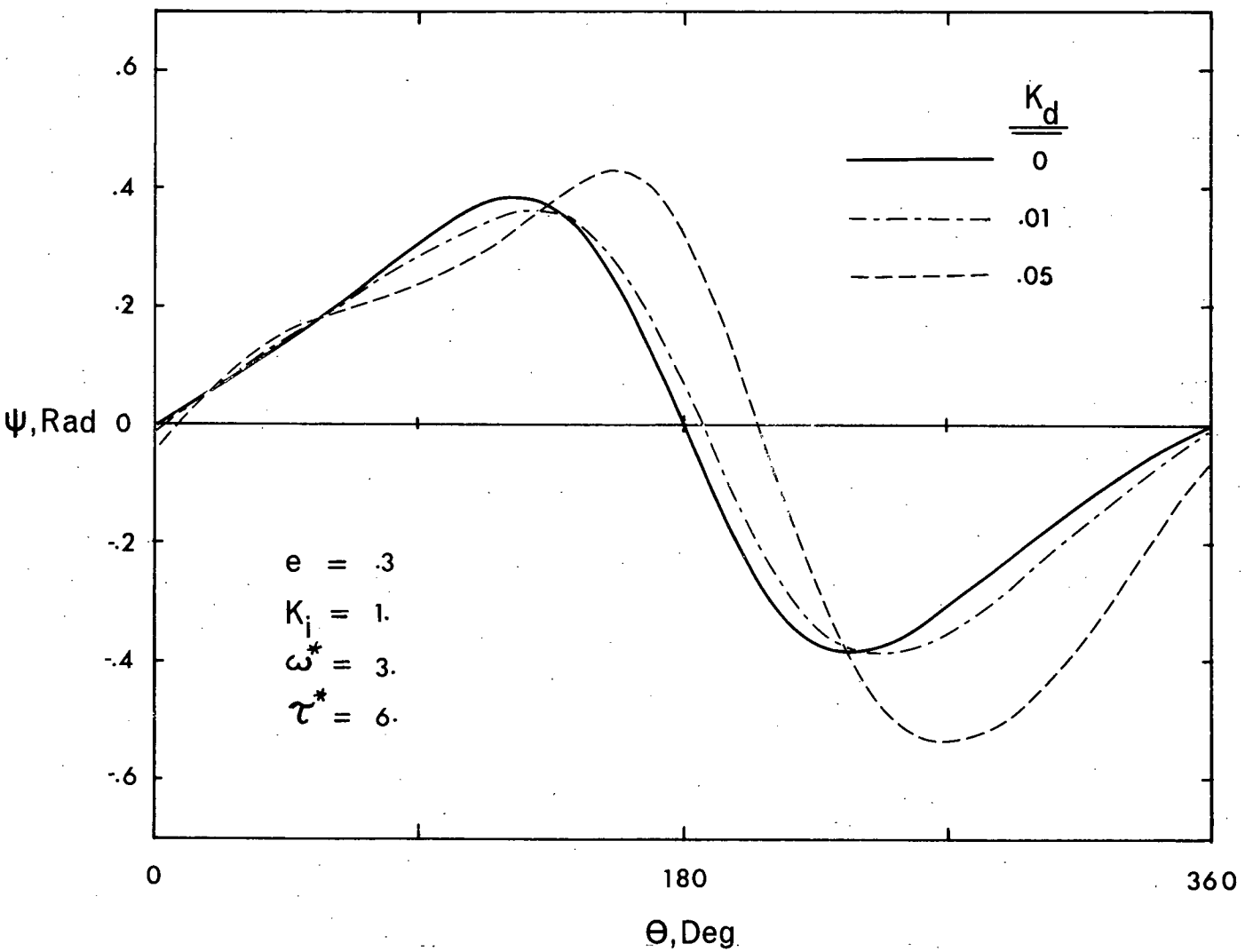

Figure 3-8 Limit cycles (K_i = 1.0, e = 0.3)

periodic solutions available for a given set of parameters (e, K_i) only the one with the smallest amplitude was suitable for comparison. For small dampers ($K_d \ll 1$) and sufficiently high natural frequencies ($\omega_d^2 \gg 3\omega_e^2$) the two types of solution are virtually identical.

The introduction of damping causes the limit cycle to lag behind the periodic solution obtained for $K_d = 0$. The varying gravitational gradient and orbital angular velocity interact with this lag and can often lead to an increase in the amplitude of the motion although the nonlinearity of the system precludes any definite prediction of this nature.

Note that a very low natural frequency of the damper can create a problem because the coefficient of equation (3.13) which represents the spring "constant" becomes negative. The motion of the damper mass then becomes unstable and the equations cease to describe the system.

3.3 Conclusions

The addition of a damper to a rigid satellite results in the disappearance of the invariant manifolds discussed in Chapter 2. The accompanying limit cycles are independent of the initial conditions and, for small dampers, are nearly identical with one of the periodic solutions obtained for the undamped case. The equations of motion in the two cases are similar and the presence of damping merely causes the trajectory in phase space to spiral inwards.

The limits of stability determined in Chapter 2 may

be regarded as approximately valid for the lightly damped satellite. The presence of damping causes the satellite to become stable eventually, irrespective of the initial condition. However, if the state of the satellite can be expressed by a point inside the appropriate limiting manifold of Chapter 2, and the damping is small, the subsequent motion should remain stable and approach the limit cycle. In doing so the representative point drifts inwards across the intermediate invariant surfaces which were determined for the undamped case. Therefore, it may be concluded that the small amplitude periodic solutions obtained for the undamped satellite represent a limiting case approached by all real satellites.

4. PLANAR LIBRATIONS OF A LONG FLEXIBLE SATELLITE

4.1 Preliminary Remarks

Gravity-gradient stabilization of satellites requires that the inertia of the satellite be large so that the available torque is sufficiently great to overcome the effects of external disturbances. To a certain extent, this problem has been overcome by the use of the de Havilland STEM (Self-storing Tubular Extensible Module)[24] which is capable of extending a tubular boom up to several hundred feet long (Table III).

The STEM boom is typically about one inch in diameter, or less, with a wall thickness of about .002 inches. This thin, slender, tubular member is quite flexible and hence susceptible to external disturbances. Thus a long boom which provides a large stabilizing effect can also introduce substantial externally induced forces. Preliminary analysis[24] indicates that among the various forms of disturbance (section 1.1) the thermal deformation of the boom is likely to have the most significant effect on the performance.

The problem in general is extremely complex as it involves the solution of a set of simultaneous differential equations with a large number of parameters. To initiate the study of such a difficult problem, a simplified model is considered.

TABLE III

CHARACTERISTICS OF REPRESENTATIVE STEM CONFIGURATIONS[35,36]

	Alouette I	Alouette II	Units
Material	Steel	Beryllium copper	
Radius, a_b	0.475	0.25	inches
Wall thickness, b_b	0.006	0.002	inches
Density, ρ_b	0.286	0.32	lb/in^3
Thermal conductivity, k_b	26	50	BTU/hr ft ^oF
Specific heat, c_b	0.11	0.092	BTU/lb ^oF
Coefficient of thermal expansion, α_t	6.5×10^{-6}	10×10^{-6}	$^oF^{-1}$
Absorptivity (solar), α_s	0.9	0.45	-
Emissivity, ϵ_b	0.8	0.25	-
Bending stiffness, $\mathcal{E}I$	351	15.5	$lb\ ft^2$
Mass/length, m_s	0.068	0.0142	lb/ft

This chapter studies the planar librations of a slender, flexible satellite of constant cross-section under the influence of solar heating. The solar flux is taken to be direct and continuous, and the resulting bending is assumed to take place in the plane of the orbit. The concept of the phase space representation of the motion is extended to a deformable system and the corresponding limiting invariant surfaces are obtained. Charts are presented which indicate the effect of orbit eccentricity, solar aspect angle, and the satellite's

physical properties on the allowable disturbances for stable operation.

4.2 Formulation of the Problem

Consider a slender flexible satellite with centre of mass at S, deformed due to solar heating, and executing planar librational motion while moving in an elliptic orbit about the centre of force O (Figure 4-1). The kinetic energy for an element of the satellite located at

$$\begin{aligned} x &= x(s,t) \\ z &= z(s,t) \end{aligned} \tag{4.1}$$

can be written as

$$\begin{aligned} dT = \frac{1}{2} dm_b \Big\{ & \left(-\dot{r}\,\mathrm{Sin}\,\psi + r\dot{\theta}\,\mathrm{Cos}\,\psi + z(\dot{\theta}+\dot{\psi}) + \dot{x}\right)^2 \\ & + \left(\dot{r}\,\mathrm{Cos}\,\psi + r\dot{\theta}\,\mathrm{Sin}\,\psi - x(\dot{\theta}+\dot{\psi}) + \dot{z}\right)^2 \Big\} \\ = \frac{1}{2} dm_b \Big\{ & \dot{r}^2 + r^2\dot{\theta}^2 + (\dot{\theta}+\dot{\psi})^2(x^2+z^2) + \dot{x}^2 + \dot{z}^2 \\ & - 2\dot{r}(\dot{\theta}+\dot{\psi})(x\,\mathrm{Cos}\,\psi + z\,\mathrm{Sin}\,\psi) \\ & + 2r\dot{\theta}(\dot{\theta}+\dot{\psi})(z\,\mathrm{Cos}\,\psi - x\,\mathrm{Sin}\,\psi) \\ & + 2\dot{x}(-\dot{r}\,\mathrm{Sin}\,\psi + r\dot{\theta}\,\mathrm{Cos}\,\psi + z(\dot{\theta}+\dot{\psi})) \\ & + 2\dot{z}(\dot{r}\,\mathrm{Cos}\,\psi + r\dot{\theta}\,\mathrm{Sin}\,\psi - x(\dot{\theta}+\dot{\psi})) \Big\}. \end{aligned} \tag{4.2}$$

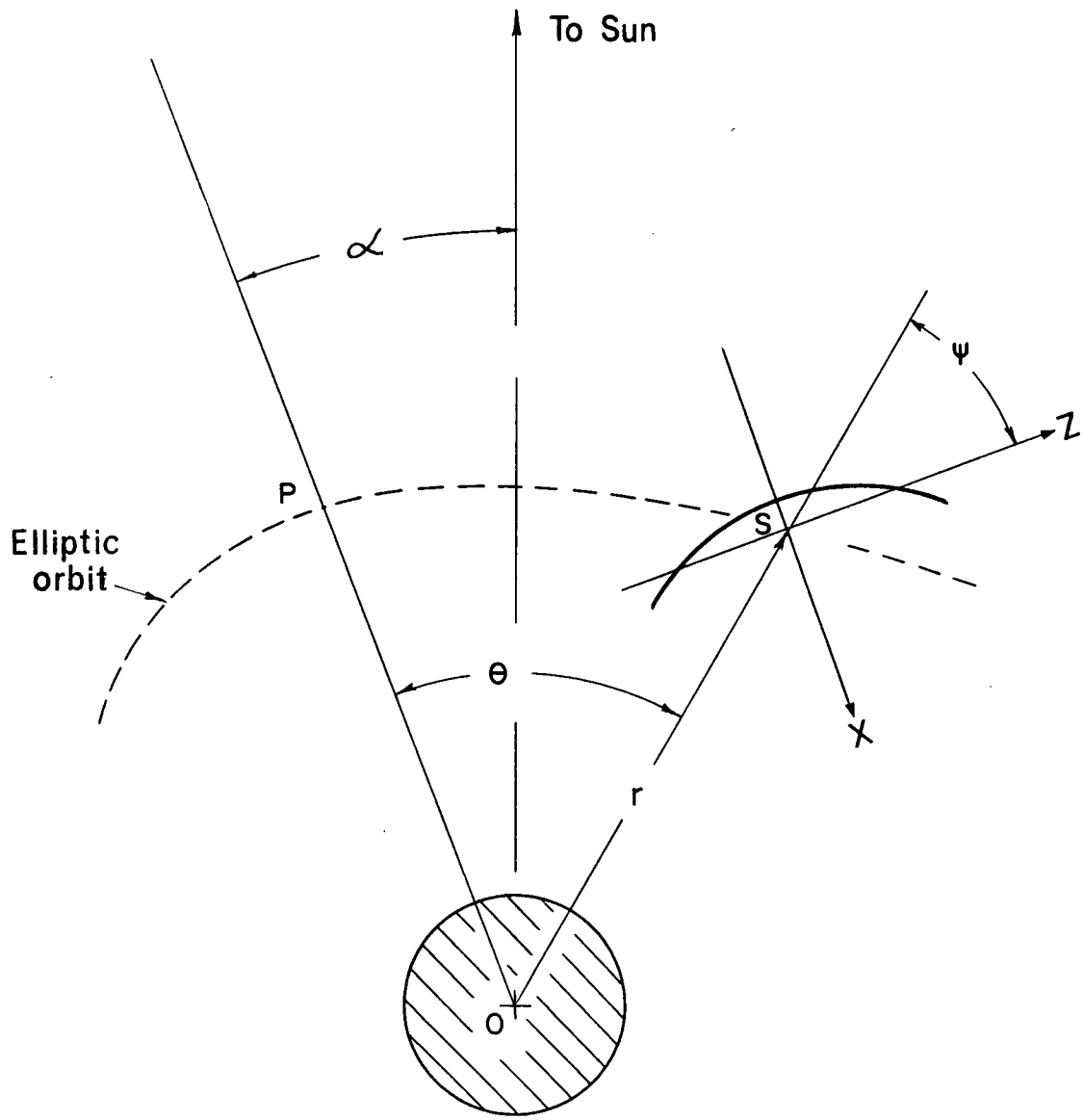

Figure 4-1 Geometry of motion of flexible satellite

Because S is the centre of mass, the relations

$$\int x\,dm_b = \int \dot{x}\,dm_b = \int z\,dm_b = \int \dot{z}\,dm_b = 0 \tag{4.3}$$

permit writing the total kinetic energy as

$$\begin{aligned} T = {} & \tfrac{1}{2} m_b (\dot{r}^2 + r^2\dot{\theta}^2) + \tfrac{1}{2} I_{yy}(\dot{\theta}+\dot{\psi})^2 \\ & + \tfrac{1}{2}\int (\dot{x}^2 + \dot{z}^2)\,dm_b + (\dot{\theta}+\dot{\psi})\int (\dot{x}z - x\dot{z})\,dm_b \end{aligned} \tag{4.4}$$

where

$$I_{yy} = \int (x^2 + z^2)\,dm_b = I_{xx} + I_{zz}\,. \tag{4.5}$$

The quantity

$$\int (\dot{x}z - x\dot{z})\,dm_b = h_s \tag{4.6}$$

represents the angular momentum of the satellite with respect to the rotating x, z-axes. The choice

$$h_s = 0 \tag{4.7}$$

indicates that the axes rotate in a manner equivalent to that of axes which are fixed in a rigid body. This device separates the librational degree of freedom, described by the co-ordinate ψ, and the vibrational degrees of freedom which employ the x,z-co-ordinates.

If the x,z-axes are taken to be the principal axes of the deformed body, the potential energy due to the

gravitational field is (equation (2.7))

$$U_g = -\frac{\mu m_b}{r} + \frac{\mu}{2r^3}\left\{I_{xx}(1-3\cos^2\psi) + I_{zz}(1-3\sin^2\psi)\right\}. \tag{4.8}$$

There is also the elastic potential energy

$$U_e = \frac{1}{2}\int \frac{EI_b}{R_c^2}\,ds\,. \tag{4.9}$$

Using Lagrange's equations the motion of the centre of mass can be described by the equations

$$\ddot{r} - r\dot{\theta}^2 + \frac{\mu}{r^2} = \frac{3\mu}{2m_b r^4}\left\{I_{xx}(1-3\cos^2\psi) + I_{zz}(1-3\sin^2\psi)\right\} \tag{4.10}$$

$$r^2\dot{\theta} + \frac{I_{yy}(\dot{\theta}+\dot{\psi})}{m_b} = h_\theta \tag{4.11}$$

while the librational motion is governed by

$$\frac{d}{dt}\left\{I_{yy}(\dot{\theta}+\dot{\psi})\right\} + \frac{3\mu}{r^3}\left(I_{xx} - I_{zz}\right)\sin\psi\cos\psi = 0 \tag{4.12}$$

which requires that the deflection of the beam be known.

This is a very complex problem. As a first approximation let

$$\left(\frac{\partial x}{\partial z}\right)^2 \approx \left(\frac{\partial x}{\partial s}\right)^2 << 1\,. \tag{4.13}$$

To this degree of approximation

$$\dot{z}^2 << \dot{x}^2 \tag{4.14}$$

and hence the co-ordinates of an element of the boom are given by

$$\begin{aligned} z &\approx s \\ x &= x(s,t). \end{aligned} \tag{4.15}$$

The deflection of an isolated beam with no external forces present is given by the partial differential equation

$$\frac{\partial^2}{\partial s^2}\left[\mathcal{E} I_b \frac{\partial^2 x}{\partial s^2}\right] + m_s \frac{\partial^2 x}{\partial t^2} = 0 \tag{4.16}$$

which has the solution

$$x(s,t) = \sum_{i=1}^{\infty} A_i(t) X_i(s) \tag{4.17}$$

where the mode shapes, $X_i(s)$, and the amplitudes, $A_i(t)$, satisfy the differential equations

$$\ddot{A}_i + \omega_i^2 A_i = 0 \tag{4.18}$$

$$\frac{d^2}{ds^2}\left[\mathcal{E} I_b \frac{d^2 X_i}{ds^2}\right] - m_s \omega_i^2 X_i = 0 \tag{4.19}$$

subject to the appropriate initial and boundary conditions.

The X_i may be thought of as generalized co-ordinates and the A_i as the amplitudes. The X_i are orthogonal; that is

$$\int X_i \, X_j \, dm_b = \begin{cases} I_i \, ; & i = j \\ 0 \, ; & i \neq j \end{cases} \tag{4.20}$$

also, for a free-free beam,

$$\int X_i \, s \, dm_b = \int X_i \, z \, dm_b = 0 \, ; \quad (i = 1, 2, \cdots) \tag{4.21}$$

so that the x, z-axes remain the principal axes of the deformed body.

The kinetic energy of vibration may be written in terms of the A_i

$$\begin{aligned} T_v &= \frac{1}{2}\int (\dot{x}^2 + \dot{z}^2)\, dm_b \approx \frac{1}{2}\int \dot{x}^2 dm_b \\ &= \frac{1}{2}\int \left(\sum_{i=1}^{\infty} \dot{A}_i X_i \right)^2 dm_b \\ &= \frac{1}{2}\int \sum_{i=1}^{\infty} \sum_{j=1}^{\infty} \dot{A}_i \dot{A}_j X_i X_j \, dm_b \\ &= \frac{1}{2} \sum_{i=1}^{\infty} \dot{A}_i^2 I_i \, . \end{aligned} \tag{4.22}$$

The expression for the elastic potential energy

$$U_e = \frac{1}{2}\int_0^L \frac{\mathcal{E} I_b}{R_c^2}\, ds = \frac{1}{2}\int_0^L \mathcal{E} I_b \left(\frac{\partial^2 \chi}{\partial s^2}\right)^2 ds \tag{4.23}$$

may be integrated by parts twice to give

$$U_e = \frac{1}{2}\left\{ \mathcal{E} I_b \frac{\partial^2 \chi}{\partial s^2}\frac{\partial \chi}{\partial s}\Big|_0^L - \frac{\partial}{\partial s}\left(\mathcal{E} I_b \frac{\partial^2 \chi}{\partial s^2}\right)\chi\Big|_0^L + \int_0^L \frac{\partial^2}{\partial s^2}\left(\mathcal{E} I_b \frac{\partial^2 \chi}{\partial s^2}\right)\chi\, ds \right\}. \tag{4.24}$$

Since the satellite is completely free, the bending moment, $\mathcal{E} I_b \frac{\partial^2 \chi}{\partial s^2}$ and the shear force, $\frac{\partial}{\partial s}\left(\mathcal{E} I_b \frac{\partial^2 \chi}{\partial s^2}\right)$, are zero at the ends and hence

$$\begin{aligned} U_e &= \frac{1}{2}\int_0^L \frac{\partial^2}{\partial s^2}\left(\mathcal{E} I_b \frac{\partial^2 \chi}{\partial s^2}\right)\chi\, ds \\ &= \frac{1}{2}\int_0^L \sum_{i=1}^{\infty}\sum_{j=1}^{\infty} \omega_i^2 A_i A_j X_i X_j m_s\, ds \\ &= \frac{1}{2}\sum_{i=1}^{\infty} \omega_i^2 A_i^2 I_i \,. \end{aligned} \tag{4.25}$$

The inertias of the beam are given approximately by

$$\begin{aligned} I_{zz} &= \int x^2 dm_b = \sum_{i=1}^{\infty} A_i^2 I_i \\ I_{xx} &= \int z^2 dm_b \approx \int s^2 dm_b = I_r \end{aligned} \tag{4.26}$$

$$I_{yy} = I_{xx} + I_{zz} \approx I_r + \sum_{i=1}^{\infty} A_i^2 I_i \qquad (4.26)\ \text{cont'd}$$

The expressions for the kinetic and potential energies may then be written as

$$T = \tfrac{1}{2} m_b (\dot{r}^2 + r^2\dot{\theta}^2) + \tfrac{1}{2}\left(I_r + \sum_{i=1}^{\infty} A_i^2 I_i\right)(\dot{\theta}+\dot{\psi})^2 + \tfrac{1}{2}\sum_{i=1}^{\infty} \dot{A}_i^2 I_i \qquad (4.27)$$

$$U = -\frac{\mu m_b}{r} + \frac{\mu}{2r^3}\left\{I_r(1-3\cos^2\psi) + \sum_{i=1}^{\infty} A_i^2 I_i (1-3\sin^2\psi)\right\} + \tfrac{1}{2}\sum_{i=1}^{\infty} \omega_i^2 A_i^2 I_i$$

and therefore the equations of motion governing the amplitudes of the vibrational modes are

$$\ddot{A}_i + \left\{\omega_i^2 + \frac{\mu}{r^3}(1-3\sin^2\psi) - (\dot{\theta}+\dot{\psi})^2\right\} A_i = F_i . \qquad (4.28)$$

Here the F_i represent the generalized forces due to thermal bending. The dependence of these forces on the orientation of the satellite leads to coupling between equations (4.12) and (4.28). This analysis parallels that of Etkin and Hughes[35] who took $\dot{\psi}^2 \gg \dot{\theta}^2, \mu/r^3$.

The natural frequencies of a uniform, free-free beam

can be determined from[37]

$$\omega_i^2 = \frac{E I_b}{m_s L^4} (kL)_i^4 \tag{4.29}$$

where

$$\cos(kL)_i \cosh(kL)_i = 1. \tag{4.30}$$

The values of $(kL)_i$ are

i	$(kL)_i$
1	4.73004
2	7.85320
3	10.99561
4	14.13717
5	17.27876
$i \geq 6$	$\frac{(2i+1)}{2}\pi$.

(4.31)

For the representative STEM configurations (Table III) the lowest natural frequency is

$$\omega_1^2 = \frac{17.5 \times 10^6}{L^4} \tag{4.32}$$

(L in feet) which for lengths typical of present practice (50-500 feet) leads to values for the fundamental period of from 3.75 to 375 seconds. It may be noted that the period of the vibration is much less than that of the orbital motion.

The results of Chapter 2 showed that the value of $\dot{\psi}$

is of the same order as $\dot{\theta}$. Also μ/r^3 is approximately equal to $\dot{\theta}^2$ so that in equation (4.28) all terms due to the gravitational field can be completely ignored compared to the relatively high natural frequency of the boom. The deflection of the boom can be approximated by the normal modes thus reducing the equations of motion corresponding to the elastic degrees of freedom to

$$\ddot{A}_i + \omega_i^2 A_i = F_i \; ; \; (i = 1,2,\cdots). \tag{4.33}$$

4.3 Thermal Analysis of the Boom

At this stage information concerning the deformation of the satellite under the influence of solar heating is essential to proceed further. Figure 4-2 illustrates the assumed cross-section of the flexible satellite which may be thought of as approximating the STEM.

Consider an element of the beam as shown in Figure 4-3. Taking the thickness of the wall to be much less than its radius, ignoring longitudinal conduction and performing a heat balance for the element gives the equation

$$\frac{k_b b_b}{a_b^2} \frac{\partial^2 T_b}{\partial \Omega^2} + \left\{ q_{ext} + q_{int} - 2\sigma \epsilon_b T_b^4 \right\} = c_b \rho_b b_b \frac{\partial T_b}{\partial t}. \tag{4.34}$$

This equation represents a significant improvement on the work of Etkin and Hughes[35] in that the effect of thermal conductivity is considered.

The thermal input to the boom from the sun can be

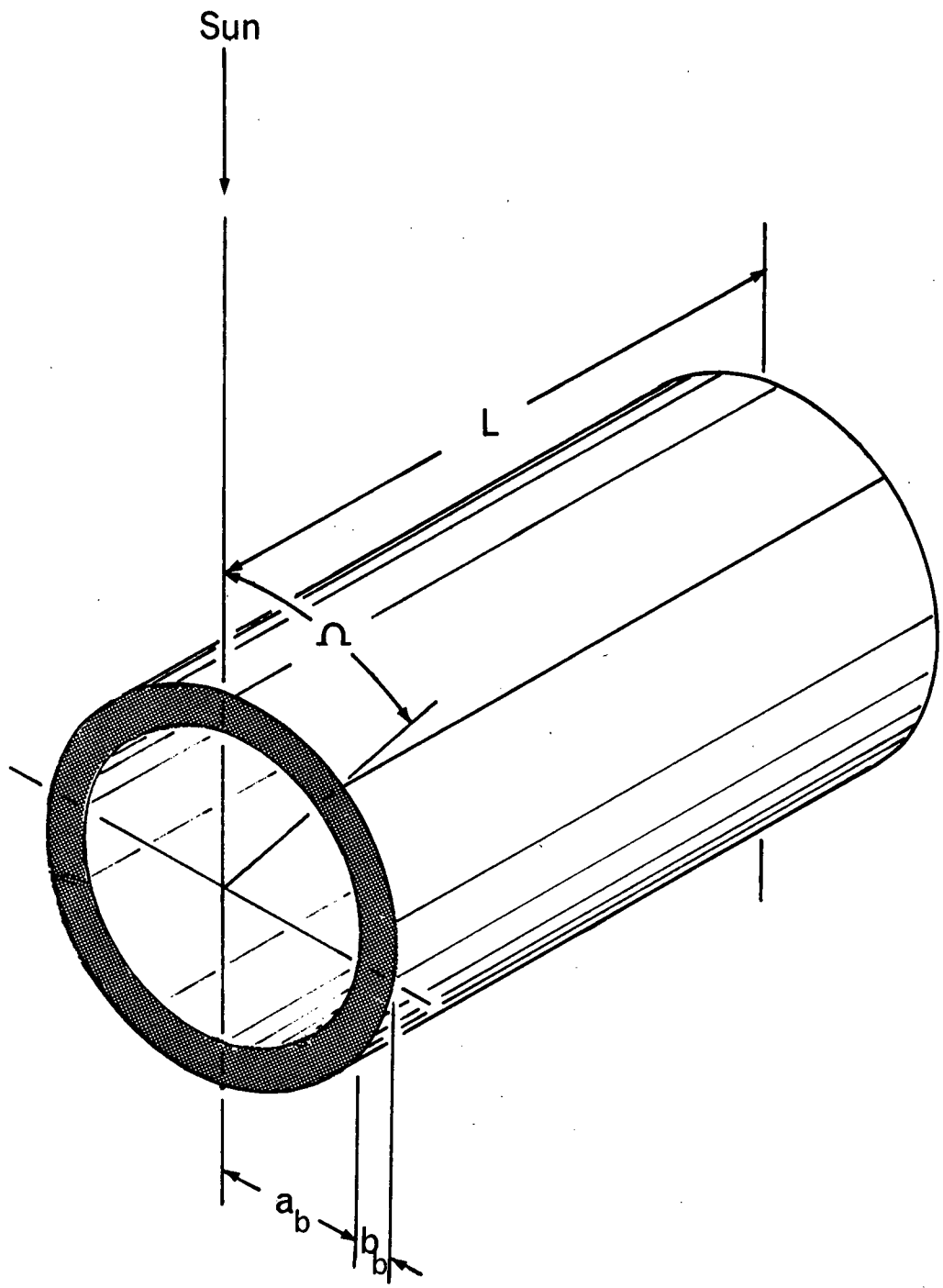

Figure 4-2 Assumed cross-section of satellite boom

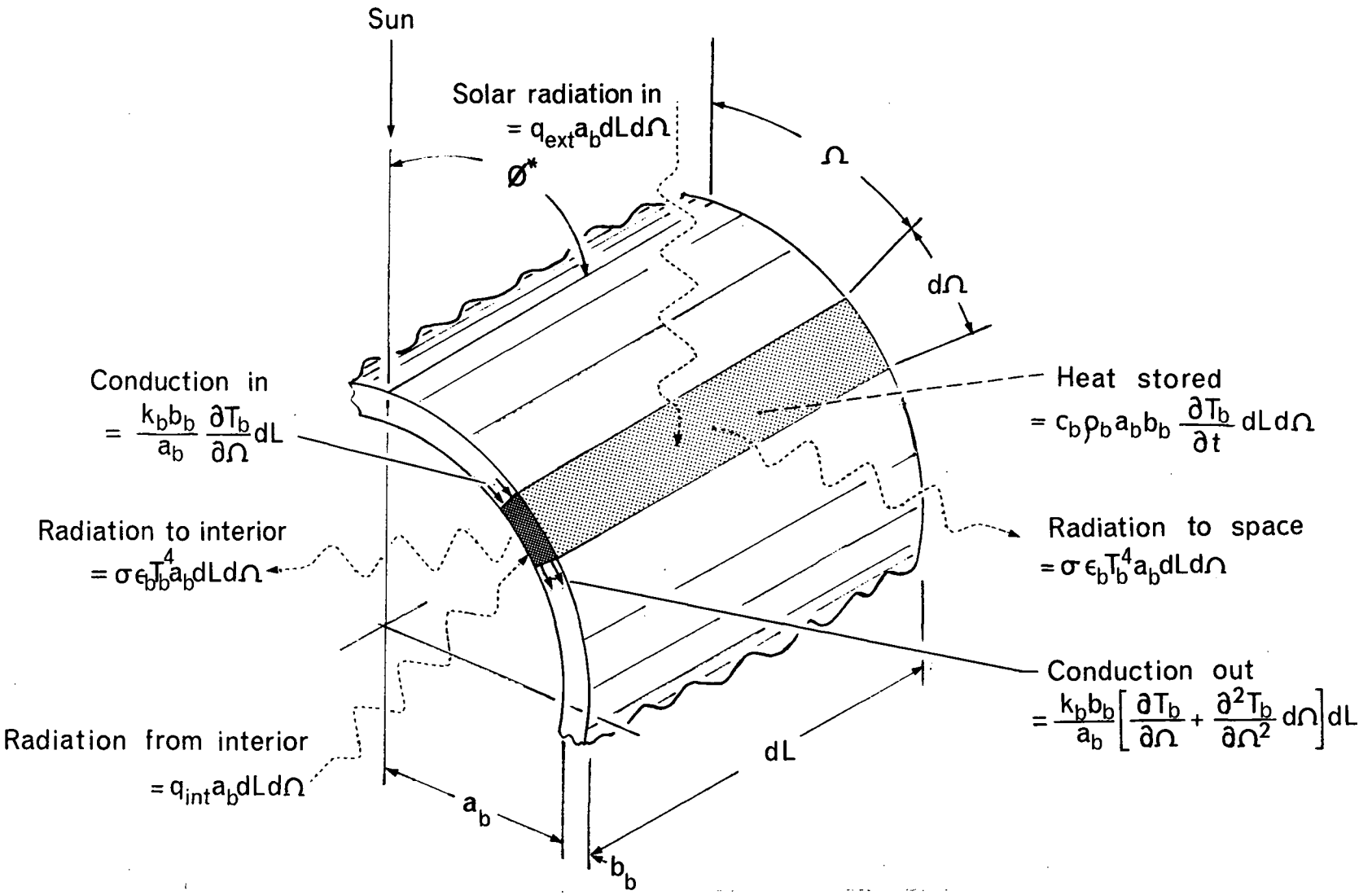

Figure 4-3 Heat balance for an element of the satellite boom

written as

$$q_{ext} = \begin{cases} q_s \alpha_s \sin\phi^* \cos\Omega \; ; -\frac{\pi}{2} \leq \Omega \leq \frac{\pi}{2} \\ 0 \qquad\qquad\qquad ; \text{ elsewhere} \end{cases} \tag{4.35}$$

where ϕ^* is the angle between the longitudinal axis of the boom and the sun. This may be written as a Fourier series

$$q_{ext} = q_s \alpha_s \sin\phi^* \sum_{n=0}^{\infty} C_{s,n} \cos n\Omega \tag{4.36}$$

where

$$C_{s,n} = \begin{cases} \frac{1}{\pi} & ; \; n = 0 \\ \frac{1}{2} & ; \; n = 1 \\ \frac{2(-1)^{n/2}}{\pi(n^2-1)} & ; \; n \text{ even}, \neq 0 \\ 0 & ; \; n \text{ odd}, \neq 1. \end{cases} \tag{4.37}$$

To determine the amount of radiation incident on the interior of the boom consider the radiation emitted by an element of area (dA_e) on the inside of the tube (Figure 4-4)

$$\frac{d\dot{Q}}{dA_e} = \epsilon_b \sigma \left[T_b (\mu_r + \Omega)\right]^4. \tag{4.38}$$

Assuming that the radiation obeys Lambert's law, the radiation which falls on the second element of area (dA_{in}) is

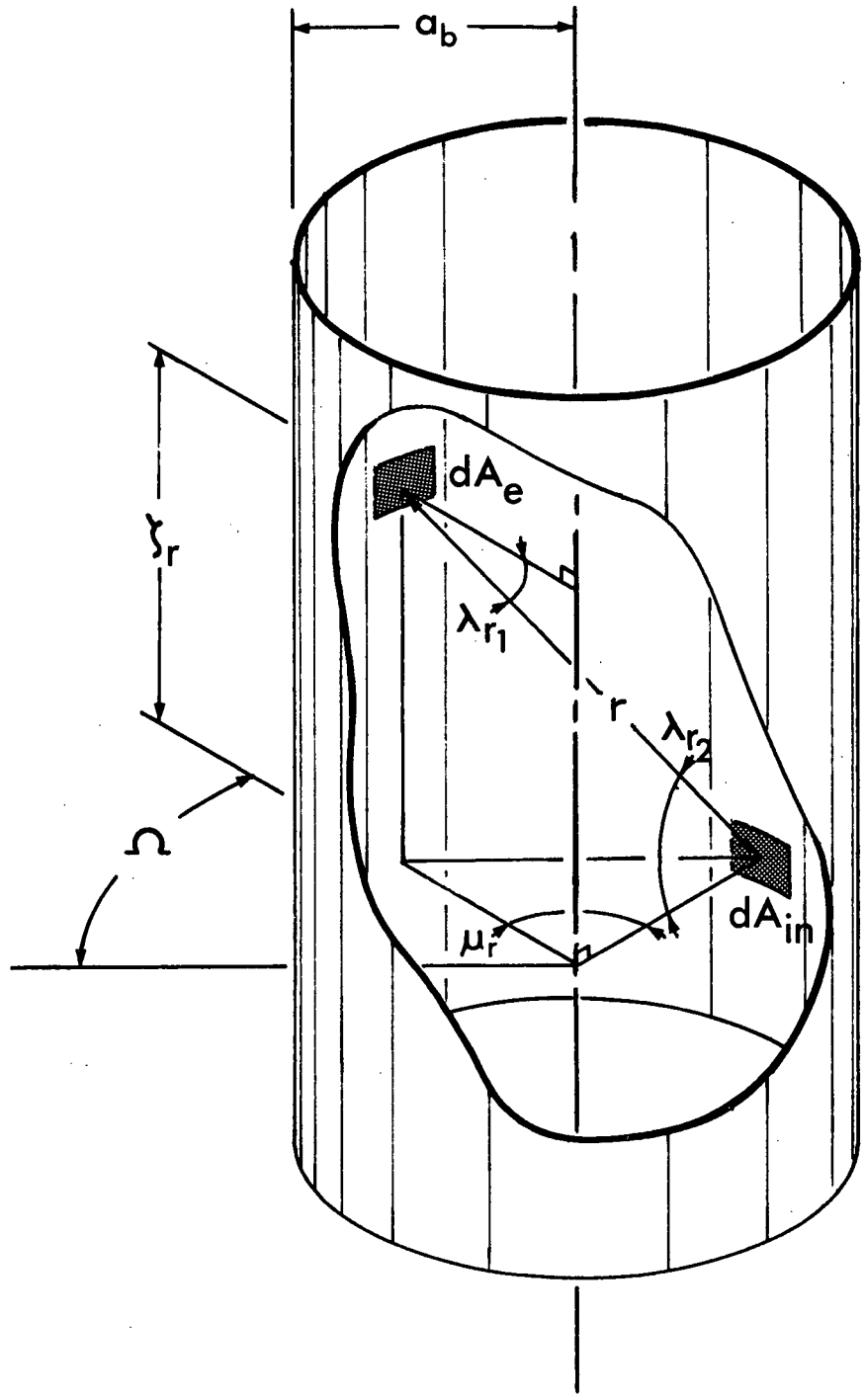

Figure 4-4 Geometry of radiant heat transfer in the interior of the satellite boom

$$\frac{d^2\dot{Q}}{dA_e\, dA_{in}} = \frac{1}{\pi}\epsilon_b \sigma \left[T_b(\mu_r+\Omega)\right]^4 \cos\lambda_{r_1} \frac{d\omega}{dA_{in}} \tag{4.39}$$

where $d\omega$ is the solid angle subtended by dA_{in} as seen from dA_e

$$d\omega = \frac{\cos\lambda_{r_2}\, dA_{in}}{r^2} . \tag{4.40}$$

From Figure 4-4 it is evident that

$$\lambda_{r_1} = \lambda_{r_2} = \lambda_r \tag{4.41}$$

$$r^2 = \rho_r^2 + 2a_b^2(1-\cos\mu_r) \tag{4.42}$$

and

$$a_b^2 + \rho_r^2 = a_b^2 + r^2 - 2a_b r\cos\lambda_r \tag{4.43}$$

so that

$$\cos\lambda_r = \frac{a_b}{r}(1-\cos\mu_r) \tag{4.44}$$

The radiation incident on dA_{in} from dA_e is then given by

$$\frac{d^2\dot{Q}}{dA_e\, dA_{in}} = \frac{\epsilon_b \sigma \left[T_b(\mu_r+\Omega)\right]^4 a_b^2 (1-\cos\mu_r)^2}{\pi\left[\rho_r^2 + 2a_b^2(1-\cos\mu_r)\right]^2} \tag{4.45}$$

and since

$$dA_e = a_b \, d\rho_r \, d\mu_r \tag{4.46}$$

$$\frac{d\dot{Q}}{dA_{in}} = q_{in} = \int_0^{2\pi}\int_{-\infty}^{\infty} \frac{\epsilon_b \sigma \left[T_b(\mu_r+\Omega)\right]^4 a_b^3 \left(1-\cos\mu_r\right)^2}{\pi\left[\rho_r^2 + 2a_b^2(1-\cos\mu_r)\right]^2} d\rho_r \, d\mu_r$$

$$= \frac{\epsilon_b \sigma}{4\sqrt{2}} \int_0^{2\pi} \sqrt{1-\cos\mu_r}\left[T_b(\mu_r+\Omega)\right]^4 d\mu_r. \tag{4.47}$$

4.4 Solution of the Heat Balance Equation

Representing the temperature distribution in the boom by a series of the form

$$T_b(\Omega) = \sum_{n=0}^{\infty} T_{b,n}(t) \cos n\Omega \tag{4.48}$$

where it may be assumed that

$$T_{b,0}(t) >> T_{b,n}(t); \quad n = 1, 2, \cdots \tag{4.49}$$

leads to the series

$$\left[T_b(\mu_r+\Omega)\right]^4 \approx T_{b,0}^4(t) + 4T_{b,0}^3(t)\sum_{n=1}^{\infty} T_{b,n}(t)\cos n(\mu_r+\Omega). \tag{4.50}$$

Hence the radiation incident upon the interior immediately following emission is

$$q_{in} = \frac{\epsilon_b \sigma}{4} \int_0^{2\pi} \left[T_{b,0}^4 + 4 T_{b,0}^3 \sum_{n=1}^{\infty} T_{b,n} \cos n(\mu_r + \Omega) \right] \sin \frac{\mu_r}{2} \, d\mu_r$$

$$= \epsilon_b \sigma \left[T_{b,0}^4 + 4 T_{b,0}^3 \sum_{n=1}^{\infty} \frac{T_{b,n} \cos n\Omega}{1 - 4n^2} \right]. \tag{4.51}$$

A fraction, ϵ_b, of this radiation is absorbed,

$$q_{abs} = \epsilon_b^2 \sigma \left[T_{b,0}^4 + 4 T_{b,0}^3 \sum_{n=1}^{\infty} \frac{T_{b,n} \cos n\Omega}{1 - 4n^2} \right] \tag{4.52}$$

and a quantity $(1 - \epsilon_b)$ is reflected,

$$q_{ref} = (1 - \epsilon_b) \epsilon_b \sigma \left[T_{b,0}^4 + 4 T_{b,0}^3 \sum_{n=1}^{\infty} \frac{T_{b,n} \cos n\Omega}{1 - 4n^2} \right]. \tag{4.53}$$

If the reflection is assumed diffuse, the reflected radiation is again incident upon the interior of the boom in a manner analogous to that employed in the derivation of equation (4.51). The total incident heat flux on the interior of the boom wall is then given by

$$q_{int} = \epsilon_b^2 \sigma \sum_{m=0}^{\infty} (1 - \epsilon_b)^m \left[T_{b,0}^4 + 4 T_{b,0}^3 \sum_{n=1}^{\infty} \frac{T_{b,n} \cos n\Omega}{(1 - 4n^2)^{m+1}} \right]. \tag{4.54}$$

Now,

$$\sum_{m=0}^{\infty}(1-\epsilon_b)^m = \left[1-(1-\epsilon_b)\right]^{-1} = \frac{1}{\epsilon_b} \tag{4.55}$$

$$\sum_{m=0}^{\infty}\frac{(1-\epsilon_b)^m}{(1-4n^2)^{m+1}} = \frac{1}{(1-4n^2)}\sum_{m=0}^{\infty}\left(\frac{1-\epsilon_b}{1-4n^2}\right)^m$$

$$= \frac{1}{\epsilon_b - 4n^2} \tag{4.56}$$

so that

$$q_{int} = \epsilon_b \sigma T_{b,o}^4 + 4\epsilon_b^2 \sigma T_{b,o}^3 \sum_{n=1}^{\infty}\frac{T_{bn}\cos n\Omega}{\epsilon_b - 4n^2} \; . \tag{4.57}$$

The final form of the heat balance equation can now be written

$$-\frac{k_b b_b}{a_b^2}\sum_{n=0}^{\infty} T_{b,n} n^2 \cos n\Omega + q_s \alpha_s \sin\phi^* \sum_{n=0}^{\infty} C_{s,n}\cos n\Omega$$

$$-\epsilon_b \sigma T_{b,o}^4 + 4\epsilon_b^2 \sigma T_{b,o}^3 \sum_{n=1}^{\infty}\frac{T_{bn}\cos n\Omega}{\epsilon_b - 4n^2} \tag{4.58}$$

$$-8\epsilon_b \sigma T_{b,o}^3 \sum_{n=1}^{\infty} T_{b,n}\cos n\Omega$$

$$= c_b \rho_b b_b \sum_{n=0}^{\infty} \dot{T}_{b,n}\cos n\Omega$$

which is of the form

$$\sum_{n=0}^{\infty} C_{b,n} \cos n\Omega = 0 \tag{4.59}$$

where the $C_{b,n}$ depend on time, but are independent of Ω. This leads to the series of equations

$$c_b \rho_b b_b \dot{T}_{b,0} + \epsilon_b \sigma T_{b,0}^4 = \frac{1}{\pi} q_s \alpha_s \sin\phi^* \tag{4.60}$$

$$c_b \rho_b b_b \dot{T}_{b,n} + \left\{ \frac{k_b b_b}{a_b^2} n^2 + 4\epsilon_b \sigma T_{b,0}^3 \left[2 + \frac{\epsilon_b}{4n^2 - \epsilon_b} \right] \right\} T_{b,n} = C_{s,n} q_s \alpha_s \sin\phi^*; \quad (n = 1, 2, \cdots) \tag{4.61}$$

where

$$C_{s,n} = \begin{cases} \frac{1}{2} & ; \quad n = 1 \\ \frac{2(-1)^{n/2}}{\pi(n^2-1)} & ; \quad n \text{ even}; \neq 0 \\ 0 & ; \quad n \text{ odd}, \neq 1. \end{cases} \tag{4.62}$$

The first of these equations is non-linear. The remaining equations, although linear, contain time varying coefficients which depend on the solution of (4.60).

Fortunately it is not necessary to solve the equations in detail. Considerable information can be obtained by determining the approximate time constant and the steady state solution.

The time constant of the nth term of the series (4.48) is given by

$$\tau_n = \frac{c_b \rho_b b_b}{\left[\frac{k_b b_b n^2}{a_b^2} + 4\epsilon_b \sigma T_{b,0}^3 \left(2 + \frac{\epsilon_b}{4n^2 - \epsilon_b}\right)\right]} < c_b \rho_b a_b^2 / k_b n^2 \tag{4.63}$$

and the steady state solution for the same term is

$$T_{n,steady} = \frac{C_{s,n} q_s \alpha_s \sin \phi^*}{\left[\frac{k_b b_b n^2}{a_b^2} + 4\epsilon_b \sigma T_{b,0}^3 \left(2 + \frac{\epsilon_b}{4n^2 - \epsilon_b}\right)\right]} \tag{4.64}$$

The analysis of Etkin and Hughes,[35] referred to earlier, ignores the term involving conductivity in the denominator of equation (4.64). This is usually the dominant term and hence their analysis overestimates the effect of solar heating. For the representative configurations (Table III)

$$\tau_{n(max)} \approx \frac{12}{n^2} \tag{4.65}$$

and therefore τ_1 is very short, of the order of 12 seconds.

The short time constant implies that the F_i depend directly on the solar aspect angle as the thermal lag is negligible compared to the librational and orbital periods. The presence of internal damping will cause the complementary solutions of equation (4.33) to damp out leaving only the forced motion of the boom. As the F_i depend essentially

on the position of the satellite, the rate of change of which is of the order of the orbital period, the $\ddot{A}_i$ term in (4.33) may also be neglected so that

$$A_i = \frac{F_i}{\omega_i^2} . \tag{4.66}$$

Thus the instantaneous configuration of the satellite is represented by its steady state deflection corresponding to the orientation. This in effect eliminates equations (4.33) leaving only (4.12), containing variable inertias, to be solved.

4.5 Thermal Deflection of the Boom

Consider an element of the boom of width $a_b d\Omega$ (Figure 4-5). The length of the strip is

$$\ell_b(\Omega) = \left(R_c + a_b \cos\Omega\right)\phi_b . \tag{4.67}$$

If ℓ_{ref} denotes the original length of the strip at a reference temperature, T_{ref}, this length can be obtained by altering the temperature and stressing the material

$$\ell_b(\Omega) = \ell_{ref}\left[1 + \alpha_t\left(T(\Omega) - T_{ref}\right) + \frac{\sigma_b(\Omega)}{E}\right], \tag{4.68}$$

hence

$$\sigma_b(\Omega) = E\left[\left(\frac{R_c\phi_b}{\ell_{ref}} - 1\right) + \frac{a_b\phi_b}{\ell_{ref}}\cos\Omega - \alpha_t\left(T(\Omega) - T_{ref}\right)\right]. \tag{4.69}$$

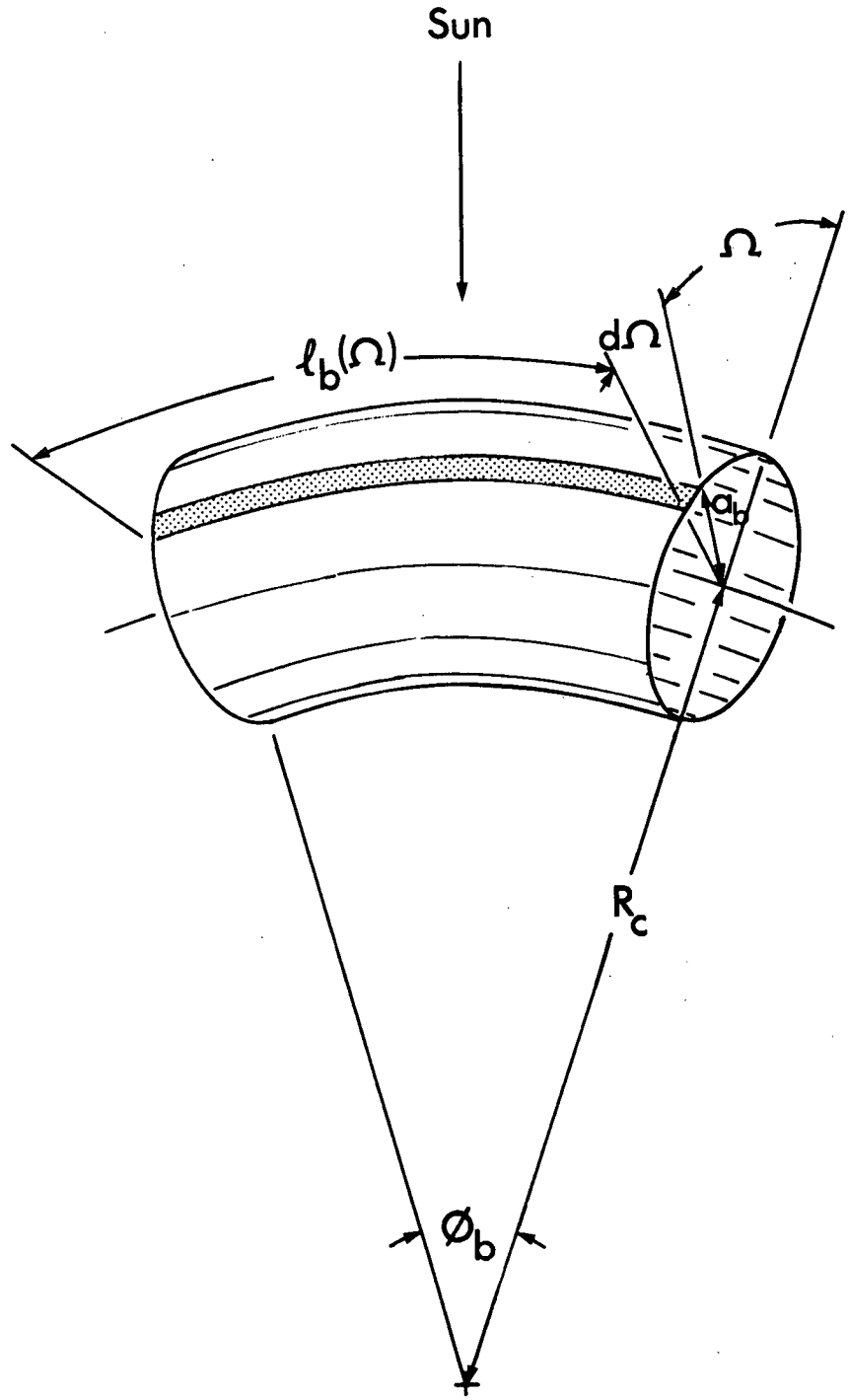

Figure 4-5 Thermal deflection of the satellite boom

The longitudinal force on the element is

$$F_L = \int_0^{2\pi} \sigma(\Omega)\, a_b\, b_b\, d\Omega$$

$$= 2\pi a_b b_b E\left\{\left(\frac{R_c \phi_b - l}{l_{ref}}\right) - \alpha_t\left(T_{b,o} - T_{ref}\right)\right\} \tag{4.70}$$

where

$R_c \phi_b = l(\pi/2)$ = mean length of the element.

During orbital motion the longitudinal force on the satellite is negligibly small so that

$$\frac{l(\pi/2) - l}{l_{ref}} = \alpha_t\left(T_{b,o} - T_{ref}\right) \tag{4.71}$$

which represents the longitudinal thermal expansion.

The moment produced by the stresses on the section is

$$\Gamma_b = \int_0^{2\pi} \sigma(\Omega)\, a_b^2\, b_b \cos\Omega\, d\Omega$$

$$= \pi a_b^2 b_b E\left\{\frac{a_b \phi_b}{l_{ref}} - \alpha_t T_{b,1}\right\} \tag{4.72}$$

If the frequency of the thermal driving force is much lower than the natural frequency of the beam, the beam will be in equilibrium and the moment will be zero. That is

$$\frac{\phi_b}{l_{ref}} = \frac{1}{R_c} = \frac{\alpha_t T_{b1}}{a_b} . \tag{4.73}$$

Let the ξ_b, η_b-co-ordinate system be defined so that the ξ_b, η_b-plane lies in the plane of motion with the sun on the negative η_b-axis (Figure 4-6). From elementary calculus

$$\frac{1}{R_c} = \frac{d^2\eta_b/d\xi_b^2}{\left[1 + (d\eta_b/d\xi_b)^2\right]^{3/2}} = \frac{1}{l^*\left[1 + (d\eta_b/d\xi_b)^2\right]^{1/2}} \tag{4.74}$$

or

$$\frac{d^2\eta_b}{d\xi_b^2} = \frac{1}{l^*}\left[1 + \left(\frac{d\eta_b}{d\xi_b}\right)^2\right] \tag{4.75}$$

where

$$l^* = \frac{2a_b}{\alpha_s \alpha_t q_s}\left[\frac{k_b b_b}{a_b^2} + 4\epsilon_b \sigma T_{b,0}^3 \left(\frac{\theta - \epsilon_b}{4 - \epsilon_b}\right)\right]. \tag{4.76}$$

Taking

$$\eta_b(0) = \frac{d\eta_b}{d\xi_b}(0) = 0 \tag{4.77}$$

gives

$$\eta_b = -l^* \ln \cos(\xi_b/l^*). \tag{4.78}$$

This solution is illustrated in Figure 4-6.

If s is the arc length of the curve

$$s = \ell^* \ln \left| \tan\left(\frac{\varepsilon_b}{2\ell^*} + \frac{\pi}{4}\right)\right| \tag{4.79}$$

and the solution can be written in the parametric form

$$\varepsilon_b = \ell^* \sin^{-1}\left[\tanh\left(s/\ell^*\right)\right] \tag{4.80}$$

$$\eta_b = \ell^* \ln \cosh\left(s/\ell^*\right). \tag{4.81}$$

A satellite of given length can be easily fitted along an arc of the curve in Figure 4-6, hence its centre of mass, orientation of principal axes, and the corresponding moments of inertia can be determined as indicated in Figure 4-7. The results of this analysis are plotted in Figures 4-8 and 4-9. The variation is expressed by the factors

$$K_x = \frac{I_r - I_{xx}}{I_r - I_{xx_{min}}} \tag{4.82}$$

$$K_z = \frac{I_{zz}}{I_{zz_{max}}}$$

where I_r represents the inertia of the rigid satellite about the x- and y-axes. It is interesting to note that $I_r - I_{xx_{min}}$ is nearly three times $I_{zz_{max}}$ and

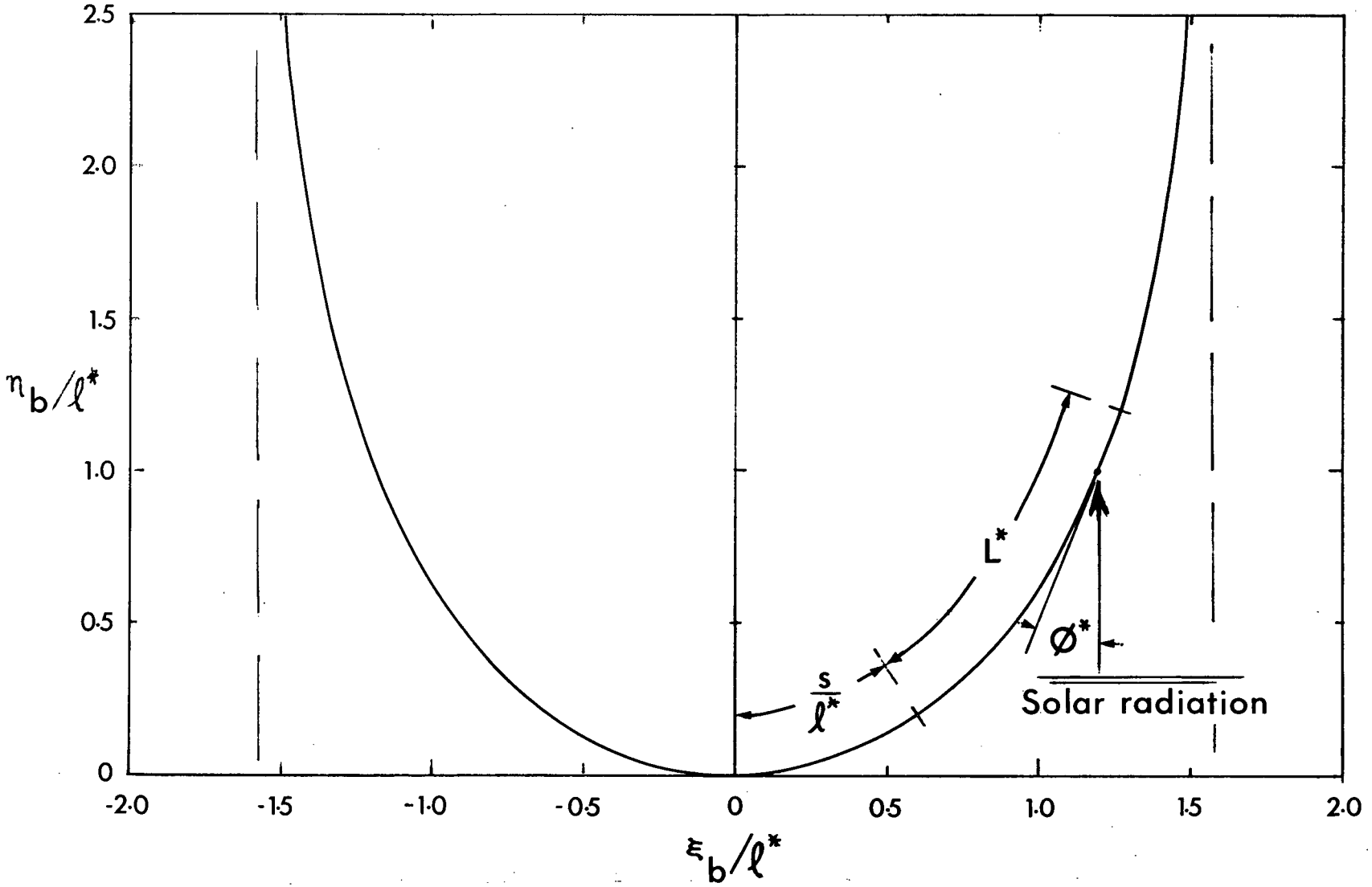

Figure 4-6 Shape of thermally deflected satellite boom

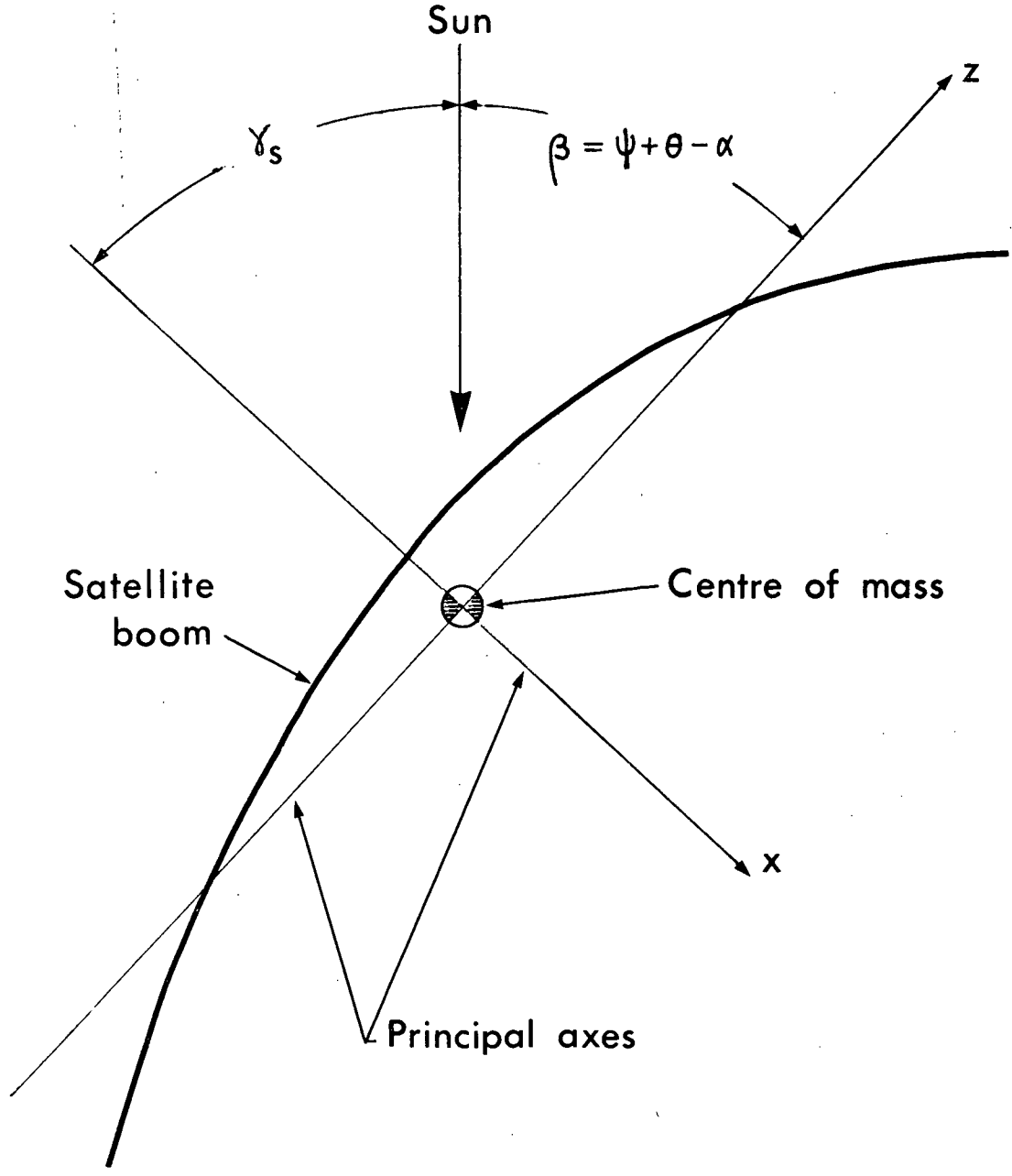

Figure 4-7 Illustration of the principal axes of the deflected satellite

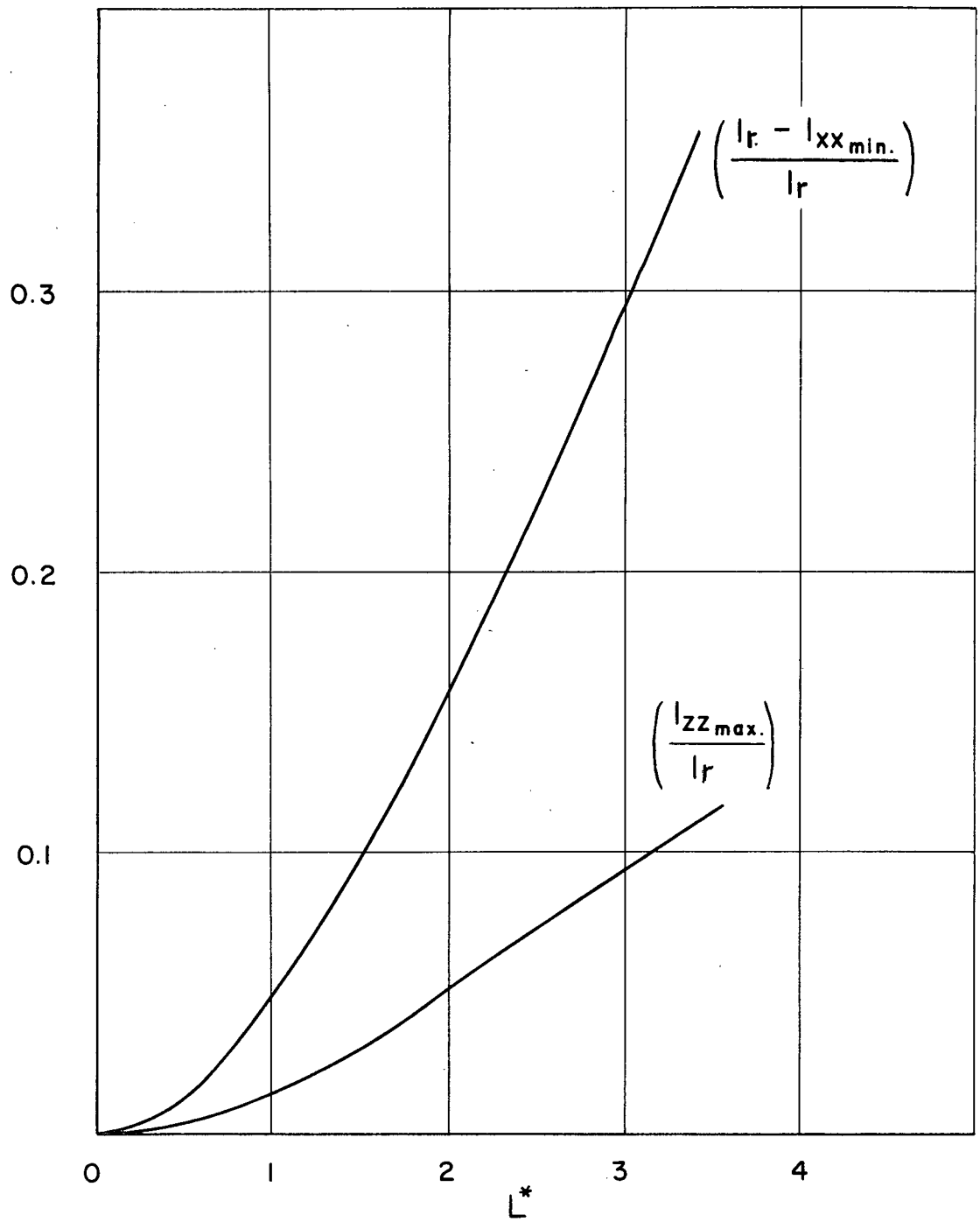

Figure 4-8 Maximum inertia variations as functions of boom length

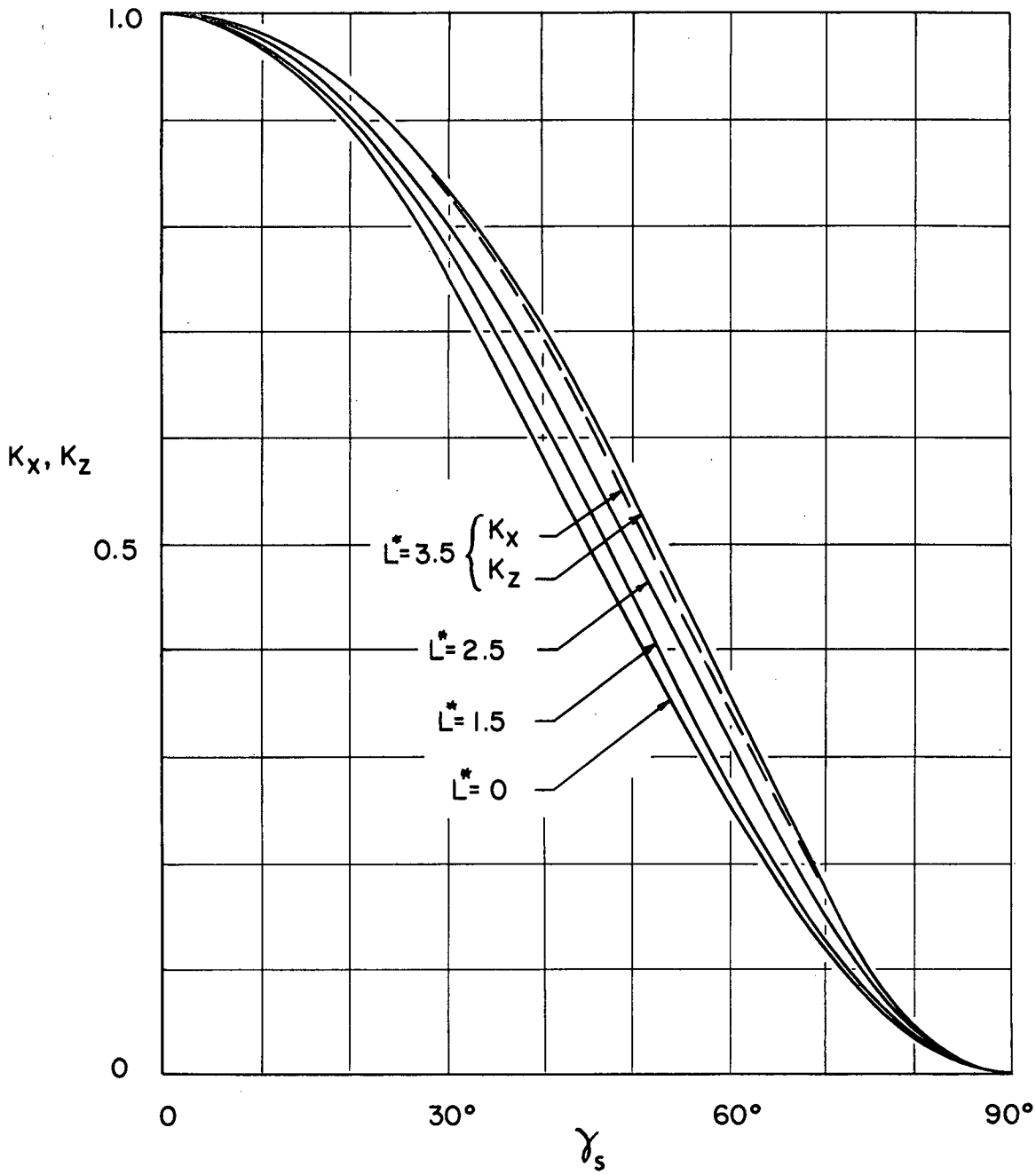

Figure 4-9 Relative inertia variation as a function of the angle between the sun and the x-axis

$$K_x \approx K_z \approx \cos^2 \gamma_s \tag{4.83}$$

so that

$$I_{zz} \approx I_{zz_{max}} \cos^2 \gamma_s \tag{4.84}$$

$$I_{xx} \approx I_r - (I_r - I_{xx_{min}}) \cos^2 \gamma \approx I_r - 3 I_{zz_{max}} \cos^2 \gamma_s .$$

Noting again that

$$\frac{d}{dt} = \frac{h_\theta}{r^2} \frac{d}{d\theta} \tag{4.85}$$

$$\frac{d^2}{dt^2} = \frac{h_\theta^2}{r^4} \frac{d^2}{d\theta^2} - \frac{2h_\theta^2}{r^5} \frac{dr}{d\theta} \frac{d}{d\theta}$$

and representing

$$I_{yy} \approx I_r (1 - 2\bar{I} \sin^2 \beta)$$

$$I_{xx} - I_{zz} \approx I_r (1 - 4\bar{I} \sin^2 \beta) \tag{4.86}$$

equation (4.12) becomes

$$\begin{aligned} &(1 - 2\bar{I} \sin^2 \beta)(1 + e \cos\theta)\psi'' \\ &\quad - 2(\psi' + 1)\{(1 + e\cos\theta)\bar{I}(\psi' + 1) \sin 2\beta \\ &\qquad + e \sin\theta (1 - 2\bar{I} \sin^2 \beta)\} \end{aligned} \tag{4.87}$$

$$+ 3(1 - 4\bar{I}\sin^2\beta)\sin\psi\cos\psi = 0. \qquad (4.87)\ \text{cont'd}$$

4.6 Stability Analysis

The governing non-linear, non-autonomous differential equation (4.87) with periodic coefficients is of the same form as (2.14). Hence the solution of the equation when represented in the three dimensional phase space generates integral manifolds with properties similar to those discussed in Chapter 2.

The solution of the equation was obtained for a wide range of initial conditions using a digital computer. The satellite was taken to be stable if it did not tumble within fifty orbits. The trajectory starting from stable initial conditions generates a surface in phase space of the form shown in Figure 4-10. It is still sufficient to extend the phase space co-ordinate θ only up to 2π because when a trajectory arrives at $\theta = 2\pi$ with certain values of ψ and ψ', it may be extended by considering another trajectory starting from $\theta = 0$ with the same values of ψ and ψ'. This is identical with the procedure adopted in Chapter 2.

The search for the limiting initial conditions which result in stable librational motion is thus a search for

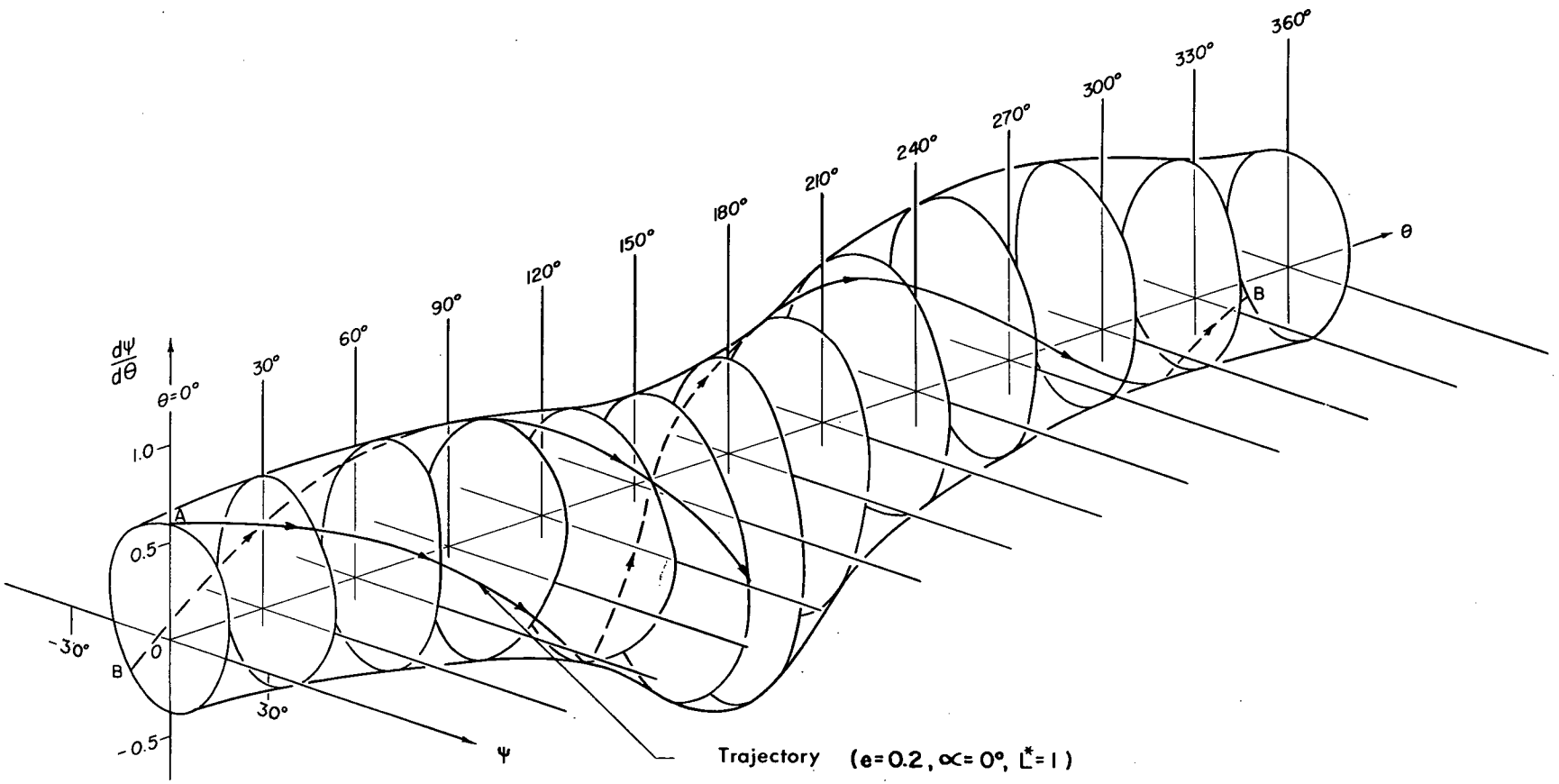

Figure 4-10 Typical invariant surface (e = 0.2, $\alpha = 0^{\circ}$, L* = 1)

the largest such surface. Any state of motion which lies within this surface generates a trajectory, and hence a new surface, which remains inside the limiting manifold. Therefore, the region enclosed by the limiting surface is the region of stability.

The usefulness of such a phase space was explained in section 2.4. For given eccentricity, satellite characteristics, and solar aspect angle it provides all possible combinations of disturbances to which the satellite may be subjected without causing it to tumble. The effect of solar aspect angle on the stability region is illustrated in Figures 4-11 and 4-12 where cross-sections of the stability region at several values of the orbit angle are presented.

A convenient condensation of data may be effected by plotting the intercepts of the ψ'-axis with the phase space cross-sections at $\theta = 0$ as shown in Figures 4-13 and 4-14. It is apparent that with increasing eccentricity the stability region decreases in size and beyond a critical value ceases to exist.

The accuracy with which the limiting manifolds were determined is approximately the same as discussed in Chapter 2. The calculations were carried out with the same precision and therefore the error in the region of stability is approximately $\pm$ .03 units in ψ'.

Several symmetry properties exhibited by equation (4.87) simplify the presentation of the numerical results.

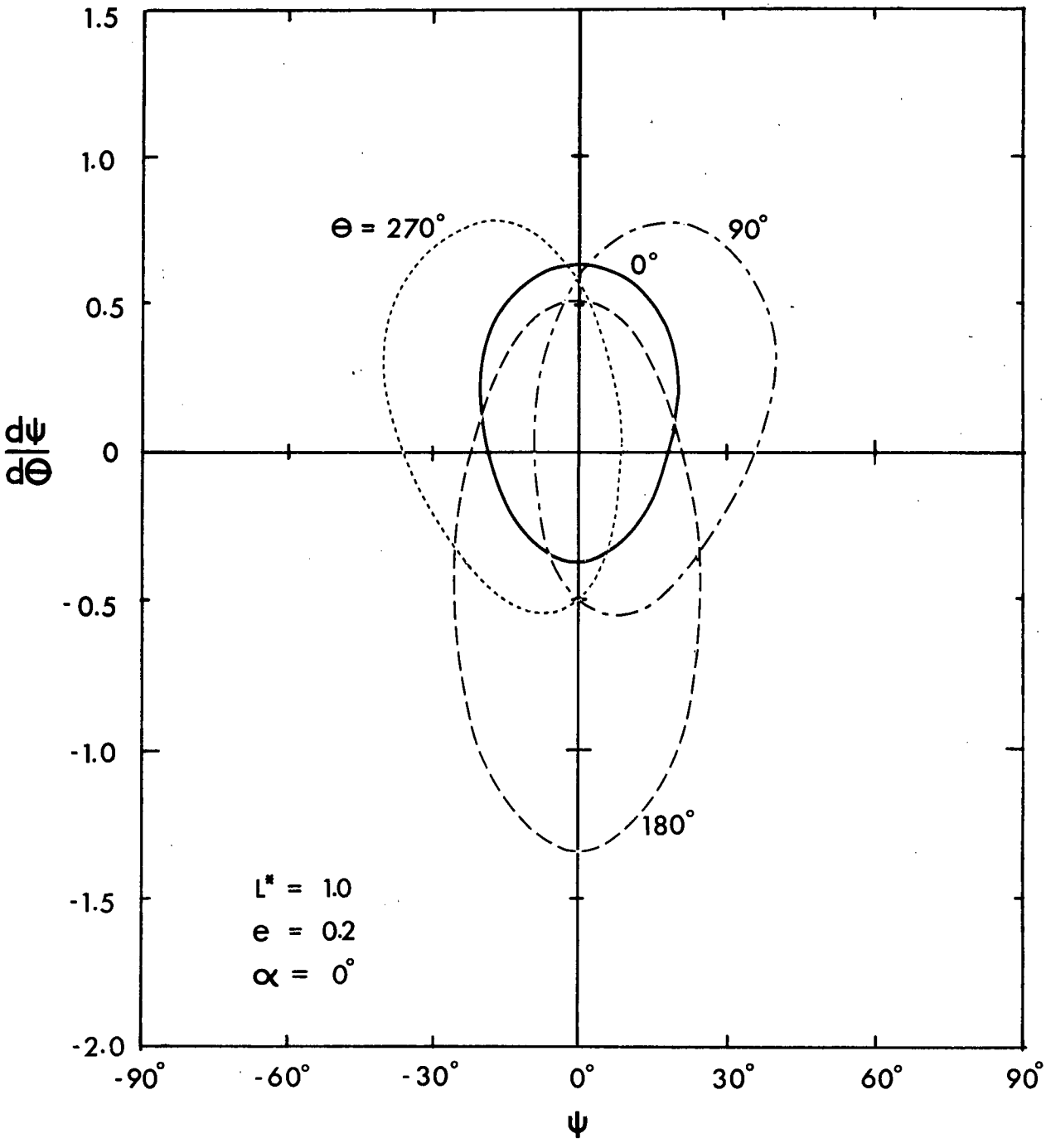

Figure 4-11 Variation of the cross-section of a limiting invariant surface with orbit angle ($e = 0.2$, $\alpha = 0^{\circ}$, $L^* = 1$)

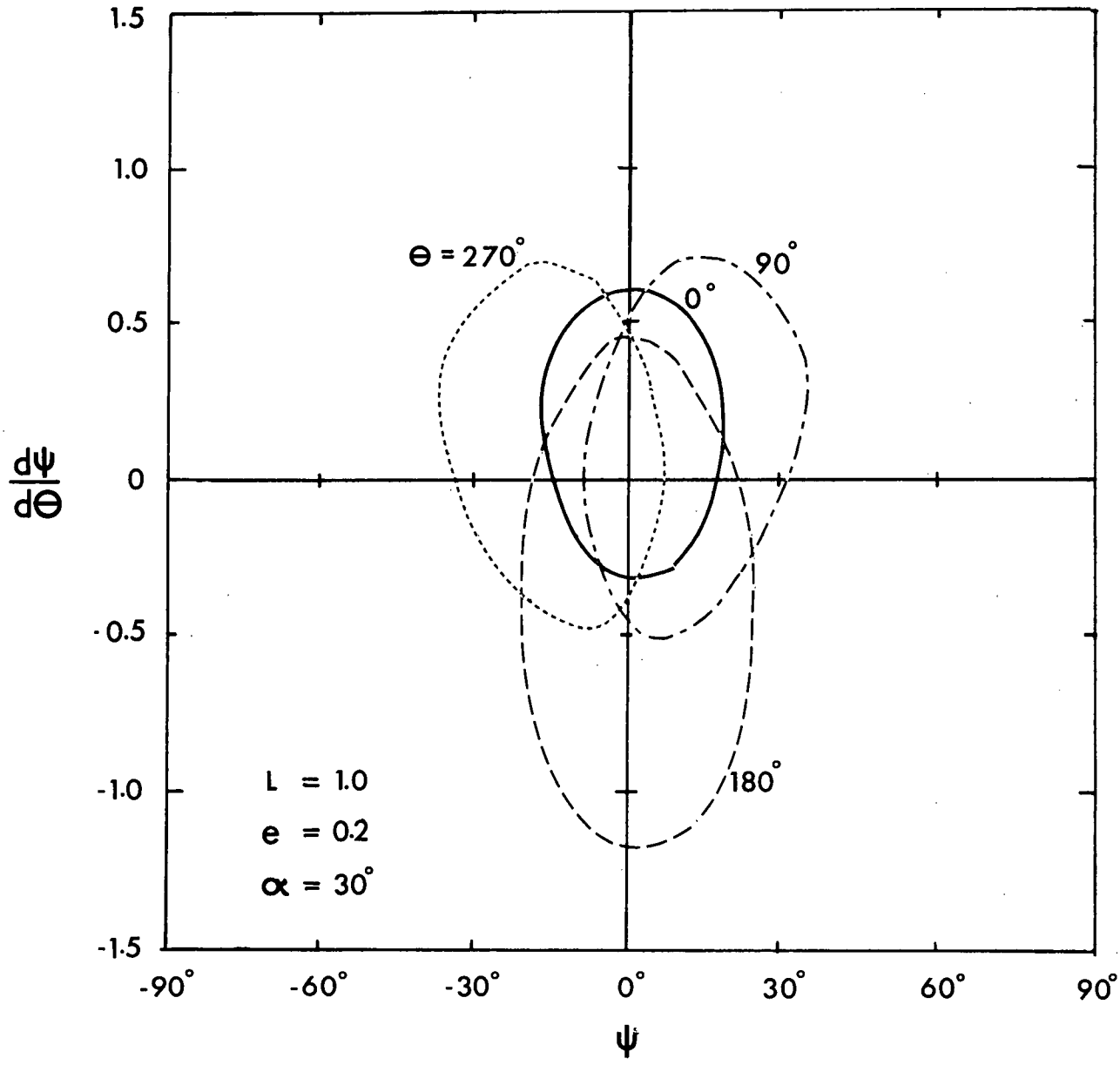

Figure 4-12 Variation of the cross-section of a limiting invariant surface with orbit angle (e = 0.2, $\alpha = 30^{\circ}$, L* = 1)

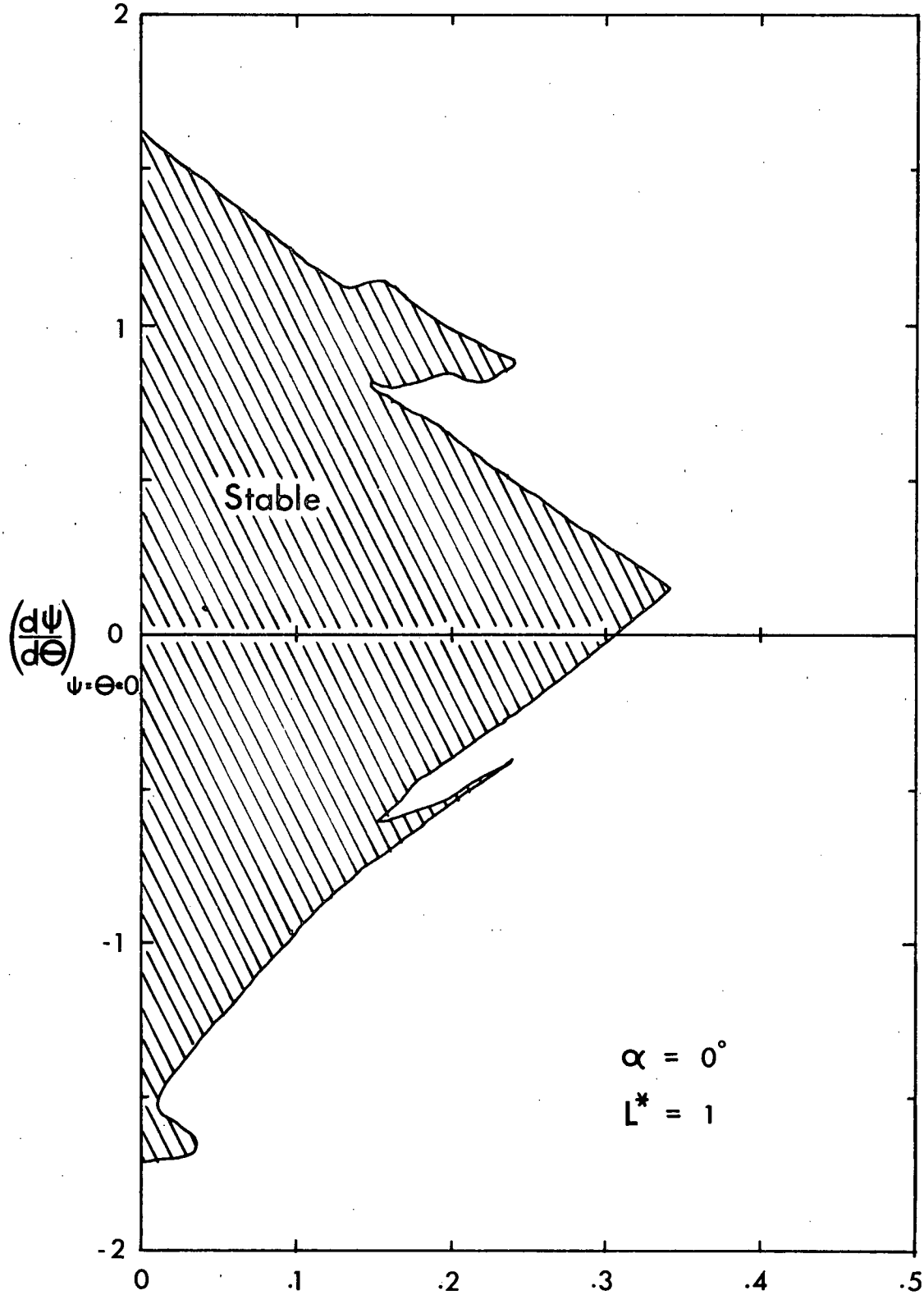

Figure 4-13-i Range of values of the derivative when $\psi = \theta = 0$ for stable motion ($L^* = 1$) ($\alpha = 0^\circ$)

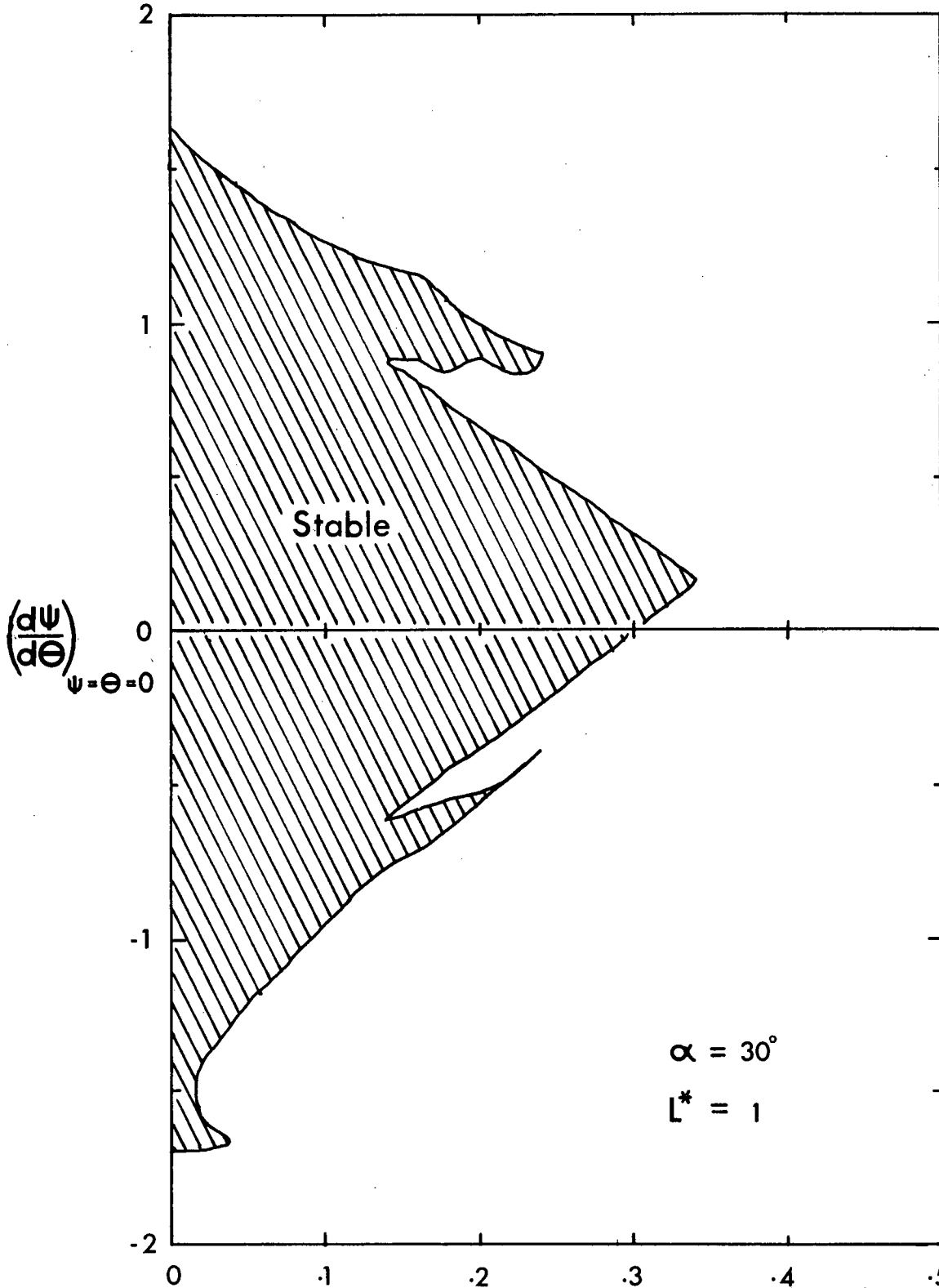

Figure 4-13-ii Range of values of the derivative when $\psi = \theta = 0$ for stable motion ($L^* = 1$) ($\alpha = 30^\circ$)

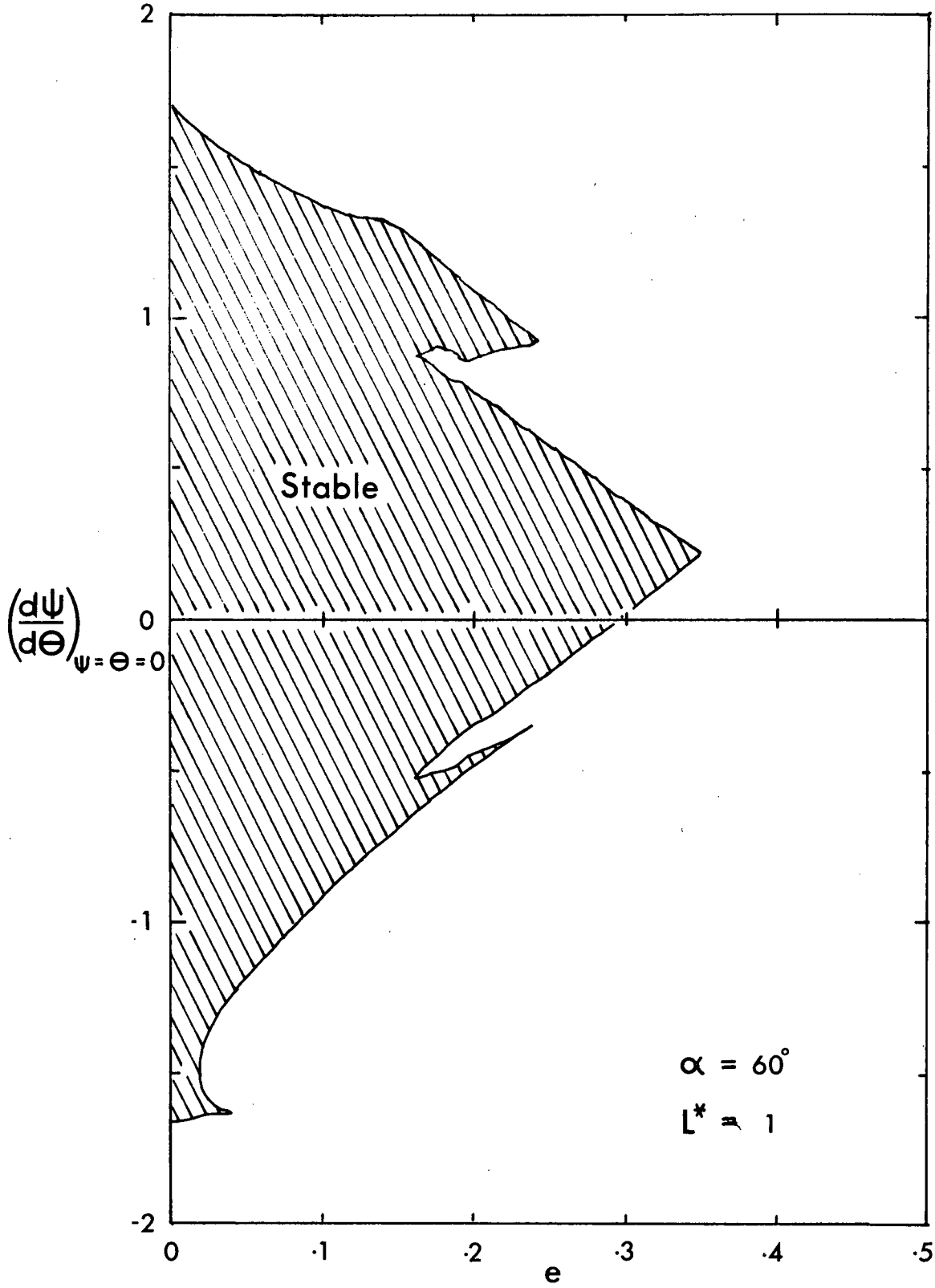

Figure 4-13-iii Range of values of the derivative when $\psi = \theta = 0$ for stable motion ($L^* = 1$) ($\alpha = 60^\circ$)

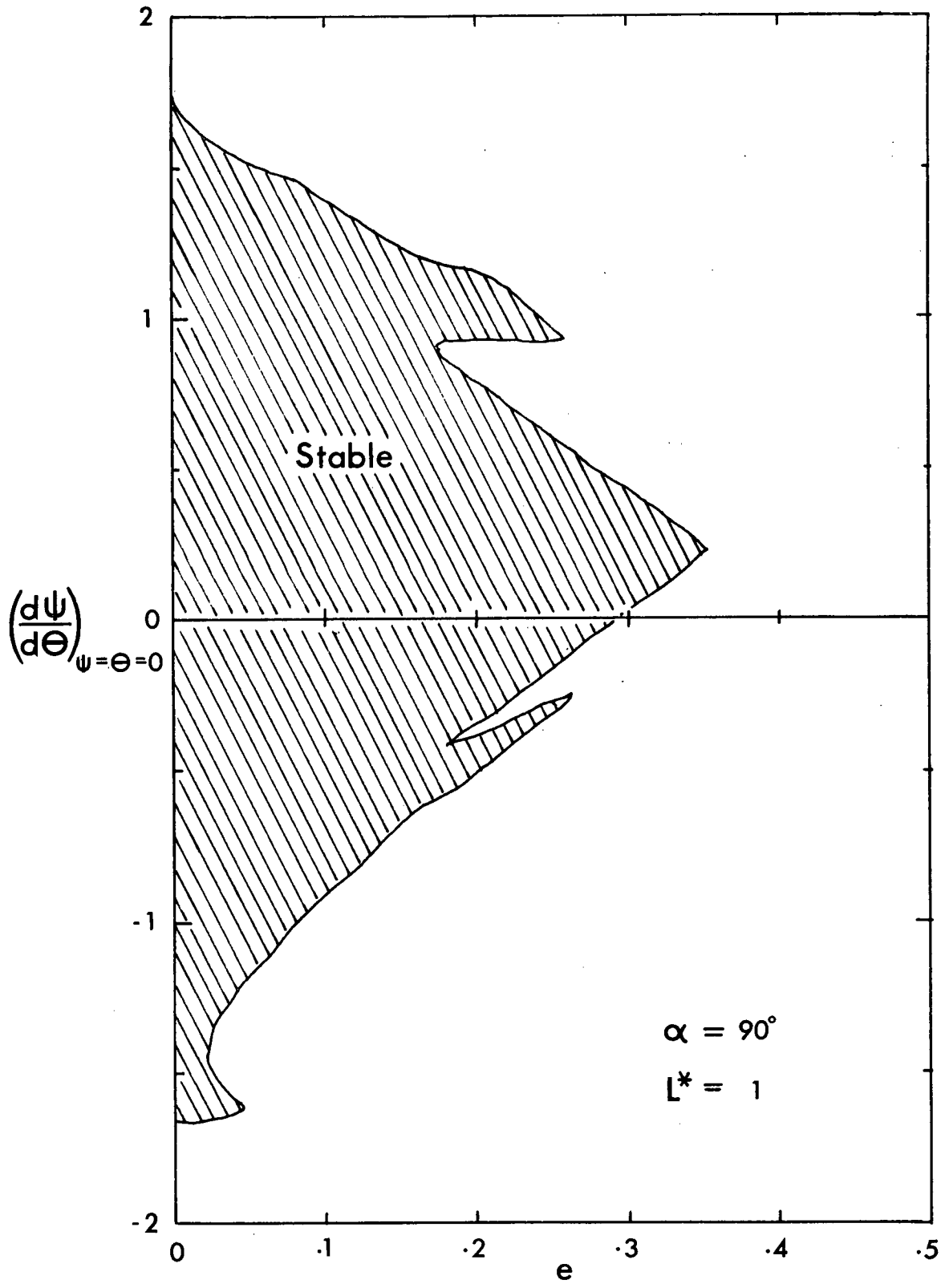

Figure 4-13-iv Range of values of the derivative when $\psi = \theta = 0$ for stable motion ($L^* = 1$) ($\alpha = 90^\circ$)

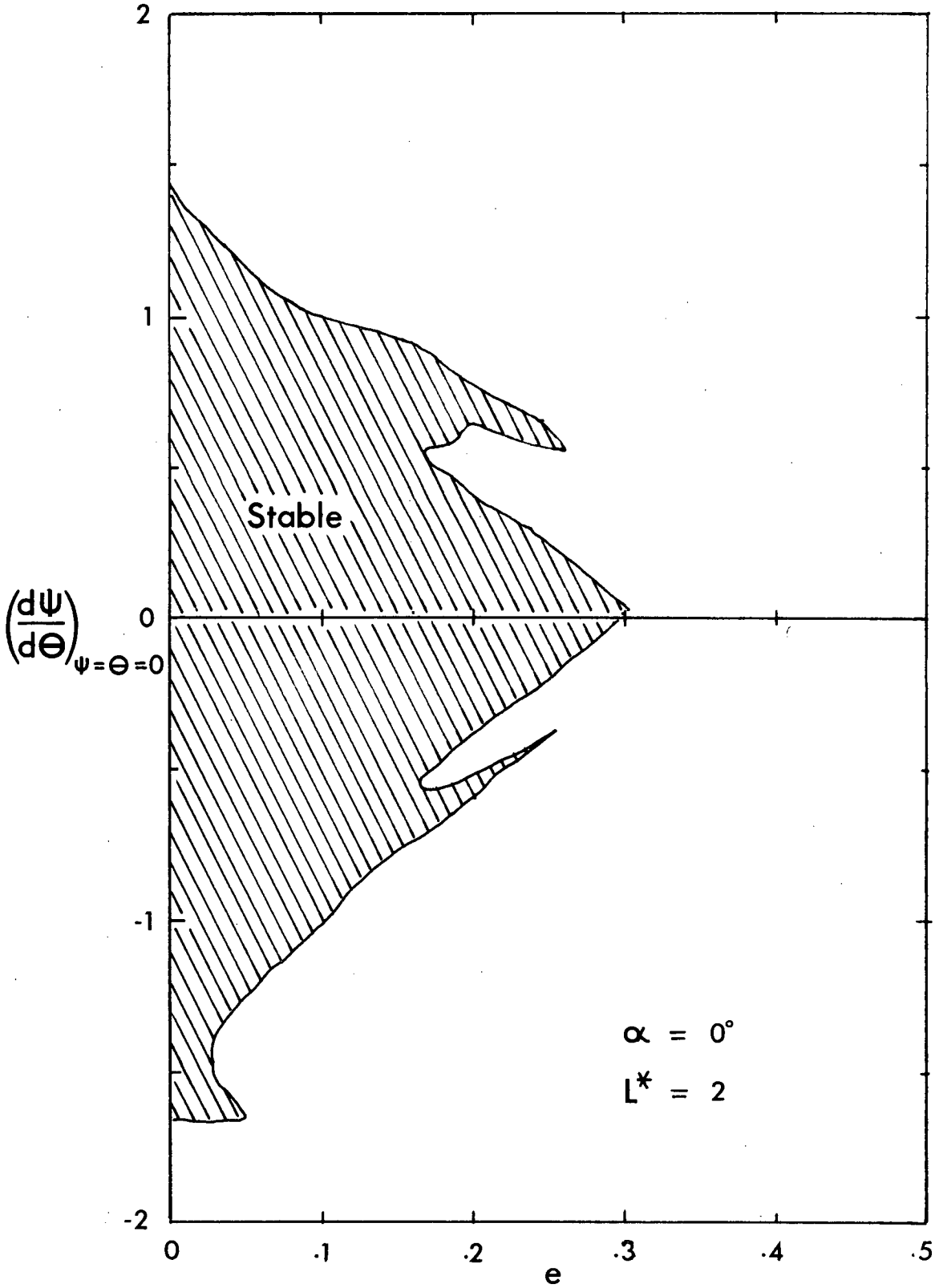

Figure 4-14-i Range of values of the derivative when $\psi = \theta = 0$ for stable motion ($L^* = 2$) ($\alpha = 0^\circ$)

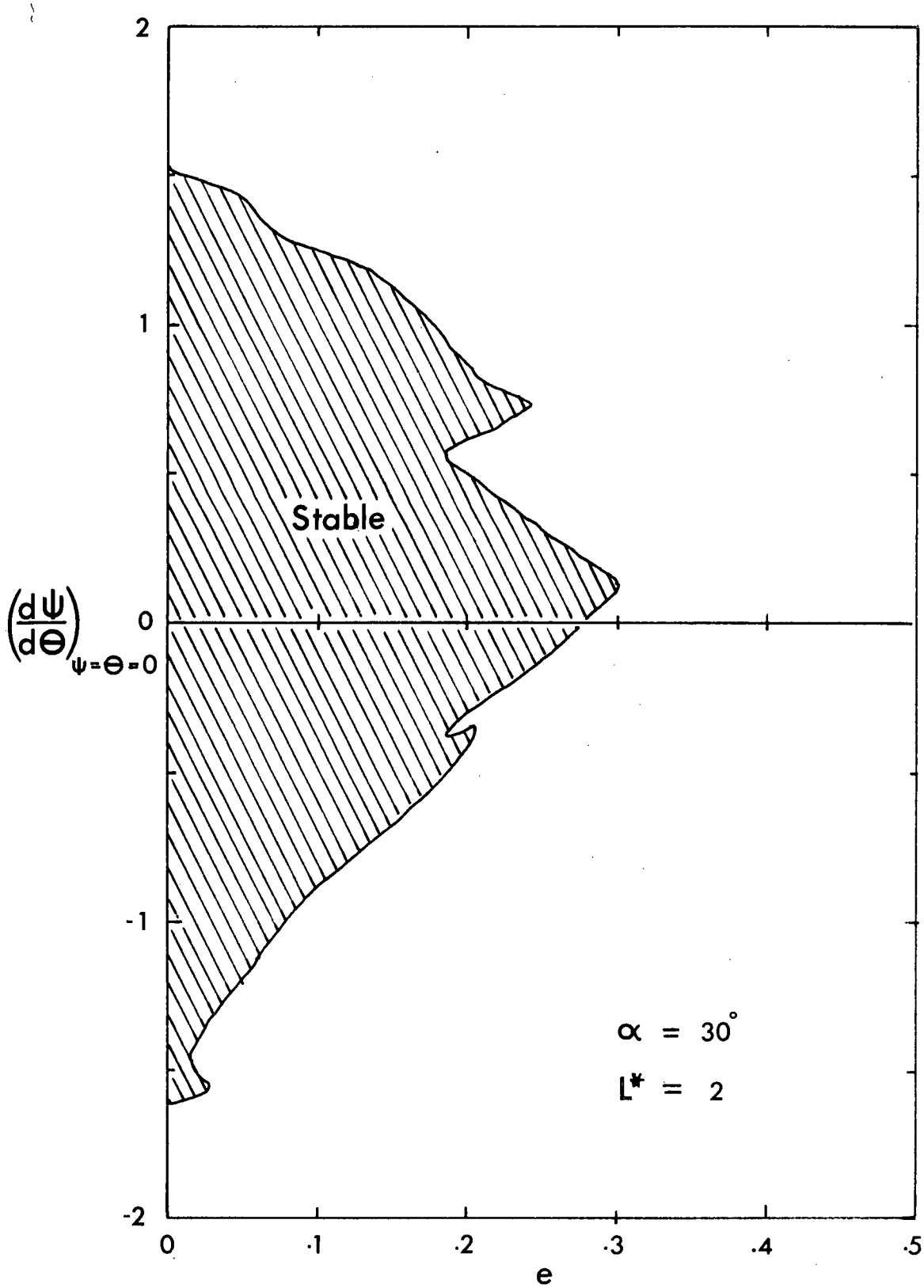

Figure 4-14-ii Range of values of the derivative when $\psi = \theta = 0$ for stable motion (L* = 2) ($\alpha = 30^{\circ}$)

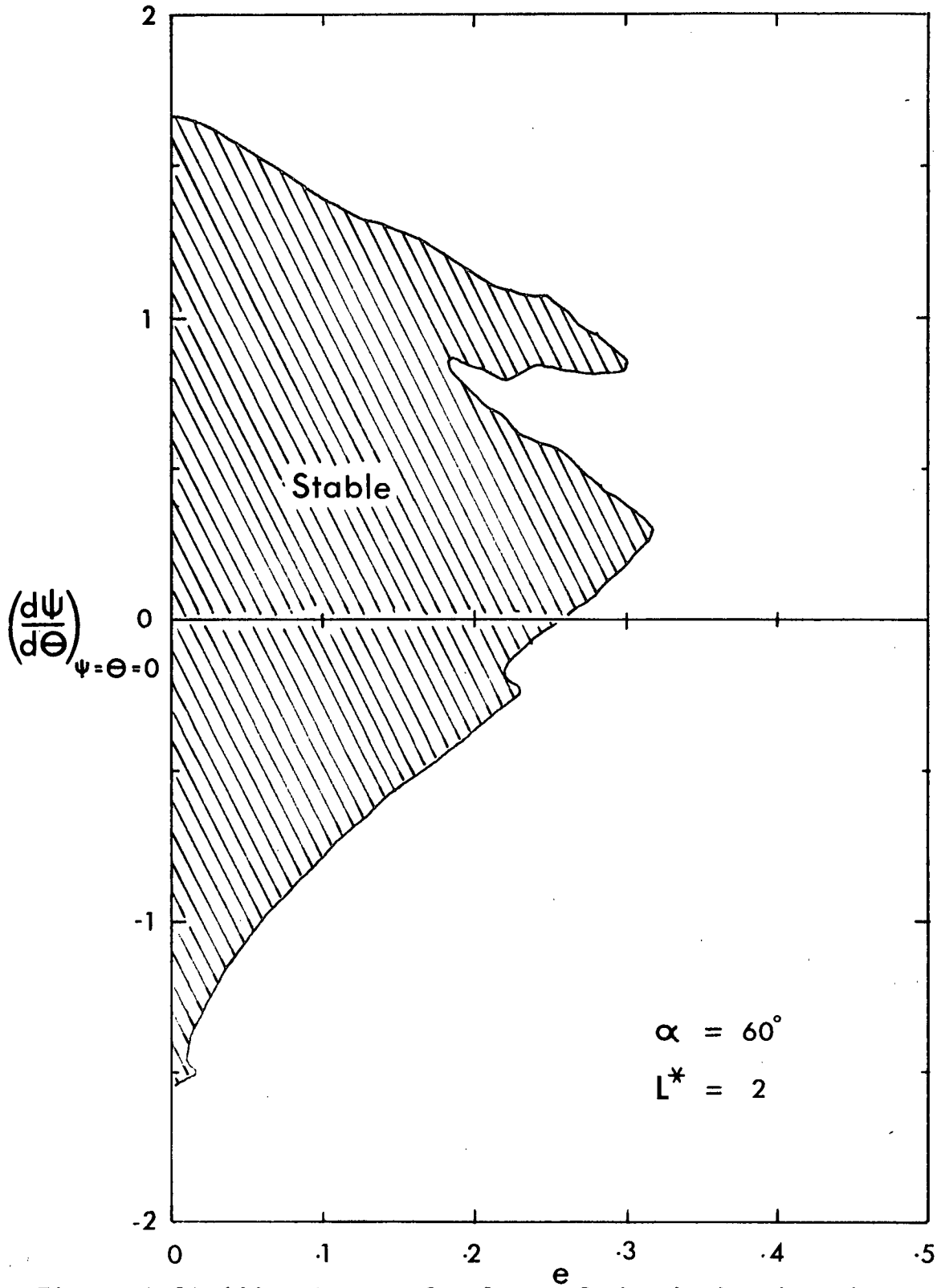

Figure 4-14-iii Range of values of the derivative when $\psi = \theta = 0$ for stable motion ($L^* = 2$) ($\alpha = 60^\circ$)

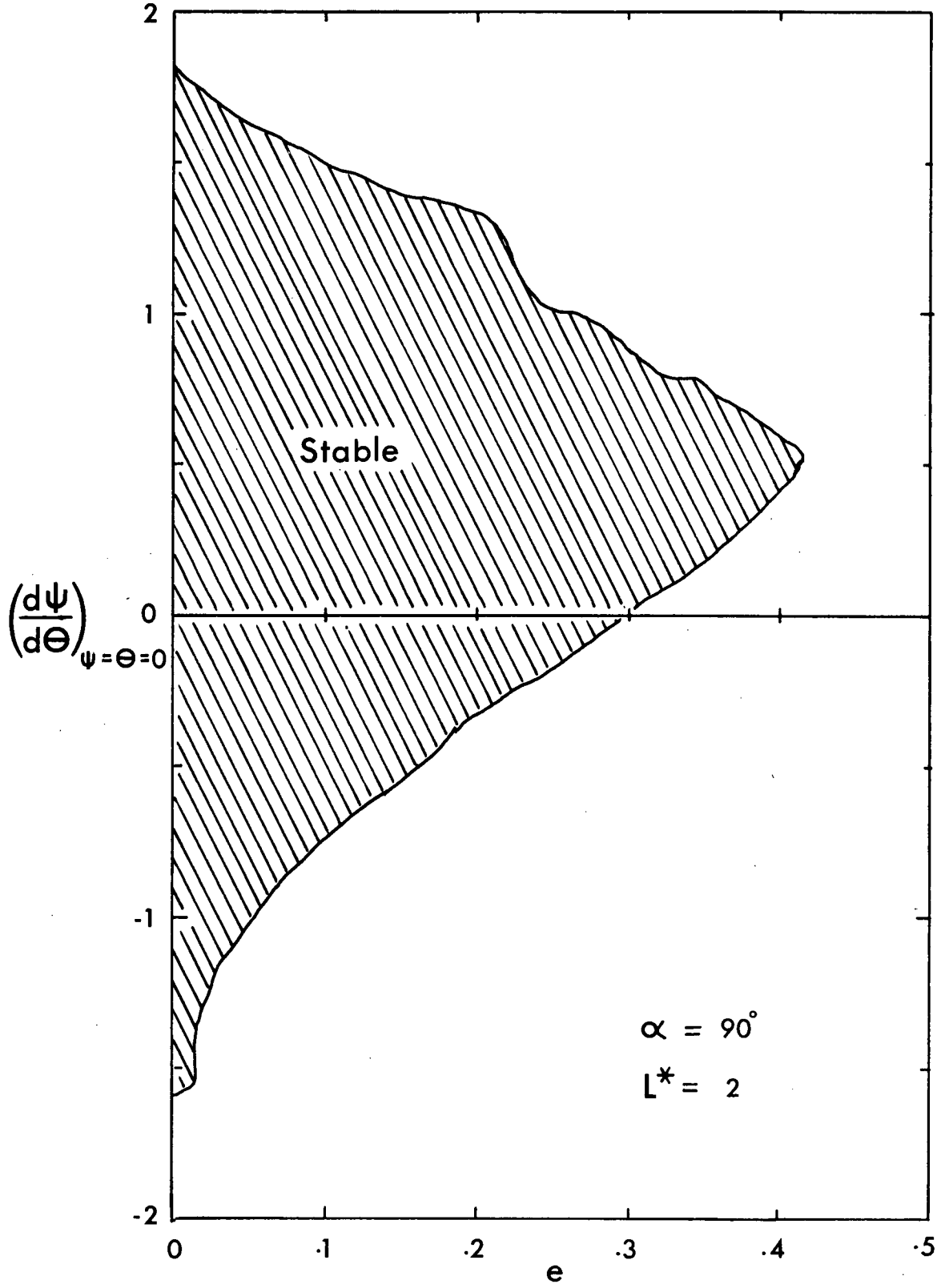

Figure 4-14-iv Range of values of the derivative when $\psi = \theta = 0$ for stable motion ($L^* = 2$) ($\alpha = 90^\circ$)

Note that substituting $\alpha + \pi$ for α results in no change in the trajectories as the equation is invariant under this substitution. For negative α, say $\alpha = -\alpha_\theta$, the solution for ψ obtained by integrating in the direction of increasing θ from the initial conditions $\psi = 0$, $\psi' = \psi'_o$, is exactly opposite in sign to that obtained by integrating backwards from the same initial conditions but with $\alpha = \alpha_\theta$. Hence the trajectories formed in the phase space for $-\alpha$ become mirror images of those obtained for $+\alpha$. In particular, the cross-sections for $\alpha = -\alpha_\theta$ at $\theta = 0, \pi$ are mirror images about the ψ'-axis of the cross-sections obtained for $\alpha = +\alpha_\theta$. Thus the intercepts of the ψ'-axis with the limiting surface at $\theta = 0$ do not change when α changes sign or increases by 180°.

Hence the stability region varies periodically with α. As the solar aspect angle would vary due to orbit precession and the motion of the planet about the sun, only those regions of the stability charts which actually overlap guarantee long term stability (Figure 4-15).

The spikes appearing in Figures 4-13 and 4-14 represent the secondary stability regions. They are associated with different periodic solutions to equation (4.87), and appear as small helical regions surrounding the main stable region of phase space. As the narrowness of these secondary regions makes them unsuitable for any practical operation, the appearance of spikes reduces the practical upper limit on eccentricity for stable operation.

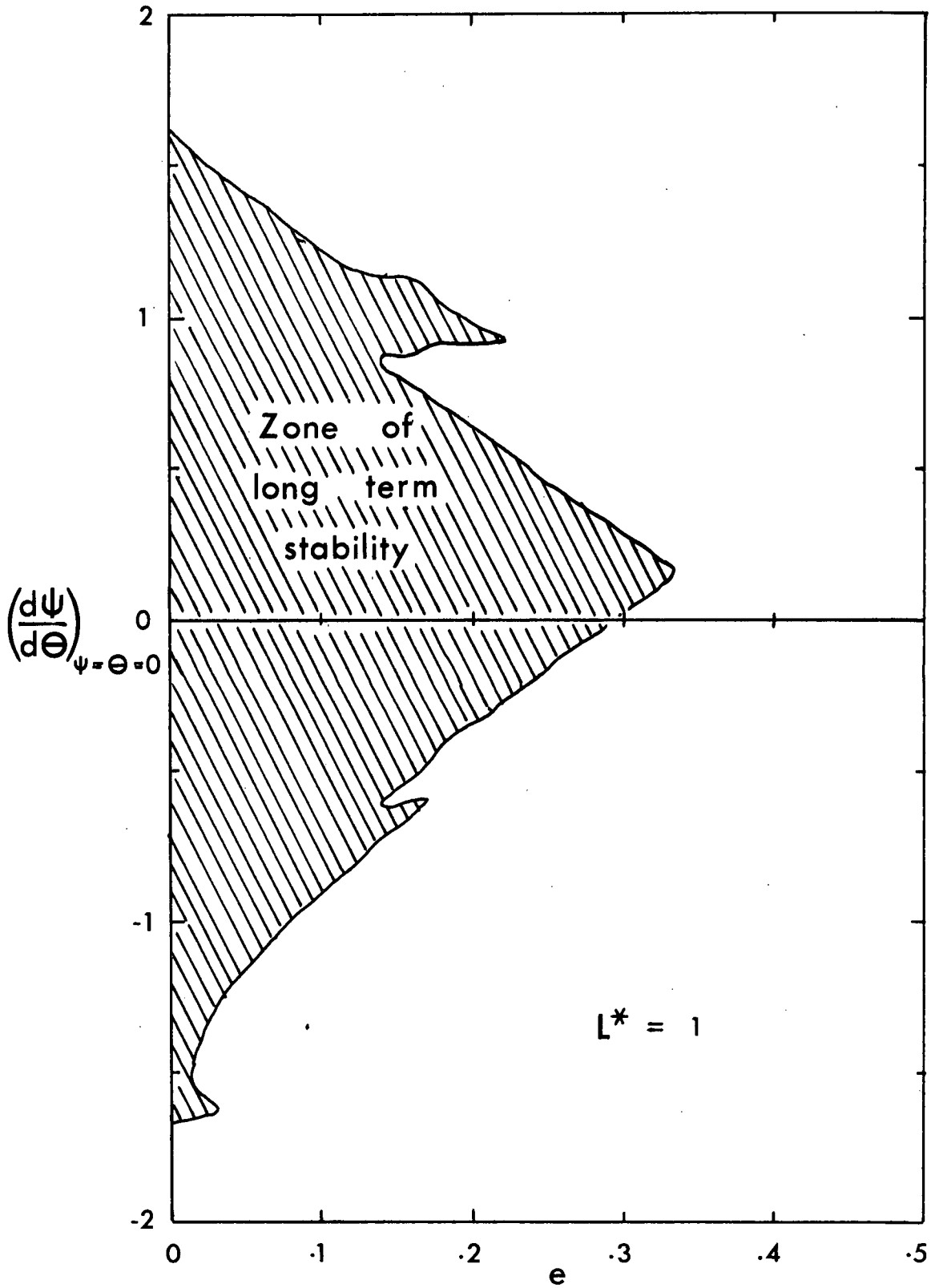

Figure 4-15-i Range of value of the derivative when $\psi = \theta = 0$ for long term stability ($L^* = 1$)

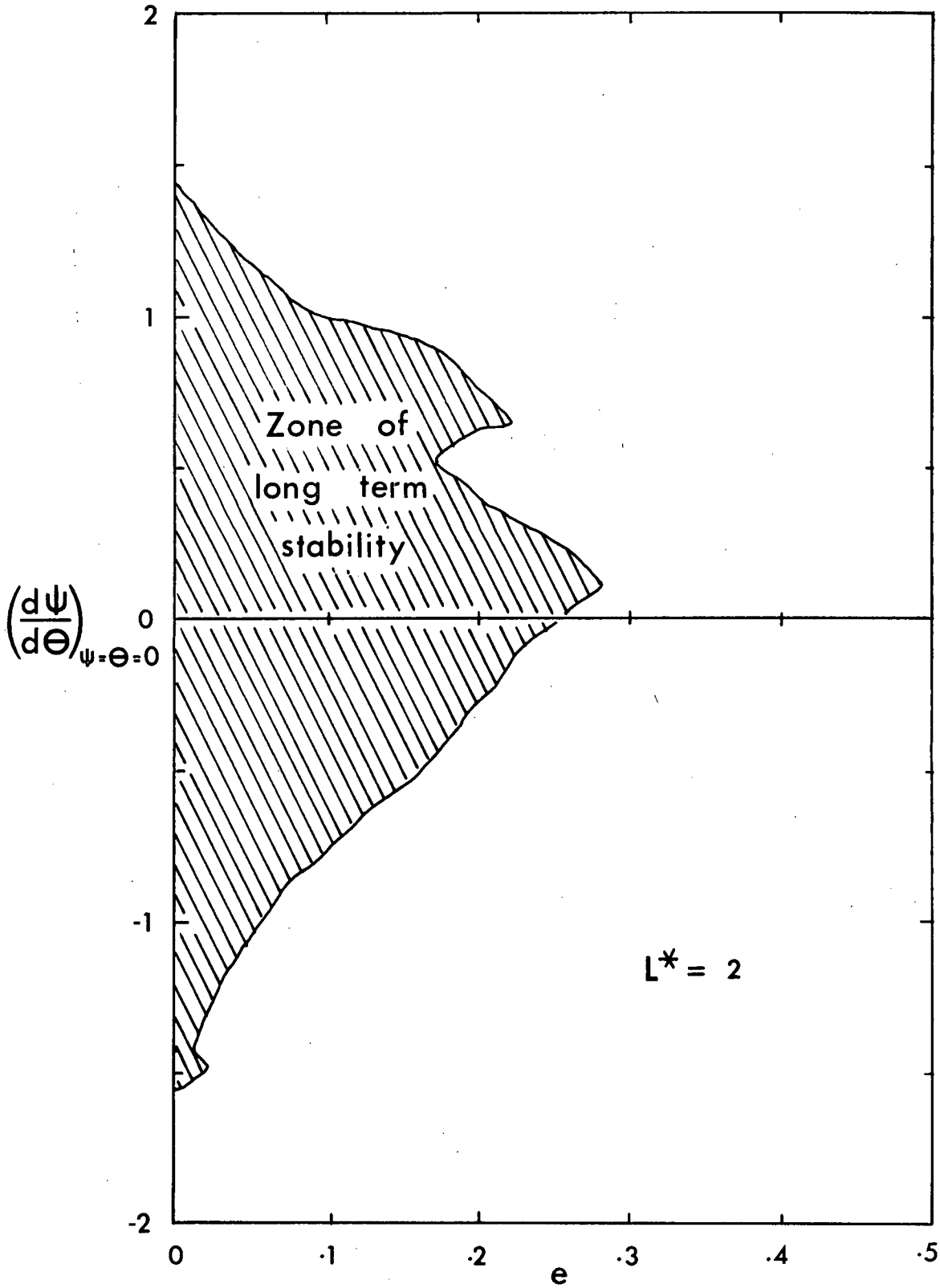

Figure 4-15-ii Range of value of the derivative when $\psi = \theta = 0$ for long term stability ($L^* = 2$)

4.7 Concluding Remarks

Based on the analysis the following observations may be made:

(i) The method employed in this chapter is restricted to "short" satellites for two reasons. The fundamental frequency of the beam must be much higher than the orbital frequency in order that the approximation employed in equation (4.33) remain valid. Also, the relations (4.84) which represent the variable inertias introduce considerable error for long satellites.

(ii) The stability limits for a slender flexible satellite, free to deform under the action of solar heating, have been obtained using the concepts of phase space and integral manifolds. This determines the critical values of initial disturbances to which a satellite may be subjected without causing it to tumble.

(iii) In general a small value of eccentricity would help to ensure stability. The critical value of eccentricity is affected by the dimensionless length L^*, as well as the solar aspect angle, α. When L^* is specified, the critical eccentricity varies periodically with α in such a manner that it increases with increasing α for $0 \leq \alpha \leq 90^\circ$. For the cases considered, it appears that gravitational gradient stabilization of an undamped satellite is not possible under any circumstances for $e > 0.425$ (Figure 4-12).

(iv) The flexible nature of the satellite causes a reduction in the size of the stability region for almost all

values of α. This reduction is not severe. It is concluded that satellite flexibility of this nature does not have a strong destabilizing influence.

(v) The critical eccentricity based on the long term stability analysis would be considerably lower than the one specified above in (iii). This is because of the periodic variation of the stability region with α.

(vi) The presence of spikes further reduces the practical upper limit on eccentricity. If the depth of the stability diagrams (Figures 4-11, 4-12, 4-13) is interpreted as a measure of the disturbance which the satellite would tolerate without becoming unstable, it is apparent that even quite moderate values of eccentricity seriously reduce the ability of the satellite to withstand external disturbances. The effect of increasing L^* is similar but not as severe.

(vii) It must be pointed out that eclipses of the sun by the planet were not considered in this analysis and may contribute to a further loss of stability. These occurrences would excite the vibrational modes of the boom and a more detailed analysis of the decay of the vibrations would be required.

5. TWO DIMENSIONAL MOTION OF AN AXI-SYMMETRIC SATELLITE IN A CIRCULAR ORBIT

5.1 Introductory Remarks

The review of the literature (Section 1.2) suggests that the planar motion of a rigid satellite in a gravity-gradient field has been the subject of considerable investigation. In contrast, the dynamical study of a satellite executing librational motion out of the orbital plane has received comparatively little attention. Such an investigation is important because, as pointed out by Kane,[38] for large amplitudes the transverse motion is strongly coupled with that in the plane.

The lack of information may be partly attributed to the fact that the governing equations of motion are non-linear, non-autonomous, and coupled. They also involve a large number of parameters and hence are not amenable to any simple concise analysis. Some simplification of the problem is achieved by restricting the satellite to move in a circular orbit. For this case, as indicated by Auelmann,[13] closed zero-velocity curves exist under certain conditions which limit the amplitude of motion.

In this chapter, the stability bounds for coupled librational motion of an axi-symmetric satellite in a circular orbit are obtained numerically. The zero-velocity curves suggest possible regions of stability and instability.

Regular and ergodic types of stable motion are discussed and the behaviour of the system in the transition region is explained. Using the concept of an invariant surface, it is shown that stable motion can result even when the zero velocity curves are open. Limiting invariant surfaces are presented and provide a comprehensive summary of the initial disturbances to which a satellite may be subjected without causing it to become unstable.

5.2. Formulation of the Problem

Consider a rigid satellite with mass centre at S in an orbit about the centre of force O (Figure 5-1). Let S-xyz be the principal body axes of the satellite and the triad S-$x_o y_o z_o$ be chosen so that the z_o-axis is directed outward along the local vertical and the y_o-axis is parallel to the orbital angular momentum vector. The position of the mass centre is given by the distance r between O and S and the orbit angle θ.

The orientation of the satellite may be specified by a set of rotations taken in the following order: a rotation, ψ, about the y_o-axis, giving the $x_1 y_1 z_1$-axes; a rotation, ϕ, about the x_1-axis resulting in the $x_2 y_2 z_2$ triad; and a rotation, λ, about the z_2-axis which yields the principal body axes xyz.

Using the principal axes the kinetic energy of the satellite can be written as

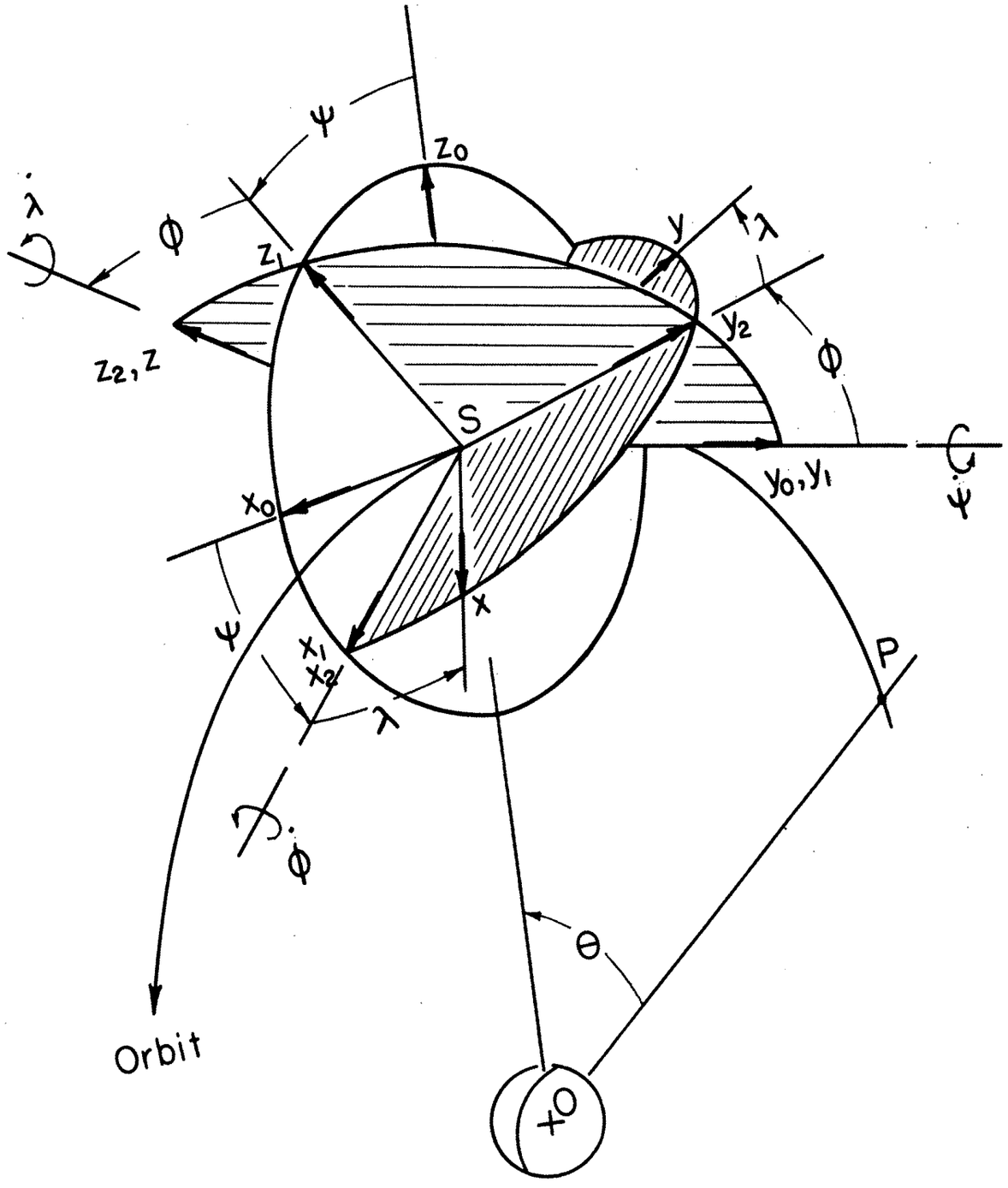

Figure 5-1 Geometry for the two dimensional motion of a satellite

$$T = \tfrac{1}{2} m_b (\dot{r}^2 + r^2\dot{\theta}^2) + \tfrac{1}{2}(I_{xx}\omega_x^2 + I_{yy}\omega_y^2 + I_{zz}\omega_z^2). \qquad (5.1)$$

Noting that

$$\begin{aligned} \omega_x &= \dot{\phi}\,\mathrm{Cos}\,\lambda + (\dot{\theta} + \dot{\psi})\,\mathrm{Cos}\,\phi\,\mathrm{Sin}\,\lambda \\ \omega_y &= -\dot{\phi}\,\mathrm{Sin}\,\lambda + (\dot{\theta} + \dot{\psi})\,\mathrm{Cos}\,\phi\,\mathrm{Cos}\,\lambda \qquad (5.2) \\ \omega_z &= \dot{\lambda} - (\dot{\theta} + \dot{\psi})\,\mathrm{Sin}\,\phi \end{aligned}$$

so that

$$\begin{aligned} T = {} & \tfrac{1}{2} m_b (\dot{r}^2 + r^2\dot{\theta}^2) \\ & + \tfrac{1}{2}\dot{\phi}^2(\mathrm{Cos}^2\lambda\, I_{xx} + \mathrm{Sin}^2\lambda\, I_{yy}) \\ & + \dot{\phi}(\dot{\theta} + \dot{\psi})\,\mathrm{Cos}\,\phi\,\mathrm{Sin}\,\lambda\,\mathrm{Cos}\,\lambda(I_{xx} - I_{yy}) \qquad (5.3) \\ & + \tfrac{1}{2}(\dot{\theta} + \dot{\psi})^2\mathrm{Cos}^2\phi(\mathrm{Sin}^2\lambda\, I_{xx} + \mathrm{Cos}^2\lambda\, I_{yy}) \\ & + \tfrac{1}{2}(\dot{\lambda} - (\dot{\theta} + \dot{\psi})\,\mathrm{Sin}\,\phi)^2 I_{zz} \,. \end{aligned}$$

To determine the potential energy, consider an element of mass, dm, with co-ordinates x,y,z,. The distance between the mass element and the centre of force can be written as

$$r = [(x + rl_x)^2 + (y + rl_y)^2 + (z + rl_z)^2]^{1/2} \qquad (5.4)$$

where the direction cosines ℓ_x, ℓ_y, ℓ_z between the outward local vertical and the xyz-axes are

$$\ell_x = -\sin\psi\cos\lambda + \cos\psi\sin\phi\sin\lambda$$

$$\ell_y = \sin\psi\sin\lambda + \cos\psi\sin\phi\cos\lambda \qquad (5.5)$$

$$\ell_z = \cos\psi\cos\phi \,.$$

The potential energy of the satellite is

$$U = -\mu\int\frac{dm_b}{r}$$

$$= -\frac{\mu}{r}\int\left[1 + \frac{2}{r}(x\ell_x + y\ell_y + z\ell_z) + \frac{x^2+y^2+z^2}{r^2}\right]^{-1/2} dm_b \qquad (5.6)$$

$$= -\frac{\mu}{r}\int\left[1 - \frac{1}{r}(x\ell_x + y\ell_y + z\ell_z)\right.$$

$$\left. - \frac{1}{2r^2}(x^2+y^2+z^2) + \frac{3}{2r^2}(x\ell_x + y\ell_y + z\ell_z)^2 + \cdots\right] dm_b \,.$$

As S is the centre of mass

$$\int x\,dm_b = \int y\,dm_b = \int z\,dm_b = 0 \qquad (5.7)$$

and since xyz are principal axes

$$\int xy\, dm_b = \int yz\, dm_b = \int zx\, dm_b = 0. \tag{5.8}$$

With this the expression for the potential energy simplifies to

$$U = -\mu m_b/r + \frac{\mu}{2r^3}\int\left[x^2(1-3l_x^2)+y^2(1-3l_y^2)+z^2(1-3l_z^2)\right]dm_b \tag{5.9}$$

Now,

$$\int x^2 dm_b = \frac{1}{2}\left(I_{yy} + I_{zz} - I_{xx}\right)$$

$$\int y^2 dm_b = \frac{1}{2}\left(I_{zz} + I_{xx} - I_{yy}\right) \tag{5.10}$$

$$\int z^2 dm_b = \frac{1}{2}\left(I_{xx} + I_{yy} - I_{zz}\right)$$

so that there results

$$U = -\frac{\mu m_b}{r} + \frac{\mu}{4r^3}\left(I_{xx} + I_{yy} + I_{zz}\right)$$

$$-\frac{3\mu}{4r^3}\left\{\sin^2\psi\left[I_{zz} - (I_{xx} - I_{yy})(\cos^2\lambda - \sin^2\lambda)\right]\right. \tag{5.11}$$

$$\left. + 4\sin\psi\cos\psi\sin\phi\sin\lambda\cos\lambda\,(I_{xx} - I_{yy})\right.$$

$$+ \cos^2\psi \sin^2\phi \left[I_{zz} - (I_{xx} - I_{yy})(\sin^2\lambda - \cos^2\lambda) \right.$$
$$\left. + \cos^2\psi \cos^2\phi \left(I_{xx} + I_{yy} - I_{zz} \right) \right\}. \qquad (5.11) \text{ cont'd}$$

For a slender axi-symmetric satellite

$$I_{xx} = I_{yy} = I > I_{zz} \qquad (5.12)$$

hence equations (5.3) and (5.11) assume the much simpler forms

$$T = \frac{1}{2} m_b \left(\dot{r}^2 + r^2 \dot{\theta}^2 \right) + \frac{1}{2} I \left(\dot{\phi}^2 + (\dot{\theta} + \dot{\psi})^2 \cos^2\phi \right)$$
$$+ \frac{1}{2} I_{zz} \left(\dot{\lambda} - (\dot{\theta} + \dot{\psi}) \sin\phi \right)^2 \qquad (5.13)$$

$$U = - \frac{\mu m_b}{r}$$
$$+ \frac{\mu}{2 r^3} \left(I - I_{zz} \right) \left(1 - 3 \cos^2\psi \cos^2\phi \right). \qquad (5.14)$$

The generalized momenta can be expressed as

$$p_\psi = \frac{\partial \mathcal{L}}{\partial \dot{\psi}} = I \cos^2\phi \left(\dot{\theta} + \dot{\psi} \right) - I_{zz} \left(\dot{\lambda} - (\dot{\theta} + \dot{\psi}) \sin\phi \right) \sin\phi$$
$$p_\phi = \frac{\partial \mathcal{L}}{\partial \dot{\phi}} = I \dot{\phi} \qquad (5.15)$$

$$p_\lambda = \frac{\partial \mathcal{L}}{\partial \dot{\lambda}} = I_{zz}\left(\dot{\lambda} - (\dot{\theta}+\dot{\psi})\sin\phi\right). \qquad (5.15)\ \text{cont'd}$$

Because $\partial \mathcal{L}/\partial \lambda = 0$ in this case, the momentum conjugate to the co-ordinate λ is constant. This momentum can be identified with the spin of the satellite about the z-axis,

$$p_\lambda = I_{zz}\left(\dot{\lambda} - (\dot{\theta}+\dot{\psi})\sin\phi\right) = \text{constant}. \qquad (5.16)$$

For a non-spinning satellite the constant must be zero, therefore

$$T = \tfrac{1}{2} m_b\left(\dot{r}^2 + r^2\dot{\theta}^2\right) + \tfrac{1}{2} I\left(\dot{\phi}^2 + (\dot{\theta}+\dot{\psi})^2\cos^2\phi\right). \qquad (5.17)$$

Using the Lagrangian formulation the governing equations of motion for the ψ and ϕ degrees of freedom can be written as

$$\ddot{\psi} + \ddot{\theta} - 2\dot{\phi}(\dot{\theta}+\dot{\psi})\tan\phi + \frac{3\mu}{r^3} K_i \sin\psi\cos\psi = 0 \qquad (5.18)$$

$$\ddot{\phi} + \left\{(\dot{\theta}+\dot{\psi})^2 + \frac{3\mu}{r^3} K_i \cos^2\psi\right\}\sin\phi\cos\phi = 0. \qquad (5.19)$$

Noting that

$$\begin{aligned} \dot{\psi} &= \psi' \dot{\theta} \\ \ddot{\psi} &= \psi'' \dot{\theta}^2 + \psi' \ddot{\theta} \\ \ddot{\phi} &= \phi'' \dot{\theta}^2 + \phi' \ddot{\theta} \end{aligned} \tag{5.20}$$

and for a circular orbit

$$\begin{aligned} \frac{\mu}{r^3} &= \dot{\theta}^2 = \text{constant} \\ \ddot{\theta} &= 0 \end{aligned} \tag{5.21}$$

hence the equations of motion may be written as

$$\psi'' - 2\phi'(\psi'+1)\,\mathrm{Tan}\,\phi + 3K_i \sin\psi \cos\psi = 0 \tag{5.22}$$

$$\phi'' + \left\{(\psi'+1)^2 + 3K_i \cos^2\psi\right\} \sin\phi \cos\phi = 0 . \tag{5.23}$$

5.3 The Hamiltonian and Zero-Velocity Curves

Ignoring the r, θ, and λ co-ordinates the Lagrangian for the system can be written as

$$\mathcal{L} = \frac{1}{2} I \left(\dot{\phi}^2 + (\dot{\theta} + \dot{\psi})^2 \cos^2\phi \right) + \frac{3\mu}{2r^3} (I - I_{zz}) \cos^2\psi \cos^2\phi \,. \tag{5.24}$$

Thus for a circular orbit, the Lagrangian function corresponding to the librational motion does not involve time explicitly hence the corresponding Hamiltonian is a constant of motion and is given by

$$H = \sum p_i \dot{q}_i - \mathcal{L}$$

$$= \frac{1}{2} I \left(\dot{\phi}^2 + (\dot{\psi}^2 - \dot{\theta}^2) \cos^2\phi \right) - \frac{3\mu}{2r^3} (I - I_{zz}) \cos^2\psi \cos^2\phi \tag{5.25}$$

and using (5.21) equation (5.25) may be rewritten as

$$\frac{2H}{I\dot{\theta}^2} = \phi'^2 + \cos^2\phi \left(\psi'^2 - 1 - 3K_i \cos^2\psi \right) = C_H. \tag{5.26}$$

Auelmann's paper[13] contains an error in the statement of this equation.

Defining a new variable

$$\hat{\psi}' = \psi' \cos\phi \tag{5.27}$$

equation (5.26) becomes

$$\phi'^2 + \hat{\psi}'^2 = \cos^2\phi \left(1 + 3K_i \cos^2\psi \right) + C_H. \tag{5.28}$$

Setting $\phi' = \hat{\psi}' = 0$ gives the zero-velocity curves for the motion ($|\psi|$, $|\phi| < \pi/2$) which are presented for various values of C_H in Figure 5-2. Since the right hand side of (5.28) is a maximum at $\phi = \psi = 0$, the sum of the squares of the velocities is positive only inside the zero-velocity curves. Therefore the zero-velocity curves represent bounds for the motion. It is thus possible to conclude that for:

$$
\begin{aligned}
C_H &< -(1 + 3K_i), && \text{no motion is possible,} \\
-(1 + 3K_i) \leq C_H &\leq -1, && \text{the motion is bounded,} \\
-1 < C_H &\leq 0, && \text{instability can arise only in the } \psi\text{-direction,} \\
0 < C_H, & && \text{unbounded motion is possible in both directions.}
\end{aligned}
$$

5.4 Phase Space and Trajectories

The equation of motion (5.12) and (5.23) may be written as a set of four first order differential equations

$$
\begin{aligned}
\frac{d\psi}{d\theta} &= \frac{\hat{\psi}'}{\cos\phi} \\
\frac{d\hat{\psi}'}{d\theta} &= \phi'\hat{\psi}'\tan\phi + 2\phi\sin\phi \\
&\quad - 3K_i \sin\psi\cos\psi\cos\phi \\
&= F_1(\psi, \phi, \hat{\psi}', \phi')
\end{aligned}
\qquad (5.29)
$$

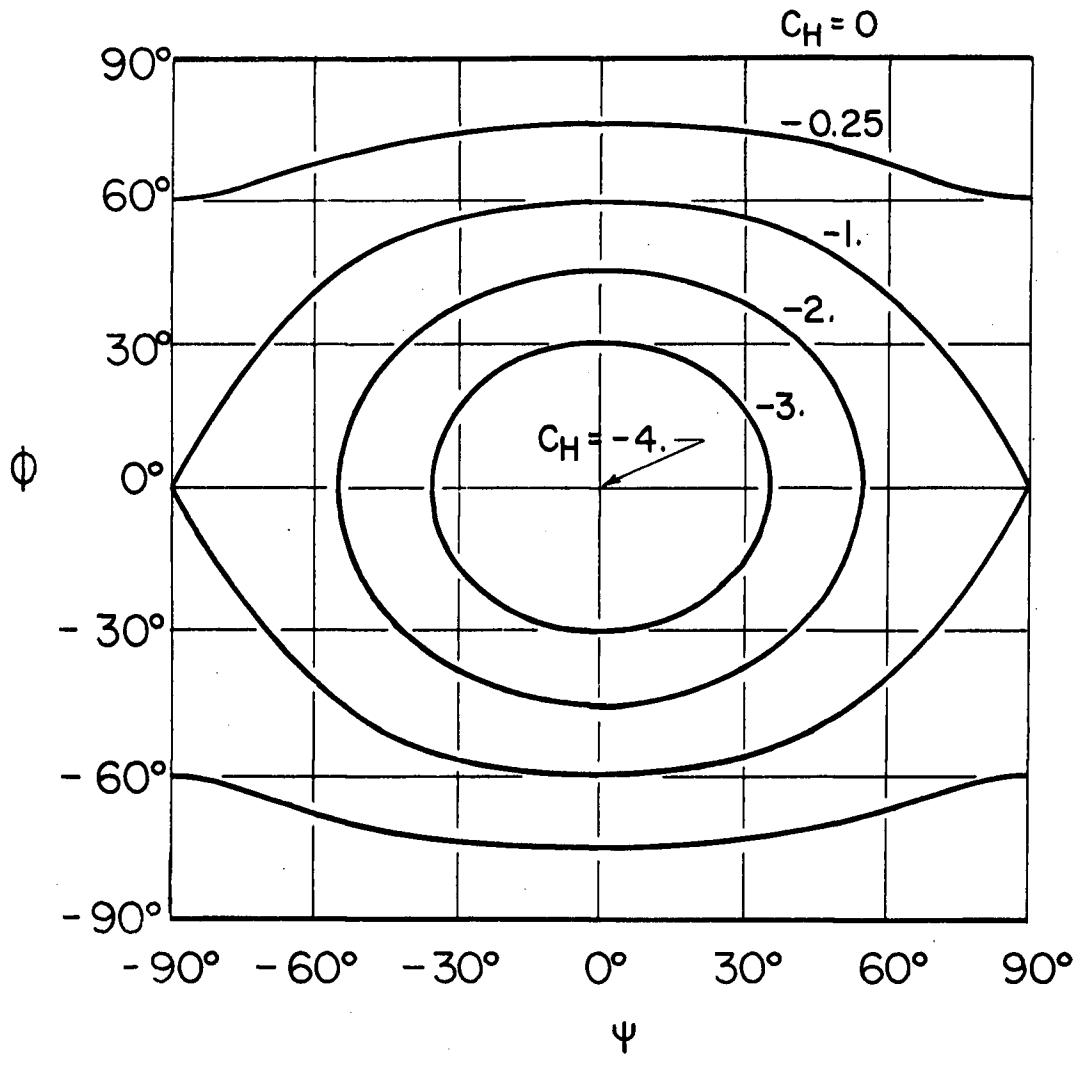

Figure 5-2 Zero-velocity curves for an axi-symmetric satellite in a circular orbit ($K_i = 1$)

$$\frac{d\phi}{d\theta} = \phi' \qquad (5.29)$$

cont'd

$$\frac{d\phi'}{d\theta} = -\left\{\left(\frac{\hat{\psi}'}{\cos\phi} + 1\right)^2 + 3K_i \cos^2\psi\right\} \sin\phi \cos\phi$$

$$= F_2(\psi, \phi, \hat{\psi}').$$

These may be rearranged in the form

$$d\theta = \frac{\cos\phi \, d\psi}{\hat{\psi}'} = \frac{d\hat{\psi}'}{F_1} = \frac{d\phi}{\phi'} = \frac{d\phi'}{F_2} \qquad (5.30)$$

which defines a trajectory in a four-dimensional phase space. The Hamiltonian (5.28) permits determining any one phase space co-ordinate in terms of the other three. Solving for Cos ϕ gives,

$$\cos\phi = \pm\left(\frac{\phi'^2 + \hat{\psi}'^2 - C_H}{1 + 3K_i \cos^2\psi}\right)$$

or

$$\phi = \pm\cos^{-1}\left[\pm\left(\frac{\phi'^2 - \hat{\psi}'^2 - C_H}{1 + 3K_i \cos^2\psi}\right)\right] \qquad (5.31)$$

The ambiguity as to sign indicates that the information derived from the Hamiltonian cannot differentiate between

$+\phi$, $-\phi$, $\pi + \phi$, and $\pi - \phi$. This information can usually be obtained from a consideration of the continuity of the solution.

If ϕ is taken to be positive and less than $\pi/2$, equation (5.31) is unambiguous and equation (5.30) defines a unique trajectory

$$\frac{d\psi}{\hat{\varphi}'}\cos\phi(\psi,\hat{\varphi},\phi,c_H) = \frac{d\hat{\varphi}'}{F_1(\psi,\hat{\varphi}',\phi',c_H)} = \frac{d\phi'}{F_2(\psi,\hat{\varphi}',\phi',c_H)} \tag{5.32}$$

in a three-dimensional ψ, $\hat{\varphi}'$, ϕ'-space. A similar equation holds for $\phi < 0$ and defines equally unique trajectories in another phase space. Certain symmetry properties, however, permit the elimination of one of the spaces.

5.5 Symmetry Properties

On substituting

$$\begin{aligned} \theta &= -\theta \\ \psi &= -\psi \\ \phi &= \phi \end{aligned} \tag{5.33}$$

in equations (5.22 - 5.23) it is observed that $\hat{\varphi}' = \hat{\varphi}'$, $\phi' = -\phi'$, $\psi'' = -\psi''$, $\phi'' = -\phi''$ and the equations of motion are unchanged. Thus a trajectory defined by (5.22 - 5.23) or the equivalent (5.32), which passes through the point $(\psi, \hat{\varphi}', \phi')$ possesses a mirror trajectory which passes

through the point $(-\psi, \hat{\varphi}', -\phi')$. Therefore the trajectory which passes through the point $(0, \hat{\varphi}', 0)$ exhibits symmetry about the $\hat{\varphi}'$-axis.

When the substitutions

$$\begin{aligned} \theta &= -\theta \\ \psi &= -\psi \\ \phi &= -\phi \end{aligned} \tag{5.34}$$

are made in equations (5.22 - 5.23) $\hat{\varphi}' = \hat{\varphi}'$, $\phi' = \phi'$ and the form of the equations is invariant. Therefore the trajectory passing through the point $(\psi, \hat{\varphi}', \phi')$ with $\phi' > 0$ possesses a mirror trajectory which passes through the point $(-\psi, \hat{\varphi}', \phi')$ where $\phi < 0$. Hence the trajectory defined by the equations of motion in the phase space is, for $\phi > 0$, a mirror image about the $\hat{\varphi}', \phi'$-plane of the trajectory defined for $\phi < 0$.

5.6 Numerical results

It was pointed out in section (5.3) that initial conditions corresponding to $-(1 + 3K_i) \leq C_H \leq -1$ always lead to stable motion. However, there appear to be two types of trajectories which indicates the existence of two classes of solutions.

The first class of solutions is illustrated in Figure 5-3. Here an invariant surface is defined in the three-dimensional phase space. That is an "isolating" integral

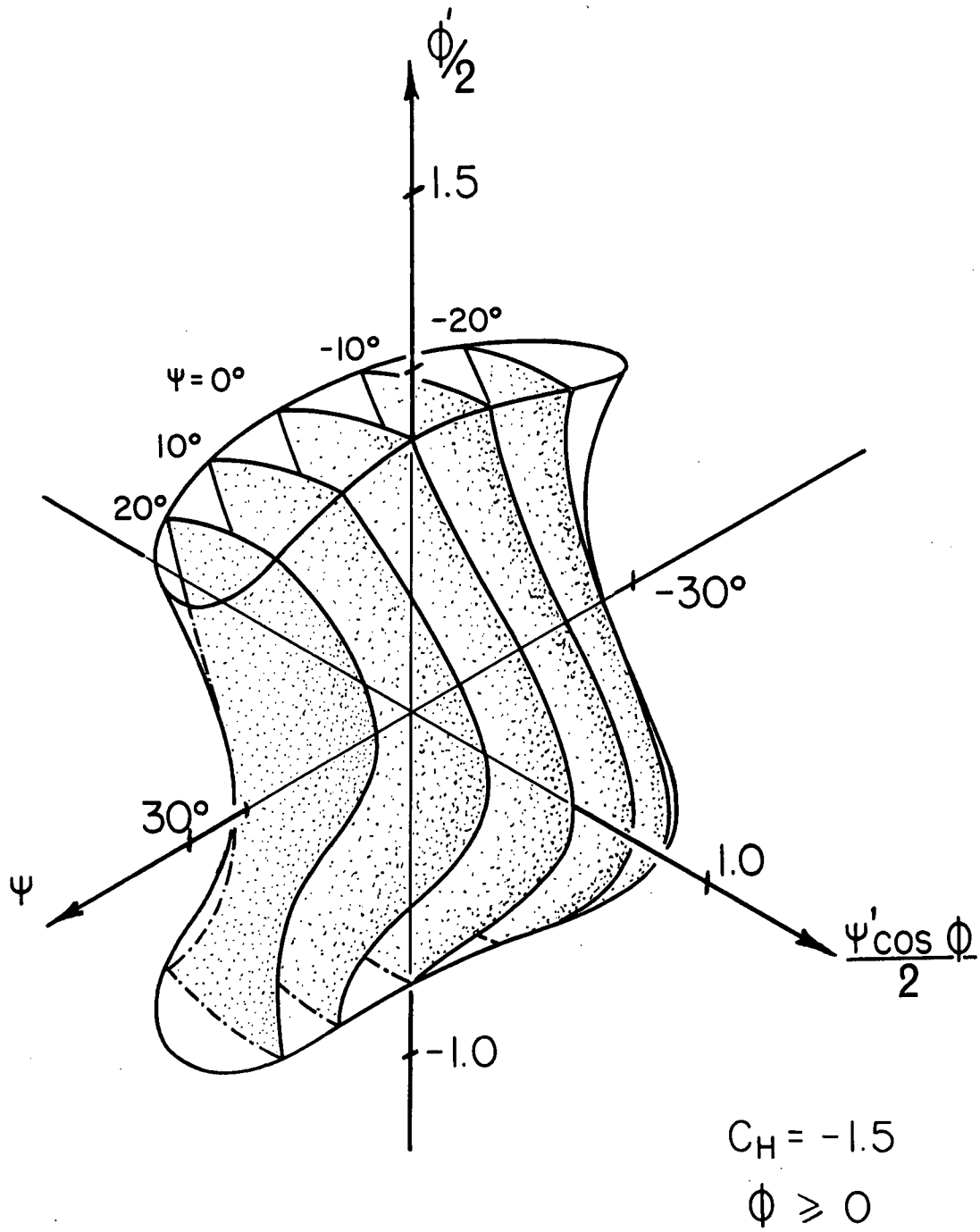

Figure 5-3 Invariant surface resulting from the first class of solutions

has been determined numerically. Figure 5-4 indicates the cross-section of a similar surface in the plane $\psi = 0$. It should be noted that the points of intersection of the trajectory with the plane $\psi = 0$ define a smooth boundary.

The second type of behaviour is illustrated in Figure 5-5. As before it represents the state of motion of the system in the plane $\psi = 0$ with the identical co-ordinates. However, in this case the points appear to be scattered randomly over regions in the plane indicating the "ergodic" nature of the motion.

Kane[38] has indicated that the motion normal to the orbital plane may exhibit a type of beat phenomenon with a very long period, typically 35 to 45 orbits. This type of behaviour would lead to a plot of the type presented in Figure 5-5. A large number of points would have to be determined before periodicity becomes evident. Such motion could best be described as "quasi-ergodic."

The behaviour of the solution in the transition region between the large simple surfaces of the first type and the ergodic behaviour of the second type lends support to the concept of quasi-ergodicity. In the transition region, "chains of islands" appear which become smaller and more numerous as the ergodic region is approached[31] (Figure 5-6).

For $C_H > -1$ there is a possibility that the motion may be unstable. The numerical results indicate that a stable initial condition results in a solution of the first type and hence in the generation of an invariant surface

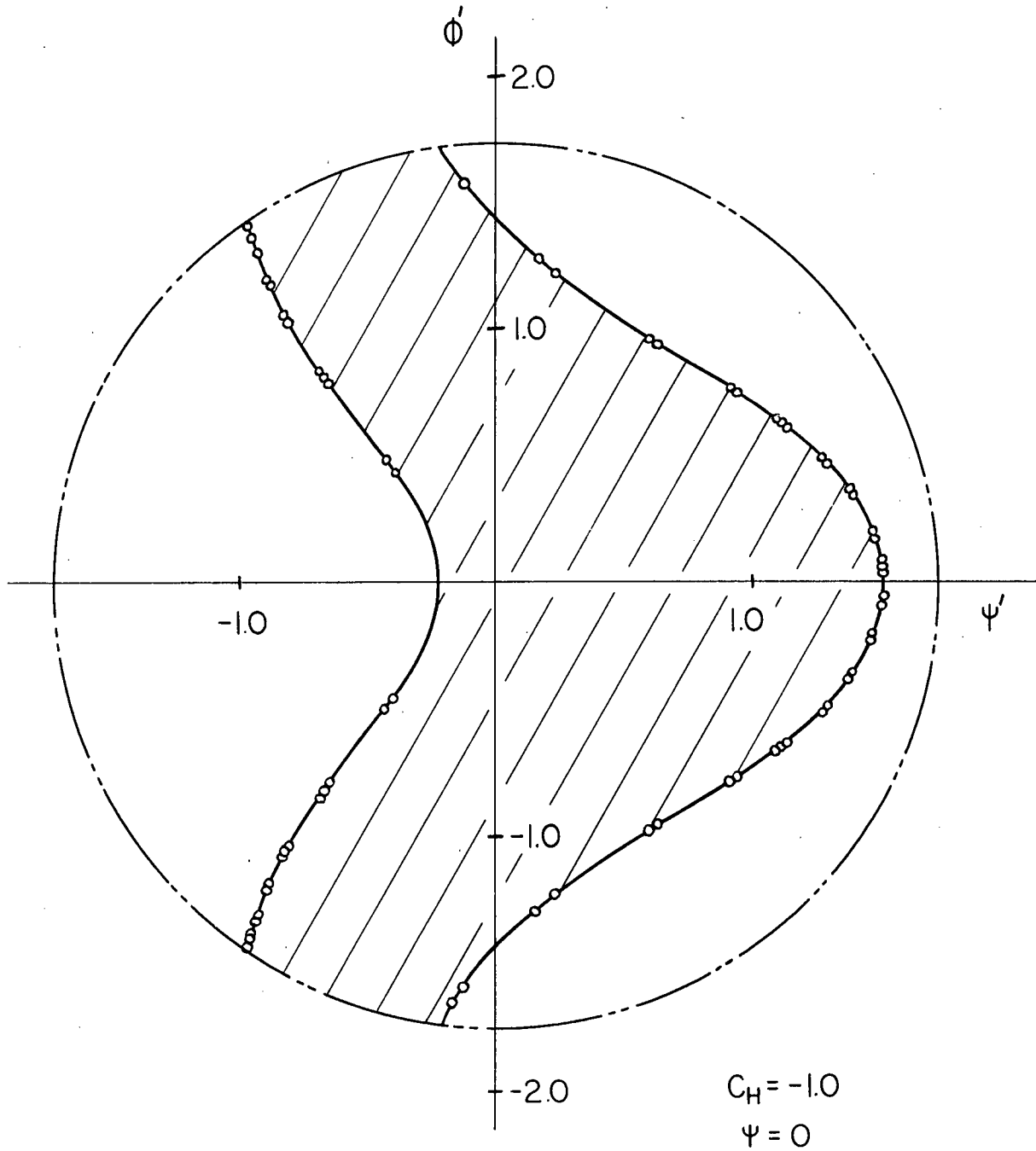

Figure 5-4 Cross-section of a surface similar to that presented in Figure 5-3 when $\psi = 0$

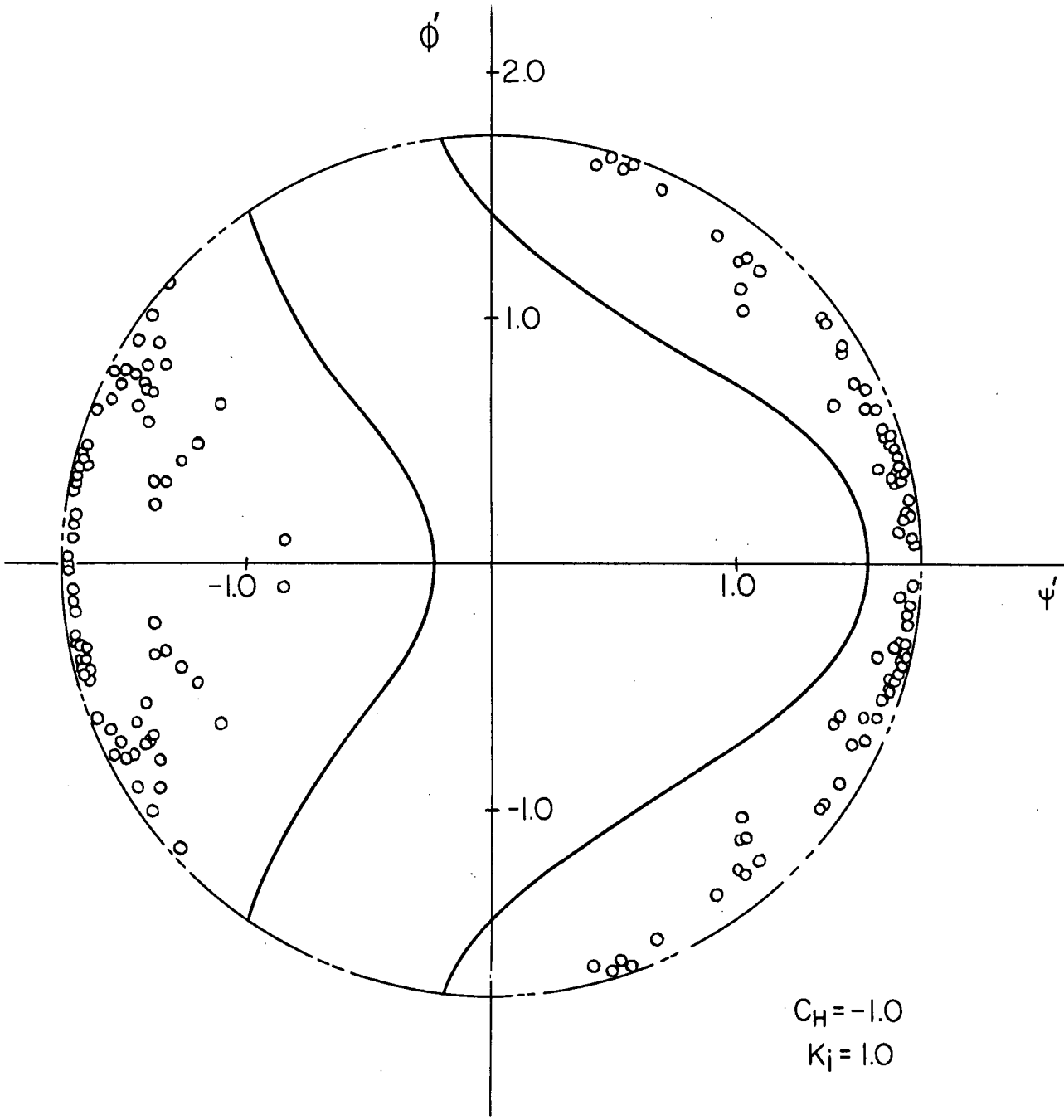

Figure 5-5 The cross-section $\psi = 0$ in phase space illustrating the ergodic nature of the second class of solutions

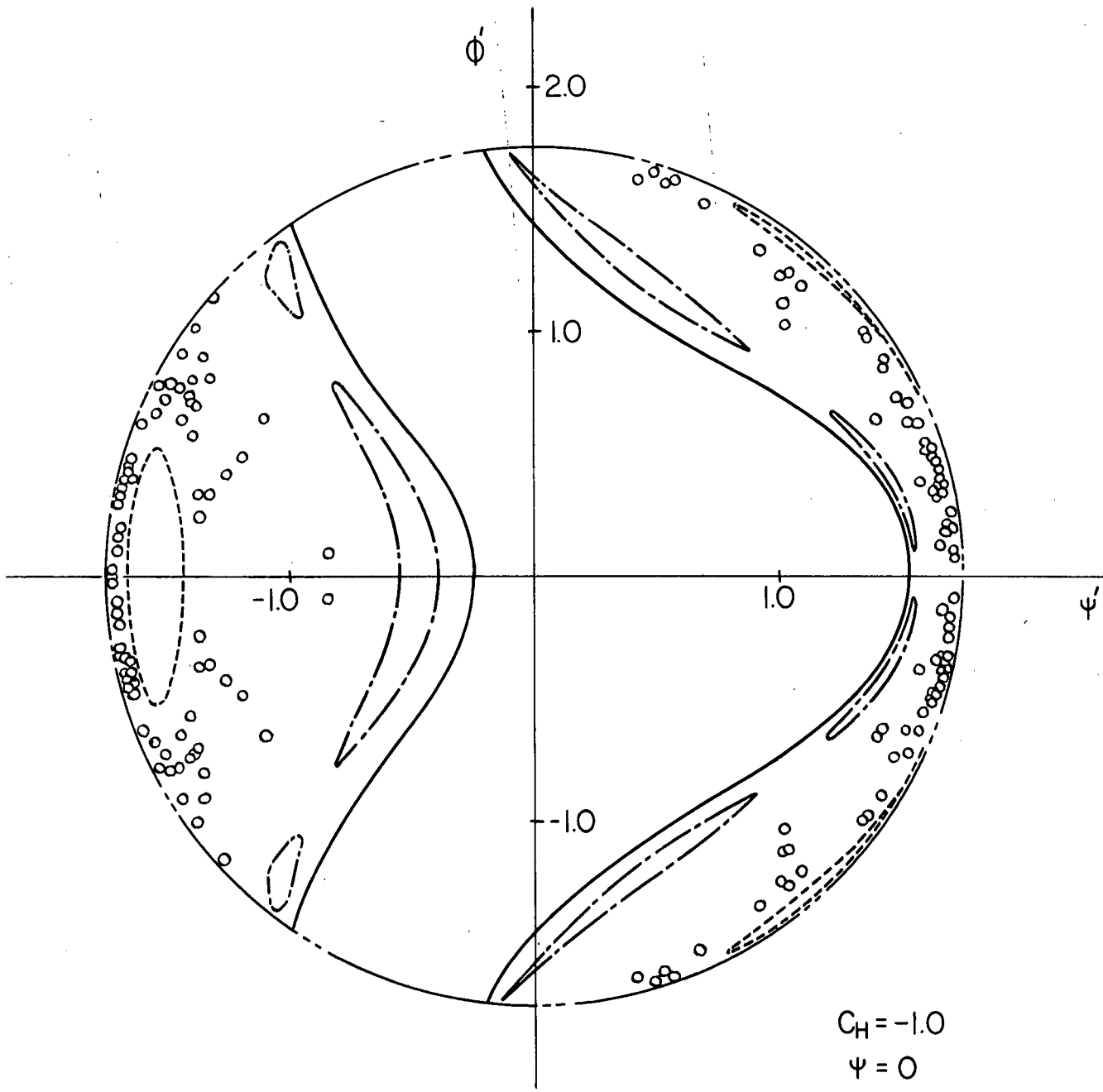

Figure 5-6 The cross-section $\psi = 0$ in phase space illustrating the transition from a large simple "mainland" to an ergodic trajectory via a number of "islands"

(Figure 5-7). Certainly, if there is such a surface, the trajectory can never leave it and stability is guaranteed. Further, the numerical analysis suggests that the ergodic type of trajectories are not consistent with stability for $C_H > -1$.

For a given value of C_H, suitable initial conditions can be chosen to generate different surfaces. The largest such surface is referred to as a limiting surface. Thus the interior of a limiting surface represents all possible states of the system, consistent with the fixed value of the Hamiltonian, corresponding to stable motion.

The numerical work indicates the existence of invariant surfaces up to at least $C_H = 0.5$. For $C_H \geq 0.6$ invariant surfaces do not appear to exist. Figures 5-8-i to 5-8-iii show several limiting surfaces for representative values of C_H ($\phi \geq 0$). The symmetry properties of section 5.5 (illustrated in Figure 5-8-iii) may be used to determine the surfaces for $\phi < 0$.

The limiting surfaces provide useful information concerning the nature of the motion. At high values of C_H the limiting surfaces for both $\phi \geq 0$ and $\phi \leq 0$, when drawn in the same diagram (Figure 5-8-iii), appear as a twisted figure eight. It is interesting to note that both motions are quasi-periodic with the period of the out-of-plane motion approximately double that of the in-plane librations. Figure 5-9 illustrates this behaviour for a specific set of

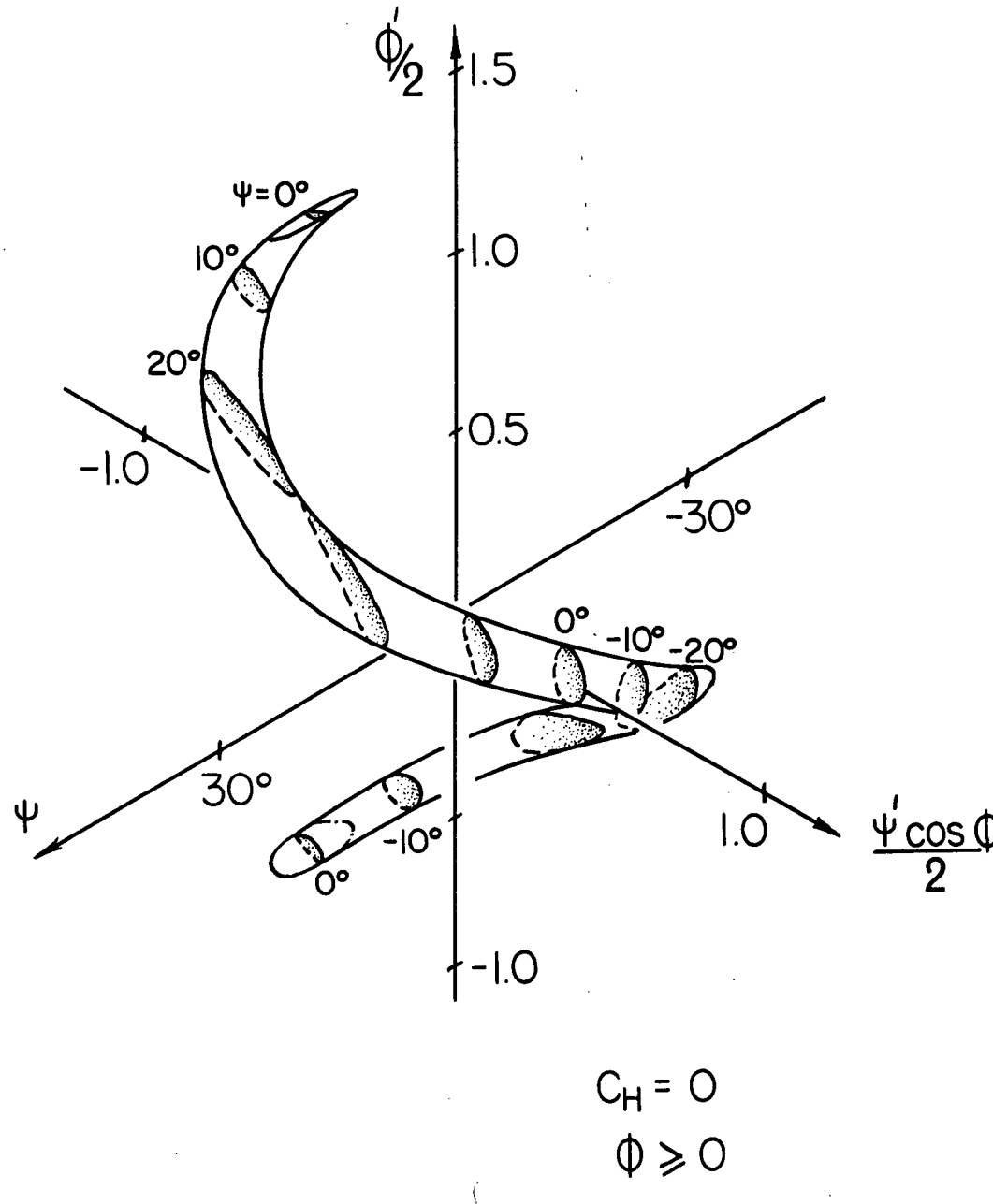

Figure 5-7 Typical invariant surface when $C_H > -1$

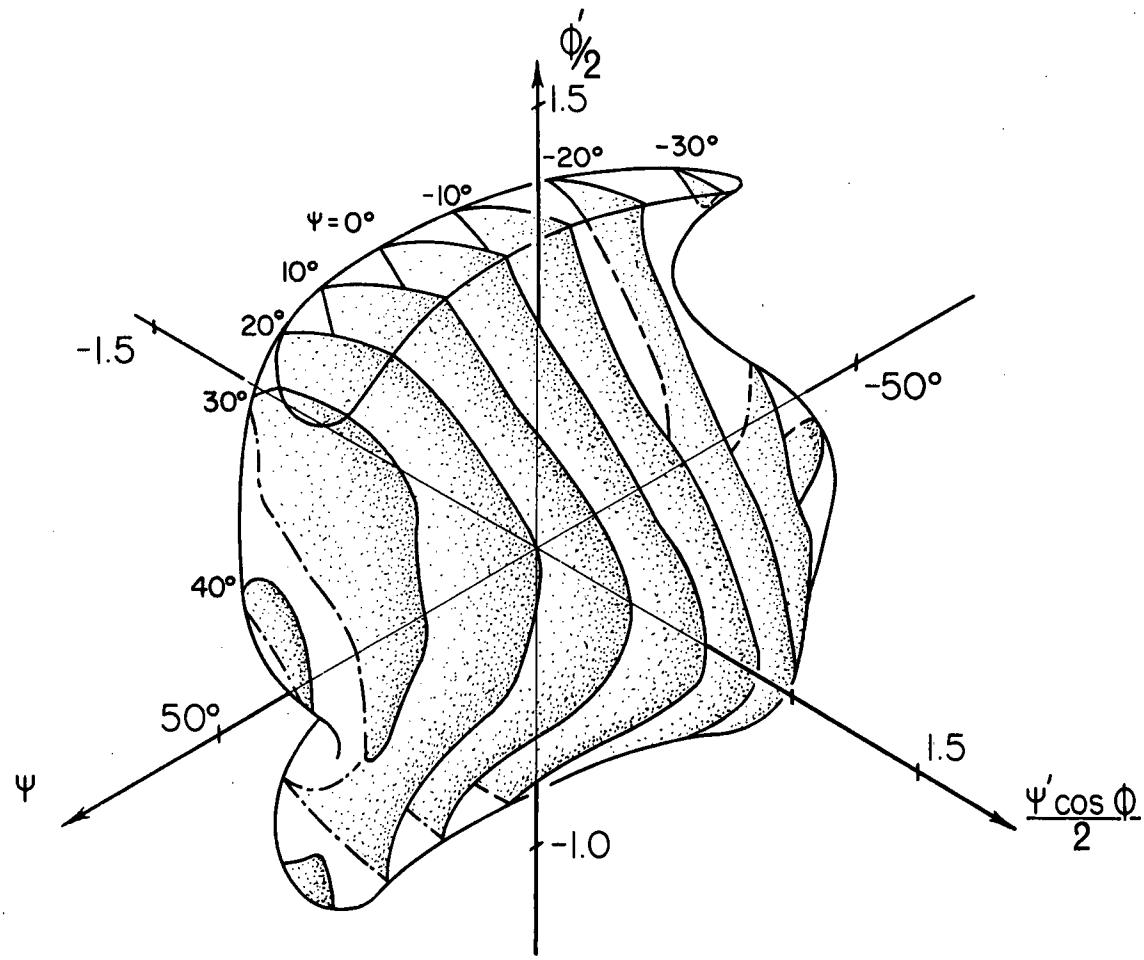

Figure 5-8-i Limiting invariant surface ($C_H = -0.5$)

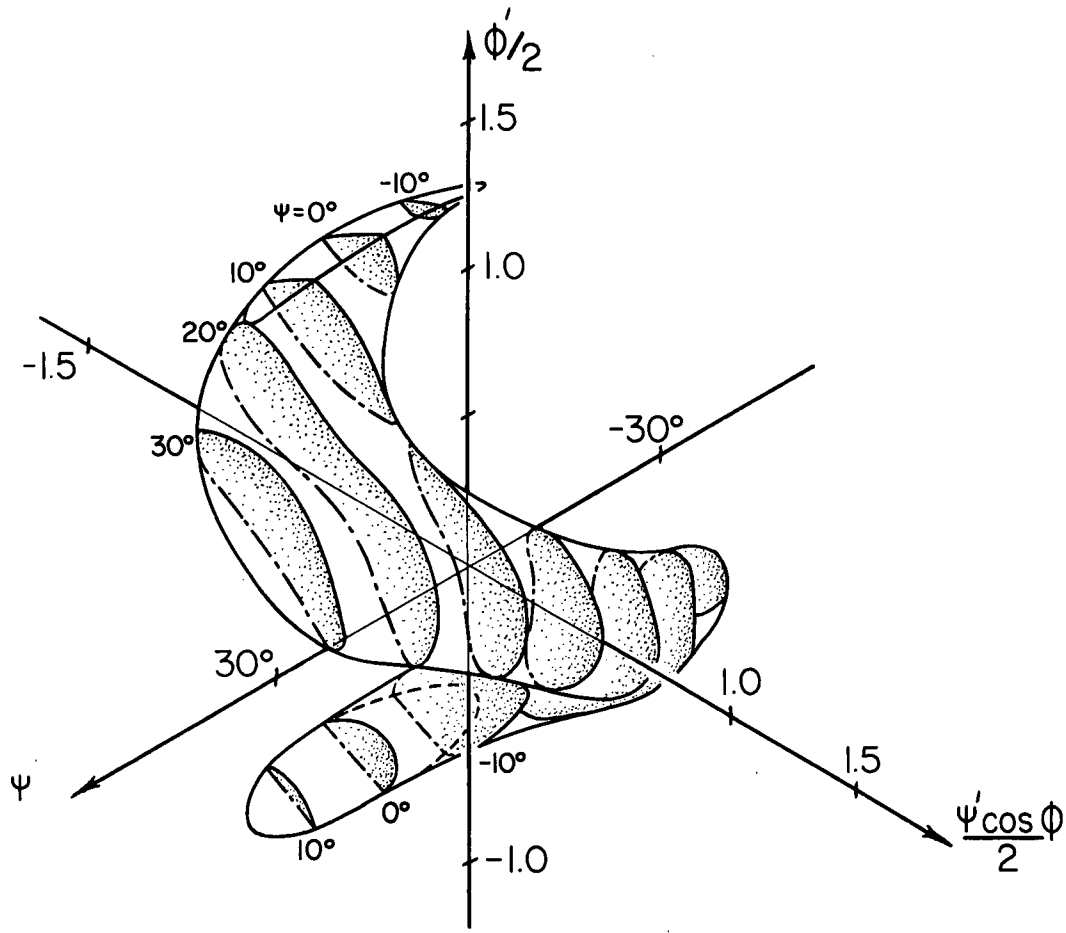

$C_H = 0$

$\Phi \geq 0$

Figure 5-8-ii Limiting invariant surface ($C_H = 0$)

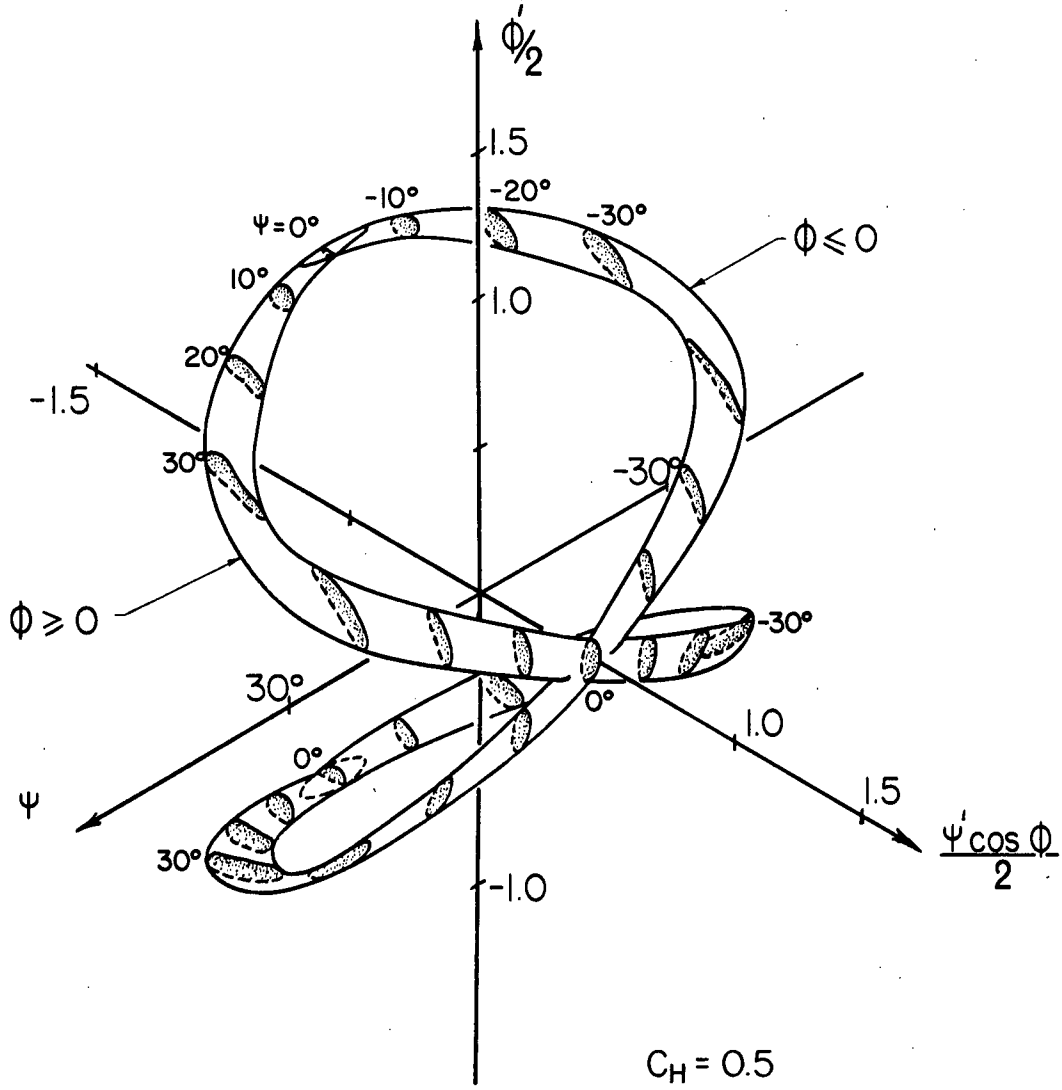

Figure 5-8-iii Limiting invariant surface ($C_H = 0.5$)

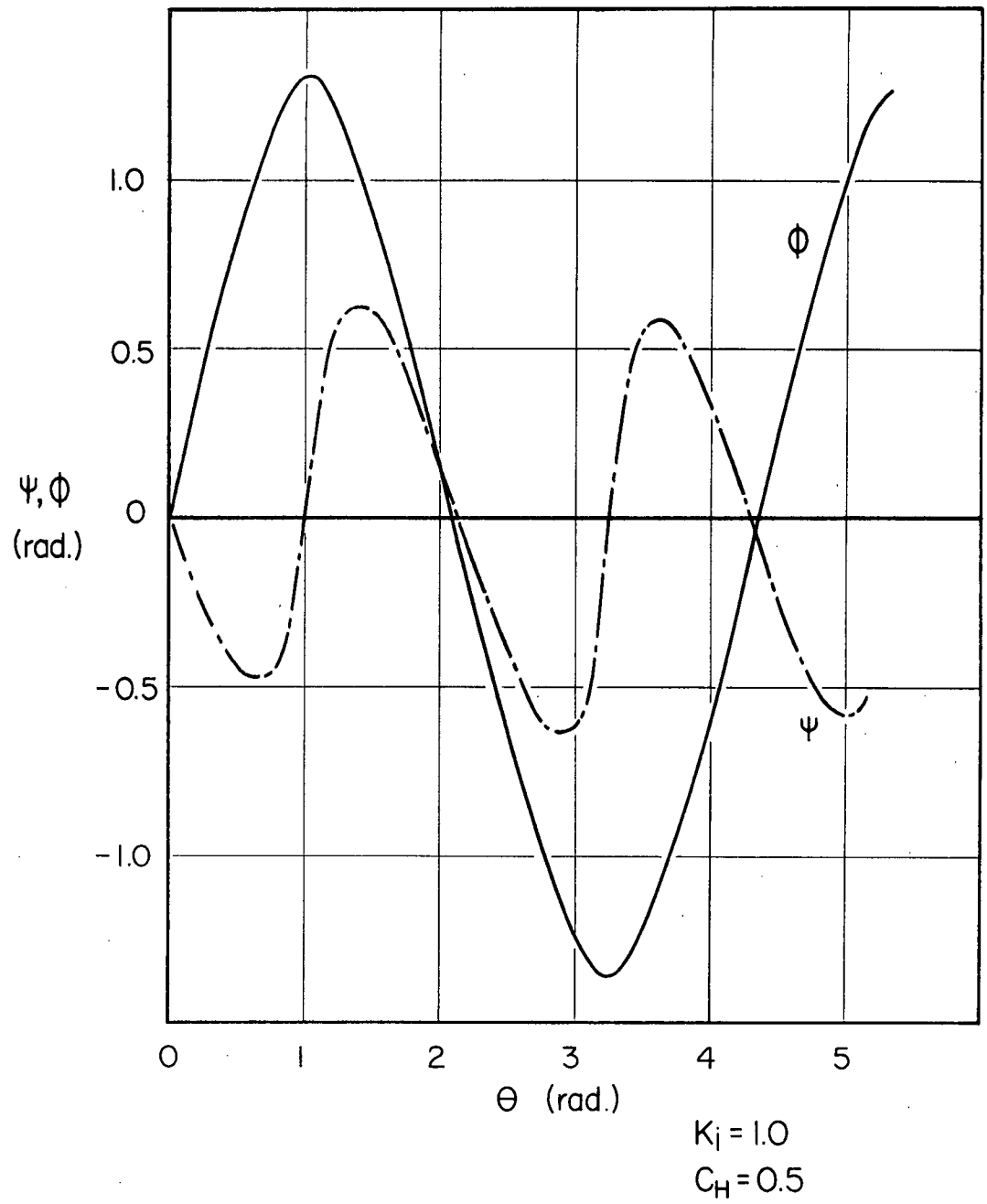

Figure 5-9 Solution of the equations of motion for specific initial conditions, illustrating the quasi-periodic nature of the motion

initial conditions.

The results displayed in Figures 5-8-i to 5-8-iii may be presented in a more informative manner. If ψ and ϕ are fixed, a constant value of C_H describes a circle in a $\hat{\psi}'$, ϕ'-plane. A point in this plane specifies value of the angular velocities of the body and hence gives a complete set of initial conditions. If the velocities are zero, the point lies at the origin and the Hamiltonian has its minimum value. For values of ψ and ϕ such that $C_H = -1$ defines a real radius, there exists a circle inside which stability is guaranteed. Larger values of C_H result in stability for varying arc lengths of the constant C_H circles.

Figures 5-10-i to 5-10-iii show the stable regions in $\hat{\psi}'$, ϕ'-planes for various combinations of ψ and ϕ. It is possible to make an observation concerning the relative sensitivity of the satellite in the position of stable equilibrium to disturbances in the ψ and ϕ directions. It is evident from Figure 5-10-i that for $\psi = \phi = 0$, the coupled motion can remain stable even when subjected to the angular velocities $\psi' = -1.15$, $\phi' = \pm 1.75$. The resultant velocity of approximately 2.1 is considerably above the value of $\sqrt{3}$ which holds for the planar case. Thus motion restricted to the orbital plane appears to be less stable than the more general two dimensional motion.

5.7 Concluding Remarks

The results show that there are two distinct types

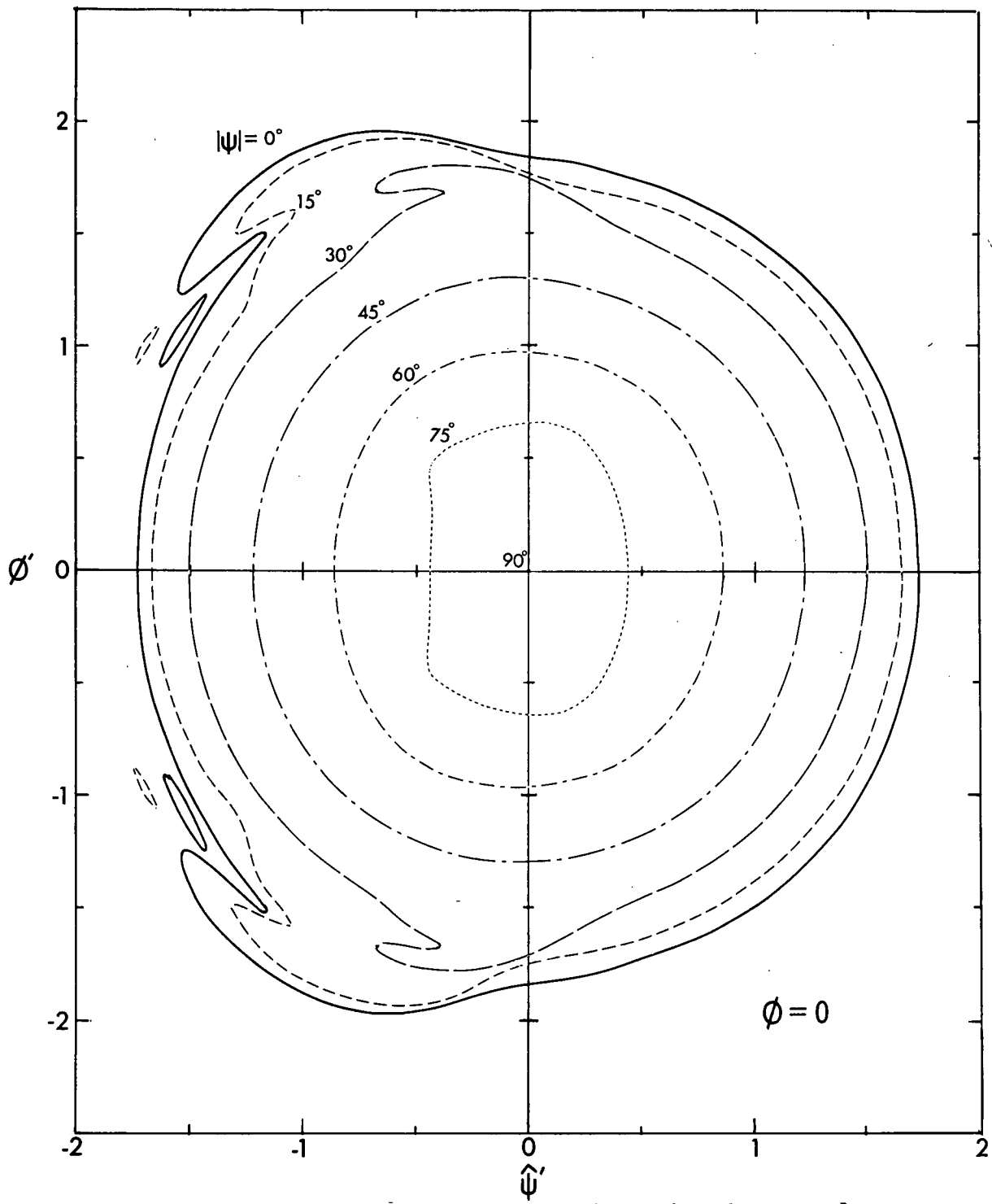

Figure 5-10-i Allowable variations in the angular velocities which may be imposed on an axi-symmetric satellite when in a specified orientation ($\emptyset = 0$)

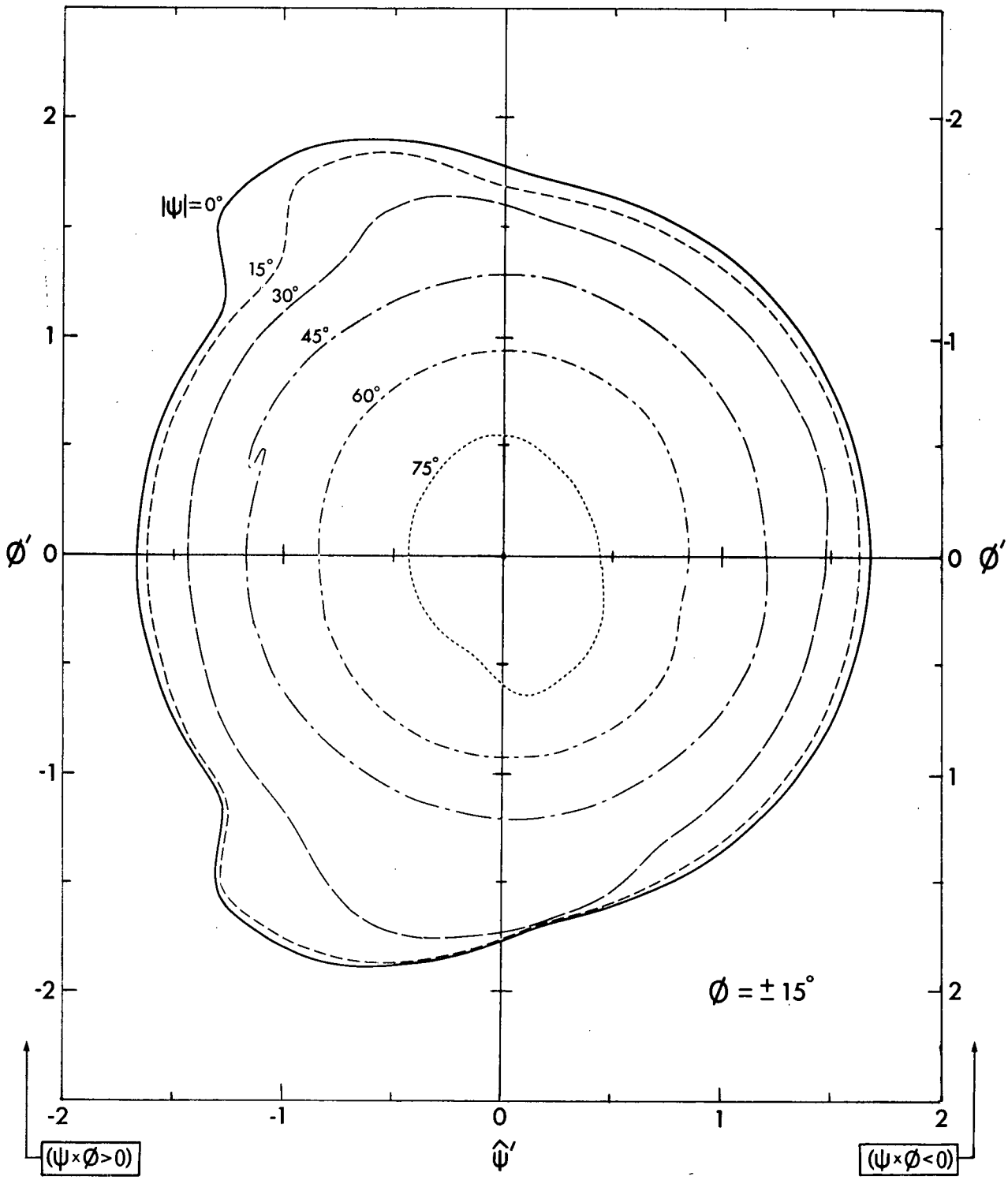

Figure 5-10-ii Allowable variations in the angular velocities which may be imposed on an axi-symmetric satellite when in a specified orientation ($\emptyset = \pm 15^{\circ}$)

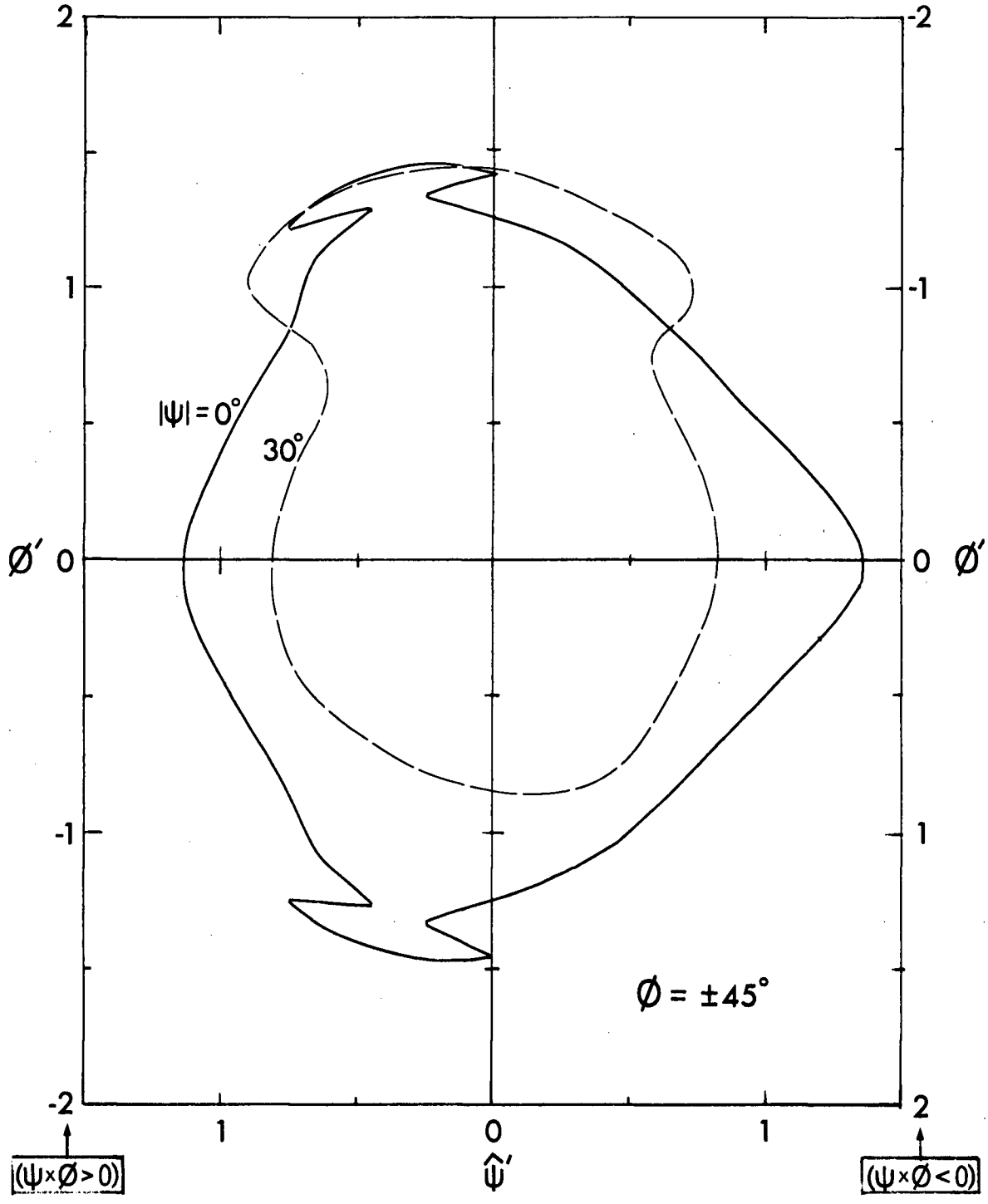

Figure 5-10-iii Allowable variations in the angular velocities which may be imposed on an axi-symmetric satellite when in a specified orientation ($\emptyset = \pm 45^{\circ}$)

of stability associated with the coupled librational motion of a gravity-gradient oriented satellite. For values of C_H less than -1 unconditional stability is guaranteed by the existence of closed zero velocity curves about the equilibrium position. On the other hand, if $-1 < C_H < C_{H_{max}} \approx 0.55$, the system possesses conditional stability which depends upon the initial conditions imposed and corresponds to the existence of an invariant surface in the phase space. Thus stable motion can result even when the zero velocity curves are not closed.

From the limiting invariant surfaces presented here it can be concluded that with increasing C_H the region of stability diminishes rapidly in size. For $C_H \approx 0.55$ it ceases to exist altogether. This imposes upper bounds on the disturbances which a satellite can tolerate without becoming unstable.

The librational motions, both in and normal to the orbital plane, are quasi-periodic. This is particularly noticeable at high values of C_H where the motion in the orbital plane occurs at a frequency approximately double that of the motion normal to the orbital plane.

The analysis suggests that the coupled librational motion is more sensitive to the in-plane disturbances compared to those normal to the orbital plane. This indicates that design analyses performed using planar motion are conservative and that the actual motion is at least as stable as indicated by the simplified study.

6. CONCLUDING REMARKS

6.1 General Conclusions

The results presented have shown the usefulness of adopting a phase space which possesses a sufficient number of dimensions so that the state of the system under study is uniquely represented by the co-ordinates of a point. In the great majority of the cases studied, the numerical integration of the equations of motion led to the generation of an invariant surface. That is, an "isolating" integral manifold could be obtained which forms a surface in the phase space and represents a reduction in the number of co-ordinates by unity.

In those cases where no integral manifold could be found, the motion was either unstable or a type of long period beat phenomenon was observed. In the latter case, there is evidence that the invariant surface breaks up into a tortuous structure which gives the motion a random appearance.

The invariant surfaces are non-intersecting. This is their most important property as it increases their usefulness in the study of the general motion and the conditions which yield stability.

There is an inherent limitation to the practical application of the concept in that it is difficult to conceive of a space possessing more than three dimensions.

Hence systems requiring more than three co-ordinates for their description are too complex for this approach to yield really useful information. Where the system involves three state variables, or less, and particularly in the case of the general second order differential equation, the method is extremely valuable.

6.2 Recommendations for Future Work

There are many possibilities for extension of the work presented here. It would, for example, be useful to obtain an approximate analysis of the planar motion of a rigid satellite which is capable of predicting the size and shape of the limiting invariant surface. One possible way of making this study would be to investigate the transformation concept introduced in Section 2.4 and to determine approximations to the mapping which yield the results with a considerable reduction in computational effort.

The analysis of the damped satellite could be extended considerably. The damper employed in Chapter 3 is complex and inefficient as compared to other devices. The configuration studied by Zajac[16] may prove to be useful in approximating practical satellites. There is a large amount of literature concerning the small amplitude motions of these devices, but very little effort has been made in considering the inherent non-linearity of the equations or the problem of capture of the satellite by the gravitational gradient field.

The problem of the "long" elastic satellite also

remains to be treated. There is at least one scientific experiment that has been proposed which would require very long antennae.[39] The analysis becomes much more difficult as the parametric excitation of the boom becomes significant as a result of the low natural frequency and interacts with the non-linearity of the large thermal deflections.

A study of the general motion of a non-spinning satellite would involve a massive amount of work. If the orbit is elliptical, the Hamiltonian varies with time and hence the state of the system (equations 5.18 and 5.19) depends on the five variables; Θ, ψ, ψ', ϕ, ϕ' as well as the parameters K_i and e. By fixing the values of Θ, K_i, and e and assuming that an integral manifold exists, it should be possible to determine ϕ, for example, as a function of ψ, ψ', and ϕ' for a specified set of initial conditions. The determination of such a function would be extremely interesting, but it would involve the integration of the equations of motion for approximately one thousand orbits if the resulting accuracy is to be equivalent to that in Chapter 5. The determination of the limiting manifold will thus be a very time consuming process. A comprehensive study of the effects of variations in the parameters K_i and e thus appears to be unrealistic.

A contribution could be made by attempting an approximate solution of the equations of motion and by comparing the results with the numerical work. This is a more elaborate problem than that proposed for the approximate solution of

the planar motion and it is assumed that the planar work would be completed before the more complicated analysis is attempted.

It would also be useful to perform a detailed simulation of an actual satellite in order to assess more accurately the magnitude of the effects of various disturbances. The design of a satellite might well form the ultimate goal of this work and such a simulation would be required in any engineering study and would be essential in determining the effects of design changes on the performance.

BIBLIOGRAPHY

1 Jensen, J., Townsend, G., Kork, J., and Kraft, D., Design Guide to Orbital Flight, McGraw-Hill, New York, 1962, pp. 752-753.

2 Wiggins, Lyle E., "Relative Magnitudes of the Space Environment Torques on a Satellite," AIAA Journal, Vol. 2, No. 4, April 1964, pp. 770-771.

3 Glasstone, Samuel, Sourcebook on the Space Sciences, Van Nostrand, Princeton, N.J., 1965, Chap. 8.

4 King-Hele, Desmond, Satellites and Scientific Research, revised ed., Routledge and Kegan, London, 1962, p. 114.

5 Piscane, Vincent L., Pardoe, Peter P., and Hook, P. Joy, "Stabilization System Analysis and Performance of the Geos-A Gravity-Gradient Satellite (Explorer XXIX)," Proceedings of the AIAA/JACC Guidance and Control Conference, American Institute of Aeronautics and Astronautics, 1966, pp. 226-237.

6 Moran, John P., "Effects of Plane Librations on the Orbital Motion of a Dumbbell Satellite," ARS Journal, Vol. 31, No. 8, Aug. 1961, pp. 1089-1096.

7 Yu, E.Y., "Long-term Coupling Effects Between the Librational and Orbital Motions of a Satellite," AIAA Journal, Vol. 2, No. 3, Mar. 1964, pp. 553-555.

8 Nelson, Walter C., and Loft, Ernest E., Space Mechanics, Prentice-Hall, Englewood Cliffs, N.J., 1962, pp. 160-165.

9 Klemperer, W.B., "Satellite Librations of Large Amplitude," ARS Journal, Vol. 30, No. 1, Jan. 1960, pp. 123-124.

10 Schechter, Hans B., "Dumbbell Librations in Elliptic Orbits," AIAA Journal, Vol. 2, No. 6, June 1964, pp. 1000-1003.

11 Baker, Robert M.L., Jr., "Librations on a Slightly Eccentric Orbit," ARS Journal, Vol. 30, No. 1, Jan. 1960, pp. 124-126.

12 Zlatousov, V.A., Okhotsimsky, D.E., Sarghev, V.A., and Torzhevsky, A.P., "Investigation of a Satellite Oscillations in the Plane of an Elliptic Orbit," Proceedings of the Eleventh International Congress of Applied Mechanics, Gortler, Henry, ed., Springer-Verlag, Berlin, 1964, pp. 436-439.

13 Auelmann, Richard R., "Regions of Libration for a Symmetrical Satellite," AIAA Journal, Vol. 1, No. 6, June 1963, pp. 1445-1446.

14 DeBra, D., "The Large Attitude Motions and Stability, Due to Gravity, of a Satellite With Passive Damping in an Orbit of Arbitrary Eccentricity About an Oblate Body," Ph.D. dissertation, Stanford University, June 1962.

15 Hartbaum, H., Hooker, W., Leliakov, I., and Margulies, G., "Configuration Selection for Passive Gravity-Gradient Satellites," Paper presented at the Symposium on Passive Gravity Gradient Stabilization, Ames Research Center, Moffett Field, Calif., May 10-11, 1965.

16 Zajac, E.E., "Damping of a Gravitationally Oriented Two-Body Satellite," ARS Journal, Vol. 32, No. 12, Dec. 1962, pp. 1871-1875.

17 Etkin, B., "Attitude Stability of Articulated Gravity-Oriented Satellites. Part I - General Theory and Motion in Orbital Plane," Report No. 89, University of Toronto, Institute of Aerophysics, Nov. 1962.

18 Etkin, B., "Dynamics of Gravity-Oriented Orbiting Systems With Application to Passive Stabilization," AIAA Journal Vol. 2, No. 6, June 1964, pp. 1008-1014.

19 Fletcher, H.J., Rongved, L., and Yu, E.Y., "Dynamics Analysis of a Two-Body Gravitationally Oriented Satellite," Bell System Technical Journal, Vol. 42, 1963, pp. 2239-2266.

20 Paul, B., West, J.W., and Yu, E.Y., "A Passive Gravitational Attitude Control System for Satellites," Bell System Technical Journal, Vol. 42, 1963, pp. 2195-2238

21 Hughes, P.C., "Optimized Performance of an Articulated Gravity Gradient Satellite at Synchronous Altitude," Report No. 118, University of Toronto, Institute of Aerospace Studies, Nov. 1966.

22 Paul, B., "Planar Librations of an Extensible Dumbbell Satellite," AIAA Journal, Vol. 1, No. 2, Feb. 1963, pp. 411-418.

23 Buxton, A.C., Campbell, D.E., and Losch, K., "Rice/Wilberforce Gravity-Gradient Damping System," Paper presented at the Symposium on Passive Gravity Gradient Stabilization, Ames Research Center, Moffett Field, Calif., May 10-11, 1965

24 Katucki, R.J., and Moyer, R.J., "Systems Analysis and Design for a Class of Gravity Gradient Satellites Utilizing Viscous Coupling Between the Earth's Magnetic and Gravity Fields," Paper presented at the Symposium on Passive Gravity Gradient Stabilization, Ames Research Center, Moffett Field, Calif., May 10-11, 1965.

25 Ashley, Holt, "Observations on the Dynamic Behaviour of Large Flexible Bodies in Orbit," AIAA Journal, Vol. 5, No. 3, Mar. 1967, pp. 460-469.

26 Dow, P.C., Schammell, F.H., Murray, F.T., Carlson, N.A., and Buck, I.H., "Dynamic Stability of a Gravity Gradient Stabilized Satellite Having Long Flexible Antennas," Proceedings of the AIAA/JACC Guidance and Control Conference, American Institute of Aeronautics and Astronautics, 1966, pp. 285-303.

27 Weygandt, P., and Moyer, R., "Attitude Control for the Gravity Gradient Test Satellite," Proceedings of the AIAA/JACC Guidance and Control Conference, American Institute of Aeronautics and Astronautics, 1966, pp. 238-248.

28 Cunningham, W.J., Introduction to Nonlinear Analysis, McGraw-Hill, New York, 1958, pp. 250-257.

29 Ince E.L., Ordinary Differential Equations, Dover, New York, 1956, pp. 114-132.

30 McLachlan, N.W., Theory and Application of Mathieu Functions, Dover, New York, 1964, pp. 57-60.

31 Hénon, M., and Heiles, C., "The Applicability of Third Integral of Motion: Some Numerical Experiments," Astronomical Journal, Vol. 69, No. 1, Feb. 1964, pp. 73-79.

32 Moser, Jurgen, "Perturbation Theory for Almost Periodic Solutions for Undamped Nonlinear Differential Equations," International Symposium on Nonlinear Differential Equations and Nonlinear Mechanics, edited by LaSalle, J.P., and Lefschetz, S., Academic Press, New York, 1963, pp. 71-79.

33 Hamming, R.W., Numerical Methods for Scientists and Engineers, McGraw-Hill, New York, 1962, pp. 183-222.

34 Mitropolskiy, Y.A., "The Method of Integral Manifolds in the Theory of Nonlinear Oscillations," International Symposium on Nonlinear Differential Equations and Nonlinear Mechanics, edited by LaSalle, J.P., and Lefschetz, S., Academic Press, New York, 1963, pp. 1-15.

35 Etkin, B., and Hughes, P.C., "Spin Decay of a Class of Satellites Caused by Solar Radiation," Report No. 107, University of Toronto, Institute for Aerospace Studies, July, 1965.

36 Marks, Lionel S., Mechanical Engineer's Handbook, 5th ed., McGraw-Hill, New York, 1951, pp. 586-600.

37 Webster, A.G., Partial Differential Equations of Mathematical Physics, 2nd ed., Dover, New York, 1955, pp. 138-142.

38 Kane, T.R., "Attitude Stability of Earth-Pointing Satellites," AIAA Journal, Vol. 3, No. 4, April 1965, pp. 726-731.

39 Stone, Robert G., "RAE - 1500-Foot Antenna Satellite," Astronautics and Aeronautics, Vol. 3, No. 3, March 1965, pp. 46-49.